ATTACHMENT B:

Attainment Demonstration Technical Support Document

Prepared for:

Clark County
Department of Environment and Sustainability, Division of Air Quality
4701 W. Russell Road, Suite 200
Las Vegas, NV 89118

Prepared by:

Ramboll Americas Engineering Solutions, Inc.
7250 Redwood Blvd., Suite 105
Novato, California 94945

June 28, 2024
16900026273

Technical Support Document: Attainment Demonstration for the Clark County Ozone State Implementation Plan

Final

RAMBOLL Bright ideas. Sustainable change.

Technical Support Document: Attainment Demonstration for the Clark County Ozone State Implementation Plan

Ramboll
7250 Redwood Boulevard
Suite 105
Novato, CA 94945
USA

T +1 415 899 0700
https://ramboll.com

CONTENTS

Table of Figures

Table of Tables

1.0 INTRODUCTION

1.1 Purpose

In June 2018, the US Environmental Protection Agency (EPA) designated a portion of Clark County, Nevada as a Marginal Nonattainment area under the 2015 ozone National Ambient Air Quality Standard (NAAQS) of 0.070 parts per million by volume (ppm) (Federal Register, 2018). The nonattainment boundary is defined as the Las Vegas Valley (LVV), hydrographic area 212 (HA 212), as recommended by the Nevada Division of Environmental Protection (NDEP) and Clark County (2018). In July 2022, the EPA reclassified the Clark County Nonattainment Area (CCNAA) from Marginal to Moderate due to continued exceedances of the standard through 2020 (Federal Register, 2022, 2023). Moderate areas are subject to additional reporting, management, and emission reduction requirements, including the submittal and approval of an ozone State Implementation Plan (SIP). An approvable SIP must demonstrate, according to photochemical modeling and other weight-of-evidence analyses, that the area will attain the NAAQS by August 3, 2024.

The purpose of this project was to conduct and document the photochemical modeling and ancillary weight-of-evidence analyses that support an ozone attainment demonstration for the CCNAA Moderate Ozone SIP. The project included developing and modeling a set of future control measures, including a mandatory 15% Rate-of-Progress (ROP) Plan for volatile organic compound (VOC) emissions, and developing an on-road mobile source conformity budget. The project was conducted by Ramboll Americas Engineering Solutions, Inc. (Ramboll) under contract to the Clark County Department of Environment and Sustainability (DES), Division of Air Quality (DAQ).

This report comprises the Technical Support Document for the attainment demonstration. Procedures described herein follow the Modeling Protocol (Ramboll, 2022a), developed at the start of this project, and adhere to the most recent photochemical modeling guidance from EPA (2018a). Additional historical context, details and procedural information are provided in the Modeling Protocol.

1.2 Background

The 2015 ozone NAAQS is set at 0.070 parts per million by volume (ppm). The form of the NAAQS is based on quality-assured, certified monitoring data reported as maximum daily 8-hour average (MDA8) ozone concentrations. An area's status relative to the NAAQS is determined by its monitored "design value" (DV), which is defined as the three-year average of the fourth highest MDA8 ozone concentration in each year. The EPA designates areas as nonattainment when DVs exceed the NAAQS. Monitored ozone concentrations are reported as parts per billion by volume (ppb); EPA's convention is to truncate ozone DVs to the nearest whole ppb, so a DV exceeding 70.9 ppb violates the 0.070 ppm ozone NAAQS.

In June 2018, the EPA designated the CCNAA as Marginal based on the maximum 2015-2017 DV of 74 ppb reported among all official monitoring sites within the basin (Federal Register, 2018). The final SIP implementation requirements rule for the 2015 ozone NAAQS was signed by the EPA Administrator on November 7, 2018 (EPA, 2018b). Accordingly, Marginal areas were expected to attain the ozone standard by August 3, 2021 based on their 2018-2020 DV. In July 2022, the EPA reclassified the CCNAA from Marginal to Moderate based on the maximum 2018-2020 DV of 74 ppb. Moderate nonattainment areas are to attain the ozone standard by August 3, 2024 based on their 2021-2023 DV.

The DES/DAQ has submitted "exceptional event" demonstrations to the EPA (e.g., Sonoma Technology, 2021), which show that several ozone exceedance days during 2018 through 2020 were

influenced by large wildfires and stratospheric intrusions impacting air quality in the CCNAA. If approved, those specific exceedance days impacted by exceptional events would not count toward the calculation of the area's 2018-2020 DV. However, EPA has indicated that not all exceptional event demonstration days will be approved, and so the revised 2018-2020 DV with the approved exceptional event days excluded will continue to exceed the 2015 ozone NAAQS.

1.2.1 8-Hour Ozone Trends

Figure 1-1 presents the 23-year history of peak 8-hour ozone DVs in Clark County along with the three ozone NAAQS that have been promulgated over the same period. The year 2022 is the most recent year of quality-assured, certified monitoring data reported by the County, while 2020 was the year when attainment of the 2015 ozone NAAQS was required for Marginal nonattainment areas to avoid reclassification to Moderate. Areas of the County have been designated nonattainment for the 1997 and 2015 standards. Over this period, peak ozone levels have decreased, particularly during the recession years of 2008-2011. Since that period, however, ozone has remained fairly constant with small variations caused by interannual variability in summer weather and external uncontrollable factors such as wildfires.

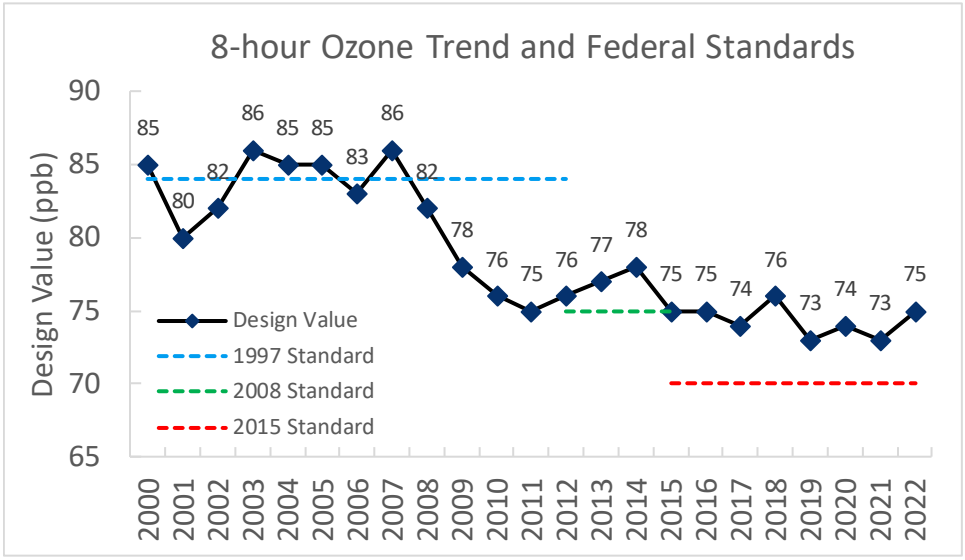

Figure 1-1. History of peak 8-hour ozone design values in Clark County and the three ozone NAAQS that have been in effect since 2000. Data from https://www.epa.gov/air-trends/air-quality-design-values#report.

1.2.2 Recent Ozone Air Quality in Clark County

As of 2022, the DES/DAQ operates 13 ambient ozone monitoring sites in the region, most of which also measure other pollutants and meteorological parameters. Figure 1-2 shows the location of the 14 ozone monitoring sites used in this study that operated in 2016, most of which continue to operate today. DAQ's ambient air monitoring network meets the monitoring requirements for criteria pollutants pursuant to Title 40, Part 58, of the Code of Federal Regulations (CFR), Appendix D (EPA, 2008). The DES/DAQ submits quality-assured monitoring data to the EPA's Air Quality System (AQS). The monitoring sites characterize urban/basin ozone patterns in Las Vegas, as well as air quality upwind and downwind of the LVV. For example, the southern Jean monitoring site along the I-15 corridor generally characterizes transport into the LVV, whereas the Apex and Indian Springs sites to the north characterize outflow from the LVV.

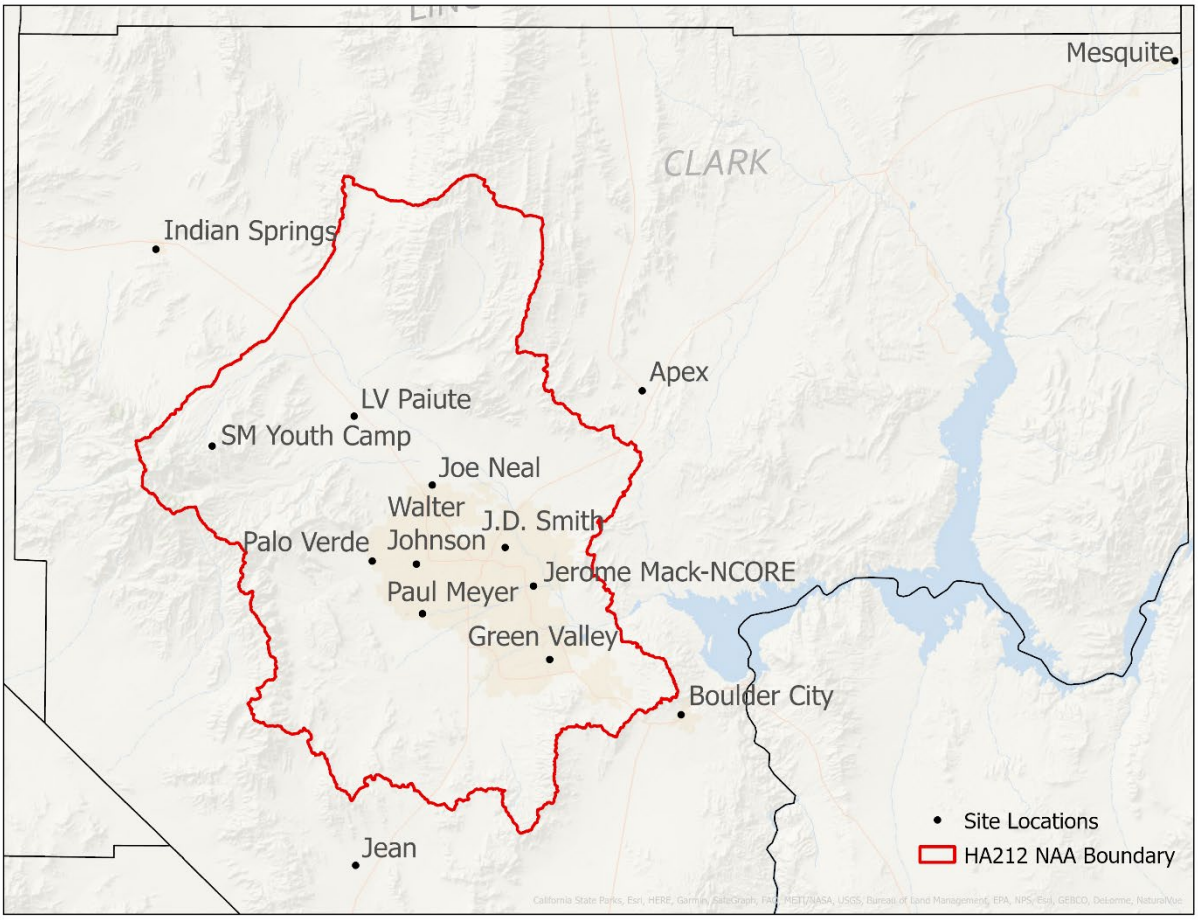

Figure 1-2. Clark County ozone monitoring sites used in this study that operated in 2016 .

Figure 1-3 shows the spatial distribution of 2020 DVs, when attainment was required for Marginal nonattainment areas, at the 10 ozone monitoring sites within and immediately surrounding the CCNAA (sites shown in grey were not official ozone monitors). Sites exceeding the 2015 ozone standard are shown in dark blue and are centered in the LVV and near Henderson. Two sites within the CCNAA, and all other sites outside, did not exceed the standard. The figure indicates the highest ozone levels in the basin occur over a distinct urban-oriented spatial pattern.

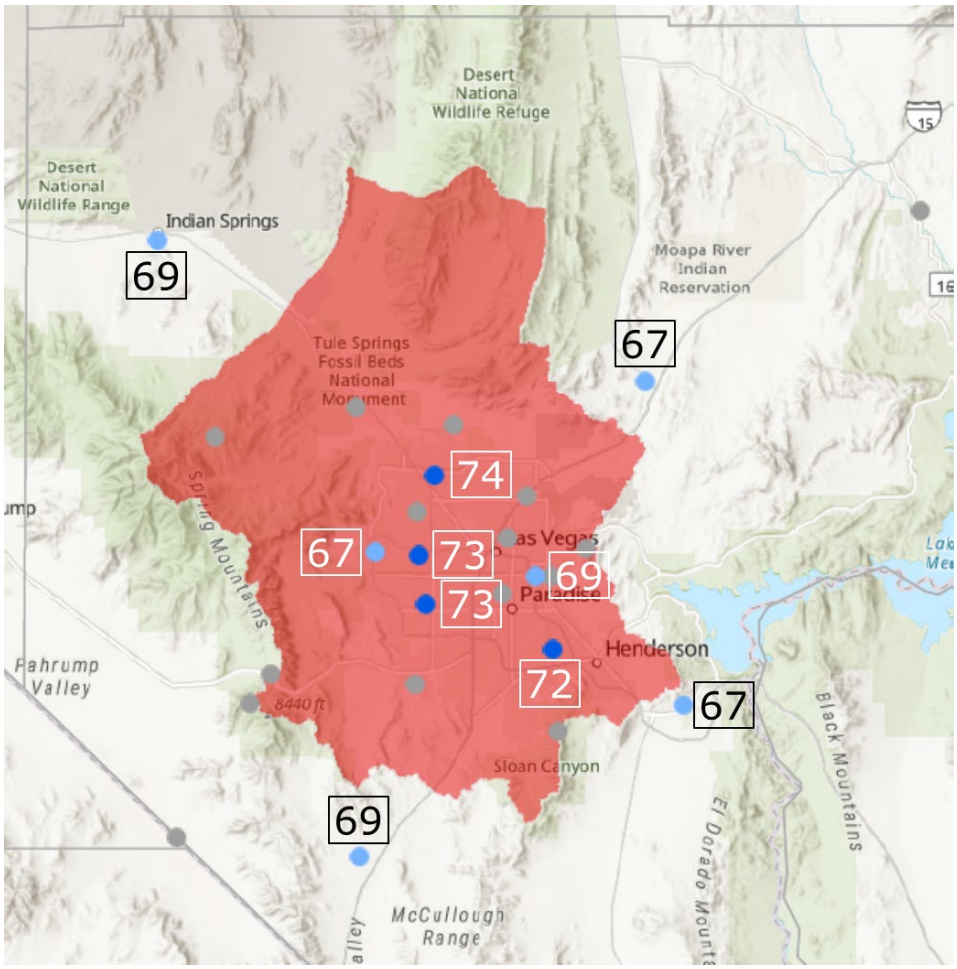

Figure 1-3. Spatial distribution of 2020 design values at 10 ozone monitoring sites within and immediately surrounding the CCNAA, as depicted by orange shading. Sites shown in grey are not official ozone monitors. Background image from https://epa.maps.arcgis.com/apps/MapSeries/index.html?appid=bc6f3a961ea14013afb2e0d0e450b0d1.

1.2.3 Conceptual Model of High Ozone Levels in Clark County

This section is largely based on the summary from Sonoma Technology (2021). Clark County is located in southern Nevada and borders California and Arizona. Clark County includes the Las Vegas – Henderson – Paradise Metropolitan Area, one of the fastest growing metropolitan areas in the United States with a 2020 population of 2.2 million (US Census Bureau, 2020). The LVV consists of a 1,600 km^2 basin that lies between 500-900 m above sea level (Langford et al., 2015). It is surrounded by the Spring Mountains to the west (3,000 m) and the Sheep Mountain Range to the north (2,500 m). Three mountain ranges comprise the southern end of the valley. The valley floor slopes downward from west to east, which influences surface weather and runoff patterns. The I-15 corridor to the southwest is an important atmospheric transport pathway from the Los Angeles Basin into the LVV (Langford et al., 2015).

The LVV experiences abundant sunshine and average summer high temperatures ranging 34 to 40°C (93 to 104°F). The urban heat island effect causes large temperature gradients within the LVV, with generally cooler temperatures on the eastern side. Winds tend to come from the southwest during

spring and summer and from the northwest in the fall and winter. The bounding mountain ranges direct basin-wide wind flows while inducing upslope/downslope circulations during weak flow conditions. The altitudes of these ranges are roughly equivalent to the summer daily boundary layer depth, leading to the trapping of pollutants within the basin during stagnant conditions. The surrounding mountains also affect precipitation patterns, contributing to low annual rainfall accumulations of 107 mm (4.2 in), 22% of which occurs during the summer monsoon season in July through September (National Weather Service Forecast Office, 2020).

During the May-September season, ozone concentrations are influenced by the photochemical oxidation of local precursor emissions comprising nitrogen oxides (NOx) and volatile organic compounds (VOC), regional and intercontinental transport into the region, and by exceptional events such as wildfires and stratospheric intrusions (Langford et al., 2015; Clark County, 2019). Local ozone production is maximized during hot, stagnant conditions when strong regional high pressure suppresses boundary layer depth and reduces basin ventilation. Transport from upwind source regions, particularly the Los Angeles Basin, occurs during southwesterly winds, while southerly transport from Mexico dominates later in the season due to the summer monsoon (Langford et al., 2015; Zhang et al., 2020).

Local precursor emissions in Clark County include NOx and VOC from mobile and stationary sources, NOx from natural-gas power generation, and VOC from consumer products and biogenic sources (vegetation). According to the 2017 CCNAA emission inventory developed in this study (Ramboll, 2024b), local anthropogenic sources emit 95 tons of NOx per day and 108 tons of VOC per day during a typical ozone season weekday (Table 1-1). On-road mobile sources comprise 38% of total NOx emissions while total mobile emissions comprise 77% of total NOx emissions during the ozone season. Nonpoint (area) sources contribute 52% of total VOC emissions. Biogenic emissions are not reported here as their estimates range by several orders of magnitude depending on which biogenic emission model is employed (as detailed in Section 8.4.10).

Table 1-1. 2017 CCNAA anthropogenic emissions (TPD) for a typical summer weekday.

Source Category	2017 NOx	2017 VOC
Point source	2.92	1.25
Nonpoint source	6.15	57.72
On-road mobile	37.91	24.81
Non-road mobile	36.98	24.03
Airports (commercial & Federal)	11.90	1.96
Locomotives	0.80	0.04
Total	**96.66**	**109.81**

1.2.4 2013 Las Vegas Ozone Study

This summary is extracted from Langford (2014). The 2013 Las Vegas Ozone Study (LVOS) assessed the influences from stratospheric and long-range transport from Asia on surface ozone concentrations in Clark County and determined if these processes contributed to exceedances of the NAAQS. The study also characterized local photochemical production and regional transport from the Los Angeles Basin and impacts from wildland fires. Measurements were made at a former US Air Force radar station ~45 km northwest of Las Vegas on Angel Peak (~2,700 m above sea level) in the Spring Mountains. The study consisted of two extended lidar ozone profiler measurement periods in late May and late June from the surface to ~2,500 m above ground level (~5,200 m above sea level), and

continuous in situ measurements of ozone, carbon monoxide, and meteorological parameters at the surface. Measurement activities were guided by forecasts and analyses from the National Oceanic and Atmospheric Administration's (NOAA) FLEXPART particle dispersion model and the Real Time Air Quality Modeling System (RAQMS), while measurement interpretation was aided by the NOAA GFDL-AM3 chemistry-climate model. The 2008 ozone NAAQS was exceeded in Clark County on 6 days during LVOS and analyses showed that stratospheric ozone had major contributions on 4 exceedance days while transported pollution from Asia had smaller contributions on 3 exceedance days. Modeling analyses suggested that wildland fires were partly responsible for 3 exceedance days outside the LVOS measurement period. Thus, results suggested that all 6 exceedance days were influenced by transport from outside the county, and further indicated that stratospheric, Asian, and wildfire contributions will be a greater concern with the lower 2015 NAAQS.

1.2.5 2017 Fires, Asian, and Stratospheric Transport–Las Vegas Ozone Study

The summaries below are extracted from Langford (2022) and Zhang et al (2020). The 2017 Fires, Asian, and Stratospheric Transport–Las Vegas Ozone Study (FAST-LVOS) was a follow-on study of ozone transport to Clark County. The field campaign was conducted from mid-May through June using lidar, ozonesonde, aircraft, and in situ measurements. In conjunction with a variety of models, the study characterized ozone and related species above southern Nevada and California and assessed the influence of stratospheric intrusions, wildfires, Asian transport, as well as local and regional contributions on surface ozone concentrations in the LVV. Campaign measurements (Langford, 2022) found elevated ozone layers above Las Vegas on more than 75% (35 of 45) of the sample days and showed that entrainment of these layers contributed to mean regional background concentrations of 50–55 ppb, or 70-80% of the 2015 ozone NAAQS. The detection and attribution of high background ozone events in the southwest US is challenging but relevant to the 2015 ozone NAAQS and possible lower standards in the future.

Simulations were conducted with two global models (GFDL-AM4 and GEOS-Chem) to study local to global contributions during high ozone events (Zhang et al., 2020). While ozone produced from regional anthropogenic emissions dominate pollution events in the LVV, stratospheric intrusions can elevate surface ozone above 70 ppb. Modeling showed stratospheric influences on 4 out of the 10 days when MDA8 ozone exceeded 65 ppb in Clark County. GFDL-AM4 captured key characteristics of deep stratospheric intrusions consistent with FAST-LVOS profile and surface measurements at Angel Peak, whereas GEOS-Chem did not simulate observed features as well and underestimated surface observations by ~20 ppb. On days when observed MDA8 ozone exceeded 65 ppb and GFDL-AM4 simulated 20–40 ppb stratospheric enhancements, GEOS-Chem simulated ~15 ppb lower background ozone. However, during a wildfire event, GEOS-Chem estimated ~15 ppb more ozone, in better agreement with lidar observations, while at the surface, the two models bracketed observed MDA8 ozone. Both models captured large-scale transport of Asian pollution, but neither could resolve fine-scale pollution plumes sensed by the numerous measurement platforms. US background ozone estimated from the two models differed by 5 ppb on average (greater in GFDL-AM4) and up to 15 ppb episodically.

1.2.6 2021 Field Measurements and Modeling

The NOAA Chemical Sciences Laboratory (CSL) and the Cooperative Institute for Research in Environmental Sciences (CIRES) at the University of Colorado conducted an intensive field measurement campaign during July through September 2021 (NOAA, 2022). The study addressed organic compound emissions and chemistry in Clark County, including: (1) measuring VOC from volatile chemical products (VCP), mobile sources, cooking, and industrial facilities; (2) characterizing their spatial distribution; (3) identifying chemical tracers to apportion VOCs among VCP, energy-

related, cooking, and biogenic sources; (4) measuring the composition of gas- and aerosol phase organics in the urban atmosphere; and (5) quantifying anthropogenic nitrogen oxide (NOx = NO + NO_2) emission from mobile sources, buildings, industrial facilities, and outlying agricultural regions and power generation. A comprehensive list of VOC, NOx, ozone and greenhouse gases were measured by the NOAA Mobile Laboratory and at the Jerome Mack site. Atmospheric profiles of winds and aerosol backscatter were measured by LIDAR at the North Las Vegas airport.

Photochemical box modeling representative of conditions at the Jerome Mack monitoring site was conducted using emissions estimated from the field measurements to assess organic gas reactivity and ozone sensitivity to VOC and NOx perturbations. Results indicated that ozone production is more NOx sensitive but within the transition zone where ozone would respond to both NOx and VOC reductions. The authors suggested that "in other regions of Las Vegas, where urban NOx might be larger than at Jerome Mack, ozone production could be NOx saturated."

Three-dimensional photochemical transport modeling was also performed using the Weather Research Forecasting with Chemistry (WRF-Chem) model. Results verified that transported regional/background of ~60 ppb is a significant fraction of MDA8 ozone during high temperature events. Reducing local NOx emissions by 50% can reduce MDA8 ozone by ~10 ppb, which is consistent with box modeling. However, effects from reducing local VOC emissions is mixed and WRF-Chem results are inconsistent with box modeling; biogenic VOC emission estimates were noted as a key uncertainty. Modeling also confirmed that wildfires are potentially a significant source of ozone pollution in Clark County.

While the field study final report has just been completed and the collected data are not directly useable for the photochemical modeling described here, we refer to certain general results from the field study to qualitatively assess modeling conducted for the SIP and to provide information for the weight of evidence.

1.2.7 EPA Modeling Platform

The EPA routinely develops national photochemical modeling platforms (MP) to evaluate air quality impacts of national rules and to conduct transport and contribution assessments. The national MPs typically coincide with the triennial National Emission Inventory (NEI[1]) years (e.g., 2014 and 2017). Below we discuss the EPA's most recent MP.

The EPA and Multi-Jurisdictional Organizations (MJO) conducted an inventory collaborative study[2] to develop a 2016 emissions inventory of comparable quality to the NEI. EPA developed several versions of the 2016 MP based on a continental US modeling domain with 12 km grid resolution (referred to as "12US2") and an expanded North American domain with 36 km resolution ("36US3"). Meteorological inputs were based on a 2016 WRF simulation conducted by EPA (2019a) while initial and boundary conditions (IC/BC) for the 36US3 domain were based on a 2016 hemispheric CMAQ simulation (EPA, 2022a). EPA has released several versions of their 2016 MP:

- 2016v7.1 Alpha[3] (2016fd emissions): available in June 2019 based mainly on 2014 NEIv7.1 emissions.

[1] https://www.epa.gov/air-emissions-inventories/national-emissions-inventory-nei

[2] http://views.cira.colostate.edu/wiki/wiki/10197

[3] https://www.epa.gov/air-emissions-modeling/2016-alpha-platform

- 2016v7.2 Beta (2016ff emissions): updated 2016 emissions from the joint EPA/MJO emissions collaborative study, originally released in March 2019 through the Intermountain West Data Warehouse (IWDW[4]).
- 2016v7.2 Beta Prime (2016fg emissions): EPA made updates for their preliminary 2028 regional haze modeling (EPA, 2019b).
- EPA 2016v1[5] (2016fh emissions): released in November 2019, with several updates made in the following months (EPA, 2021), including emission projections for 2023 and 2028.
- 2016v2[6] (2016fj emissions): uses the same meteorological and IC/BC data as 2016v1 and includes emissions scenarios for 2016, 2023, 2026 and 2032 (EPA, 2022b). EPA applied the MOtor Vehicle Emissions Simulator (MOVES3) for all years to generate Emissions Factor (EF) lookup tables for processing model-ready on-road mobile source emissions. The 2016v2 MP contains several major updates as follows:
  - Use of the MOVES3[7] mobile source emissions model instead of MOVES2014 used in the 2016v1 MP.
  - Updated non-point inventory from the 2017 NEI[8] including a new volatile chemical products (VCP) emissions inventory approach (Seltzer et al., 2021).
  - Updated oil and gas emissions for the western states using data provided by WRAP.
  - Corrections for double counting of emissions at airports.
  - Updated emissions for Canada and Mexico.
  - Updated biogenic emissions using a newer version of the Biogenic Emission Inventory System and the Biogenic Emissions Landuse Database (BEIS3.7/BELD5) instead of BEIS3.61/BELD4 used in the 2016v1 MP.

EPA (2022c) released the 2016v2 MP in January 2022[9]. The 2016v2 MP has been used to project future ozone DVs for the years 2023, 2026 and 2032. EPA estimated that ozone DVs in Clark County may not attain the 2015 ozone NAAQS in 2023 but would attain in 2026 and 2032 (Table 1-2).

EPA also used the 2016v2 MP for the preliminary interstate ozone transport modeling for the 2015 ozone NAAQS (EPA, 2022d), in which 2023 DV contributions were estimated from individual states, foreign sources, fires and biogenic emissions. EPA estimated that California's contribution to ozone DVs in Clark County is roughly as large as Nevada's own contribution, while most ozone is transported into the LVV from BCs (Table 1-3) reflecting total global contributions. Fires and biogenic emissions are estimated to be minor contributors (1-3 ppb) and Canada and Mexico contribute even less (1-2 ppb).

[4] http://views.cira.colostate.edu/iwdw/
[5] https://www.epa.gov/air-emissions-modeling/2016v1-platform
[6] https://www.epa.gov/air-emissions-modeling/2016v2-platform
[7] https://www.epa.gov/moves/latest-version-motor-vehicle-emission-simulator-moves
[8] https://www.epa.gov/air-emissions-inventories/2017-national-emissions-inventory-nei-data
[9] https://gaftp.epa.gov/Air/aqmg/2016v2_Platform_Modeling_Data/

Table 1-2. Projected 2023, 2026 and 2032 ozone DVs (ppb) at all Clark County ozone monitoring sites based on EPA's 2016v2 modeling platform (from https://gaftp.epa.gov/Air/aqmg/2016v2_Platform_Modeling_Data/ accessed April 2022).

Site ID	2023fj Avg 3x3	2023fj Max 3x3	2026fj Avg 3x3	2026fj Max 3x3	2032fj Avg 3x3	2032fj Max 3x3
320030022 Apex	66.1	67.7	65.3	66.9	64.4	65.9
320030023 Mesquite	58.3	59.0	57.9	58.5	57.3	58.0
320030043 Paul Meyer	68.5	69.5	67.8	68.7	66.9	67.8
320030071 Walter Johnson	67.7	69.3	66.7	68.3	65.7	67.2
320030073 Palo Verde	67.7	68.4	66.7	67.4	65.7	66.3
320030075 Joe Neal	70.0	**71.0**	69.0	69.9	67.8	68.7
320030298 Green Valley	66.6	66.6	65.6	65.6	64.4	64.4
320030540 Jerome Mack	65.0	66.3	64.1	65.3	63.1	64.3
320030601 Boulder City	61.8	62.7	61.0	62.0	60.1	61.0
320031019 Jean	64.8	66.4	64.2	65.8	63.6	65.2
320032002 J.D. Smith	67.9	68.4	66.9	67.4	65.7	66.2
320037772 Indian Springs	65.1	65.6	64.6	65.1	63.9	64.4

Table 1-3. Projected 2023 ozone DV contributions (ppb) from Nevada, other states, foreign sources, fires, and biogenic emissions at 10 LVV ozone monitoring sites based on EPA's 2016v2 modeling platform (https://gaftp.epa.gov/Air/aqmg/2016v2_Platform_Modeling_Data/ accessed April 2022).

Site ID	AZ	CA	NV	Canada +Mexico	2023 Fires	IC/BC	Biogenic
320030022 Apex	0.31	6.90	6.58	1.33	1.57	47.03	1.83
320030043 Paul Meyer	0.37	6.96	8.19	1.48	2.30	46.43	1.94
320030071 Walter Johnson	0.19	7.40	6.31	1.31	3.10	46.72	1.70
320030073 Palo Verde	0.19	7.40	6.31	1.31	3.10	46.72	1.70
320030075 Joe Neal	0.21	7.44	8.46	1.28	0.67	49.59	1.75
320030298 Green Valley	0.46	7.60	6.47	1.84	1.77	45.58	1.99
320030540 Jerome Mack	0.42	6.89	8.45	1.73	1.84	42.94	1.86
320031019 Jean	0.13	6.66	0.99	1.61	2.21	51.22	1.42
320032002 J.D. Smith	0.36	7.79	10.57	1.31	0.78	44.48	1.97
320037772 Indian Springs	0.07	5.54	1.66	0.79	1.90	53.25	1.29

2.0 MODEL SELECTION

The model selection process for the CCNAA ozone attainment demonstration followed EPA (2018a) guidance. The EPA recommends that models be selected for ozone SIP studies on a case-by-case basis, yet explicitly mentions the Community Multiscale Air Quality (CMAQ) model and the Comprehensive Air quality Model with extensions (CAMx) as the most commonly used photochemical grid models (PGM) for this purpose. Thus, both satisfy EPA's selection criteria and are preferred over other PGMs. EPA's ozone modeling guidance lists several criteria for model selection that are paraphrased as follows:

- It should not be proprietary.
- It should have received a scientific peer review.
- It should be demonstrated to be applicable to the problem on a theoretical basis.
- It should be used with available data bases that are adequate to support its application.
- It should be shown to have performed well in past modeling applications.
- It should be applied consistently with an established protocol on methods and procedures.
- It should have a user's guide and technical description.
- The availability of advanced features (e.g., probing tools or science algorithms) is desirable.
- When other criteria are satisfied, resource considerations may be important and are a legitimate concern.

For more than a decade, the Clark County DES/DAQ has employed WRF, SMOKE, MOVES, BEIS and CAMx to study ozone air quality in the LVV. Therefore, DAQ staff are very familiar with the operation and performance of each model and so for the CCNAA ozone demonstration the model selection is weighted toward this system of models. Furthermore, the EPA, MJOs, states, and many local air quality agencies have successfully applied these models in other ozone regulatory programs throughout the US.

2.1 Weather Research and Forecasting Model

The Weather Research and Forecasting (WRF) model, Advanced Research WRF (ARW) core, supported the CCNAA attainment demonstration modeling by providing meteorological inputs required by the PGM. WRF is a mesoscale numerical weather prediction system designed to serve both operational forecasting and atmospheric research needs (Skamarock et al., 2019). WRF is flexible and efficient computationally, while offering advanced physics, numerical, and data assimilation capabilities contributed by the research community. It features a software architecture allowing for computational parallelism and system extensibility. WRF is suitable for a broad spectrum of applications across scales ranging from sub-kilometer to thousands of kilometers. The effort to develop WRF has been a collaborative partnership, principally among the National Center for Atmospheric Research (NCAR), the National Oceanic and Atmospheric Administration (NOAA), the National Centers for Environmental Prediction (NCEP) and the Forecast Systems Laboratory (FSL), the Air Force Weather Agency (AFWA), the Naval Research Laboratory, the University of Oklahoma, and the Federal Aviation Administration (FAA).

WRF is publicly available, has full documentation, and possesses two decades of demonstrated success in simulating meteorological conditions and driving PGM simulations throughout the US specifically for regulatory and research air quality studies.

2.2 Emissions Models

2.2.1 Sparse Matrix Operator Kernel Emissions Processing System

The Sparse Matrix Operator Kernel Emissions (SMOKE) processing system prepared emission inputs for the PGM. SMOKE is an efficient, modern tool that generates temporally, spatially, and chemically allocated emission inputs from on- and non-road mobile, point, non-point (area), biogenic, and fire sources (UNC, 2020). Except for mobile and biogenic emissions, which are developed from separate models and processed through SMOKE, its purpose is to convert an existing annual emissions inventory by county and individual point source into the specific formatted emission files required by PGMs. SMOKE performs three main functions for this purpose: (1) spatially allocates county-level emissions to PGM grid cells using a surrogate distribution (e.g., population, land use, etc.); (2) temporally allocates annual emissions to a specific time (e.g., monthly or seasonally, day of week, and hour); and (3) chemically maps criteria pollutant emissions to the individual compounds needed by the PGM chemical mechanism (most important for VOC and particulate matter).

SMOKE is the most current and widely used emissions processor that supports regulatory modeling activities throughout the US. It is designed specifically to translate US NEI datasets to the CMAQ and CAMx models and is flexible to incorporate local and special emissions data. It includes capabilities to directly process mobile source emissions from MOVES and biogenic emissions from BEIS.

2.2.2 MOtor Vehicle Emissions Simulator

The MOtor Vehicle Emissions Simulator version 3 (MOVES3) estimated emission rates from on-road and non-road motor vehicle sources. MOVES3 is EPA's latest mobile source emissions model (EPA, 2020a, 2021a) that estimates emissions at the national, county, and project level for criteria air pollutants, greenhouse gases, and air toxics. Updates from the previous version include:

- The latest data on vehicle populations, travel activity, and emission rates as well as updated fuel supply information at the county level.
- Better accounting for vehicle starts, long-haul truck hoteling, and off-network idling.
- Incorporation of the impacts of the Heavy-Duty Greenhouse Gas Phase 2 rule and the Safer Affordable Fuel-Efficient (SAFE) Vehicles Rule.
- Improved user interface to make the model easier to use and updated for compatibility with newer software.

These updates ensure that MOVES3 is a state-of the-science model and the most accurate tool for estimating emissions from the transportation sector for most purposes. Outside of California, it is the only EPA-approved mobile source emissions model available in the US.

2.2.3 SMOKE-MOVES

The "SMOKE-MOVES" processing stream converted emission factors (EF) generated by MOVES3 to emission inputs required by the PGM. It combines data from several MOVES3 EF look-up tables, vehicle activity (e.g., vehicle miles travelled or VMT), and meteorological data (typically from WRF) to generate hourly, gridded, speciated mobile source emissions input files. SMOKE-MOVES was used in the standard convention by using representative county-level activity data provided by Clark County and EPA (for areas outside of Clark County) to generate on-road mobile source emission inputs.

2.2.4 Biogenic Emission Inventory System

The Biogenic Emission Inventory System (BEIS) estimated natural VOC emissions from vegetation and NOx from soil (EPA, 2022e). Built into SMOKE to specifically support CMAQ, BEIS is driven by ambient

meteorology and land cover data from the Biogenic Emissions Landuse Database (BELD). BELD data provide distributions of hundreds of vegetation classes at 1 km resolution over most of North America.

Several versions of BEIS have been developed and applied during the evolution of the EPA 2016 emissions modeling platforms. BEIS3.61/BELD4 was used for the 2016v1 MP. Updates from previous versions included incorporating the US National Land Cover Data (NLCD) into BELD4 and calculating leaf temperature using a canopy model instead of 2-meter temperature directly. BEIS3.7/BELD5 was used for the 2016v2 MP. This version uses updated biomass and emissions factors and several updates to the landuse database. BEIS4/BELD6 is the latest version, released in mid-2022, that includes fundamental updates to the landuse database.

As described in Section 8.4.10, each of these three BEIS versions result in substantially different estimates in biogenic VOC emissions in Clark County. BEIS3.7/BELD5 was initially selected for CCNAA modeling to be consistent with the EPA 2016v2 MP. After review of the PGM performance, additional sensitivity tests using BEIS3.6/BELD4 and BEIS4/BELD6 were conducted and evaluated. We also compared emission estimates from all three versions of BEIS to the latest version of the Model of Emissions of Gases and Aerosols from Nature (MEGAN, version 3.2), developed by the University of California at Irvine (UCI, 2022). MEGAN3.2 includes expanded plant emissions data in western states and the inclusion of vegetative data for urban areas, which were implicitly zero in previous versions and led to zero urban biogenic emissions.

2.3 Comprehensive Air quality Model with extensions

The CAMx photochemical grid model was used for the CCNAA ozone attainment demonstration. CAMx is a state-of-science "one-atmosphere" multi-scale photochemical grid model capable of addressing ozone, particulate matter, toxics, visibility, and acid deposition at regional, urban, and local scales over periods of days to years (Ramboll, 2022b). CAMx is a publicly available open-source computer modeling system built on today's understanding that air quality issues are complex, interrelated, and reach beyond the urban scale. CAMx is designed to (a) simulate air quality over many temporal and geographic scales, (b) treat a wide variety of inert and chemically active pollutants, (c) provide source-receptor, sensitivity, and process analyses, and (d) be computationally efficient and flexible. CAMx v7.2 is the current version, released in May 2022.

The EPA has approved the use of CAMx for numerous ozone and PM SIPs throughout the US and has used this model to evaluate effects of national rules and regional mitigation strategies, including the Cross-State Air Pollution Rule (CSAPR; EPA, 2021b) and most recently the preliminary interstate ozone transport modeling for the 2015 ozone NAAQS (EPA, 2022d). The 2016v1 and v2 platforms include data inputs that support CAMx applications on EPA's 36 and 12 km continental grids.

2.4 Final Justification for Model Selection

The modeling system employed to support the CCNAA ozone attainment demonstration satisfies all of EPA's model selection criteria as follows:

- It should not be proprietary: The WRF, SMOKE, MOVES, BEIS, and CAMx models are all publicly available at no cost and can be downloaded from their respective websites[10,11,12,13].

[10] https://www.mmm.ucar.edu/weather-research-and-forecasting-model
[11] https://www.cmascenter.org/smoke/
[12] https://www.epa.gov/moves
[13] http://www.camx.com/

- It should have received scientific peer review: All the models considered have been published in hundreds of peer-review journal articles. CAMx has been subject to its own peer-review reports and an assessment by EPA that it is suitable for ozone SIP modeling (EPA, 2018a).
- It should be appropriate for the specific application on a theoretical basis: The WRF model was designed to simulate time varying three-dimensional meteorological fields and provides all the meteorological information necessary for ozone modeling. The SMOKE, MOVES and BEIS models provide the hourly gridded speciated emissions information required for ozone modeling. CAMx was designed to include all the processes necessary to simulate ozone formation in the troposphere over multiple scales.
- It should be used with data bases which are available and adequate to support its application: The procedures outlined to develop the 2016 CCNAA modeling platform, as described in later sections, rely on data bases that were purposely developed, or are otherwise entirely adequate, to support the meteorological, emission and photochemical model applications.
- It should be shown to have performed well in past modeling applications: The WRF/SMOKE/CAMx modeling system has a demonstrated record of simulating ozone air quality nationally (EPA platforms), throughout the western US (WRAP platforms), within western US nonattainment areas (Texas, Colorado, Utah, New Mexico, Arizona), and has been applied previously by Clark County.
- It should be applied consistently with an established protocol on methods and procedures: The WRF/SMOKE/CAMx application methodology follows the established procedures in EPA (2018a) guidance and all past modeling applications described above.
- It should have a user's guide and technical description: Each of the models cited include technical descriptions developed by the model authors and procedures for application (see websites in footnotes). CAMx includes an up-to-date and comprehensive user's guide (Ramboll, 2022b) that has a detailed technical description and procedures for application.
- The availability of advanced features (e.g., probing tools or science algorithms) is desirable: CAMx includes advanced Probing Tool features, including Ozone Source Apportionment Technology (OSAT), Decoupled Direct Method (DDM) of sensitivity analysis, Process Analysis (PA), and Reactive Tracers (RTRAC), in addition to advanced core model features (e.g., most up-to-date Carbon Bond photochemistry, and a Plume-in-Grid module).
- When other criteria are satisfied, resource considerations may be important and are a legitimate concern: CAMx is more flexible and computationally efficient than CMAQ, allows two-way nesting, and supports both Message Passing Interface (MPI) and Open Message Passing (OMP) parallel processing.

3.0 EPISODE SELECTION

The CCNAA attainment demonstration modeled May through August 2016 as the "base year" because that period adequately represents recent high ozone conditions in the basin and established 2016 modeling datasets developed and vetted by EPA were readily available. The summer of 2016 was fairly typical of climatology, wildfire activity was present but perhaps not as impactful as more recent years, and routine monitoring data exist for the period. The May-August 2016 satisfied EPA (2018a) ozone modeling guidance for selecting modeling episodes for attainment demonstrations.

3.1 EPA Episode Selection Criteria

EPA's ozone SIP modeling guidance recommends the following criteria, at a minimum, for selecting modeling periods (EPA, 2018a, page 19):

1) Model time periods that are close to the most recently compiled and quality assured NEI.
2) Model time periods when observed concentrations are close to the appropriate base year DV and ensure there are enough days so that the modeled attainment test applied at each monitor is based on multiple days.
3) Model time periods both before and following elevated pollution concentration episodes to ensure the modeling system appropriately characterizes low pollution periods, development of elevated periods, and transition back to low pollution periods through synoptic cycles.
4) Simulate a variety of meteorological conditions conducive to elevated pollutant concentrations and poor air quality.

Items 3 and 4 relate to modeling many "episodes" (i.e., multi-day periods) representing the evolution of diverse meteorological conditions, and thus potentially different source types/regions, that lead to exceedances of the ozone NAAQS in the study area. Consequently, the guidance emphasizes modeling an entire summer ozone season to capture meteorological and emissions variability and to include enough high ozone days for the attainment test. This is now common practice in other ozone nonattainment areas in the western US: e.g., Denver (Ramboll, 2019, 2022c), Phoenix (Maricopa Association of Governments, 2016), and Salt Lake City (in preparation). This approach was also adopted for CCNAA modeling.

Below we further address items 1 and 2 of EPA's episode selection criteria in more detail with respect to supporting the justification for summer 2016 as the CCNAA modeled base year.

3.1.1 National Emissions Inventory and Other Supporting Data

EPA generates comprehensive US emission inventories every 3 years (e.g., 2014, 2017, 2020, etc.), but occasionally develops inventories of the same quality for intermediate years as needed (such as for the 2016 MP). Therefore, selecting a base modeling year that aligns with national inventories was prudent, but other factors were considered including the availability of observed ambient air quality data, meteorology, special study data, and existing model-ready datasets.

The 2017 NEI was most recently updated in January 2021 (EPA, 2021c), while the 2016v2 MP is somewhat more recent (EPA, 2022b) and largely based on the 2017 NEI, but it includes some important updates such as a new VCP VOC inventory. The 2016v2 has been designed for studies focused on criteria air pollutants, includes future year projections for 2023, and has been vetted and applied for EPA's current national modeling studies. Routine air quality and meteorological data are available for both 2016 and 2017 years, so the choice of base year is not dependent on routine data. Special study data are available from the 2017 FAST-LVOS (Langford, 2022; Zhang et al., 2020), which could provide ancillary information for the PGM performance evaluation. Most importantly,

given the schedule to complete modeling analyses in time for the ozone SIP submittal in 2023, the 2016v2 MP provided a complete set of US and North American model-ready inputs for the summer of 2016, emissions projections for 2023, and a robust foundational database from which to develop inputs for the local Clark County modeling domain.

3.1.2 Observations Consistent with Base Year DVs

The 2016 ozone season is included within the 3-year DV period (2015-2017) that was used to designate the CCNAA as Marginal under the 2015 ozone NAAQS. From Figure 1-1 (Section 1), the CCNAA DV has not changed much since the 2017 DV of 74 ppb, ranging from 73 ppb to 76 ppb including 74 ppb for the 2020 DV (the Marginal attainment year) and 73 ppb for the 2021 DV. Variations are attributed to interannual meteorological variability, effects from suppressed activity due to COVID-19, and the recent drought-induced increase in massive and prolonged western US wildfires that have been shown to affect ozone levels in the LVV (e.g., Sonoma Technology, 2021, 2023).

Table 3-1 lists MDA8 ozone concentrations recorded each day at each monitoring site operating within Clark County during May through September 2016. Exceedances of the ozone standard occurred on the following 23 days, along with peak MDA8 ozone, number of exceeding sites, and a preliminary assessment of the cause of each exceedance:

- May 14: 72 ppb Single exceedance at SM Youth Camp, not official site
- May 20: 79 ppb Single exceedance at SM Youth Camp, not official site
- June 3: 71 ppb (1 site) Local production
- June 6: 73 ppb (1 site) Local production, transport from southern California
- June 7: 77 ppb (1 site) Local production, transport from southern California
- June 8: 74 ppb (1 site) Local production, transport from southern California
- June 14: 71 ppb Single exceedance at SM Youth Camp, not official site
- June 23: 72 ppb (1 site) Local production
- June 24: 84 ppb (9 sites) Southern California wildfire influence
- June 25: 73 ppb (1 site) Southern California wildfire influence
- June 27: 74 ppb (3 sites) Southern California wildfire influence
- July 1: 75 ppb (3 sites) Local production with high humidity
- July 2: 73 ppb (2 sites) Local production with high humidity
- July 13: 71 ppb (1 site) Local production, transport from southern California
- July 24: 71 ppb (1 site) Southern California wildfire influence
- July 25: 73 ppb (1 site) Southern California wildfire influence
- July 26: 77 ppb (1 site) Southern California wildfire influence
- July 27: 83 ppb (5 sites) Southern California wildfire influence
- July 28: 72 ppb (3 sites) Southern California wildfire influence
- July 29: 75 ppb (2 sites) Southern California wildfire influence
- August 23: 71 ppb (1 site) Southern California wildfire influence
- August 24: 80 ppb (6 sites) Southern California wildfire influence
- August 25: 73 ppb Single exceedance at SM Youth Camp, not official site

The maximum MDA8 ozone on these exceedance days ranged from 71 to 84 ppb, with an average of 75 ppb. No exceedance days occurred during September when ozone concentrations exceeded 55 ppb on only 9 days. Therefore, September was not included in the modeling period. Clark County did not file any exceptional event demonstrations to EPA for the year 2016. The largest number of exceedance days in 2016 occurred at the Joe Neal monitoring site, located northwest of the City of North Las Vegas.

Table 3-1. MDA8 ozone concentrations recorded each day at each monitoring site operating within Clark County during the May-September 2016 ozone season. Values highlighted in orange exceed the 70 ppb ozone standard, and values shaded in yellow are within the 55 to 70 ppb range. The site labelled "SM Youth Camp" is not an official AQS monitoring site.

Monitoring Site	May 2016																													
	1	2	3	4	5	6	7	8	9	10	11	12	13	14	15	16	17	18	19	20	21	22	23	24	25	26	27	28	29	30	31
Apex	48	50	56	62	51	51	48	57	56	60	51	57	61	57	60	49	51	46	61	67	59	55	59	54	60	60	61	64	66	60	52
Mesquite	43	47	47	55	46	51	47	50	51	50	48	50	53	42	55	44	40	45	58	56	55	50	56	52	50	55	49	54	57	53	45
Paul Meyer	51	52	57	59	49	47	47	51	51	63	55	60	61	59	56	49	52	45	61	64	52	53	56	51	60	55	53	63	60	65	51
Walter Johnson	49	51	57	58	48	48	47	50	51	65	53	60	61	59	57	48	52	44	60	64	51	52	57	51	60	55	56	64	64	65	52
Palo Verde	45	49	55	56	48	46	45	49	51	62	50	58	58	61	55	46	47	41	61	64	50	50	57	50	60	50	51	63	62	62	50
Joe Neal	48	51	58	61	50	50	53	52	54	67	53	64	62	58	55	49	54	44	62	65	53	51	59	51	62	55	61	66	68	63	52
Green Valley	46	48	52	57	50	42	47	50	50	58	49	57	56	56	55	49	48	46	59	61	52	54	57	52	58	59	54	62	61	62	57
Jerome Mack	49	50	54	58	49	46	48	52	51	62	50	61	57	53	58	48	50	46	59	62	53	56	57	NV	57	59	58	63	63	63	57
Boulder City	46	48	53	57	47	46	48	52	52	57	49	56	55	55	56	52	54	45	58	62	59	52	57	53	57	61	53	60	57	58	51
Jean	52	53	57	57	49	49	51	52	53	58	58	58	58	57	53	48	54	48	62	65	53	48	58	53	59	56	52	62	61	62	60
JD Smith	49	50	55	58	49	46	49	51	51	63	51	61	59	55	58	47	51	44	60	64	54	55	57	50	58	57	60	64	65	64	54
SM Youth Camp	50	53	60	61	56	51	52	52	55	NV	50	65	68	72	57	49	49	47	62	79	61	50	59	56	62	50	54	64	65	59	52
Indian Springs	44	48	54	60	49	50	49	51	49	50	47	57	62	57	51	48	51	39	59	68	51	44	57	51	63	46	51	61	64	54	46
Maximum Value	52	53	58	62	51	51	53	57	56	67	58	64	62	61	60	52	54	48	62	68	59	56	59	54	63	61	61	66	68	65	60

Monitoring Site	June 2016																													
	1	2	3	4	5	6	7	8	9	10	11	12	13	14	15	16	17	18	19	20	21	22	23	24	25	26	27	28	29	30
Apex	54	62	67	59	65	66	66	61	49	41	50	43	55	63	58	57	54	58	57	59	62	58	65	84	64	66	57	55	66	51
Mesquite	NA	NA	NA	NA	NA	56	58	58	51	43	42	40	47	55	56	48	43	51	45	44	52	50	55	71	56	54	48	51	53	53
Paul Meyer	59	64	67	64	63	64	69	68	51	51	53	39	47	62	50	55	48	52	56	60	62	58	64	73	68	67	70	63	64	48
Walter Johnson	54	63	66	63	62	65	70	68	47	52	52	40	47	62	52	57	47	53	60	60	62	58	66	73	69	67	71	60	65	51
Palo Verde	53	60	67	65	62	64	69	70	49	50	50	39	49	66	49	57	49	50	56	58	59	56	63	71	67	66	72	58	62	51
Joe Neal	54	65	71	65	68	73	77	74	48	52	52	42	49	62	52	59	47	55	62	61	64	64	72	83	73	70	74	58	68	56
Green Valley	61	60	63	59	68	64	68	66	49	45	47	42	48	61	54	57	56	50	57	56	57	57	62	73	66	65	62	58	66	50
Jerome Mack	58	62	63	58	68	67	67	64	50	47	48	41	49	59	50	53	52	54	57	58	57	58	64	77	67	63	61	56	67	50
Boulder City	58	53	59	53	60	60	62	58	44	41	44	39	49	55	58	48	52	56	49	56	53	54	59	68	59	58	55	55	59	55
Jean	52	57	63	59	63	62	64	65	54	50	44	38	46	62	50	55	51	48	45	51	57	58	60	68	63	62	65	59	60	54
JD Smith	55	63	66	61	68	70	70	67	55	50	51	41	48	62	53	54	50	54	58	60	59	60	65	78	70	66	65	58	67	51
SM Youth Camp	49	59	72	64	61	61	67	64	46	47	47	42	54	71	53	53	49	52	52	54	59	54	60	70	69	65	69	53	58	57
Indian Springs	48	53	56	61	61	59	55	67	44	49	44	42	44	65	44	56	51	54	46	50	55	58	67	68	58	63	61	52	55	57
Maximum Value	61	65	71	65	68	73	77	74	54	52	53	43	55	66	58	59	56	58	62	61	64	64	72	84	73	70	74	63	68	57

Monitoring Site	July 2016																													
	1	2	3	4	5	6	7	8	9	10	11	12	13	14	15	16	17	18	19	20	21	22	23	24	25	26	27	28	29	30	31
Apex	64	64	57	56	66	65	61	63	57	57	56	68	69	65	64	68	59	NV	52	51	52	63	61	48	65	63	62	67	64	60	56
Mesquite	53	57	49	47	51	58	54	50	54	55	49	56	58	49	NV	57	48	39	42	42	43	49	54	55	56	52	53	54	53	55	52
Paul Meyer	70	69	54	53	63	61	66	58	51	56	58	59	65	65	66	66	60	46	44	44	52	NA	NA	NA	NA	NV	76	63	75	59	55
Walter Johnson	74	71	57	52	61	58	66	57	51	56	59	NV	66	67	62	64	62	44	44	45	54	53	67	69	65	69	77	70	71	59	56
Palo Verde	73	70	53	52	62	58	63	55	53	49	57	59	68	66	62	64	59	49	46	43	54	53	64	69	67	68	74	65	67	54	54
Joe Neal	75	73	59	54	62	58	70	60	50	55	66	63	71	70	67	66	60	47	46	48	58	60	69	71	69	77	83	72	69	62	58
Green Valley	63	61	53	52	64	61	61	62	53	59	52	64	60	59	64	65	62	49	48	45	NV	NV	64	57	63	57	64	67	63	57	55
Jerome Mack	NV	63	56	54	63	61	66	63	52	54	56	64	64	62	63	65	62	50	50	49	54	59	67	61	65	64	69	71	67	57	55
Boulder City	59	57	45	52	56	58	51	53	55	60	53	63	58	58	60	60	53	38	44	43	47	54	55	42	57	52	55	55	60	58	54
Jean	59	59	51	52	63	63	63	59	50	59	54	NV	63	65	66	65	61	49	49	45	47	53	60	68	64	57	58	59	61	57	58
JD Smith	67	65	56	53	62	60	67	62	51	56	NV	61	66	63	62	63	60	49	47	47	54	55	66	64	65	66	75	73	70	57	55
SM Youth Camp	57	61	52	57	55	NV	65	59	50	55	59	61	65	66	63	65	62	51	50	48	50	52	61	67	69	69	64	58	61	57	60
Indian Springs	66	62	51	53	59	60	65	56	49	55	39	62	69	67	63	61	53	46	47	49	54	50	57	69	73	58	61	56	55	53	55
Maximum Value	75	73	59	56	66	65	70	63	57	60	66	68	71	70	67	68	62	50	52	51	58	63	69	71	73	77	83	72	75	62	58

Table 3-1 (concluded).

Monitoring Site	August 2016																													
	1	2	3	4	5	6	7	8	9	10	11	12	13	14	15	16	17	18	19	20	21	22	23	24	25	26	27	28	29	30	31
Apex	54	57	NA	NA	NV	42	58	62	53	49	50	60	58	59	55	63	58	54	61	61	50	55	57	68	67	44	50	50	50	47	52
Mesquite	51	56	47	55	58	40	46	55	45	36	43	48	52	NA	NV	41	38	39	40	40	40	38	39	43	44	34	35	36	34	32	37
Paul Meyer	55	61	49	55	63	49	58	57	60	59	54	62	70	62	53	64	57	54	53	60	50	58	66	71	68	47	57	64	66	55	53
Walter Johnson	56	63	53	54	65	48	58	57	60	56	52	66	70	63	53	64	59	54	54	64	52	59	56	76	67	49	57	64	63	53	53
Palo Verde	56	65	54	56	65	49	58	57	60	63	55	65	68	63	53	65	62	54	55	64	53	60	67	73	66	48	56	64	60	51	52
Joe Neal	60	65	57	59	67	51	60	59	61	54	55	65	67	64	53	65	63	59	57	68	54	64	71	80	67	52	56	55	61	53	56
Green Valley	50	54	NV	50	59	44	56	58	54	50	49	60	62	61	52	61	56	50	52	57	50	53	60	69	64	46	51	50	54	49	50
Jerome Mack	50	57	47	54	62	44	58	60	57	48	51	67	65	62	54	64	59	53	58	62	52	55	61	75	67	46	53	53	59	51	53
Boulder City	47	54	49	56	59	41	53	57	47	39	40	56	57	55	54	60	53	49	54	54	49	53	60	64	59	47	52	50	50	50	49
Jean	50	51	51	61	59	46	57	58	59	52	54	49	58	57	56	NA	NA	NV	53	58	51	55	57	60	66	47	51	54	50	47	52
JD Smith	51	57	48	52	62	45	57	59	57	48	52	66	64	61	51	62	58	53	56	63	52	57	62	79	63	46	53	53	57	49	54
SM Youth Camp	61	59	55	60	62	57	59	63	66	63	62	57	65	62	63	66	68	59	57	59	53	55	57	67	73	66	57	55	55	53	59
Indian Springs	61	58	54	56	65	52	57	58	61	58	57	54	52	56	57	64	59	55	52	57	53	58	65	55	66	56	57	51	46	48	53
Maximum Value	61	65	57	61	67	52	60	62	61	63	57	67	70	64	57	65	63	59	61	68	54	64	71	80	68	56	57	64	66	55	56

Monitoring Site	September 2016																													
	1	2	3	4	5	6	7	8	9	10	11	12	13	14	15	16	17	18	19	20	21	22	23	24	25	26	27	28	29	30
Apex	50	46	49	47	47	59	45	53	51	44	49	58	48	51	46	45	48	49	44	31	32	49	41	41	46	46	45	41	45	45
Mesquite	35	31	34	34	30	38	29	35	34	31	35	39	33	33	34	33	34	34	30	24	21	34	29	29	34	33	33	29	29	28
Paul Meyer	53	49	47	49	54	58	43	59	63	51	45	55	46	52	51	51	55	51	44	33	35	48	41	41	46	47	46	52	52	56
Walter Johnson	53	49	46	50	55	59	44	60	67	54	48	56	47	56	53	51	54	52	45	33	36	48	40	42	46	47	48	50	49	50
Palo Verde	51	49	49	52	54	56	46	59	64	49	50	57	47	53	51	48	53	53	46	32	34	47	40	43	46	46	47	48	46	49
Joe Neal	55	50	46	50	55	62	50	64	63	56	48	56	46	56	53	52	54	57	48	34	37	48	40	41	46	48	47	50	52	53
Green Valley	47	46	49	47	51	57	38	55	58	48	47	55	48	52	48	46	51	52	40	31	31	47	40	40	45	42	44	48	47	46
Jerome Mack	50	50	48	47	51	58	41	57	59	49	48	56	47	54	52	49	53	52	42	32	32	47	40	42	46	45	46	49	47	48
Boulder City	46	43	48	47	50	56	38	50	55	44	48	53	48	50	48	45	48	48	39	32	31	NA	NA	40	45	45	43	46	45	43
Jean	53	50	49	50	52	58	39	55	63	43	46	58	49	50	50	50	49	45	41	35	38	48	38	44	47	49	46	45	48	52
JD Smith	52	51	47	48	52	60	43	59	60	52	48	54	47	55	52	48	53	53	44	32	34	47	38	43	46	46	46	49	49	49
SM Youth Camp	56	54	54	55	58	60	59	68	62	52	61	62	58	46	47	47	49	59	47	38	51	52	50	48	48	50	49	53	55	60
Indian Springs	53	46	48	47	54	61	55	55	45	44	46	58	48	44	42	41	44	46	48	37	41	49	40	39	42	43	46	46	49	53
Maximum Value	55	50	49	52	55	62	55	64	67	56	50	58	49	56	53	52	55	57	48	37	41	49	41	44	47	49	48	52	52	56

3.1.3 Additional Rationale for Selecting 2016 as the Base Year

The choice to model 2016 satisfied all of the criteria listed in EPA's modeling guidance, most importantly:

1. The average MDA8 ozone over 2016 exceedance days (75 ppb) was close to the 2015-2017 DV (74 ppb) used to classify Clark County as a Marginal NAA, and to the 2018-2020 DV (also 74 ppb) that resulted in the reclassification to Moderate;
2. EPA-vetted emission inventories and modeling datasets were readily available – it was critically important to leverage existing datasets as much as possible given the very tight schedule for the ozone SIP.

There were other reasons why more recent years were not especially suited to represent the base year. Figure 3-1 shows time series of MDA8 ozone at Joe Neal spanning the years 2015 through 2020. There were 17 exceedance days at this site in 2016, although the three highest exceedances were influenced by regional wildfires. There were 13 exceedance days at this site in 2017, 10 in 2018, 1 in 2019, and 9 in 2020. Therefore, 2016 contained the largest number of exceedance days at the peak monitoring site, while 2017 contained the second most. With consistent DVs year-to-year, choosing a different modeled base year should not materially affect the 2023 DV projection.

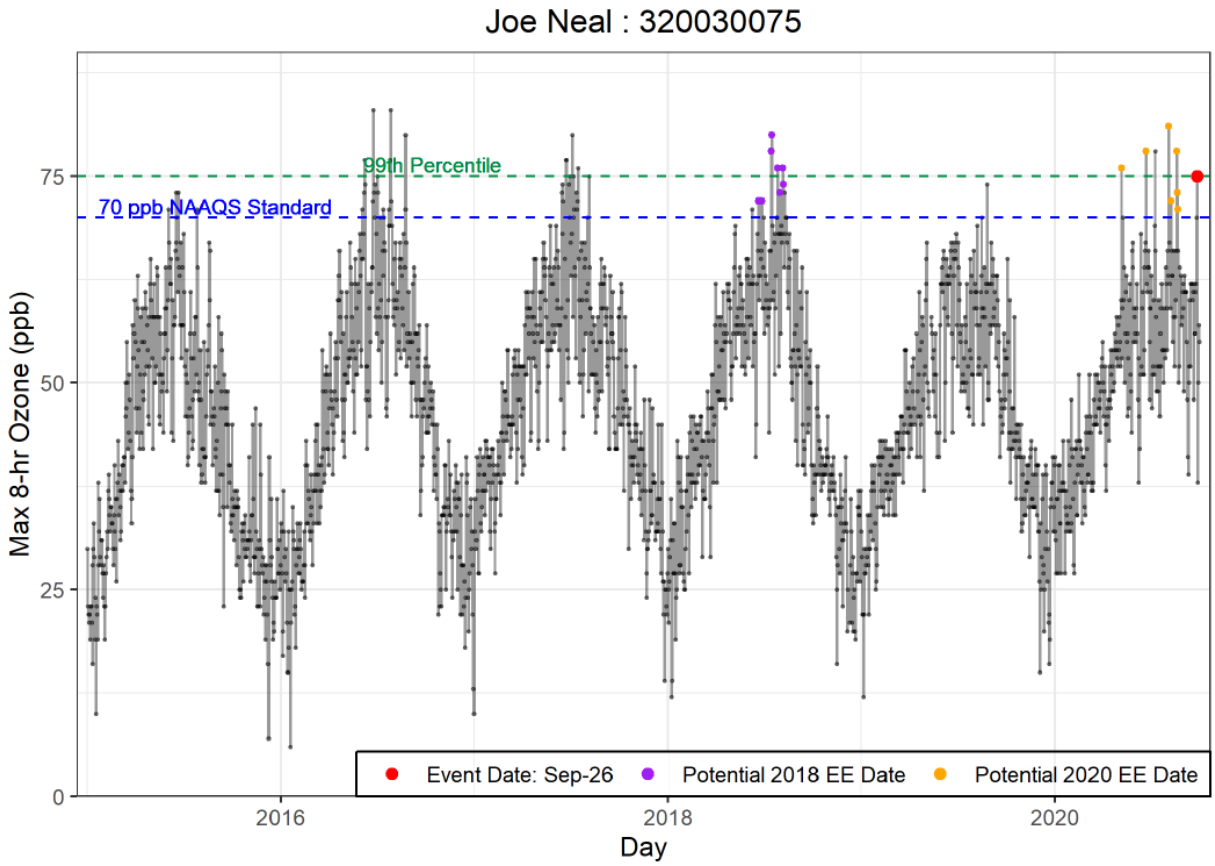

Figure 3-1. Time series of MDA8 ozone at the Joe Neal monitoring site from 2015 through 2020 (figure taken from Sonoma Technology, 2021).

Probably the biggest disadvantage of adopting a more recent year since 2017 was the dramatic increase in exceptional event-like days. Most exceedance days in 2018 and 2020 were associated with plausible wildfire exceptional events, as highlighted in Figure 3-1 (Sonoma Technology, 2021). It is important to maximize the number of high ozone days in the SIP modeling that result from local and regional anthropogenic emissions rather than wildfires. From 2017 through 2021 the western US has burned nearly continuously during the ozone season, and it is increasingly difficult to identify a period when poor air quality in Clark County is not influenced by massive regional fires. While there were potential fire influences on many ozone exceedance days in 2016, more days are believed to be influenced by "typical" local and/or regional anthropogenic emissions than in recent years.

3.2 Analysis of Regional Meteorological and Air Quality Conditions

We analyzed meteorology and air quality over the western US to evaluate the suitability of the 2016 ozone season for modeling by ensuring it represents typical conditions. The following summary is taken from the Denver ozone modeling protocol (Ramboll, 2019); see Appendix A of that document for additional details from Ramboll's extensive analysis. Our findings should be considered in the context of larger climate change trends and their influences on the current western US "mega-drought".

The Regional Technical Operations Working Group (RTOWG) of the Western Regional Air Partnership (WRAP) evaluated the representativeness of several recent years (2014, 2015 and 2016) for their

updated annual western regional photochemical modeling platform (Stoeckenius et al., 2018). Ramboll (2019) extended the analysis to include 2017. The RTOWG study noted that for regional air quality planning:

"As significant resources are required to develop and exercise an annual air quality modeling platform for analysis of the issues of concern (primarily ground-level ozone, particulate matter, regional haze, and nitrogen deposition), it is important to establish the "degree of representativeness", or the degree of difference between calendar base year(s) selected for simulation and analysis….the objective of this study is to compare and contrast the key characteristics of each year analyzed both with respect to each other and with respect to long-term averages"

The key characteristics analyzed included: meteorology (e.g., 500 hPa heights, hydrology, surface temperatures); wildfires; emissions (EGUs and on-road); and air quality (visibility, nitrogen deposition, ozone, and PM). The RTOWG study considered a large area of interest covering the entire western US.

Seasonal and regional variations led Stoeckenius et al. (2018) to conclude that each year exhibits its own unique features. For certain key characteristics analyzed, specific years were shown to exhibit specific issues. For example, 2015 exhibited severe drought conditions west of Rockies and significant fire activity in western Canada and northwest US that impacted regional air quality. Moreover, a significant increase in 2017 wildfires resulted in even larger impacts on air quality throughout the western US. The number of acres burned by western US wildfires in 2016 was approximately half that of 2017 and slightly less than 2015.

For many other characteristics, however, neither 2016 nor 2017 exhibited particularly anomalous conditions. Nevada state-wide precipitation was slightly above average for the 12 months ending August 2016, whereas it was much above average for the 12-month period ending in August 2017. Nevada June-August 2016 average temperatures were much above average, which was weighted by the warmest temperatures in June while above average temperatures occurred during July and August. In contrast, June-August 2017 average temperatures were classified as "record warmest." Between May and September 2016, the Palmer drought index fluctuated between neutral (3 months) and moderate (2 months) in southern Nevada. The drought index remained neutral throughout summer 2017.

3.3 Future Year to be Modeled

The CCNAA is currently classified as a Moderate Nonattainment Area under the 2015 ozone NAAQS because 2018-2020 ozone DVs failed to attain the standard by the August 3, 2021 attainment date for Marginal areas (Figures 1-1 and 1-3). Moderate areas must attain the NAAQS by August 3, 2024 based on the 2021-2023 DV, or risk further bump-up to Serious. Thus, attainment demonstration modeling was conducted for the 2023 future year. The 2016v2 MP includes projected national emission inventories for the 2023 year. Following EPA (2018a) guidance, CAMx modeling of May-August 2023 included the projected emissions but continued to use all other model inputs (meteorology, boundary conditions, etc.) from the 2016 base year to isolate the impacts from emission changes. Details on future year modeling procedures are presented in other sections of this report.

4.0 MODELING DOMAIN

This section describes the modeling domain and defines the PGM horizontal and vertical grid structures for the CCNAA ozone attainment demonstration modeling. Details include the map projection, domain coverage, grid resolution and grid nesting arrangement.

4.1 Horizontal Grids

The CCNAA attainment demonstration modeling employed the same nested 36/12 km grids as the EPA 2016 MP (36US3, 12US2). A third grid with 4 km grid resolution covering Clark County (CC4c2) was nested within the 12US2 grid. Figure 4-1 displays the 36US3/12US2/CC4c2 domain structure and Figure 4-2 shows the coverage of the CC4c2 grid in greater detail. The cartesian modeling domain is defined on a Lambert Conic Conformal map projection based on the parameters listed in Table 4-1. Specific coordinate and resolution information about each grid is listed in Table 4-2.

Table 4-1. Map projection parameters for the CCNAA 36US3/12US2/CC4c2 modeling domain.

Parameter	Value
Map Projection	Lambert Conic Conformal Perfect sphere, diameter 6370 km
True Latitude 1	33°N
True Latitude 2	45°N
Central Longitude	97°W
Central Latitude	40°N

Table 4-2. Coordinate and resolution parameters for each of the CCNAA modeling grids.

Parameter	36US3	12US2	CC4c2
Grid Cell Size	36 km	12 km	4 km
Total Grid Cells	172 x 148	396 x 246	50 x 62 (w/ buffer) 48 x 60 (no buffer)
SW Corner (km)	-2952, -2772	-2412, -1620	-1696, -412 (w/ buffer) -1692, -408 (no buffer)
NE Corner (km)	3240, 2556	2320, 1332	-1496, -164 (w/ buffer) -1500, -168 (no buffer)
Parent Grid X-Range	N/A	N/A (1-way nested in 36US3)	61 – 76 (in 12US2)
Parent Grid Y-Range	N/A	N/A (1-way nested in 36US3)	102 – 121 (in 12US2)
WRFCAMx I/J Offset	N/A	N/A	183, 87

The CC4c2 grid employed a horizontal resolution that EPA recommends for urban-scale PGM applications so that local influences and details in emissions, chemistry and transport throughout the basin are appropriately resolved. The 12US2 grid provides an adequate mid-level resolution to account for regional sources and transport into Clark County, particularly from California, northern Mexico and neighboring states. The 36US3 grid covers a larger expanse of Canada, Mexico, and the Pacific Ocean, and provides the mechanism by which domain BCs quantify pollutant influx into North America from around the globe.

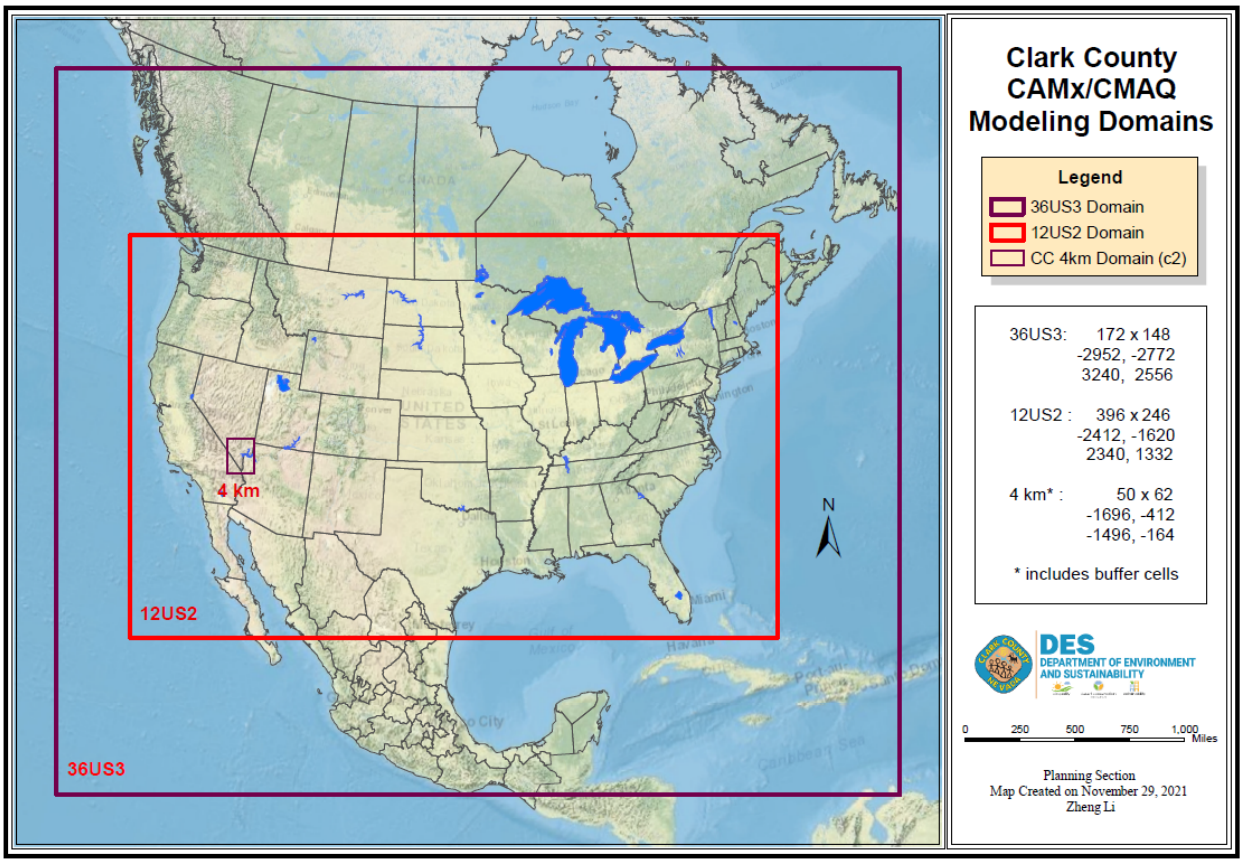

Figure 4-1. PGM nested modeling grids employed for the Clark County ozone attainment demonstration. Details on grid coordinates and number of grid cells are shown in the right inset.

For all CAMx applications, including base year model performance, sensitivity testing, and future year emission reduction scenarios, the 12US2/CC4c2 grids were run together using two-way interactive grid nesting. In initial 2016 base year runs, 12US2 BCs were taken from the 2016v2 MP, which in turn were based on EPA's 2016 CAMx run on the 36US3 grid. EPA developed global BC inputs for the 36US3 grid from their 2016 hemispheric CMAQ simulations (EPA, 2022a). In later and final 2016 base year runs, we derived a new set of 36US3 BCs from an alternative source of global modeling, re-ran the 36US3 grid in CAMx, and extracted new 12US2 BCs for the 12/4 nested runs. Details on the source of global BCs and modeling procedures are provided in Sections 7.4 and 8.4.

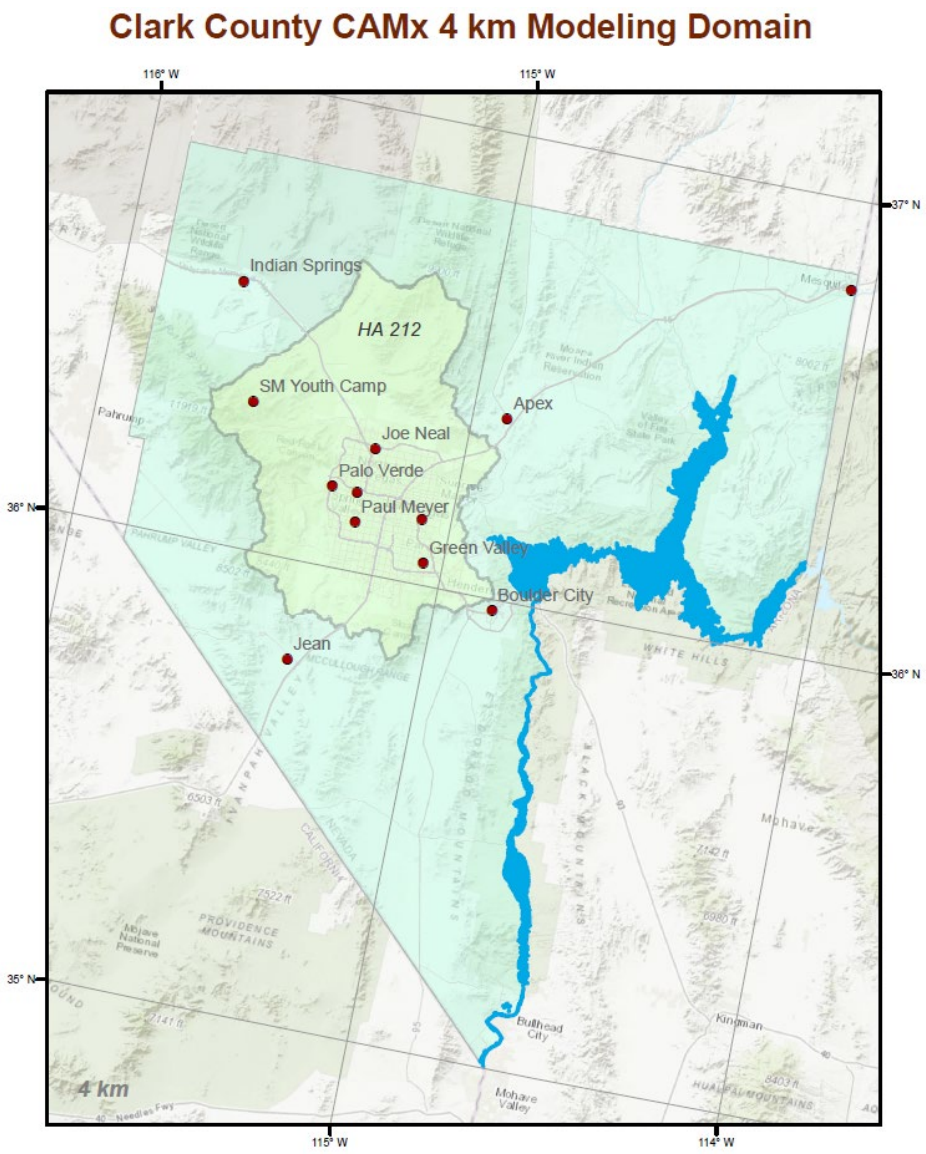

Figure 4-2. Extent of the 4 km Clark County PGM nested modeling grid (CC4c2) employed for the Clark County ozone attainment demonstration. Clark County is shaded in green while the extent of the CCNAA (labeled HA 212) comprises a smaller area of the County. The locations of 12 ozone monitoring sites are also shown for reference.

4.2 Vertical Grid Structure

The vertical grid structure used for CCNAA modeling was entirely defined by the three-dimensional datasets developed for the EPA 2016v2 MP, which in turn was based on EPA's WRF simulations developed to drive the PGM system. The WRF vertical grid comprises 35 layers extending from the surface to ~20 km (50 mb pressure altitude), as shown in Table 4-3. To remain consistent with EPA's grid system, CCNAA modeling maintained the full 35 layer structure for CAMx. The layer structure includes a 20 m deep surface layer, four layers through the lowest 100 m, 14 layers through the lowest 1000 m, and 31 layers within the troposphere (~10 km).

Table 4-3. Vertical grid structure for the EPA 2016 MP.

EPA WRF/CAMx			
Layer	**eta**	**Pressure (mb)**	**Height (m)**
35	0.00	50	20576
34	0.05	98	16297
33	0.10	146	13766
32	0.15	194	11961
31	0.20	243	10555
30	0.25	291	9372
29	0.30	339	8337
28	0.35	387	7416
27	0.40	435	6583
26	0.45	483	5822
25	0.50	532	5120
24	0.55	580	4467
23	0.60	628	3857
22	0.65	676	3284
21	0.70	724	2743
20	0.74	763	2331
19	0.77	792	2033
18	0.80	821	1744
17	0.82	840	1555
16	0.84	859	1370
15	0.86	878	1188
14	0.88	898	1010
13	0.90	917	835
12	0.91	927	748
11	0.92	936	662
10	0.93	946	577
9	0.94	955	493
8	0.95	965	409
7	0.96	975	326
6	0.97	984	243
5	0.98	994	162
4	0.985	999	121
3	0.990	1004	81
2	0.995	1008	40
1	0.9975	1011	20
0	1.0000	1013	0

5.0 BASE YEAR METEOROLOGICAL INPUTS

Ramboll utilized existing CAMx-ready meteorological modeling datasets for the 36US3 and 12US2 grids developed by EPA for their 2016 MP (EPA, 2019). Here, we describe the meteorological modeling and performance assessment for the nested CC4c2 domain covering Clark County as defined in Section 4.

Meteorological inputs for the CC4c2 domain were developed primarily from 2016 WRF simulations recently conducted by EPA on a large grid with 4 km grid spacing covering California and most of Nevada including Clark County (Figure 5-1). EPA applied the same science configuration, inputs, and application methodology as their 12US2 WRFv3.8 simulations that support their 2016 MP (EPA, 2019). The vertical grid structure for the California/Nevada WRF domain is identical to the 2016 MP (Table 4-3) and the horizontal grid aligns with the 12US2 grid with sufficient extent to fully include the CC4c2 CAMx grid. The eastern edge of the WRF grid is 24 km from the eastern edge of the CC4c2 grid, which is beyond the recommended 5 grid point buffer recommended in EPA's guidance. Furthermore, EPA used their 12US2 WRF output to drive WRF 4 km boundary conditions (a process referred to as "nest-down"), which maximizes consistency among wind and mass fields thereby reducing numerical artifacts at the boundaries. Details on the EPA WRF configuration are listed in Table 5-1.

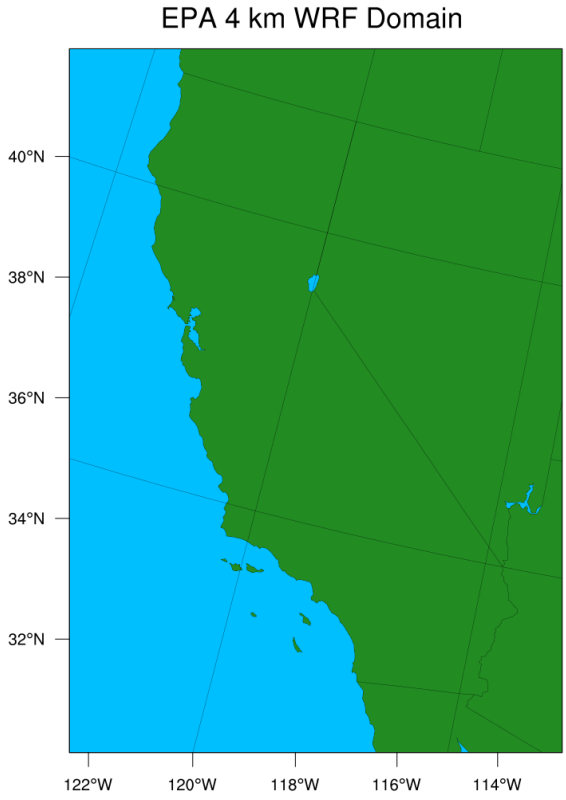

Figure 5-1. Extent of the EPA 4 km WRF domain covering California and Nevada. The domain meshes with the 2016 MP 12US2 grid and sufficiently covers the area of the CC4c2 grid.

Table 5-1. WRF configurations for the EPA and Ramboll 4 km California/Nevada meteorological modeling. The EPA configuration is taken from the 2016 MP 12US grid application. Ramboll's deviations from EPA's configuration are highlighted in red.

Model Component	EPA	Ramboll
Model Code	WRF v3.8	WRF v4.4
Modeling Period	January 1 – December 31, 2016	June 29 – July 4, 2016
Application	Continuous 365 day run	Single 5-day segment
Horizontal Grid		
Map Projection	Lambert Conic Conformal	Lambert Conic Conformal
Projection Center	-97°N / 40°W	-97°N / 40°W
True Latitudes	33°N and 45°N	33°N and 45°N
Grid Points	237 x 339	237 x 339
SW Corner coordinate	-2424, -756	-2424, -756
NE Corner coordinate	-1476, 600	-1476, 600
Vertical Grid		
Layers	35 up to 50 mb (~20 km)	35 up to 50 mb (~20 km)
Coordinate	Sigma (normalized pressure)	Sigma (normalized pressure)
Initial/Boundary Conditions	Nest-down from EPA 12US2 output	12 km North American Model (NAM)
Nudging Analyses	12 km North American Model (NAM)	12 km North American Model (NAM)
Landcover	40-category National Landcover Dataset (NLCD)	40-category National Landcover Dataset (NLCD)
Sea Surface Temperature	1 km Group for High Resolution Sea Surface Temperatures (GHRSST)	0.1 degree Fleet Numerical Meteorology and Oceanography Center Sea Surface Temperatures (FNMOC SST)
Lightning Data	National Lightning Detection Network (NLDN)	None
Physics		
Short/Longwave Radiation	Rapid Radiation Transfer Model - Global (RRTMG)	Rapid Radiation Transfer Model - Global (RRTMG)
Resolved Clouds	Morrison microphysics	Thompson microphysics
Surface Model	Pleim-Xiu (P-X)	Noah
Surface Layer	Pleim-Xiu (P-X)	MM5 Similarity
Boundary Layer	Asymmetric Convective Model (ACM2)	Yonsei University (YSU)
Sub-grid Clouds	Kain-Fritsch	Multiscale Kain-Fritsch or no sub-grid cumulus scheme
Data Assimilation/Nudging		
3-D Wind	$1x10^{-4}$ s^{-1} (above PBL)	$1x10^{-4}$ s^{-1} (all layers)
3-D Temperature	$1x10^{-4}$ s^{-1} (above PBL)	$1x10^{-4}$ s^{-1} (above PBL)
3-D Moisture	$1x10^{-5}$ s^{-1} (above PBL)	$1x10^{-5}$ s^{-1} (above PBL)
Surface Analysis Nudging	None	None
Observation Nudging	None	None
Soil Nudging	P-X temperature & moisture	None
Lightning Assimilation	On (controls deep convection)	None (not available in v4.4)

The Clark County DES/DAQ obtained EPA's WRF output files and ran the Atmospheric Model Evaluation Tool (AMET; EPA, 2022f) to generate a suite of statistical and graphical products from which to evaluate performance in replicating observed conditions. DES/DAQ sent WRF output and AMET results to Ramboll for an initial evaluation to determine if the simulation is suitable for this work. Ramboll stratified statistical performance into groups of surface meteorological stations within Las Vegas, the Mojave Desert, and other areas of Southern California. We also reviewed performance during specific high ozone periods, and qualitatively reviewed performance for the Las Vegas and San Diego radiosonde observation (RAOB) profiles.

From that initial evaluation, Ramboll determined that the EPA WRF run performed well overall, especially in the LVV, meeting statistical benchmarks. However, some larger wind and temperature errors were noted in the LVV during some high ozone periods, and particularly during July 1-2 related to poorly simulated convective activity.

5.1 WRF Modeling of June 29 – July 4, 2016

The July 1-2 period was considered key to ozone modeling as it represents a period believed to involve mostly local ozone production with perhaps some regional transport. As directed by DES/DEQ, Ramboll conducted a short WRF simulation in an attempt to improve overall performance during the July 1-2 high ozone episode. The WRF configuration was based on a simulation recently conducted for WESTAR (Ramboll, 2021a), which in turn was based on the best performing runs (considering convective rainfall) from numerous WRF comparison studies conducted for WRAP and New Mexico over the past few years. Details of the configuration of this run are listed in Table 5-1 for direct comparison to EPA's configuration.

As described below, we assessed EPA's and Ramboll's WRF model performance in more detail against standard routine local and regional observational data. The decision to use the alternative WRF simulation to bridge the July 1-2 period was based on performance comparisons for winds, temperature, humidity, and rainfall patterns. EPA's and Ramboll's WRF 4 km resuls were processed to CAMx-ready inputs on the CC4c2 modeling grid using the WRFCAMx interface program. WRF output was also processed to model-ready inputs for the Community Multiscale Air Quality (CMAQ) model using the Meteorology-Chemistry Interface Processor (MCIP) for processing on-road and biogenic emissions. Those steps are detailed in later Sections of this report.

5.2 Summary of Conclusions from the WRF Evaluation

Ramboll initially determined that the EPA WRF run performed well overall during the summer 2016 season, meeting statistical benchmarks especially in the LVV. The additional analyses described here confirmed that the EPA WRF run was applicable for CAMx photochemical modeling over the majority of the May-August 2016 ozone modeling period, for the following reasons:

- Model performance in replicating surface temperature and wind at meteorological monitoring sites within the LVV was rather good relative to other recent WRF modeling performed in the western US, meeting statistical benchmarks;
- While surface humidity tended to be overstated in EPA's modeling, that particular variable has the least influence on CAMx ozone performance;
- WRF was mostly able to replicate vertical profiles of temperature and humidity rather well, according to Las Vegas RAOB data.

Based on our detailed performance evaluation of the July 1-2 "bridge" run, we recommended supplanting EPA's WRF results with Ramboll's WRF results for the June 30 – July 2, 2016 period for

use in CAMx. In order to reduce the potential for a sudden shift in meteorological parameters on July 1, we recommended using the alternative WRF simulation starting on June 30, a day with lower ozone in the region. Our reasoning for these recommendations include:

- Dramatically improved agreement with observed temperature conditions, both at the surface and in the vertical during the July 1-2 convective period;
- Improved agreement with precipitation patterns based on observations day-by-day;
- Improved agreement with observed humidity early in the episode, although the model exhibited large under predictions later in the period;
- Improved surface winds during certain afternoon hours when spurious convection in EPA's WRF run on July 1 and 2 caused strong downdraft outflows over the LVV.

Temperature performance is critical for CAMx modeling: temperature drives the diurnal evolution of mixing depth and influences temperature-sensitive emissions and chemical rates that drive ozone formation. The removal of spurious convection greatly improved the characterization of temperature and winds influenced by simulated convective downdrafts. In summary, a drier, less cloudy, warmer environment was preferred for photochemical modeling, even if such conditions tended to be somewhat overstated, so that we maximized the potential for generating higher ozone on these important locally-drive ozone exceedance days.

5.3 Model Performance Evaluation Approach

Evaluation of EPA's California/Nevada WRF application and Ramboll's June 30 – July 4 bridge run included quantitative and qualitative methods. Quantitative evaluations statistically compare WRF predictions against surface hourly meteorological observations at multiple sites, matched by time and location. Qualitative evaluations graphically compare time series of modeled wind speed/direction, temperature, and humidity to observations at specific sites, and daily to monthly spatial patterns in precipitation. The evaluation was conducted for meteorological observation sites over southern Nevada and California, with particular focus within the LVV.

Quantitative model performance statistics were calculated using AMET and the publicly-available METSTAT tool (Ramboll, 2022d). Both generate graphical and statistical products to evaluate model performance for surface winds, temperatures, and humidity. The purpose of these evaluations is to establish a first-order acceptance/rejection of the simulation based on adequate replication of the weather phenomena in the study area. Thus, this approach screens for obvious model flaws and errors. Statistical measures include mean observation and prediction, prediction signed error (bias), and prediction unsigned error (absolute or gross error).

Mean observation (Mo) is calculated using values from 1 or many sites over a given period:

$$M_o = \frac{1}{IJ}\sum_{j=1}^{J}\sum_{i=1}^{I} O_j^i$$

where O^i_j is the individual observed quantity at site i and time j, and the summations are over all sites (I) and over time periods (J).

Mean Prediction (Mp) is calculated from simulation results that are interpolated to each observation site used to calculate the mean observation for a given period:

$$M_p = \frac{1}{IJ}\sum_{j=1}^{J}\sum_{i=1}^{I} P_j^i$$

where P^i_j is the individual predicted quantity at site i and time j. Note the predicted mean wind speed and mean resultant direction are derived from the vector-average of the east-west component u and north-south component v that are output by WRF.

Bias (B) is calculated as the mean signed difference in prediction-observation pairings with valid data within a given analysis region and for a given period:

$$B = \frac{1}{IJ}\sum_{j=1}^{J}\sum_{i=1}^{I}\left(P_j^i - O_j^i\right)$$

Gross Error (E) is calculated as the mean absolute difference in prediction-observation pairings with valid data within a given analysis region and for a given period:

$$E = \frac{1}{IJ}\sum_{j=1}^{J}\sum_{i=1}^{I}\left|P_j^i - O_j^i\right|$$

Note that the bias and gross error for winds are calculated from the predicted-observed residuals in speed and direction (not from vector components u and v). The direction error for a given prediction-observation pairing is limited to range from 0 to ±180°.

Root Mean Square Error (RMSE), which is another form of unsigned error, is calculated as the square root of the mean squared difference in prediction-observation pairings with valid data within a given analysis region and for a given period:

$$RMSE = \left[\frac{1}{IJ}\sum_{j=1}^{J}\sum_{i=1}^{I}\left(P_j^i - O_j^i\right)^2\right]^{\frac{1}{2}}$$

The RMSE, as with the gross error, is a good overall measure of model performance. However, since large errors are weighted heavily (due to squaring), large errors in a small sub-region may produce a large RMSE even though the errors may be small and quite acceptable elsewhere.

To put the statistical performance of a meteorological model simulation into context for air quality model applications, specific statistics are compared to performance benchmarks. The purpose of the benchmarks is to understand how good or poor the results are relative to the history of other model applications throughout the United States. Table 5-2 lists the meteorological model performance benchmarks that were considered in this study. The simple benchmarks (Emery et al., 2001) were developed by analyzing well-performing meteorological model results in areas of mostly flat terrain and simple meteorological conditions (e.g., stationary high pressure). The complex benchmarks (Kemball-Cook et al., 2004) were developed during the 2002 WRAP visibility modeling and are appropriate for applications in complex terrain and more variable meteorological conditions that occur in areas such as the Rocky Mountains and Alaska. McNally et al. (2008) analyzed multiple annual runs that included complex terrain conditions and suggested an alternative set of benchmarks for temperature under more complex conditions. The complex benchmarks in Table 5-2 represent the maximum among those proposed by Kemball-Cook and McNally.

Both 4 km WRF applications were statistically evaluated against these benchmarks, including bias and error in temperature, wind direction and mixing ratio, and bias and RMSE in wind speed. Observations for WRF verification and evaluation were obtained from the National Climate Data Center's (NCDC) global-scale, quality-controlled DS3505 integrated surface hourly dataset. Global hourly and synoptic observations are compiled from numerous sources into a single common text format and common data model. The DS3505 database contains records of most official surface meteorological stations from airports, military bases, reservoirs/dams, agricultural sites, and other sources dating from 1901 to the present.

Table 5-2. Meteorological model performance benchmarks for simple conditions (Emery et al., 2001) and complex conditions (Kemball-Cook et al., 2004; McNally et al, 2008).

Parameter	Simple	Complex
Temperature Bias	≤ ±0.5 K	≤ ±2.0 K
Temperature Error	≤ 2.0 K	≤ 3.5 K
Humidity Bias	≤ ±0.8 g/kg	≤ ±1.0 g/kg
Humidity Error	≤ 2.0 g/kg	≤ 2.0 g/kg
Wind Speed Bias	≤ ±0.5 m/s	≤ ±1.5 m/s
Wind Speed RMSE	≤ 2.0 m/s	≤ 2.5 m/s
Wind Dir. Bias	≤ ±10 degrees	--
Wind Dir. Error	≤ 30 degrees	≤ 55 degrees

*Dashes indicate that the parameter was not addressed by the referenced study.

The WRF surface meteorological model performance metrics were compared against the simple and complex model performance goals using "soccer plots." Soccer plots present WRF statistics as symbols in X/Y space (e.g., temperature bias as X and temperature error as Y) along with the performance benchmarks plotted as a box or "goal". The closer the symbols are to zero, the better the model performance. Statistical symbols within the goal indicate that WRF performs similarly to or generally better than the history of WRF simulations conducted for air quality modeling applications. Statistical symbols outside the goal indicate that WRF performs generally worse.

The hourly prediction and observation data that feed into the statistical calculations were plotted as time series by AMET or METSTAT. Either site-specific or site-aggregated time series can be developed. These types of plots were qualitatively reviewed to assess the ability of WRF to replicate intra-diurnal and inter-daily variations in temperature, winds, and humidity. Additionally, simulated profiles of temperature and humidity were plotted along with twice-daily Las Vegas RAOB data (KVEF). These plots provide an important assessment of the vertical structure of the atmosphere. The surface and profile assessments focused on periods when ozone was high or exceeded the NAAQS to evaluate the extent to which meteorology is properly characterized during these most important events.

A proper simulation of precipitation is also critically important for modeling ozone formation within, and regional transport into the CCNAA. Plots were generated to assess precipitation patterns and rates relative to measured conditions. Oregon State University (OSU) publishes precipitation analysis fields based on observations that can be used to qualitatively evaluate the WRF precipitation fields. The Parameter-elevation Relationships on Independent Slopes Model (PRISM) is used to generate the precipitation analysis fields (Daly et al., 2008). The PRISM interpolation method develops data sets that reflect, as closely as possible, the current state of knowledge of spatial climate patterns in the United States. PRISM calculates a climate – elevation regression for each digital elevation model (DEM) grid cell, and rain gauge stations entering the regression are assigned weights based primarily on the physiographic similarity between the station and the grid cell. Factors considered are location, elevation, coastal proximity, topographic facet orientation, vertical atmospheric layer, topographic position, and orographic effectiveness of the terrain.

Spatial plots of the WRF daily and monthly precipitation fields were compared with the PRISM spatial maps in a qualitative model evaluation. We focused on WRF performance for daily convective precipitation because WRF tends to overstate it, which can suppress ozone formation and improperly influence wind, temperature, and moisture patterns. However, the PRISM precipitation interpolation scheme works better for organized synoptic weather systems than for stochastic convective showers,

which tend to be spotty and intermittent. This is the primary reason why the analysis of precipitation performance remains as a qualitative comparison of spatial patterns and magnitudes.

5.4 Evaluation of EPA WRF 4 km Run

We compared EPA WRF model performance against available observations in the LVV region during high ozone periods that occurred during the summer of 2016. For surface performance, we graphically evaluated modeled temperature, humidity and winds against observations at Harry Reid International Airport (KLAS), while statistically evaluating WRF performance for those same variables across four routine airport monitoring sites within the LVV (KLAS, KLSV, KVGT and KHND in Figure 5-2). We also evaluated model performance for vertical temperature and humidity profiles against RAOB measurements from the KVEF Las Vegas radiosonde. Finally, we graphically compared daily simulated precipitation patterns against PRISM analyses on high ozone days when either WRF or observations reported precipitation in the region. For the remainder of this discussion, we refer to the EPA WRF run as "run0" and Ramboll's alternative WRF run for June 29 – July 4 as "run1".

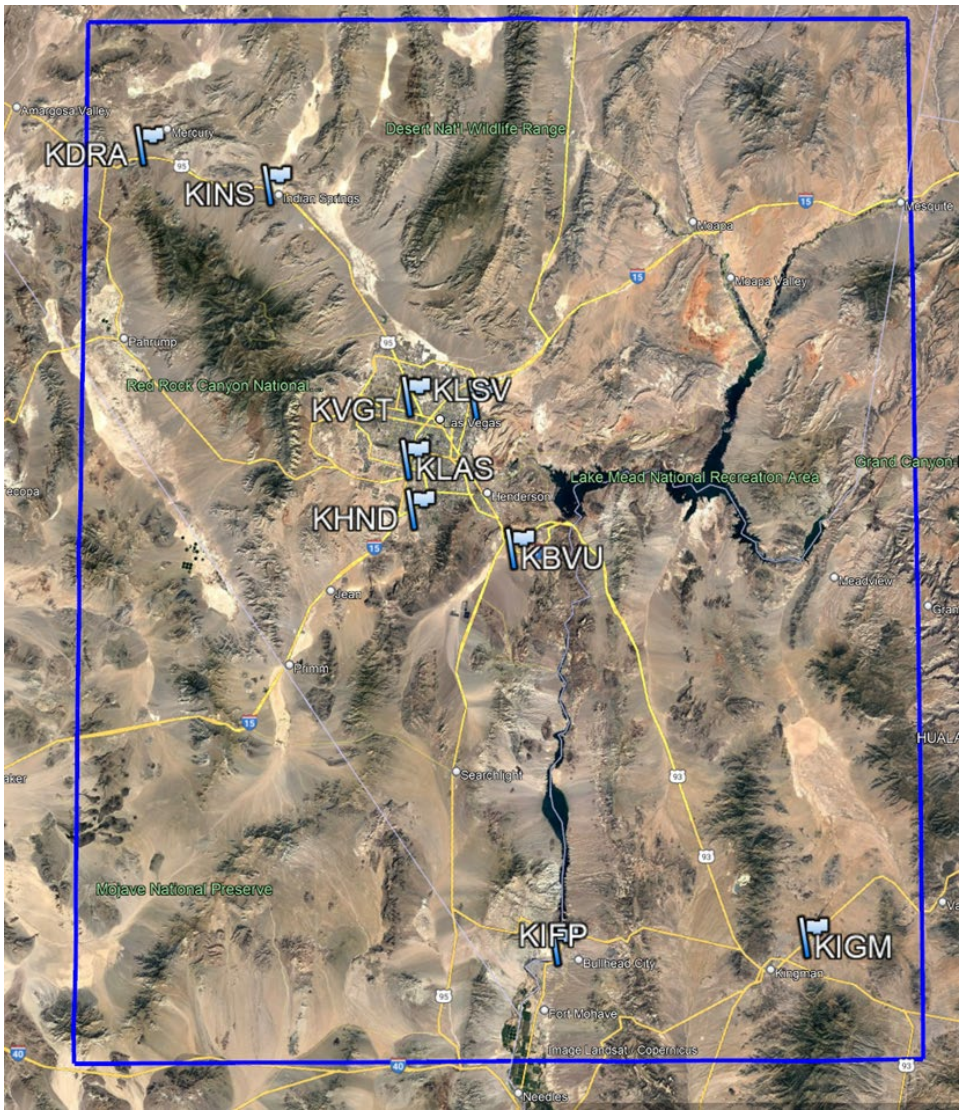

Figure 5-2. Locations of DS3505 surface airport meteorological monitoring sites (flags) within the CC4c2 CAMx domain (shown in blue).

We evaluated run0 performance for each of eight weeklong high ozone periods in 2016 as defined by Clark County DES/DAQ:

1. May 14-20
2. June 2-8
3. June 22-28
4. July 1-7
5. July 11-17
6. July 23-29
7. August 11-17
8. August 19-25

5.4.1 Surface Statistical Performance

Figure 5-3 displays soccer plots among the 8 high ozone periods (colored symbols) for wind speed (top left), wind direction (top left), temperature (bottom left) and water vapor mixing ratio (bottom left). We note that the benchmarks were designed for evaluating monthly performance across multiple sites within a region. In general, bias and error statistics look better when calculated for larger data populations (Emery et al., 2001). Therefore, we expect that statistical performance over shorter periods (as in weeklong high ozone periods) and a few sites to result in a wider range relative to benchmarks.

All 8 ozone periods show a negative wind speed bias (top left panel of Figure 5-3), with 3 of the 8 periods within the simple bias benchmark (≤±0.5 m/s) and all within the complex bias benchmark (≤±1.5 m/s). Five of the ozone periods achieve the simple benchmark for RMSE (≤2.0 m/s), and all achieve the complex benchmark (≤2.5 m/s).

Wind direction performance (top right panel of Figure 5-3) shows that 4 of the 8 high ozone periods meet the simple/complex benchmark for bias (≤±10°), and the other 4 periods are within the 10°-20° range. None of the periods meet the simple benchmark for error (≤30°), though all periods meet the complex benchmark (≤55°).

Temperature performance (bottom left panel of Figure 5-3) shows a general negative bias for 6 of the 8 high ozone periods. While all 8 periods lie within the complex benchmark (≤±2.0 K), 3 periods (May 14-20, July 11-27 and August 11-17) achieve the simple benchmark (≤±0.5 K). All 8 high ozone periods achieve the complex benchmark for error (≤3.5 K) and only one ozone period (July 1-7) lies outside the simple benchmark (≤2.0 K).

Water vapor mixing ratio performance (bottom right panel of Figure 5-3) shows a persistent positive bias across all 8 high ozone periods. Five periods meet the simple benchmark for bias (≤±0.8 g/kg), and one period (June 22-28) lies outside of the complex benchmark (≤±1.0 g/kg). All 8 high ozone periods meet the simple/complex benchmark for error (≤2.0 g/kg).

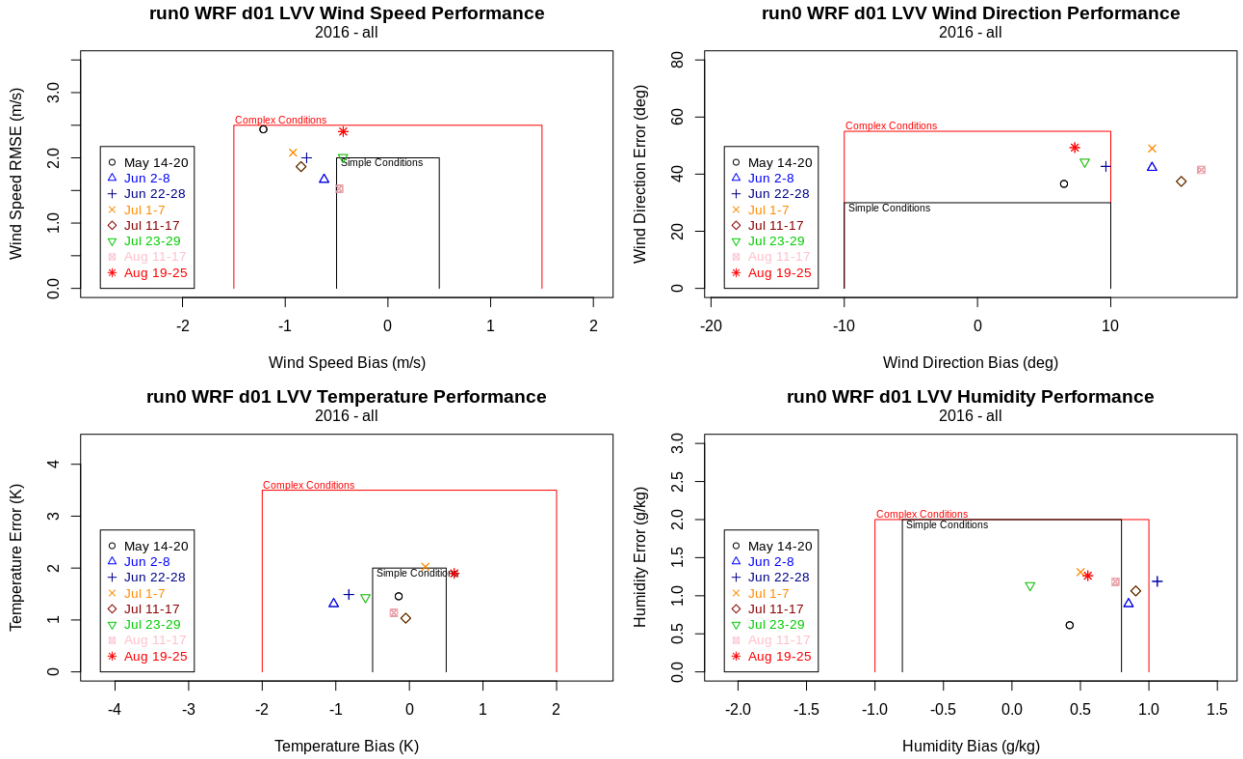

Figure 5-3. Soccer plots comparing model performance statistical metrics from EPA's WRF run against simple and complex benchmarks: 10-m wind speed (top left), 10-m wind direction (top right), 2-m temperature (bottom left) and 2-m water vapor mixing ratio (bottom right). Different symbols refer to each of the eight high ozone periods in 2016.

5.4.2 Time Series

Figures 5-4 through 5-11 show time series at KLAS from WRF run0 (red) and observations (black) for 2-m temperature (1st panel from top), 2-m water vapor mixing ratio (2nd panel), 10-m wind speed (3rd panel) and 10-m wind direction (bottom panel) for each of the 8 high ozone periods. Focusing on temperature, the model is able to replicate the daily midday peaks reasonably well on most days, but modeled temperature tends to drop off at faster rate in the late afternoon/evening hours than observed. Because temperature is tied to mixing, chemistry and emissions, this accelerated temperature drop could have implications for ozone modeling in CAMx. On several days (June 28, July 1-2, 28, August 22-23), modeled temperatures crash suddenly near midday, in contrast to observations. These temperature crashes are paired with large modeled spikes in mixing ratio, suggesting that convective activity in the model is responsible.

The persistent positive mixing ratio bias seen in the soccer plots (bottom right panel of Figure 5-3) is evident in the time series. For some ozone periods (see Figure 5-5 and Figure 5-8 for examples), run0 exhibits a +1 to +2 g/kg bias across nearly all hours.

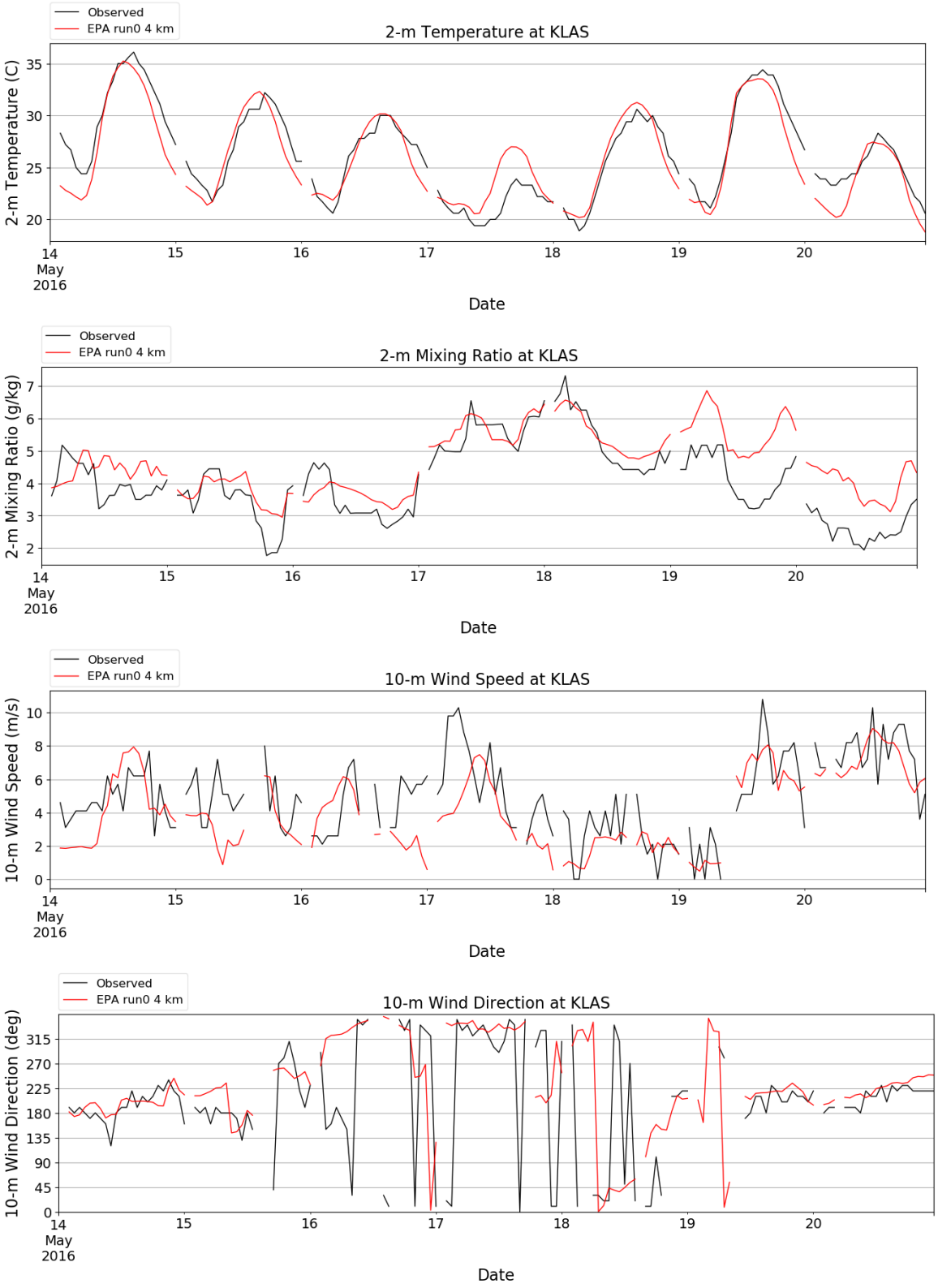

Figure 5-4. Observed (black line) and EPA WRF model (red) 2-m temperature (first panel from top), 2-m water vapor mixing ratio (second panel), 10-m wind speed (third panel) and 10-m wind direction (bottom panel) time series during May 14-20, 2016 at KLAS.

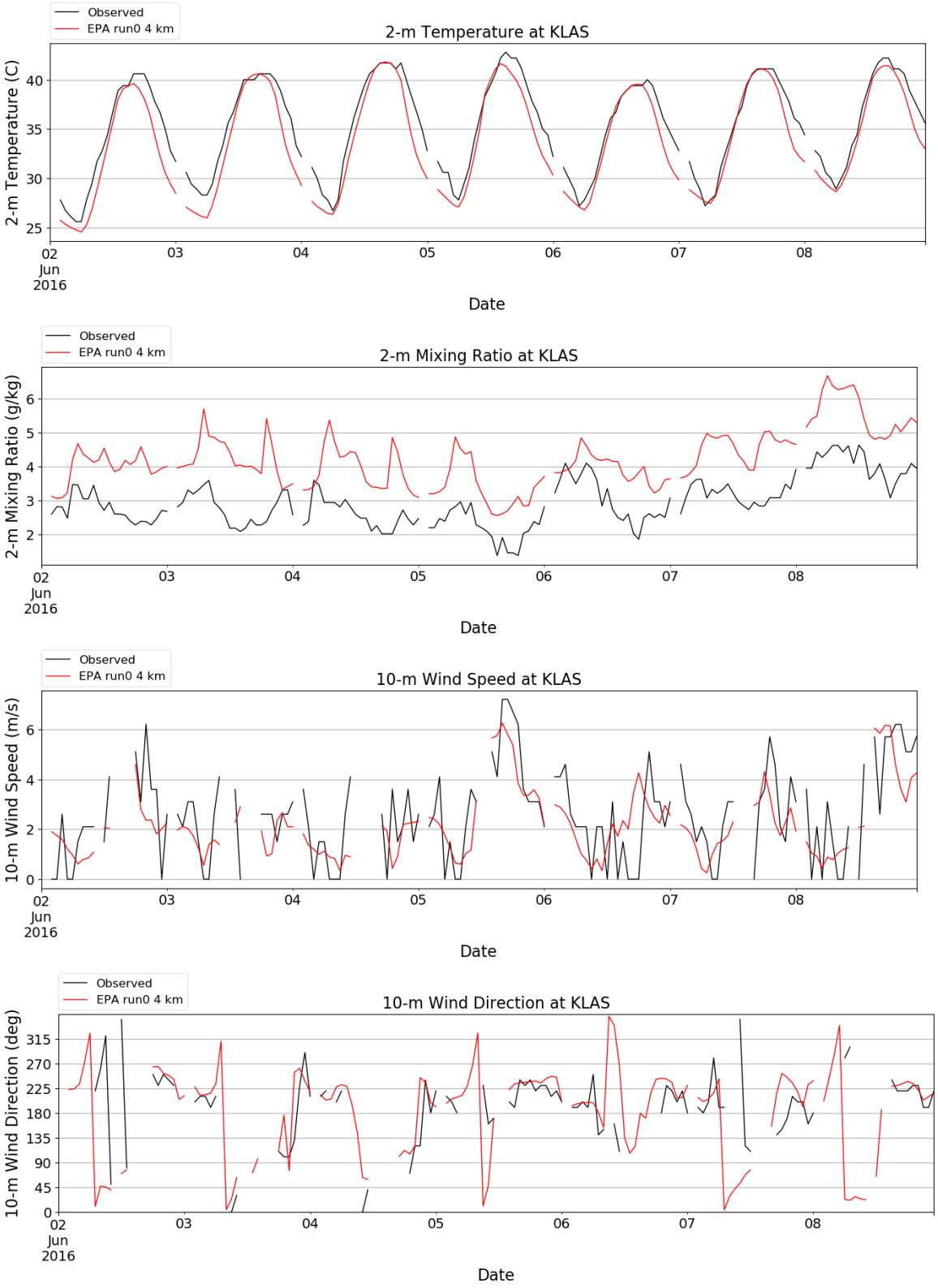

Figure 5-5. Observed (black line) and EPA WRF model (red) 2-m temperature (first panel from top), 2-m water vapor mixing ratio (second panel), 10-m wind speed (third panel) and 10-m wind direction (bottom panel) time series during June 2-8, 2016 at KLAS.

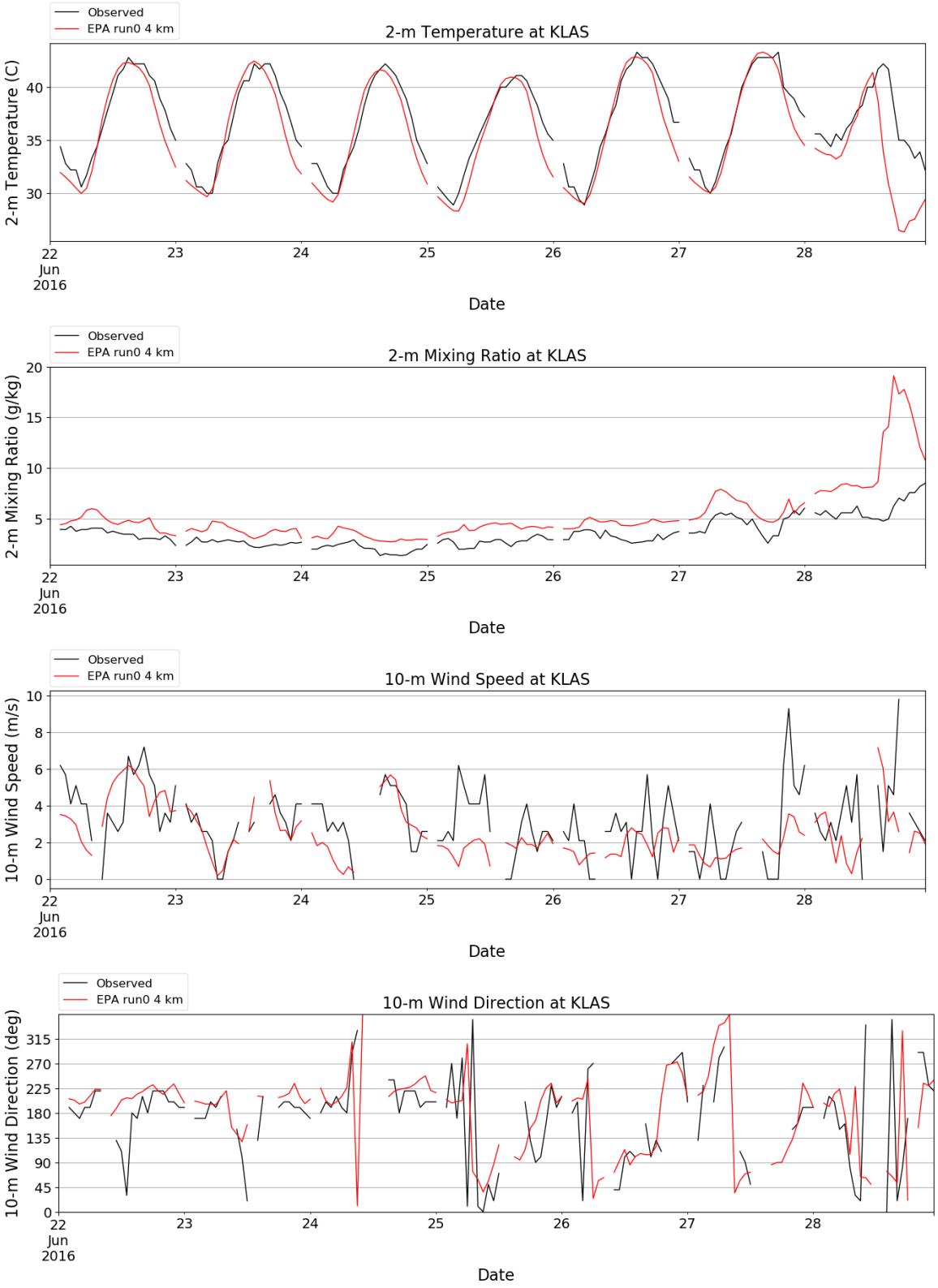

Figure 5-6. Observed (black line) and EPA WRF model (red) 2-m temperature (first panel from top), 2-m water vapor mixing ratio (second panel), 10-m wind speed (third panel) and 10-m wind direction (bottom panel) time series during June 22-28, 2016 at KLAS.

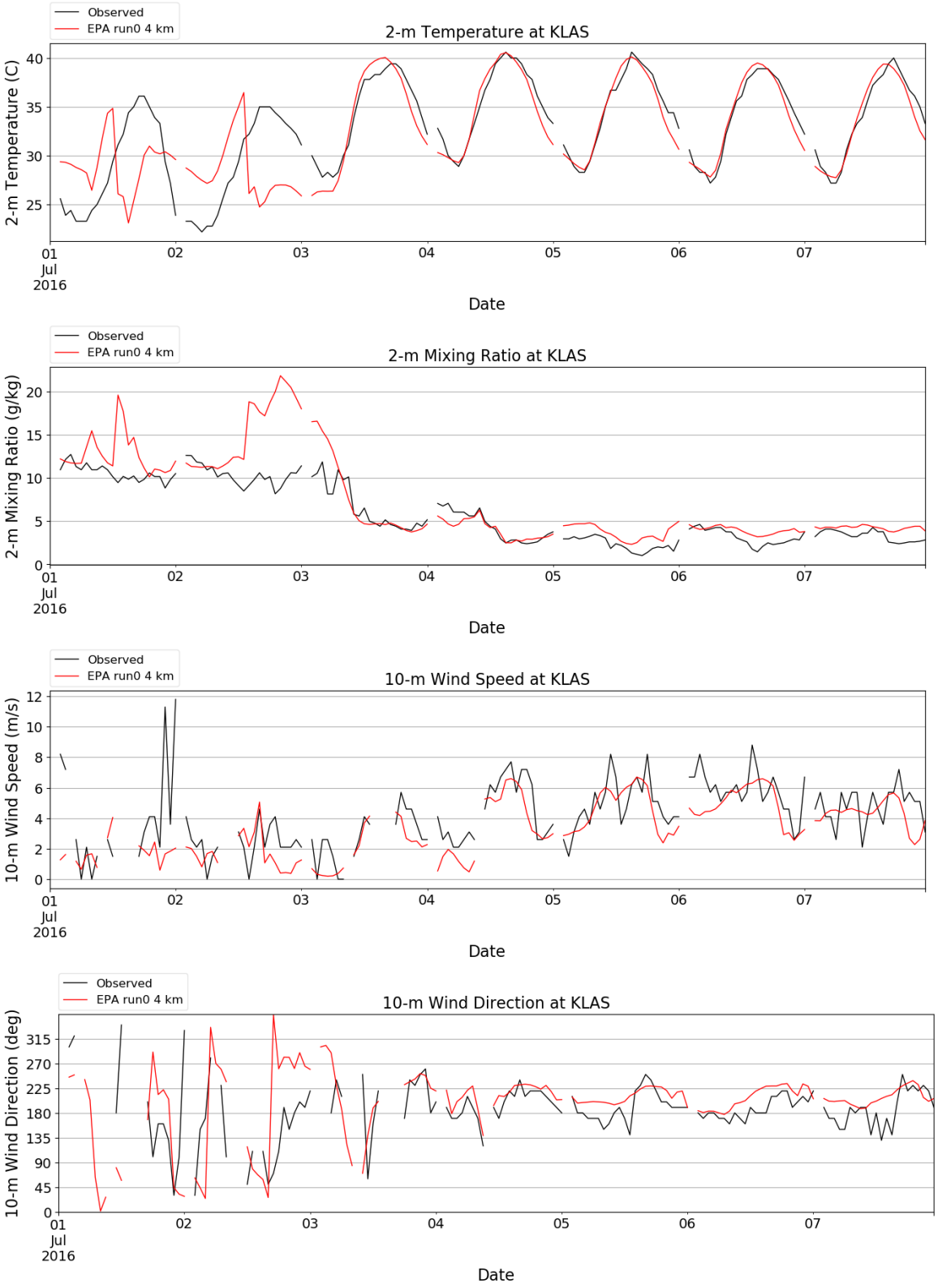

Figure 5-7. Observed (black line) and EPA WRF model (red) 2-m temperature (first panel from top), 2-m water vapor mixing ratio (second panel), 10-m wind speed (third panel) and 10-m wind direction (bottom panel) time series during July 1-7, 2016 at KLAS.

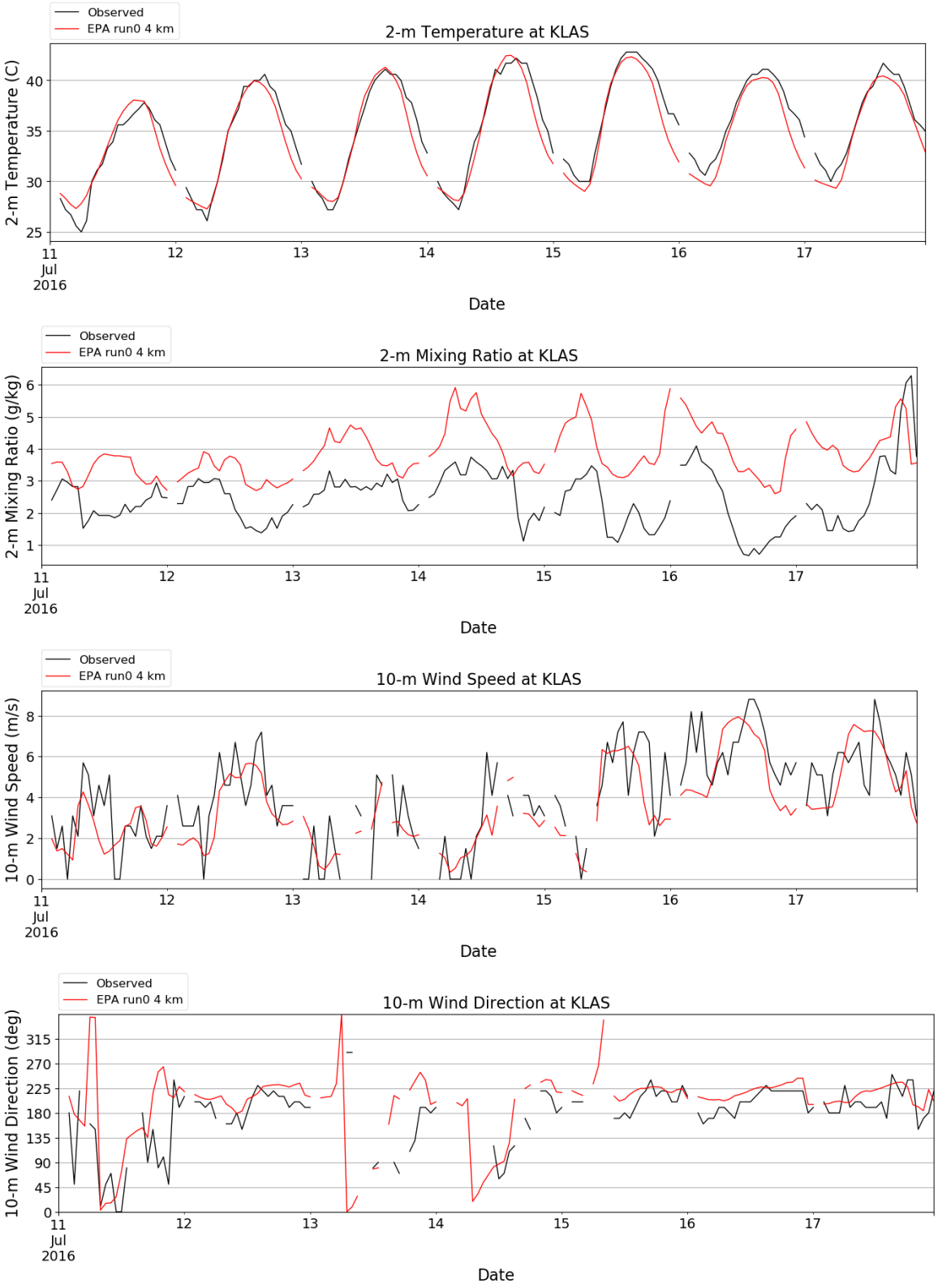

Figure 5-8. Observed (black line) and EPA WRF model (red) 2-m temperature (first panel from top), 2-m water vapor mixing ratio (second panel), 10-m wind speed (third panel) and 10-m wind direction (bottom panel) time series during July 11-17, 2016 at KLAS.

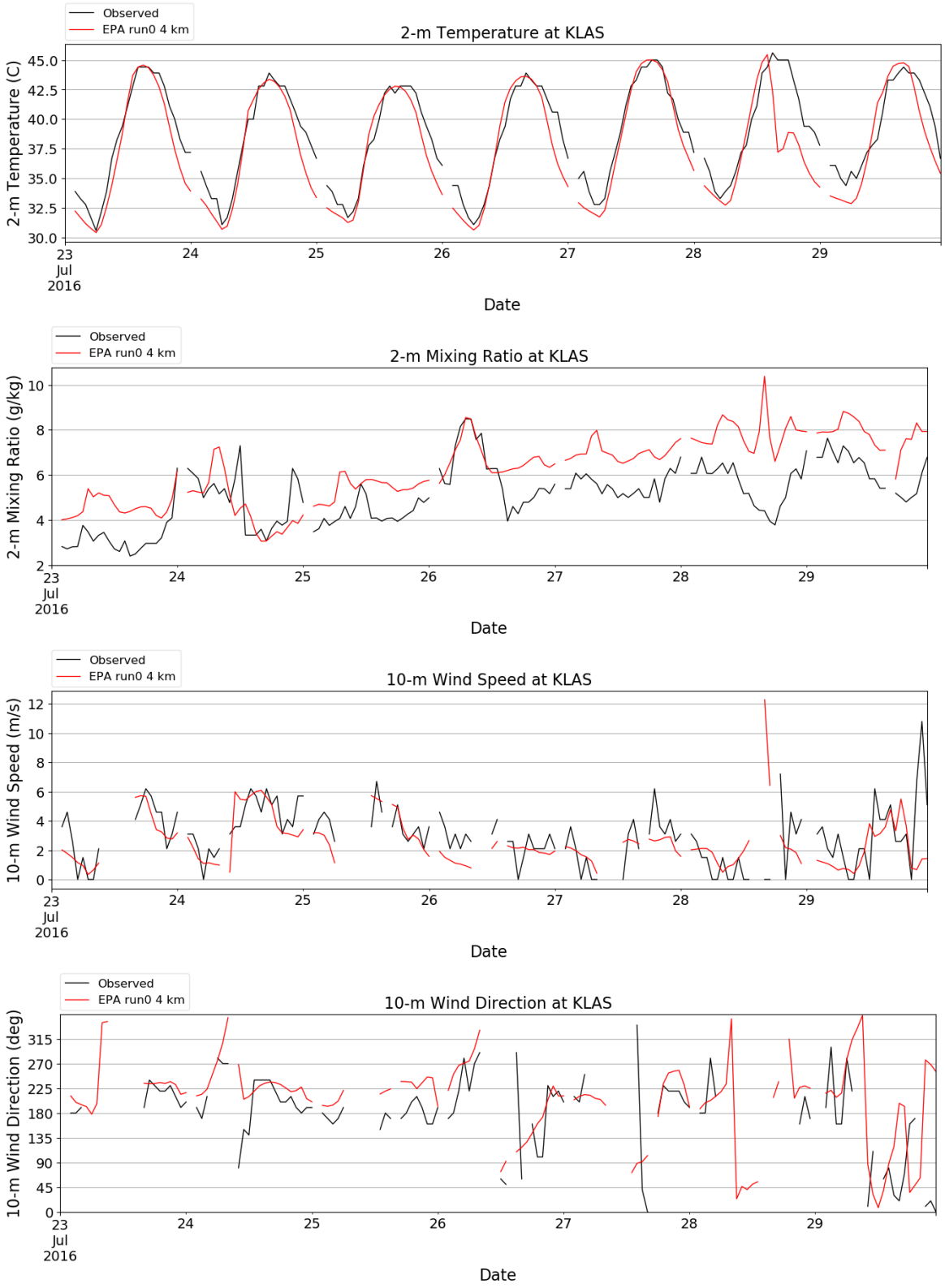

Figure 5-9. Observed (black line) and EPA WRF model (red) 2-m temperature (first panel from top), 2-m water vapor mixing ratio (second panel), 10-m wind speed (third panel) and 10-m wind direction (bottom panel) time series during July 23-29, 2016 at KLAS.

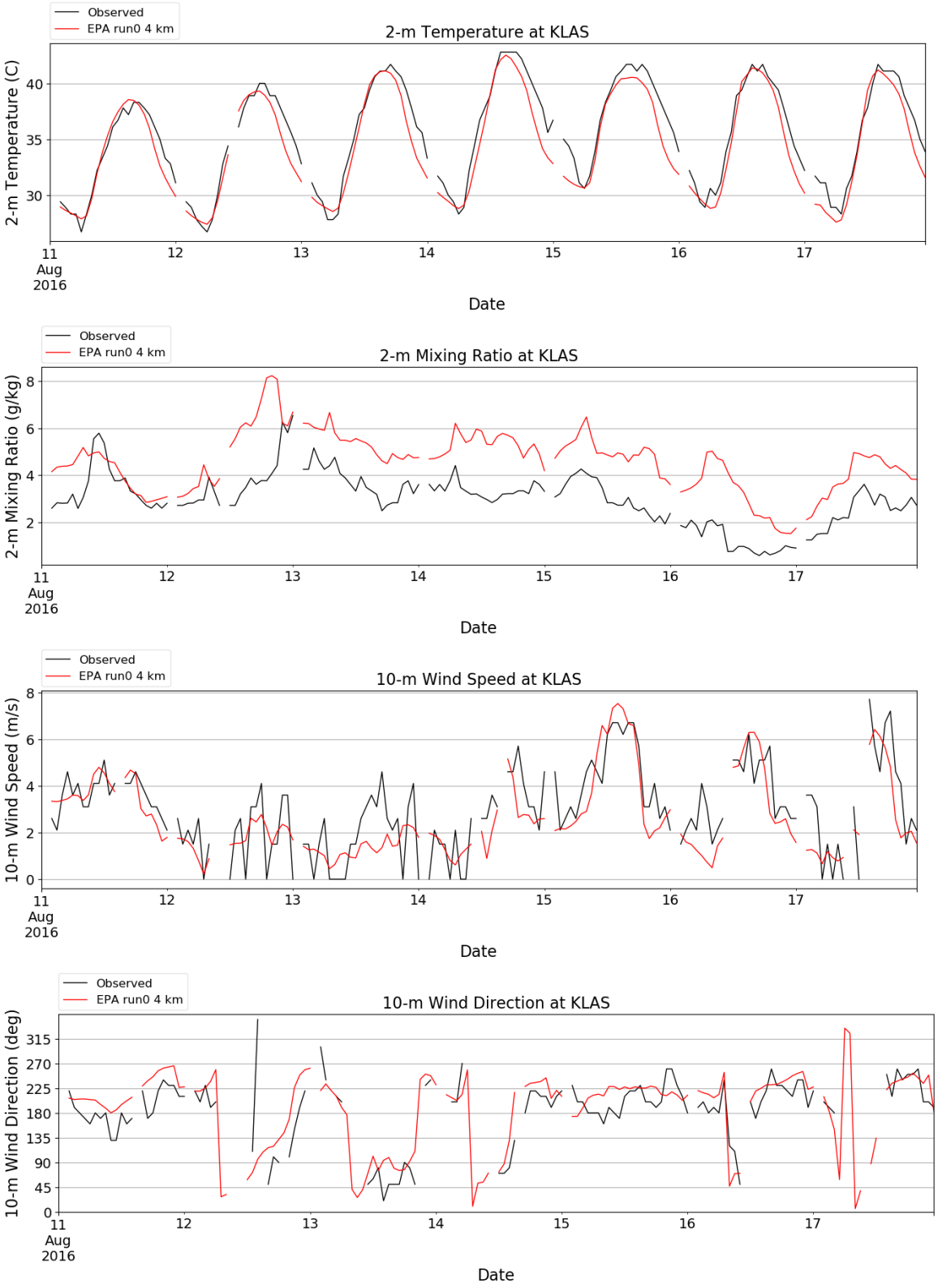

Figure 5-10. Observed (black line) and EPA WRF model (red) 2-m temperature (first panel from top), 2-m water vapor mixing ratio (second panel), 10-m wind speed (third panel) and 10-m wind direction (bottom panel) time series during August 11-17, 2016 at KLAS.

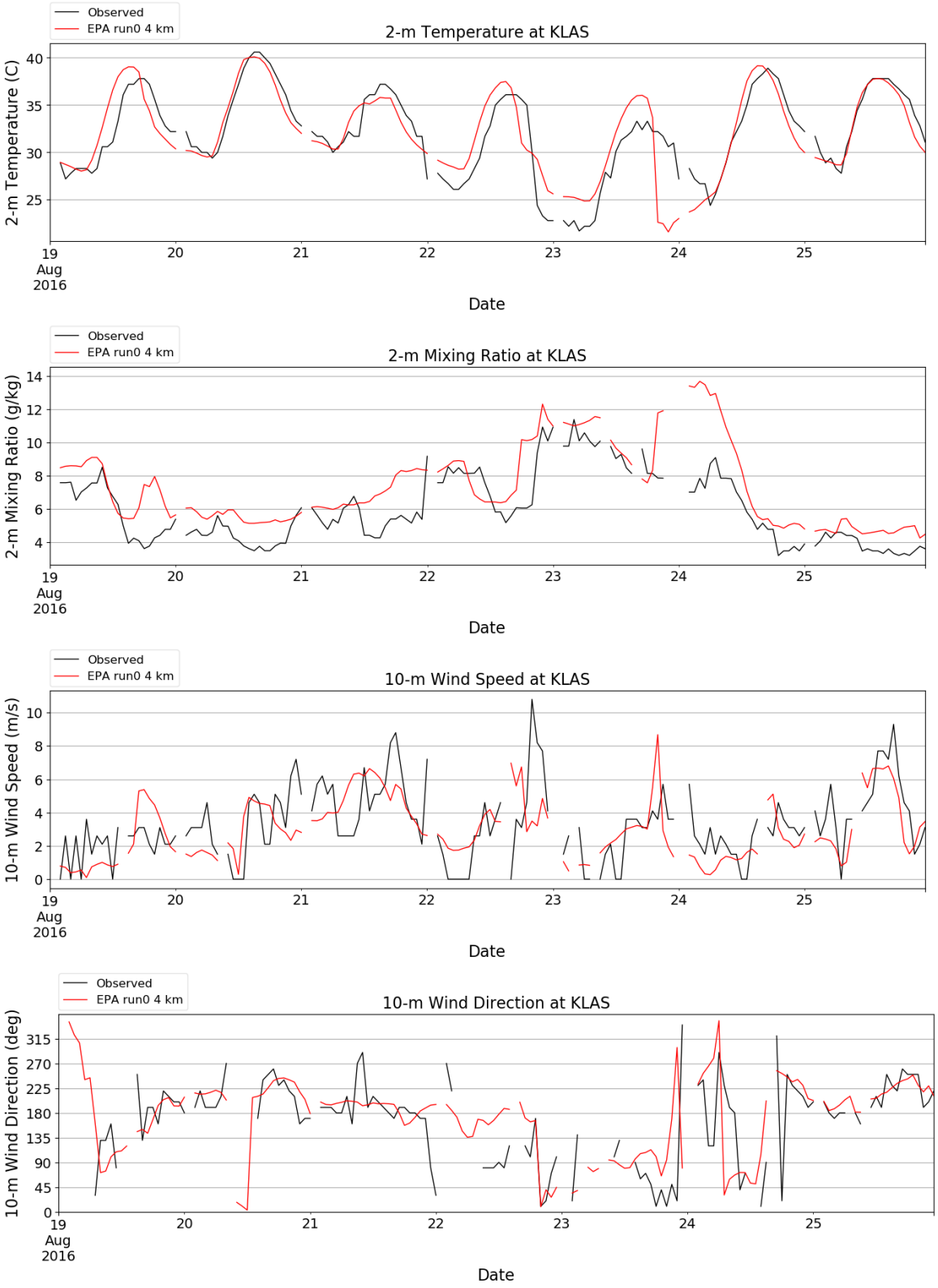

Figure 5-11. Observed (black line) and EPA WRF model (red) 2-m temperature (first panel from top), 2-m water vapor mixing ratio (second panel), 10-m wind speed (third panel) and 10-m wind direction (bottom panel) time series during August 19-25, 2016 at KLAS.

The model characterizes observed variation in wind speed reasonably well, but with a persistent negative bias. During periods of convective activity (see July 28 in Figure 5-9 for an example), the model sometimes shows large spikes in wind speed, which could be the result of resolved convective downburst winds in the model that temporarily lead to large positive wind speed biases. The model appears to capture observed wind direction shifts but does not exhibit as much hourly variation as observed. We note that missing wind direction observations due to calm wind speeds are frequent during high ozone periods.

5.4.3 Vertical Profile Comparisons

We evaluated temperature and humidity profiles from WRF run0 against measurements from the KVEF RAOB (location shown in Figure 5-12). For brevity, this section presents profile comparisons for two high ozone days at 5 PM PDT (00 UTC): July 28 and August 24. We selected these two days as generally representative of best (August 24) and worst (July 28) performance outside of the July 1-2 period.

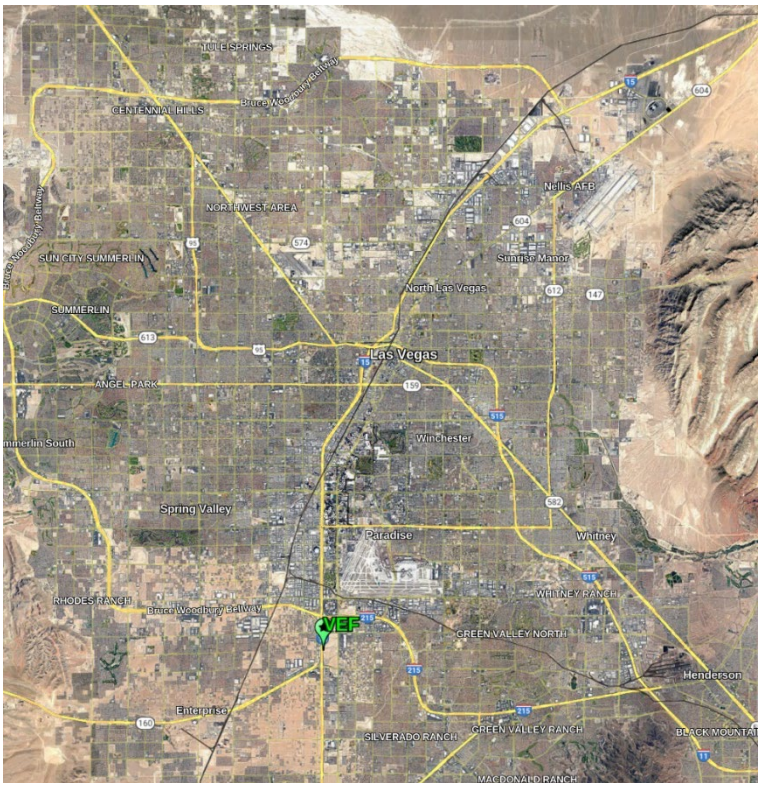

Figure 5-12. Map of Las Vegas showing location of KVEF RAOB site.

Figure 5-13 shows temperature (solid lines) and dewpoint temperature (dashed lines) profiles on August 24, 2016 at 5 PM PDT. Run0 shows good agreement with the RAOB measurements for temperature, with nearly identical profiles from the surface to about 2,400 m above mean sea level (AMSL) or about 1,700 m above ground level (AGL). Run0 dewpoint temperature is nearly identical to the corresponding KVEF observation at the surface but stays nearly constant with increasing height while the observed sounding increases markedly just above the surface, then decreases to match run0 at about 3,200 AMSL (~2,500 AGL).

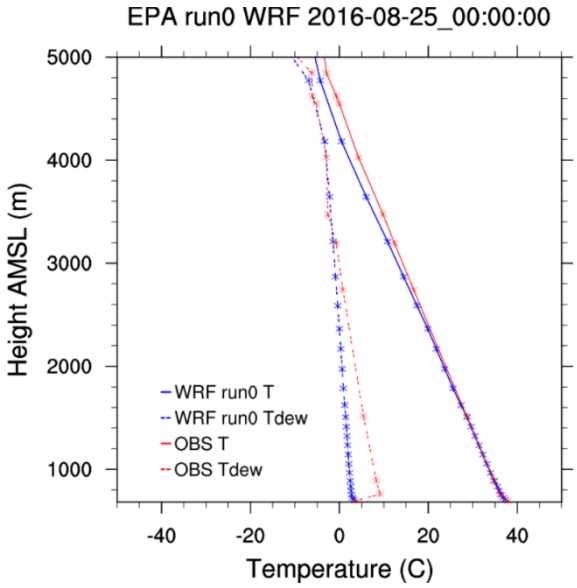

Figure 5-13. Vertical profiles from EPA WRF run0 (blue) and observed (red) temperature (solid lines) and dewpoint temperature (dashed lines) on August 24, 2016 at 5 PM PDT at KVEF.

Figure 5-14 shows the same information on July 28, 2016 at 5 PM PDT. The observed sounding shows a near-surface temperature of 44.2° C (111.6° F), compared to 37.1° C (98.8° F) for run0. The shallow temperature inversion simulated in run0 suggests surface cooling from shading or wet ground resulting from recent or concurrent precipitation. The daily precipitation plot covering this time period does show daily precipitation totaling about 0.1 inches in the vicinity of KVEF (see Figure 5-15 in next section).

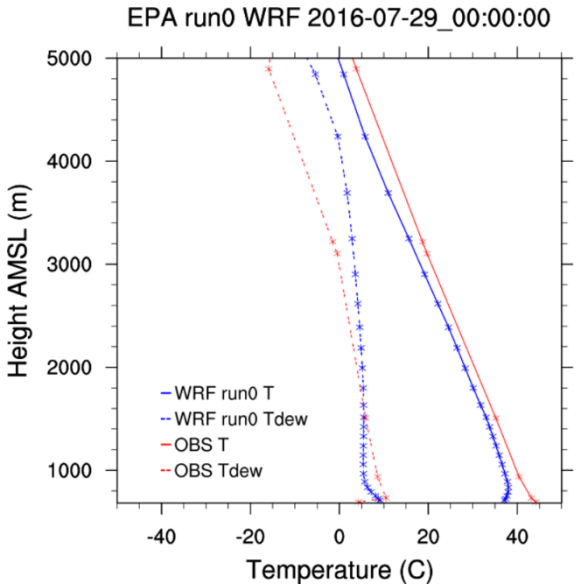

Figure 5-14. Vertical profiles from EPA WRF run0 (blue) and observed (red) temperature (solid lines) and dewpoint temperature (dashed lines) on July 28, 2016 at 5 PM PDT at KVEF.

5.4.4 Qualitative Evaluation for Precipitation

We focused this analysis on the high ozone days when some measurable precipitation was reported in the PRISM data or simulated by WRF run0: July 28-29 and August 23. We present similar precipitation comparisons for EPA's run0 and Ramboll's run1 against PRISM data covering the July 1-2 high ozone period later in this Section.

Figure 5-15 shows daily precipitation patterns from PRISM (left) and run0 (right) for the 24-hour period ending on July 29, 2016 at 5 AM PDT (12 UTC). Both plots show the locations of the DS3505 surface meteorological stations as black circles. The 3 stations in an approximate north/south line are the North Las Vegas Airport (KVGT), McCarran International Airport (KLAS) and Henderson Executive Airport (KHND). The KVEF radiosonde lies just west of KHND and shows daily precipitation around 0.1 inches. The erroneous precipitation in WRF run0 at this location is the likely cause for the substantial near-surface temperature underestimate found in Figure 5-14. Run0 shows better agreement with PRISM throughout most of the LVV with zero or near-zero (< 0.01 inches) precipitation.

Figure 5-16 shows a similar plot for the 24-hour period ending at 5 AM PDT on July 30, 2016. PRISM and run0 are in good agreement (zero or near-zero precipitation) across the LVV, except for an area extending just east and northeast of Nellis Air Force Base (KLSV; just east of VGT) where run0 shows spotty showers resulting in 0.01-0.1 inches of daily precipitation.

Finally, Figure 5-17 shows a daily precipitation comparison plot for the 24-hour period ending at 5 AM PDT on August 24, 2016. PRISM shows shower activity in the western LVV, with heavier amounts to the northwest of Las Vegas. Run0 however, centers shower activity over North Las Vegas, with daily totals exceeding 0.25 inches at KVGT (where PRISM shows < 0.01 inches).

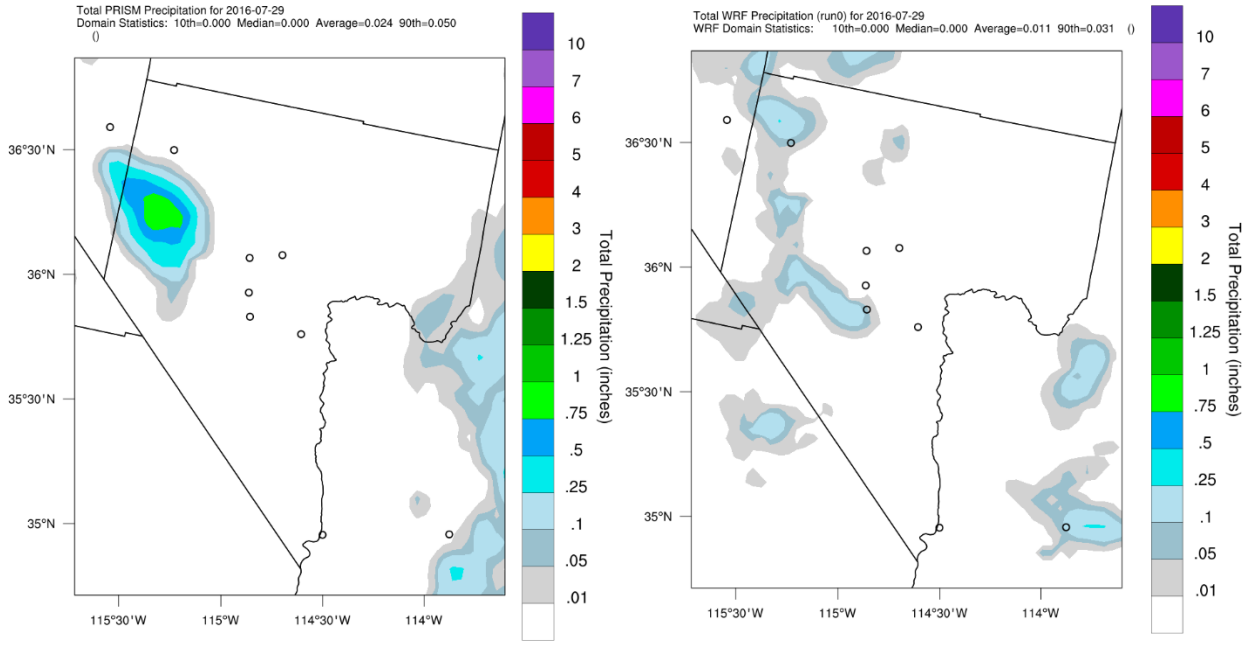

Figure 5-15. Daily precipitation patterns from PRISM based on observations (left) and modeled by EPA WRF run0 (right) for the 24-hour period ending July 29, 2016 at 5 AM PDT.

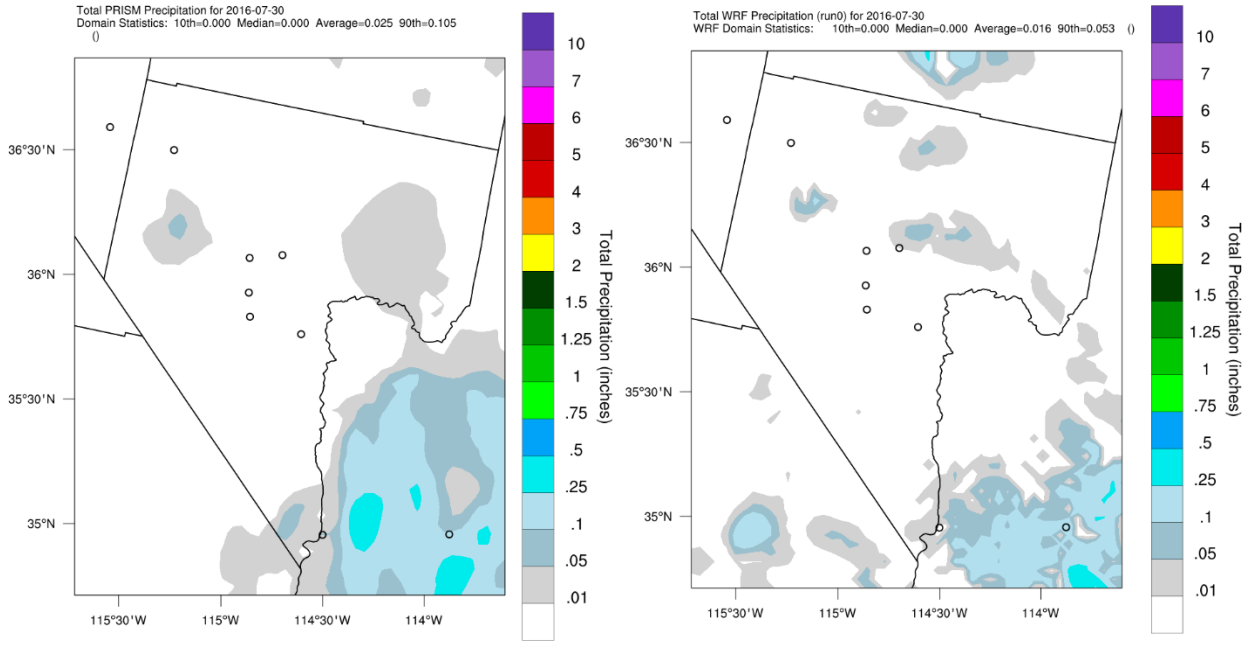

Figure 5-16. Daily precipitation patterns from PRISM based on observations (left) and modeled by EPA WRF run0 (right) for the 24-hour period ending July 30, 2016 at 5 AM PDT.

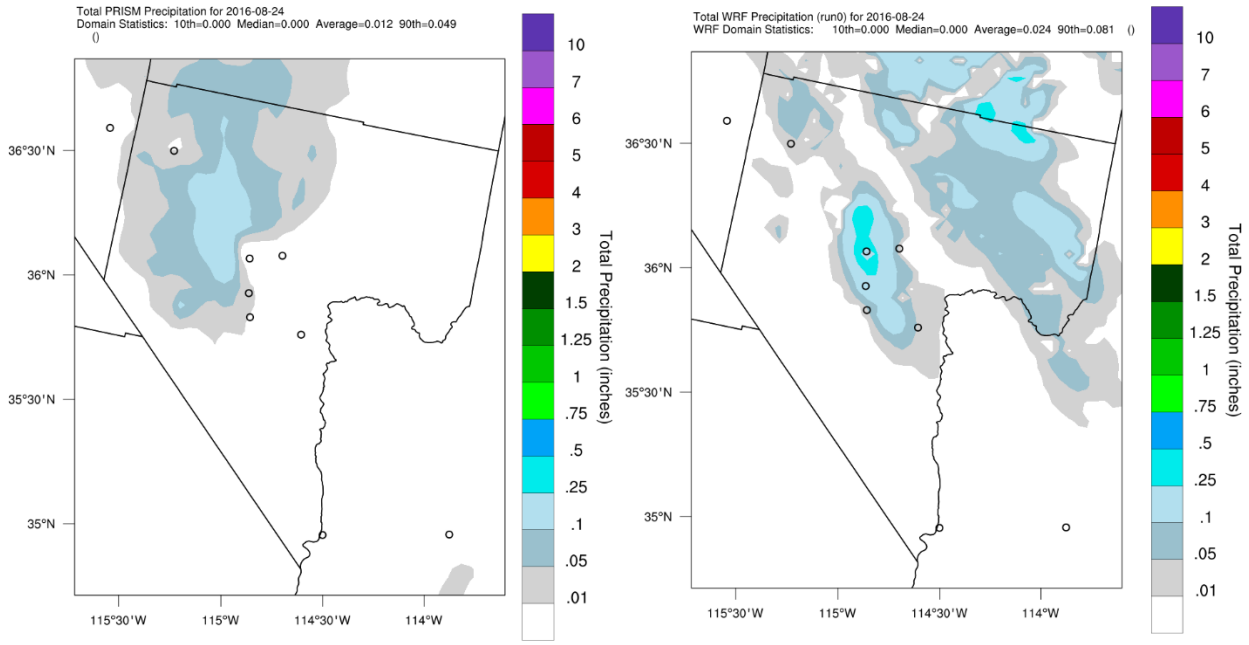

Figure 5-17. Daily precipitation patterns from PRISM based on observations (left) and modeled by EPA WRF run0 (right) for the 24-hour period ending August 24, 2016 at 5 AM PDT.

5.4.5 Phenomenological Evaluation

EPA's modeling guidance (EPA, 2018a) recommends a phenomenological or an event-based meteorological evaluation as part of any air modeling study. As part of the phenomenological evaluation for this study, we evaluated how large-scale meteorological features above terrain are simulated in WRF via observational analyses. Figure 5-18 shows an example comparison of a 700 mb upper air analysis chart (left panel; height contours in grey; temperature contours shown as red dashed lines; dewpoint temperatures exceeding -4°C shown as green lines) and 700 mb WRF 4 km run0 (right) height contours (purple), wind vectors and temperature on June 23, 2016 at 5 PM PDT. Figure 5-19 shows a similar comparison at the 500 mb level over North America from the WRF 12 km run on June 24, 2016 at 5 AM PDT. The orientation of WRF run0 height contours generally agree with those shown on the analysis chart. WRF winds tend to agree qualitatively with the upper air stations in both speed and direction. Over the southwestern US and LVV specifically, WRF winds indicate more stagnation and therefore a larger deviation in wind direction than is observed as the trough moves through Southern California and Nevada. Our examination of similar comparison plots throughout the summer 2016 modeling period revealed generally good qualitative agreement between WRF and the height contours and wind vectors as depicted on the analysis charts.

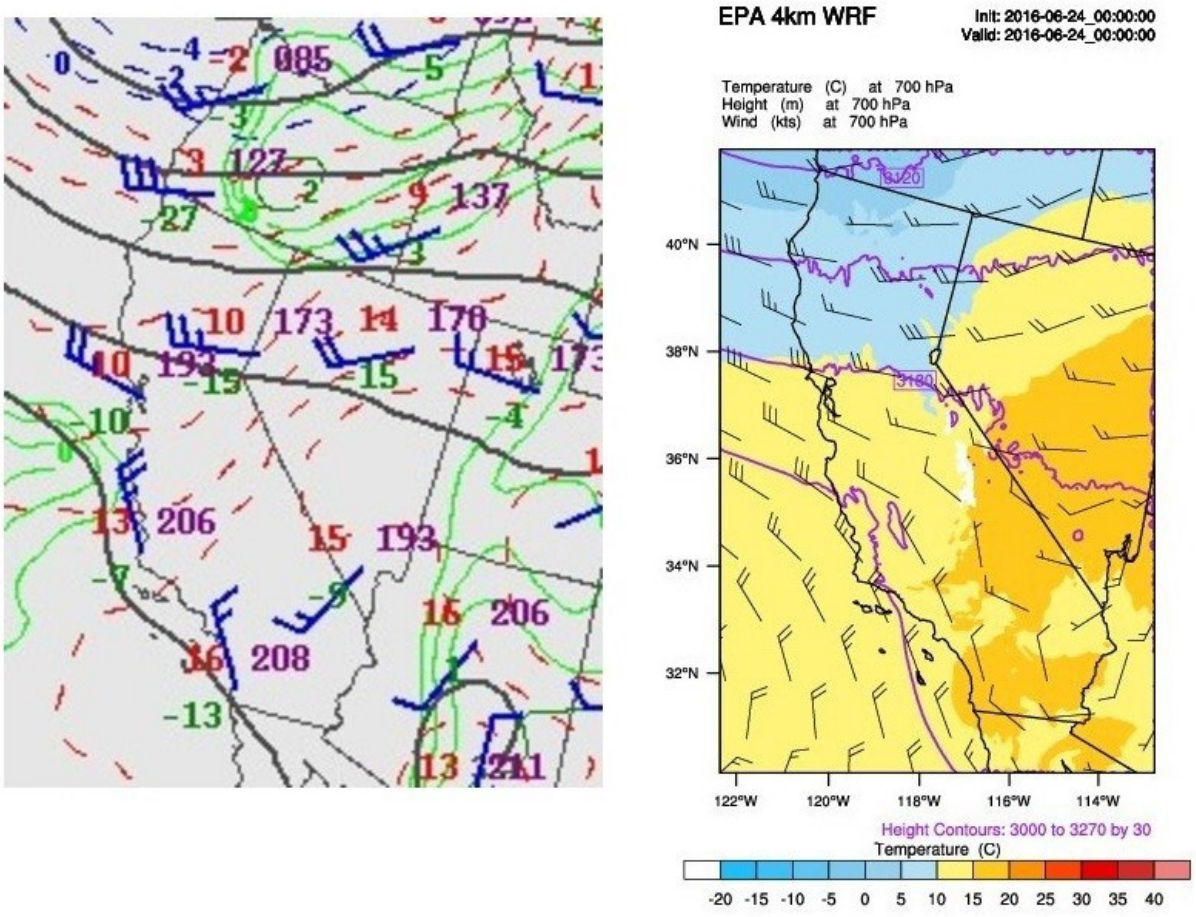

Figure 5-18. 700 mb upper air analysis chart (left; height contours in grey; temperature contours shown as red dashed lines; dewpoint temperatures exceeding -4°C shown as green lines) and 700 mb WRF 4 km run0 (right) height contours (purple), wind vectors and temperature on June 23, 2016 at 5 PM PDT.

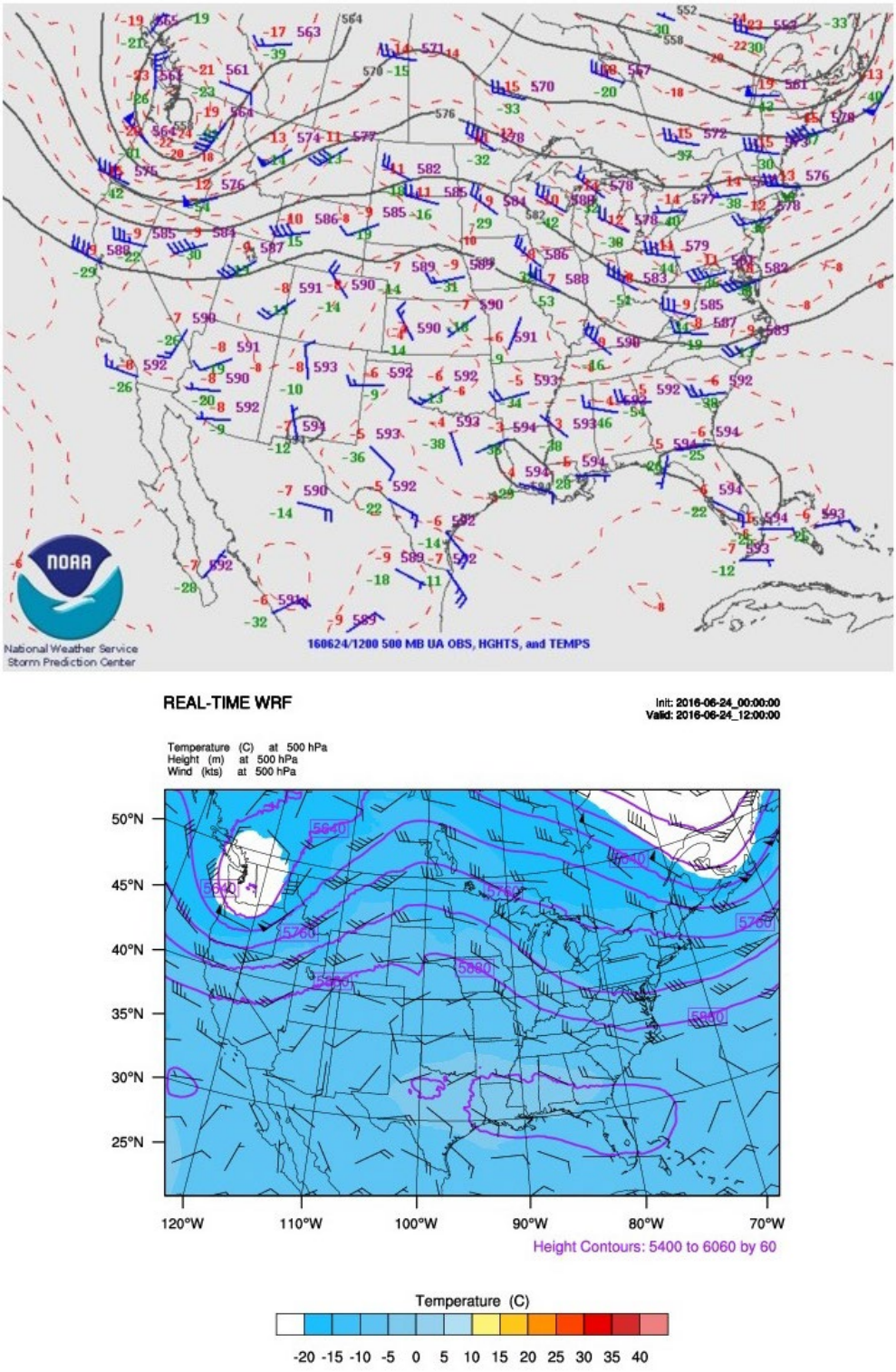

Figure 5-19. 500 mb upper air analysis chart (top; height contours in grey; temperature contours shown as red dashed lines) and 500 mb WRF 12 km (bottom) height contours (purple), wind vectors and temperature on June 24, 2016 at 5 AM PDT.

5.5 Evaluation of WRF 4 km Bridge Run

We compared WRF run1 performance for the June 30 – July 4, 2016 period against the WRF run0 results. As described previously, we configured this alternative WRF simulation in an attempt to improve overall performance during the July 1-2, 2016 high ozone days. These days are considered key to ozone modeling as they represent a period believed to involve mostly local ozone production with perhaps some regional transport.

5.5.1 Surface Statistical Performance

Table 5-3 presents daily 2-m temperature bias and error statistics from run0 and run1 for the June 30 – July 4, 2016 bridge period across the four airport sites within the LVV. The table shows complex benchmarks for bias and error as defined in Table 5-2 and as shown on the soccer plots. We again note that these benchmarks were designed for monthly evaluations across multiple sites within a region. Since we are focusing on daily statistics over an episode that exhibits the worst performance of the entire 4-month modeling period, we would not expect the models to achieve these benchmarks consistently or in unison. Bold text in the table indicates statistics within the complex benchmarks, while green highlighting denotes when daily run1 performance statistics are better (smaller absolute bias or smaller error) than run0. The low biases for run0 during July 1 (+0.8 K) and July 2 (+0.7 K) are misleading as they are the result of some large hourly positive biases nearly "cancelling out" other large hourly negative biases within the same day. This effect is clearly seen in the hourly time series in the next section. Therefore, it is more important to compare unsigned error. Run1 shows a substantially better error statistic on July 1 (2.2 K compared to 4.6 K for run0) and slightly better error statistic on July 2 (4.4 K compared to 5.0 K for run0). Run1 also exhibits a better error statistic for July 3 (0.7 K compared to 1.3 K for run0), but the errors are identical on July 4.

Table 5-3. Daily temperature bias and error statistics for WRF run0 and WRF run1 for June 30 – July 4, 2016 across the LVV. Bold text indicates statistics meeting complex benchmarks, while green highlighted cells show days where run1 outperforms run0.

	Mean Bias (K)					Mean Error (K)				
	6/30	**7/01**	**7/02**	**7/03**	**7/04**	**6/30**	**7/01**	**7/02**	**7/03**	**7/04**
Benchmark	≤ ± 2	≤ ± 2	≤ ± 2	≤ ± 2	≤ ± 2	≤ 3.5	≤ 3.5	≤ 3.5	≤ 3.5	≤ 3.5
run0	**1.9**	**0.8**	**0.7**	**-0.2**	**0.0**	**2.4**	4.6	5.0	**1.3**	**0.8**
run1	3.1	2.2	4.4	**0.0**	**-0.3**	3.8	**2.2**	4.4	**0.7**	**0.8**

Tables 5-4 through 5-6 show similar statistics for humidity, wind speed and wind direction, respectively. Run1 shows substantially better bias and error statistics for humidity (Table 5-4) during the July 1-2 period. The positive biases in run0 (July 1: +1.0 g/kg; July 2: +2.6 g/kg) result from overactive convection in the LVV, which is corroborated by the time series and precipitation analyses discussed later. Aside from July 1 (+0.2 g/kg), run1 exhibits negative mixing ratio biases on July 2 (-3.2 g/kg) and for the other 3 days. Despite these rather substantial dry biases, run1 results in better agreement with observed precipitation and near-surface temperature during this period.

Run1 exhibits generally better or similar wind speed (Table 5-5) bias and RMSE for June 30 – July 2, though the statistical differences from run0 are not large. Relative performance for wind direction (Table 5-6) is mixed and no clear conclusions can be drawn from the statistics alone. We also note that observed wind direction is flagged as missing (and therefore hourly statistics are not calculated) at low/variable wind speeds and these occurrences are generally more frequent during high ozone periods.

Table 5-4. Daily water vapor mixing ratio bias and error statistics for EPA WRF run0 and Ramboll WRF run1 for June 30 – July 4, 2016 across the LVV. Bold text indicates statistics meeting complex benchmarks, while green highlighted cells show days where run1 outperforms run0.

	Mean Bias (g/kg)					Mean Error (g/kg)				
	6/30	7/01	7/02	7/03	7/04	6/30	7/01	7/02	7/03	7/04
Benchmark	≤ ± 1	≤ ± 1	≤ ± 1	≤ ± 1	≤ ± 1	≤ 2	≤ 2	≤ 2	≤ 2	≤ 2
run0	**0.7**	**1.0**	2.6	**-0.7**	**-1.0**	**1.8**	**1.4**	3.0	**1.7**	**1.0**
run1	**-0.8**	**0.2**	-3.2	-4.8	-2.5	**1.9**	**0.8**	3.3	4.8	2.5

Table 5-5. Daily wind speed bias and error statistics for EPA WRF run0 and Ramboll WRF run1 for June 30 – July 4, 2016 across the LVV. Bold text indicates statistics meeting complex benchmarks, while green highlighted cells show days where run1 outperforms run0.

	Mean Bias (m/s)					RMSE (m/s)				
	6/30	7/01	7/02	7/03	7/04	6/30	7/01	7/02	7/03	7/04
Benchmark	≤ ±1.5	≤ ±1.5	≤ ±1.5	≤ ±1.5	≤ ±1.5	≤ 2.5	≤ 2.5	≤ 2.5	≤ 2.5	≤ 2.5
run0	**-1.0**	-1.6	**-1.2**	**-0.4**	**-0.5**	3.3	3.6	2.8	**1.4**	**1.5**
run1	**-0.2**	**-0.8**	**1.2**	**0.9**	**-0.2**	3.3	2.9	3.1	**1.8**	**2.1**

Table 5-6. Daily wind direction bias and error statistics for EPA WRF run0 and Ramboll WRF run1 for June 30 – July 4, 2016 across the LVV. Bold text indicates statistics meeting complex benchmarks, while green highlighted cells show days where run1 outperforms run0.

	Mean Bias (m/s)					Mean Error (m/s)				
	6/30	7/01	7/02	7/03	7/04	6/30	7/01	7/02	7/03	7/04
Benchmark	≤ ±10	≤ ±10	≤ ±10	≤ ±10	≤ ±10	≤ 55	≤ 55	≤ 55	≤ 55	≤ 55
run0	**8**	-17	32	11	11	64	84	98	**44**	**30**
run1	26	46	19	13	13	75	73	74	**47**	**34**

5.5.2 Time Series Comparison

Figure 5-20 shows time series at KLAS for WRF run0 (red), WRF run1 (blue) and observations (black) for 2-m temperature (1st panel from top), 2-m water vapor mixing ratio (2nd panel), 10-m wind speed (3rd panel) and 10-m wind direction (bottom panel) during June 30 – July 4, 2016. On June 30, apparent convective activity is reflected in the KLAS observations, with a sudden temperature drop around midday paired with spikes in observed mixing ratio. Run0 appears to capture the timing of the onset of convective activity as evidenced by the concurrent sharp temperature decrease and mixing ratio increase. However, run0 temperatures quickly rebound (while mixing ratio decreases), signifying an end to shower activity in the model, which contrasts with the observations that support continued shower activity in the region (temperature continues to drop while mixing ratio spikes). Run1 performs worse than run0 on June 30, with midday peak temperatures substantially overestimated (and mixing ratio underestimated) with no obvious daytime convective signal as seen in the observations and run0.

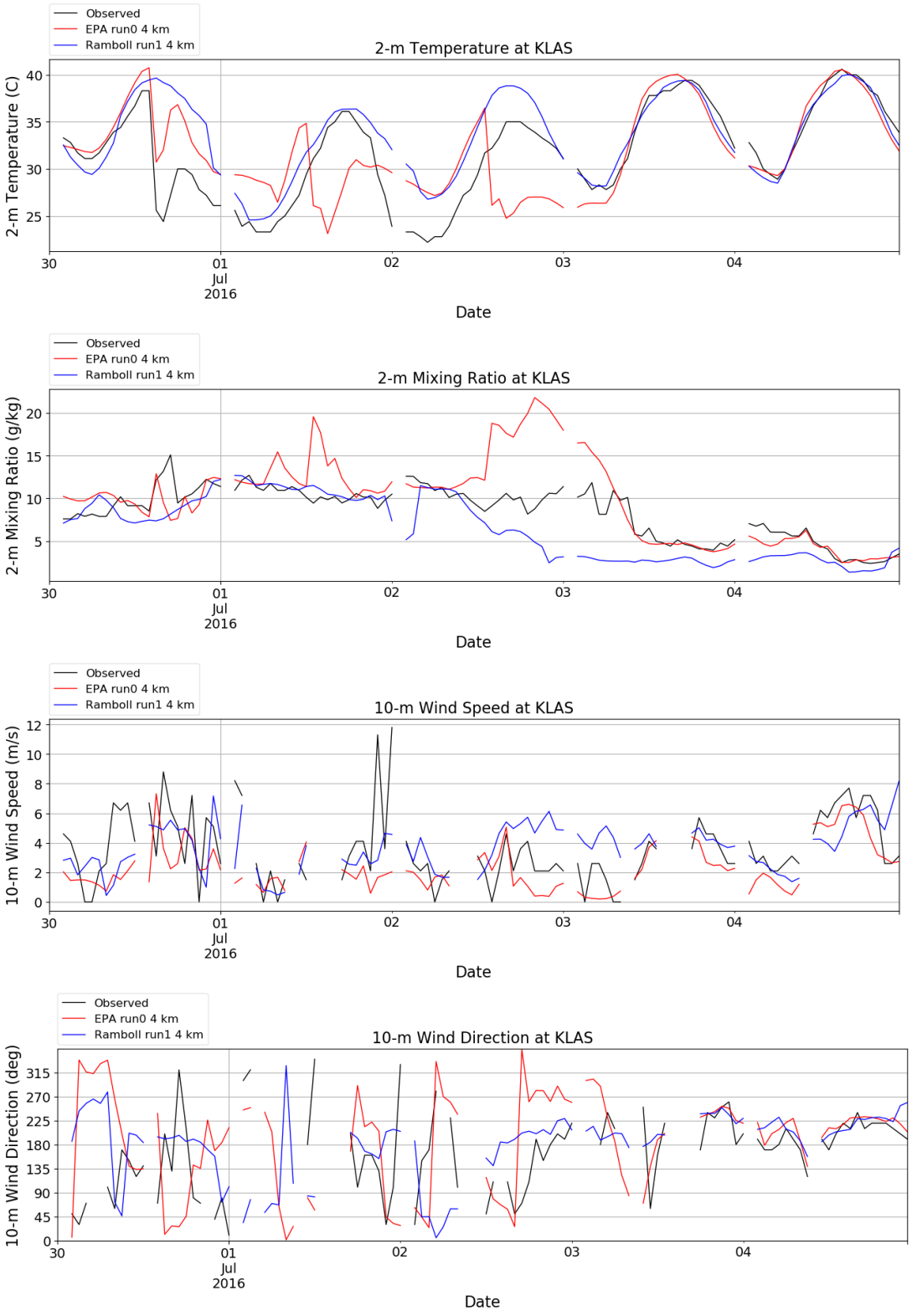

Figure 5-20. Observed (black line), EPA WRF run0 (red) and Ramboll WRF run1 (blue) 2-m temperature (first panel from top), 2-m water vapor mixing ratio (second panel), 10-m wind speed (third panel) and 10-m wind direction (bottom panel) time series for June 30 – July 4, 2016 at KLAS.

On July 1 and 2, run0 again shows daytime temperature crashes paired with large spikes in mixing ratio, indicating convective activity that does not occur in the observations. We verified that these convective events result in dramatic collapses in mixing depth, which have implications for ozone modeling in CAMx. Run1 does not exhibit such convective activity on July 1 and 2 and matches the midday temperature peak reasonably well on July 1. Overnight temperatures into July 2 for run1 remain considerably higher than observed and this positive temperature bias persists into midday, where the run1 daytime peak is about 4° C higher than observed. At the same time, run1 mixing ratio begins a downward trend around midday on July 2 leading to substantial negative biases through July 4. Temperature performance is similar between the two runs for July 3 and 4, with run1 matching observations slightly better than run0.

Wind speed and wind direction time series show no clear winner and there are many missing observations during the July 1-2 high ozone period, apparently due to calm/variable winds below measurement thresholds. From these results, we were confident that replacing run0 meteorology with run1 would not substantially degrade wind performance during the July 1-2 high ozone period.

5.5.3 Vertical Profile Comparisons

Figures 5-21 through 5-29 show vertical profiles of WRF (blue) and observed (red) temperature (soild lines) and dewpoint temperature (dashed lines) at 00Z and 12Z (5 AM and PM PDT) at the KVEF RAOB from June 30, 2016 at 5 AM PDT (Figure 5-21) through July 4, 2016 at 5 AM PDT (Figure 5-29). Solid lines in the left panels show WRF run0 profiles and solid lines in the right panels show WRF run1 profiles. The first two figures spanning June 30 (Figure 5-21 and 5-22) show that WRF run0 better matches the observed profiles than run1, but the differences are not substantial. On July 1 (Figures 5-23 and 5-24), large differences build; run0 substantially underpredicts afternoon near-surface temperature, while run1 matches the observations quite well for both temperature and dewpoint. On July 2 at 5 AM PDT (Figure 5-25), model differences decrease, and both runs show similar positive temperature biases near the surface while matching the observed dewpoint quite well. On that afternoon, however, near-surface temperatures in run0 (Figure 5-26) again exhibit a substantial underestimate, while run1 shows a smaller temperature overestimate coupled with a much drier profile than observed. Both runs do a better job matching the observed temperature profiles through the remaining soundings covering July 3 and 4, while run1 continues the trend toward much drier profiles than observed.

5.5.4 Qualitative Evaluation for Precipitation

Figure 5-30 shows the precipitation patterns from PRISM based on observations (left) and modeled by WRF run0 (middle) and run1 (right) for the 24-hour period ending July 1, 2016 at 5 AM PDT. PRISM shows lighter rain amounts (< 0.1 inches) in the northern LVV and heavier amounts to the south, including a local maximum surrounding KLAS and KHND, with over 0.5 inches. Both WRF runs show similar patterns to each other, with a general underestimate of precipitation in the LVV and overestimates to the east.

Figure 5-31 shows the same information ending on July 2, 2016 at 5 AM PDT. WRF run0 does a reasonable job matching the magnitude of PRISM precipitation amounts in the LVV. Because the time series show signatures of overstated precipitation (sudden increases in mixing ratio paired with sudden decreases in temperature relative to observations), we conclude that run0 produces precipitation at spurious times/locations during the day. Run1 is mostly dry throughout the LVV (right panel of Figure 5-31).

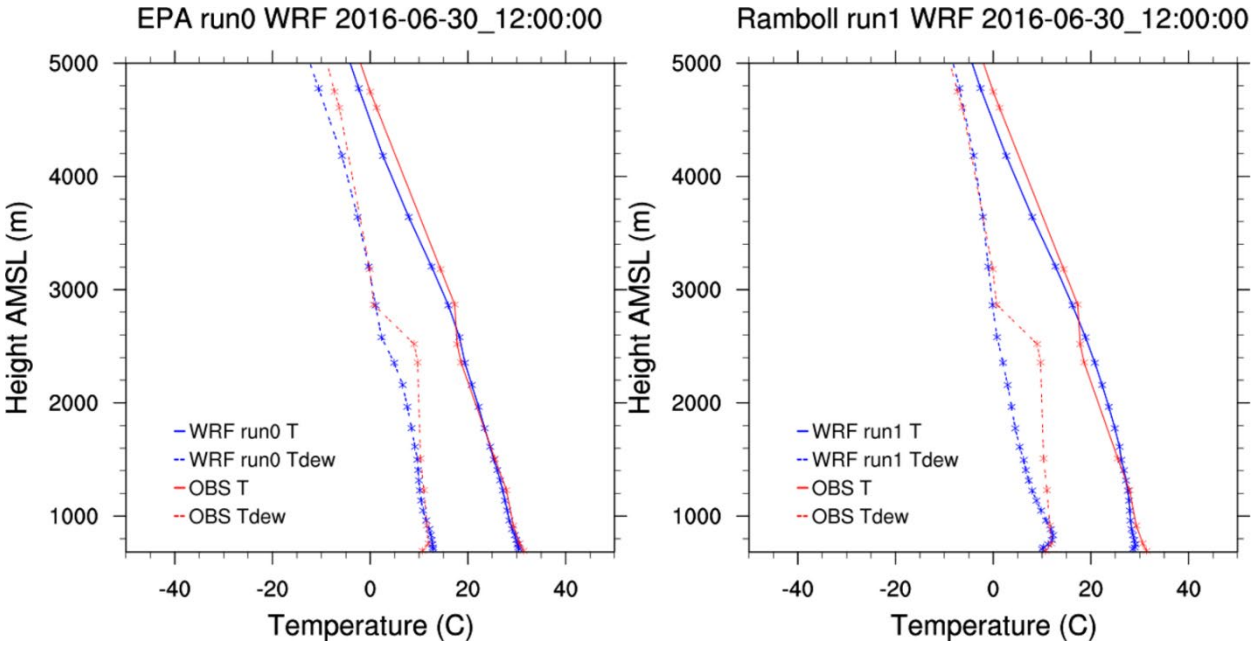

Figure 5-21. Vertical profiles at KVEF from WRF run0 (blue lines in left panel), WRF run1 (blue lines in right panel) and observed (red) temperature (solid lines) and dewpoint temperature (dashed lines) on June 30, 2016 at 5 AM PDT.

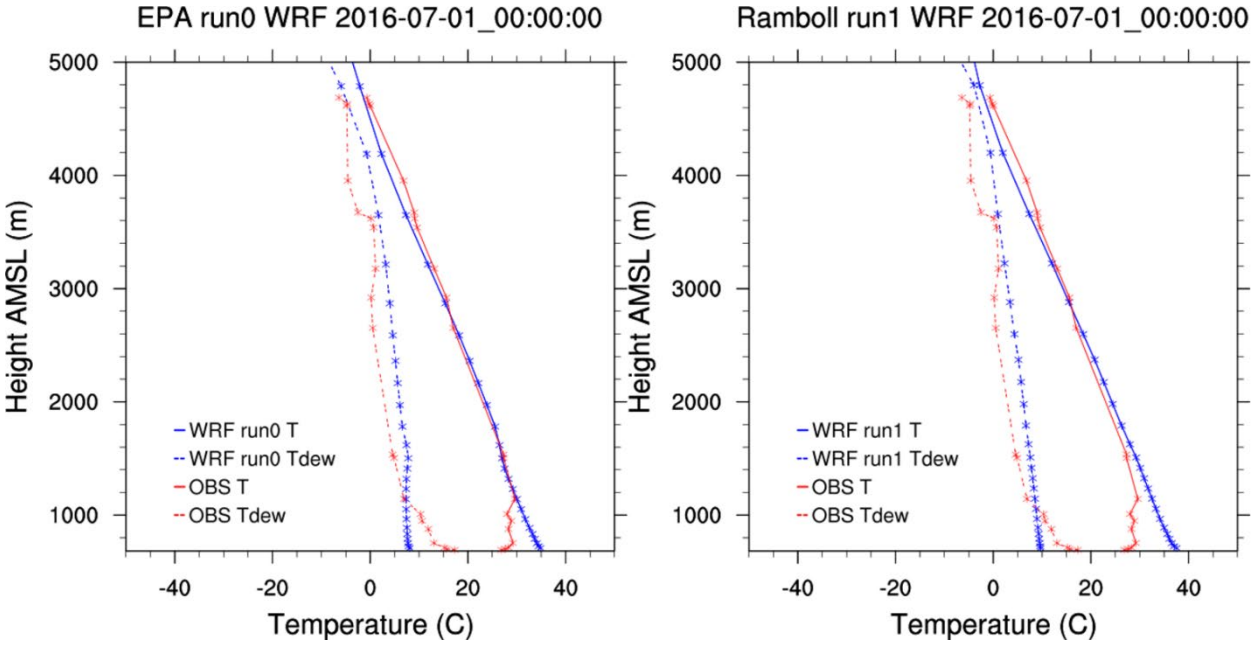

Figure 5-22. Vertical profiles at KVEF from WRF run0 (blue lines in left panel), WRF run1 (blue lines in right panel) and observed (red) temperature (solid lines) and dewpoint temperature (dashed lines) on June 30, 2016 at 5 PM PDT.

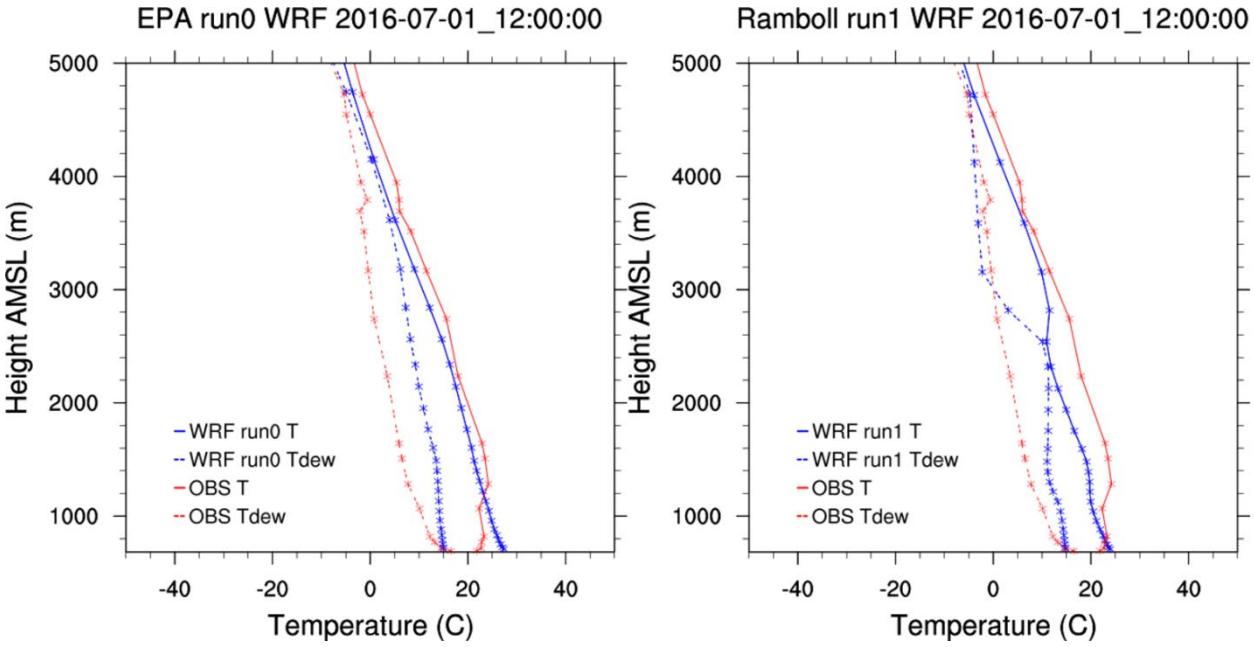

Figure 5-23. Vertical profiles at KVEF from WRF run0 (blue lines in left panel), WRF run1 (blue lines in right panel) and observed (red) temperature (solid lines) and dewpoint temperature (dashed lines) on July 1, 2016 at 5 AM PDT.

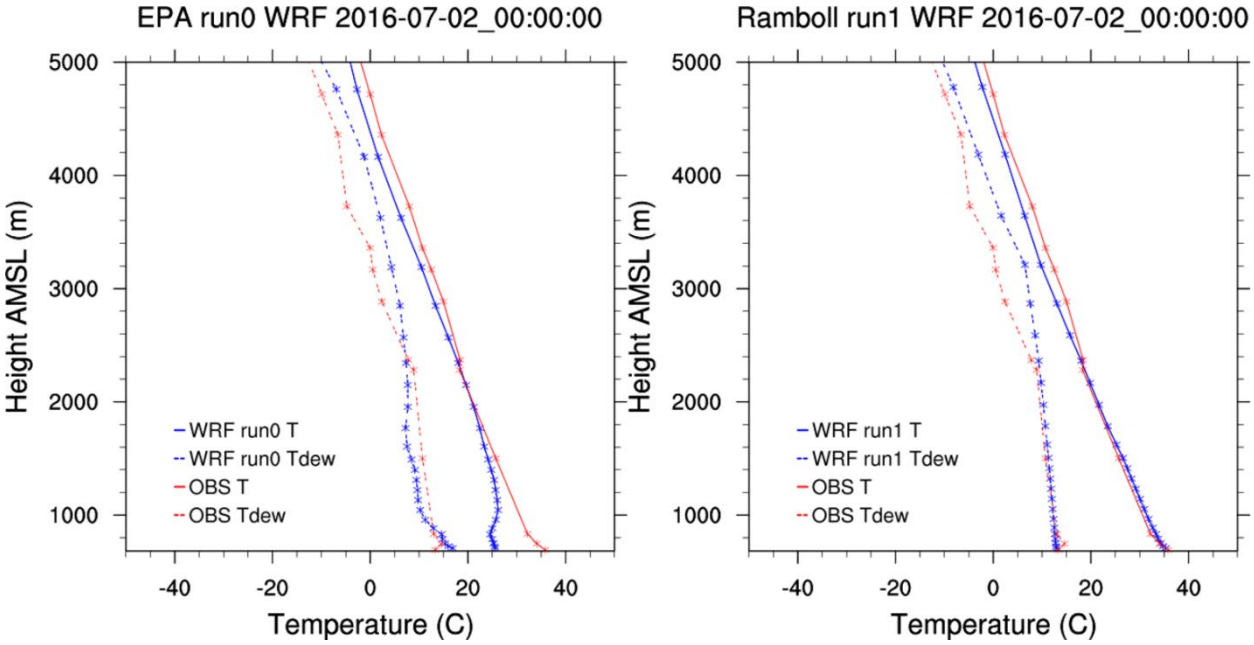

Figure 5-24. Vertical profiles at KVEF from WRF run0 (blue lines in left panel), WRF run1 (blue lines in right panel) and observed (red) temperature (solid lines) and dewpoint temperature (dashed lines) on July 1, 2016 at 5 PM PDT.

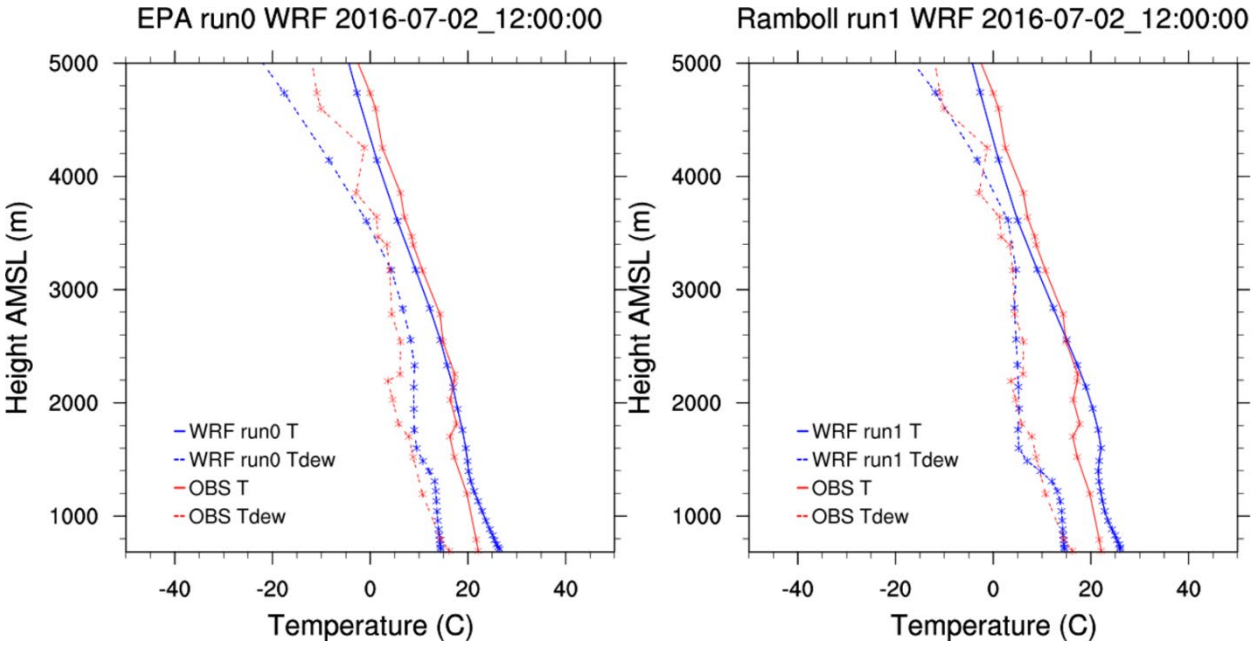

Figure 5-25. Vertical profiles at KVEF of WRF run0 (blue lines in left panel), WRF run1 (blue lines in right panel) and observed (red) temperature (solid lines) and dewpoint temperature (dashed lines) on July 2, 2016 at 5 AM PDT.

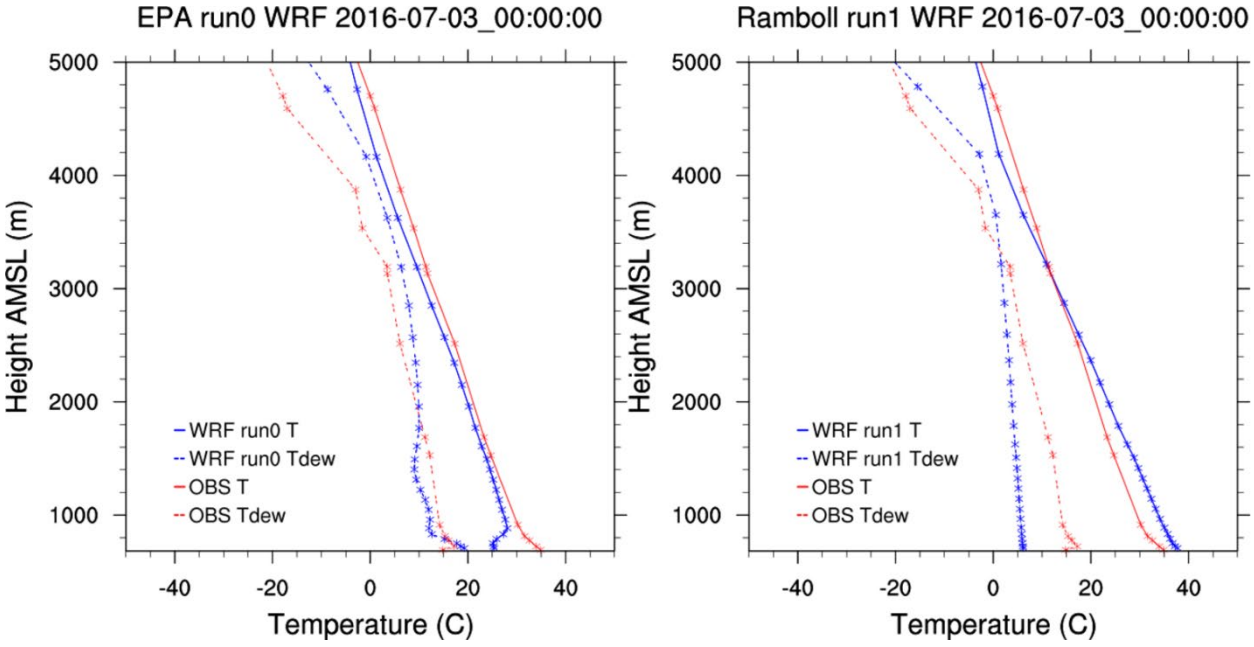

Figure 5-26. Vertical profiles at KVEF from WRF run0 (blue lines in left panel), WRF run1 (blue lines in right panel) and observed (red) temperature (solid lines) and dewpoint temperature (dashed lines) on July 2, 2016 at 5 PM PDT.

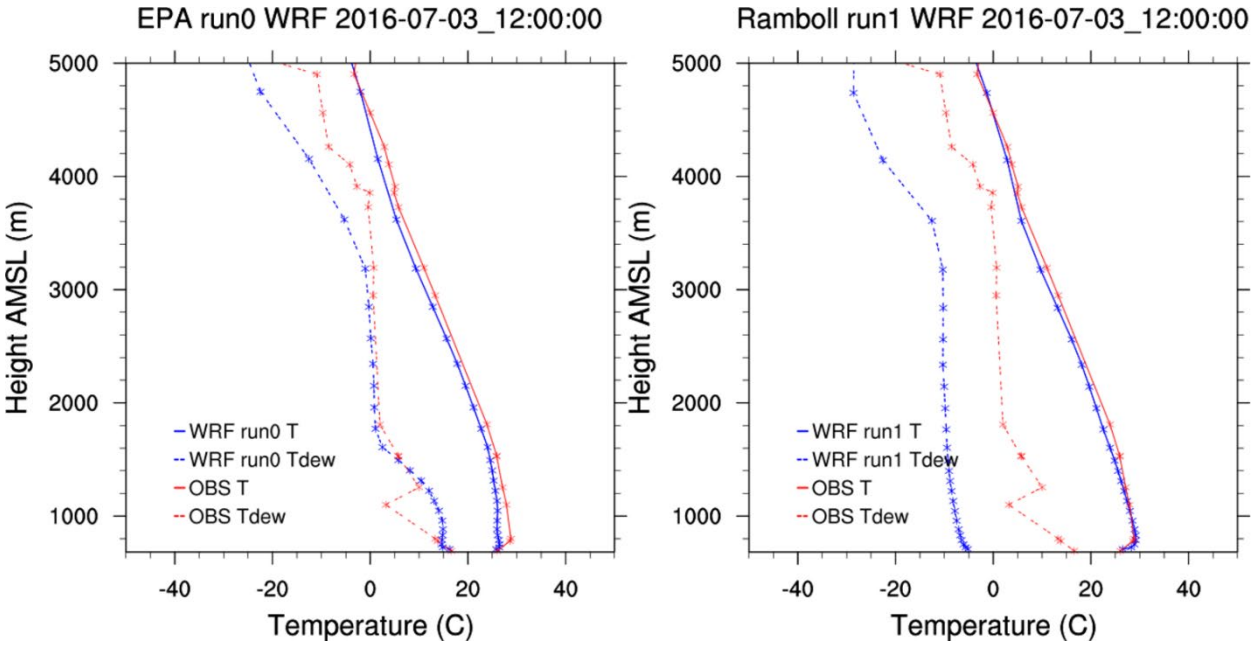

Figure 5-27. Vertical profiles at KVEF from WRF run0 (blue lines in left panel), WRF run1 (blue lines in right panel) and observed (red) temperature (solid lines) and dewpoint temperature (dashed lines) on July 3, 2016 at 5 AM PDT.

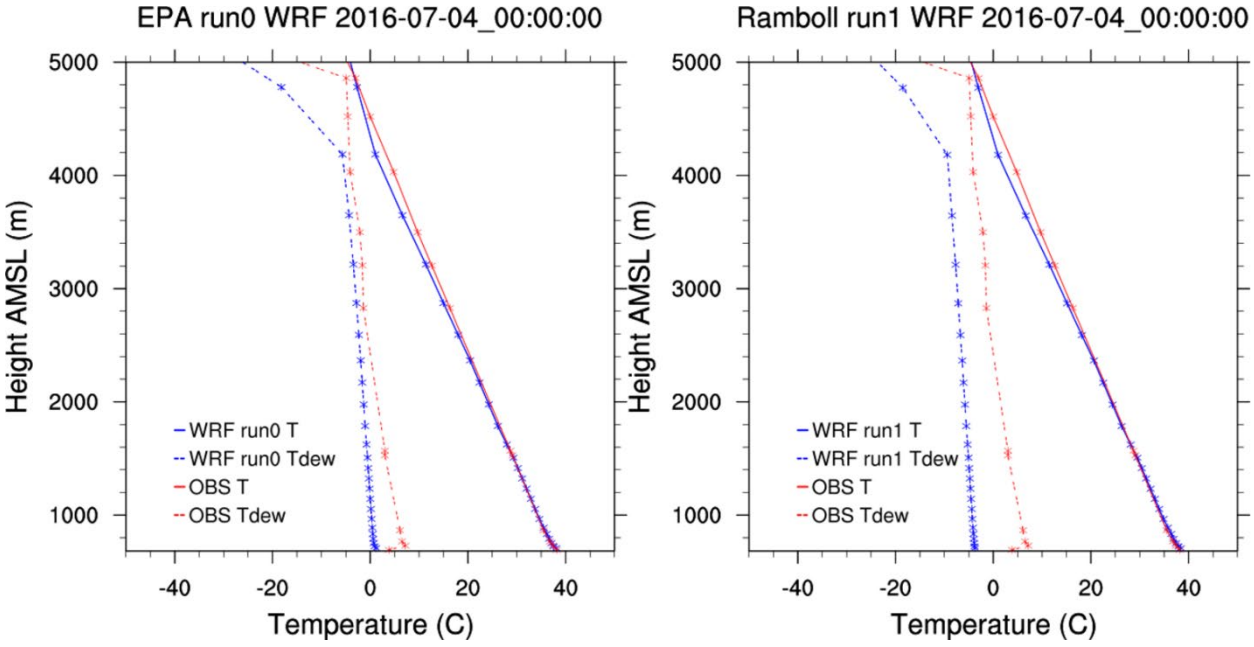

Figure 5-28. Vertical profiles at KVEF from WRF run0 (blue lines in left panel), WRF run1 (blue lines in right panel) and observed (red) temperature (solid lines) and dewpoint temperature (dashed lines) on July 3, 2016 at 5 PM PDT.

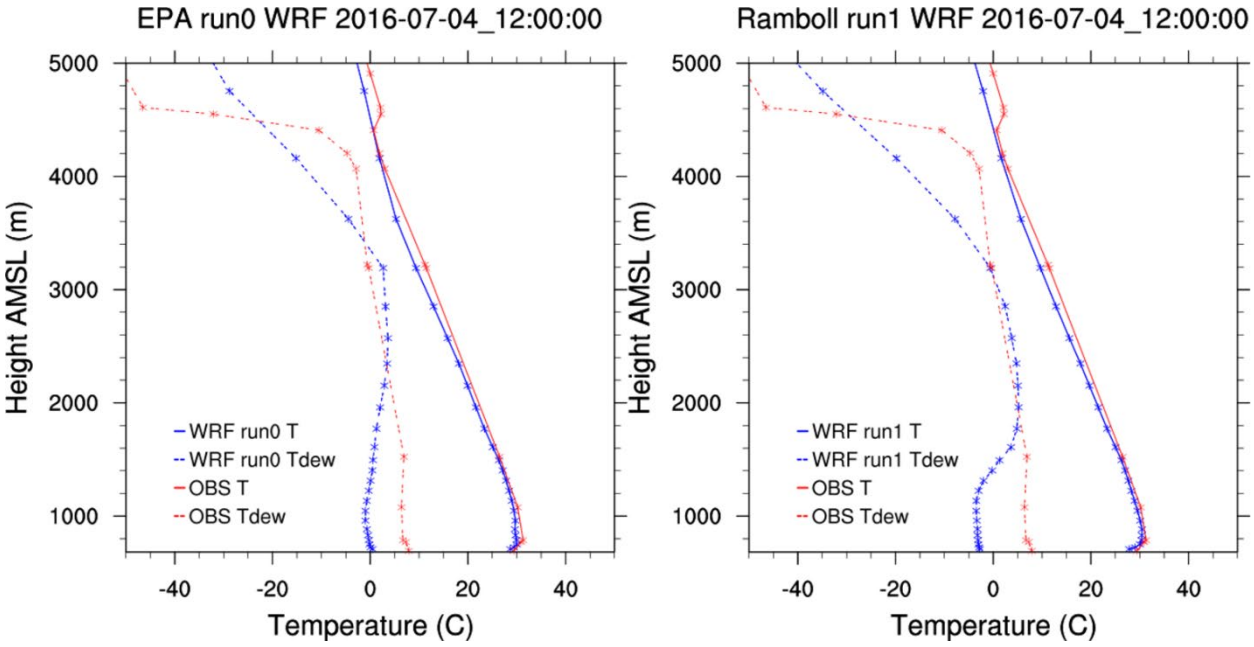

Figure 5-29. Vertical profiles at KVEF from WRF run0 (blue lines in left panel), WRF run1 (blue lines in right panel) and observed (red) temperature (solid lines) and dewpoint temperature (dashed lines) on July 4, 2016 at 5 AM PDT.

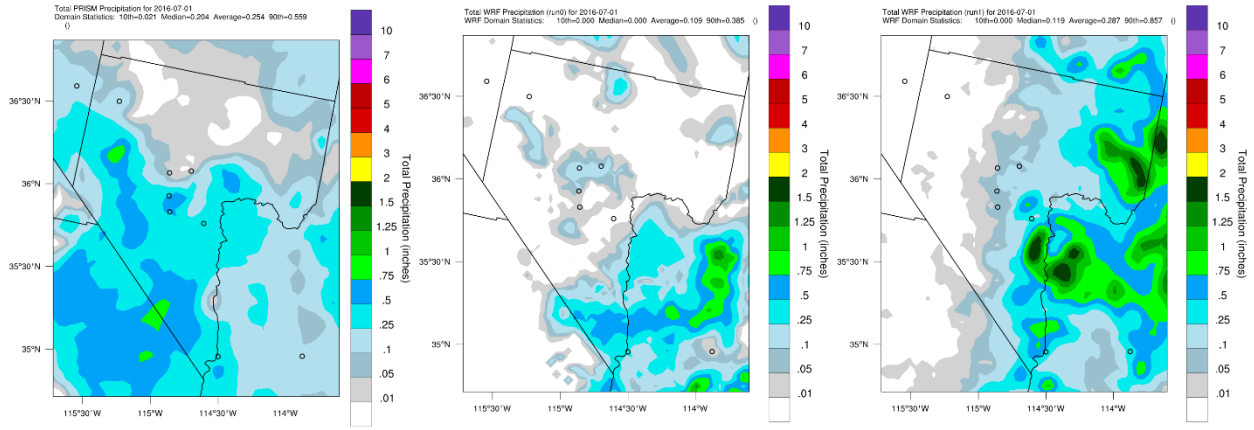

Figure 5-30. Precipitation patterns from PRISM based on observations (left) and modeled by EPA WRF run0 (middle) and Ramboll WRF run1 (right) for the 24-hour period ending July 1, 2016 at 5 AM PDT.

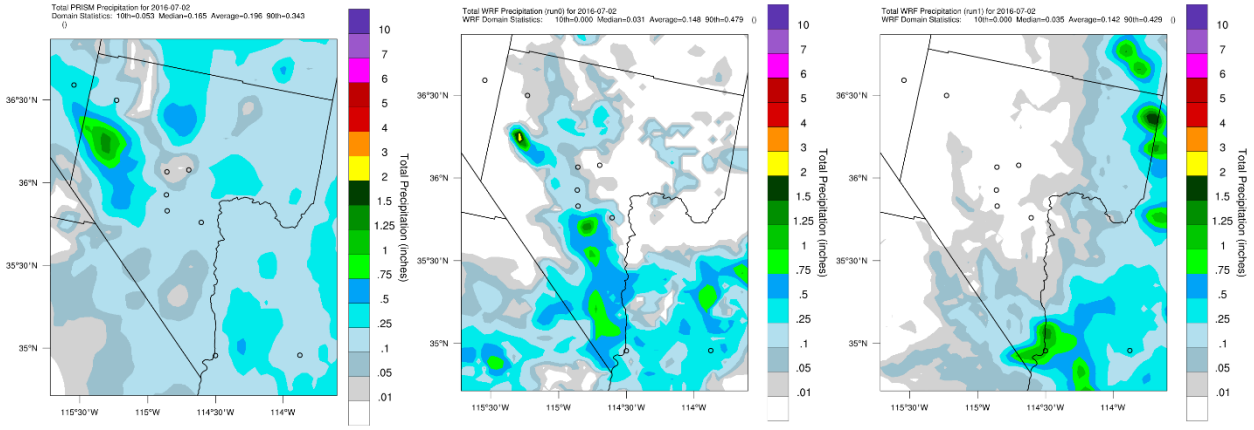

Figure 5-31. Precipitation patterns from PRISM based on observations (left) and modeled by EPA WRF run0 (middle) and Ramboll WRF run1 (right) for the 24-hour period ending July 2, 2016 at 5 AM PDT.

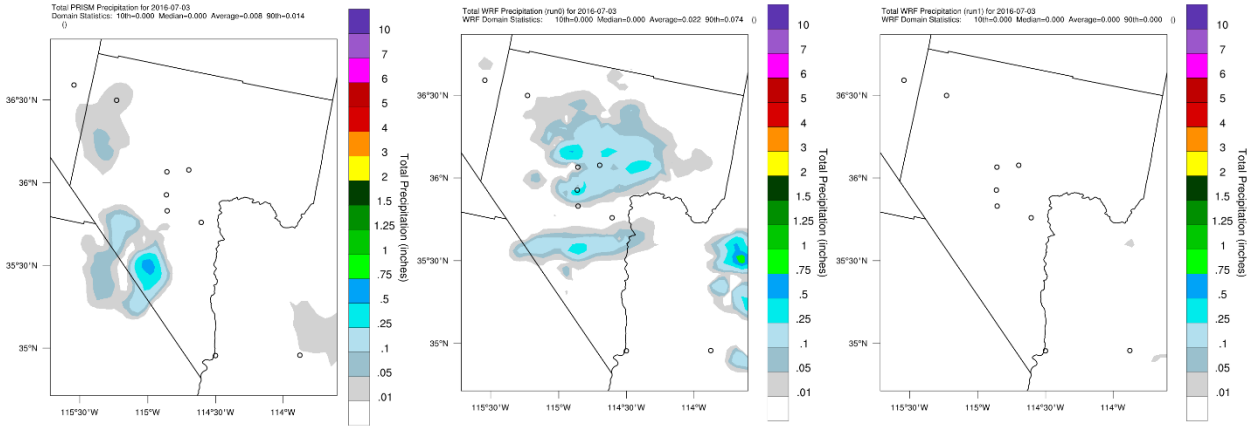

Figure 5-32. Precipitation patterns from PRISM based on observations (left) and modeled by EPA WRF run0 (middle) and Ramboll WRF run1 (right) for the 24-hour period ending July 3, 2016 at 5 AM PDT.

Finally, Figure 5-32 shows the same information ending July 3, 2016 at 5 AM PDT. PRISM shows the LVV as mostly dry during this period, while run0 continues to generate several local showers throughout the LVV with rain amounts exceeding 0.25 inches. By contrast, run1 shows no precipitation in the LVV, in better agreement with PRISM. We exclude PRISM precipitation plots for July 3-4 due to near-zero precipitation in PRISM and zero precipitation across the domain in both run0 and run1.

5.5.5 Phenomenological Evaluation

Figure 5-33 shows a comparison of the 700 mb upper air analysis chart (left panel; height contours in grey; temperature contours shown as red dashed lines; dewpoint temperatures exceeding -4°C shown as green lines) and 700 mb WRF 4 km run0 (center) and WRF 4 km run1 (right) height contours (purple), wind vectors and temperature on July 1, 2016 at 5 PM PDT. The orientation of both WRF run0 and WRF run1 height contours generally agree with those shown on the analysis chart, which indicates a broad region of flat height gradient and weak winds surrounding a weak upper-level low pressure system. Similarly, WRF run0 and WRF run1 wind speed and direction tend to agree

qualitatively with the upper air stations. The evaluation of WRF run0 and run1 at specific locations in the LVV reveal discernable performance differences on this day. Because the large-scale features seem to be represented reasonably well in both WRF simulations, we conclude that these performance differences are primarily due to mesoscale and local scale influences (e.g., convection and interactions with elevated terrain, which influence winds at 700 mb) given the rather weak synoptic scale patterns.

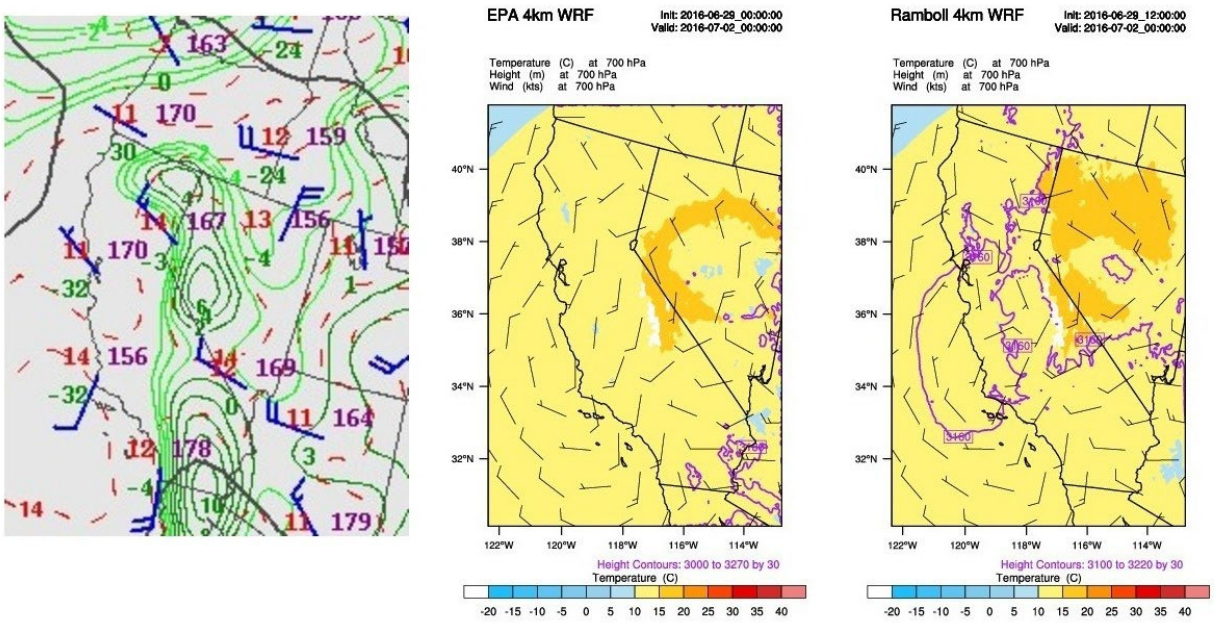

Figure 5-33. Left panel: 700 mb upper air analysis chart (height contours in grey; temperature contours shown as red dashed lines; dewpoint temperatures exceeding -4° C shown as green lines). Center panel: 700 mb WRF 4 km run0 height contours (purple), wind vectors and temperature. Right panel: same as center panel but for WRF 4 km run1. All panels show results for July 1, 2016 at 5 PM PDT.

6.0 BASE AND FUTURE YEAR EMISSION INPUTS

6.1 Emissions Data and Methods

The EPA recently developed the 2016v2 emissions modeling platform (EMP)[14], which includes a full suite of the base year (2016) and future year inventories, ancillary emissions data, and scripts and software for preparing emissions to support air quality modeling. The 2016v2 EMP incorporates emissions based on the updated MOVES3 mobile source model, the 2017 NEI non-point inventory, the WRAP oil and gas inventory, and updated inventories for Canada and Mexico. In addition, the 2016v2 EMP uses a new approach and data to estimate emissions for VCPs implemented in the VCPy framework (Seltzer et al., 2021). For this project, the EMP's 2016fj and 2023fj emission inventories were the primary sources of the CAMx emission inputs (EPA, 2022b)[15]. However, locally specific emissions data from Clark County were used for the CC4c2 modeling domain wherever feasible.

CAMx requires hourly emissions of both anthropogenic and natural sources that have been spatially allocated to the modeling grid cells and chemically speciated for the Carbon Bond version 6 (CB6; Ramboll, 2022b) chemical mechanism used in the model. The anthropogenic source categories include stationary point sources, stationary non-point (area) sources, on-road mobile sources, non-road mobile sources, airports, locomotives, ocean-going vessels, and agricultural sources. The natural sources include biogenic, lightning, oceanic, and wildfires. We processed and prepared the modeling emissions for CAMx using EPA's SMOKE software, version 4.8.1 (UNC, 2020). The sections below describe the development of the 2016 Base Case and 2023 Future Year emission inputs for CAMx modeling.

6.1.1 2016 Base Case Emissions

The sources of 2016 Base Case emissions data for each source category and each grid are presented in Table 6-1. For the 36US3 and 12US2 domains, 2016v2 CMAQ-ready emission inputs were simply converted to CAMx formats using the CMAQ2CAMx processor. Ramboll has previously conducted extensive quality assurance evaluations on these files to ensure proper conversion without loss or gain of emissions and proper formatting. These emission files have been, and continue to be, used extensively by Ramboll in other projects.

For the CC4c2 domain, the 2016fj inventory served as the primary source of emission inputs, augmented with locally specific data for airports and on-road mobile sectors provided by the Clark County DES/DAQ. Ramboll applied EPA's standard 4 km US-wide spatial surrogates to facilitate grid allocation, which EPA developed on the same Lambert map projection and grid system as their 2016 MP and thus exactly aligns with the CC4c2 grid definition. Development of the 2016 CC4c2 domain anthropogenic emission inputs is summarized below:

- On-road mobile source emissions were developed using the SMOKE-MOVES processor with:
  (1) 2016 emission factors generated by EPA's MOVES3 run provided by the 2016v2 EMP;
  (2) County-level vehicle activity data from the 2016v2 EMP; and
  (3) CC4c2 gridded hourly WRF meteorological data.
- Non-road emissions were developed from the 2016v2 EMP using SMOKE.
- 2016fj point source electric generating unit (EGU) emissions included hourly 2016 Continuous Emissions Monitoring System (CEMS) values for NOx and SO_2.

[14] https://www.epa.gov/air-emissions-modeling/2016v2-platform

[15] Technical Support Document: https://www.epa.gov/system/files/documents/2022-02/2016v2_emismod_tsd_february2022.pdf

Table 6-1. Sources of 2016 Base Case inventory sectors by domain.

Source Category	CC4c2 (Clark County 4 km Domain)	12US2 (12 km Domain)	36US3 (36 km Domain)
Area: *ag, rwc, afdust, nonpt, solvents*	EPA 2016fj inventory	EPA 2016fj model-ready files	EPA 2016fj model-ready files
Oil & Gas: *np_oilgas, pt_oilgas*	N/A	EPA 2016fj model-ready files	EPA 2016fj model-ready files
On-road Mobile: *onroad*	SMOKE-MOVES with EPA 2016fj MOVES3 emission factors, VMT, vehicle population and CC4c2 MCIP met.	EPA 2016fj model-ready files	EPA 2016fj model-ready files
Non-road: *Nonroad*	EPA 2016fj inventory	EPA 2016fj model-ready files	EPA 2016fj model-ready files
Airports: *airports*	2017 airport emissions provided by Clark County	EPA 2016fj model-ready files	EPA 2016fj model-ready files
CMV: *cmv_c1c2, cmv_c3*	N/A	EPA 2016fj model-ready files	EPA 2016fj model-ready files
Locomotives: *rail*	EPA 2016fj inventory	EPA 2016fj model-ready files	EPA 2016fj model-ready files
EGU Point: *ptegu*	EPA 2016fj model-ready files: all emissions in this sector are elevated (no low-level contribution)	EPA 2016fj model-ready files	EPA 2016fj model-ready files
Point: *ptnonipm*	EPA 2016fj model-ready files: all emissions in this sector are elevated (no low-level contribution)	EPA 2016fj model-ready files	EPA 2016fj model-ready files
Non-US: *Canada/Mexico/Offshore*	N/A	EPA 2016fj model-ready files	EPA 2016fj model-ready files
Fires	EPA 2016fj PTFIRE3D model-ready files	EPA 2016fj PTFIRE3D model-ready files	EPA 2016fj PTFIRE3D model-ready files
Biogenic	2016 BEIS4/BELD6 with CC4c2 MCIP met	2016 BEIS4/BELD6 with 12US2 MCIP met	2016 BEIS4/BELD6 with 36US3 MCIP met
Lightning NOx	12-km virtual point sources from Ramboll's LNOx processor and EPA 2016 12US2 WRF meteorology		N/A

- Non-point emissions from the EPA 2016v2 EMP were processed with SMOKE. The non-point source category includes area-wide residential, commercial, and industrial emissions, VCPs, agricultural sources, and other non-point sectors. As noted above, the 2016v2 EMP used a new approach and data to estimate emissions for VCP sources. EPA back-casted all other non-point emissions inputs from the 2017 NEI to the year 2016.
- The Clark County Department of Aviation (DOA) provided 2017 emissions for commercial aviation, which includes Harry Reid (McCarran) International Airport, North Las Vegas Airport, and Henderson Executive Airport. Federal aviation emissions consist entirely of emissions from Nellis Air Force Base (NAFB), which provided 2017 emissions to DES/DAQ. The 2017 emissions from aircraft operations were used directly for the 2016 Base Case and processed with SMOKE.

6.1.2 Biogenic Emissions

Biogenic VOC and NOx emissions were initially based on BEIS3.7 to be consistent with the EPA 2016v2 MP. BEIS is built into SMOKE and can be downloaded from the SMOKE website. The inputs to BEIS include: (1) landcover distributions that define emission factors according to biomass type, and (2) gridded hourly meteorology as biogenic VOC emissions are sensitive to temperature and solar radiation. BEIS3.7 was used in conjunction with the Biogenic Landcover Database version 5 (BELD5) and gridded hourly meteorology from the WRF 2016 simulation as described in Section 5. BELD5 data are provided by EPA covering the entire US at 4-km grid scale that exactly matches the 12US2 mapping conventions and the CC4c2 grid specifications. Therefore, no special mapping of BELD5 data to the CC4c2 grid was necessary.

BEIS3.6/BELD4, BEIS4/BELD6, and MEGAN3.2 were later evaluated as alternatives for CAMx sensitivity testing (see Section 8.4). Each of these models resulted in substantially different estimates in biogenic VOC emissions in Clark County. While modeled biogenic NOx and VOC emission rates have trended downward with succeeding versions from BEIS3.6 to BEIS4, the huge range of emission rates among these versions illustrates the remaining uncertainty in desert biogenic emission estimates and related vegetative characterization over just the last few years. Most notably, VOC emissions varied by nearly 1000-fold between BEIS3.6 and MEGAN3.2. Ultimately, we replaced BEIS3.7/BELD5 with the latest BEIS4/BELD6 biogenic emissions platform, which reduced both rural and urban isoprene emissions below both of its predecessors, in agreement with reports from EPA's early testing for the western US (Ramboll, 2022c). EPA graciously processed BELD6 vegetative cover datasets for the 12US2 and CC4c2 grids for our use with BEIS4. Ramboll processed BEIS4 biogenic emissions on the 36US3/12US2/CC4c2 grid system for the entirety of the April-August modeling period.

Table 6-2 lists 2016 summer monthly average biogenic emissions (TPD) on the CC4c2 grid as determined from the four different biogenic emission platforms. Section 8.4.10 provides additional details on biogenic emission comparisons and modeling results.

6.1.3 Other Natural Source Emissions

EPA did not develop NOx emissions from lightning for their 2016v2 MP. Therefore, Ramboll independently developed lightning NOx emissions using a CAMx processor called LNOx available from the CAMx website[16]. The LNOx processor uses WRF output fields defining convective activity (cloud top heights and convective available potential energy) to determine location, timing, and frequency of lightning to generate three-dimensional NOx emissions. LNOx emissions are developed as virtual point sources.

[16] https://www.camx.com/download/support-software/

Table 6-2. 2016 summer monthly biogenic emissions (TPD) estimated for the CC4c2 modeling domain from four biogenic modeling systems.

Biogenic Model	May	June	July	August	Average
	NOx				
BEIS3.6/BELD4 (2016v1)	6	9	9	9	8
BEIS3.7/BELD5 (2016v2)	5	7	8	7	7
BEIS4/BELD6	5	7	8	7	7
MEGAN3.2	17	32	30	27	27
Biogenic Model	**VOC**				
BEIS3.6/BELD4 (2016v1)	850	1,936	2,128	1,737	1,663
BEIS3.7/BELD5 (2016v2)	288	654	717	586	561
BEIS4/BELD6	71	154	167	139	133
MEGAN3.2	2	3	15	26	12
Biogenic Model	**Isoprene**				
BEIS3.6/BELD4 (2016v1)	145	294	304	258	250
BEIS3.7/BELD5 (2016v2)	57	114	118	101	97
BEIS4/BELD6	13	23	22	20	19
MEGAN3.2	1	1	7	2	3
Biogenic Model	**Terpene**				
BEIS3.6/BELD4 (2016v1)	253	582	653	534	505
BEIS3.7/BELD5 (2016v2)	64	148	165	135	128
BEIS4/BELD6	16	36	40	33	31
MEGAN3.2	1	1	4	2	2

Given potentially very different meteorological realizations of convective activity between the 12US2 and CC4c2 grids (as described in Section 5 for July 1-2), we adopted 12US2 LNOx emissions developed previously for another Ramboll project, which were based on EPA's WRF data. As grid-independent point sources, LNOx emits into both the 12US2 and CC4c2 grids. LNOx data are sparse in time and space and therefore the use of 12 km LNOx emissions within the CC4c2 grid does not materially affect the CC4c2 ozone results.

Open land fires (e.g., wildfires) were based on the EPA 2016v2 inventory. For fires within the United States, EPA estimated emissions using the Satellite Mapping Automated Reanalysis Tool for Fire Incident Reconciliation version 2 (SMARTFIRE2) and the BlueSky Framework (EPA, 2022b). EPA developed fire emissions from outside of the United States using the Fire Inventory from NCAR (FINN[17]). The 2016v2 platform provides three-dimensional layered CMAQ model-ready fire emissions with plume rise calculated by SMOKE. These emission files were converted into CAMx point format using the CMAQ2CAMx converter, which retained the layer-by-layer distribution of smoke emissions.

6.2 2023 Future Case Emissions

The procedures used to develop the Clark County CAMx 2023 emission inputs were similar to those for the 2016 Base Case. The sources of 2023 Future Case emissions data for each source category and each grid are presented in Table 6-3.

[17] https://www2.acom.ucar.edu/modeling/finn-fire-inventory-ncar.

Table 6-3. Sources of 2023 Future Year inventory sectors by domain.

Source Category	CC4c2 (Clark County 4 km Domain)	12US2 (12 km Domain)	36US3 (36 km Domain)
Area: *ag, rwc, afdust, nonpt, solvents*	EPA 2023fj inventory	EPA 2023fj model-ready files	EPA 2023fj model-ready files
Oil & Gas: *np_oilgas, pt_oilgas*	N/A	EPA 2023fj model-ready files	EPA 2023fj model-ready files
On-road Mobile: *onroad*	SMOKE-MOVES with EPA 2023fj MOVES3 emission factors, Clark County VMT, vehicle population and CC4c2 MCIP met.	EPA 2023fj model-ready files	EPA 2023fj model-ready files
Non-road: *Nonroad*	EPA 2023fj inventory	EPA 2023fj model-ready files	EPA 2023fj model-ready files
Airports: *airports*	2023 airport emissions provided by Clark County	EPA 2023fj model-ready files	EPA 2023fj model-ready files
CMV: *cmv_c1c2, cmv_c3*	N/A	EPA 2023fj model-ready files	EPA 2023fj model-ready files
Locomotives: *rail*	EPA 2023fj inventory	EPA 2023fj model-ready files	EPA 2023fj model-ready files
EGU Point: *ptegu*	EPA 2023fj model-ready files: all emissions in this sector are elevated (no low-level contribution)	EPA 2023fj model-ready files	EPA 2023fj model-ready files
Point: *ptnonipm*	EPA 2023fj model-ready files: all emissions in this sector are elevated (no low-level contribution)	EPA 2023fj model-ready files	EPA 2023fj model-ready files
Non-US: *Canada/Mexico/Offshore*	N/A	EPA 2023fj model-ready files	EPA 2023fj model-ready files
Fires	EPA 2016fj PTFIRE3D model-ready files	EPA 2016fj PTFIRE3D model-ready files	EPA 2016fj PTFIRE3D model-ready files
Biogenic	2016 BEIS4/BELD6 with CC4c2 MCIP met	2016 BEIS4/BELD6 with 12US2 MCIP met	2016 BEIS4/BELD6 with 36US3 MCIP met
Lightning NOx	12-km virtual point sources from Ramboll's LNOx processor and EPA 2016 12US2 WRF meteorology		N/A

The 2023 36US3 and 12US2 emissions were based on EPA's CMAQ-ready 2023fj emissions, converted to CAMx using the CMAQ2CAMx processor. Natural emissions and fires were held constant at 2016 values. Development of the 2023 CC4c2 domain anthropogenic emission inputs is summarized below:

- On-road mobile source emissions were developed using the SMOKE-MOVES processor using:
  (1) 2023 emission factors generated by EPA's MOVES3 run provided by the 2016v2 EMP;
  (2) Clark County 2023 vehicle miles traveled (VMT) and vehicle population data provided by DES/DAQ based on travel demand modeling;
  (3) Clark County 2023 vehicle starts and hours of off-network idling calculated using VMT ratios;
  (4) 2023 county-level vehicular activity data for all other counties from the 2016v2 EMP; and
  (5) CC4c2 gridded hourly WRF meteorological data.
- Non-road emission inputs were developed from the 2016v2 EMP for 2023 using SMOKE.
- Non-point emissions from the 2016v2 EMP for 2023 were processed with SMOKE. The non-point source category includes the same sources as those for the 2016 Base Case and was projected using various trends and procedures by EPA (2022b).
- The Clark County DOA provided 2023 projected emissions for commercial aviation and NAFB provided 2022 emissions, which were projected to 2023 by DES/DAQ. Both commercial and Federal aviation emissions from aircraft operations were processed with SMOKE.
- For other anthropogenic source categories, SMOKE was used to process the 2023fj emissions for the CC4c2 domain.

6.3 Quality Assurance

Quality assurance (QA) of emissions datasets is a critical step in performing air quality modeling studies. Because emissions processing is time consuming and involves complex manipulation of many different types of large databases, rigorous QA measures are a necessity to prevent errors in emissions processing from propagating to the PGM application. Ramboll performed a multistep emissions QA approach as developed for the WRAP 2002 modeling (Adelman, 2004) and following the procedures in EPA's modeling guidance (EPA, 2018a, pp. 60) and Section 2.20 of the SMOKE User's Manual (UNC, 2020, pp. 92). The following specific steps were performed to assure data quality:

1. The EPA 2016v2 platform data were reviewed and summarized to compare against any corresponding local inventory data compiled by Clark County for representativeness.
2. SMOKE is designed with flexible QA capabilities to generate standard and custom reports for checking the emissions modeling process. It includes reporting features to keep track of the adjustments at each processing stage and ensure that data integrity is not compromised. SMOKE-generates diagnostic files and summary reports were carefully reviewed for error and warning messages.
3. Visual displays were generated that include: (1) spatial plots of the emissions for each ozone precursor species (e.g., NOx, VOC, and CO); (2) summary tables of emissions for ozone precursors by major source category. This QA information was examined against the original point and area source data and summarized in an overall QA assessment.
4. Each set of biogenic emissions were carefully reviewed to ensure reasonable results consistent with input data, other modeling projects in the western US, and Ramboll's direct experience.

6.4 Summary of Emissions Results

Tables 6-4 and 6-5 present the 2016 and 2023 July weekday daily average anthropogenic emissions across the entirety of Clark County in tons per day (TPD). We calculated the average ozone season day emissions by averaging the daily emissions over the weekdays (Monday through Friday) in July

excluding July 4th holiday, which was modeled as if it was a Sunday. The results were compared against the EPA 2016v2 daily county-level emission reports[18] for QA checks, and they matched well for all sectors except on-road mobile and airports, which are based on local data developed in this study. Figure 6-1 compares daily average NOx and VOC emissions by major anthropogenic category. On-road and non-road mobile sectors were the dominant anthropogenic categories for NOx in 2016, followed by airports and industrial point source categories. There is a significant decline in on-road mobile NOx emissions between 2016 and 2023 (-59%), primarily due to fleet turnover. There are also reductions in NOx emissions between 2016 and 2023 for non-road mobile, locomotives, and industrial point sources. NOx emissions from airports and non-point area source categories increased slightly in 2023.

For VOCs, the non-point sector was the dominant anthropogenic category, followed by non-road and on-road mobile sources in 2016. On-road and non-road mobile VOC emissions decrease the most (-44% and -6%, respectively) between 2016 and 2023. VOC emissions increased slightly for the non-point category in 2023.

Table 6-4. July weekday average 2016 and 2023 anthropogenic NOx emissions (TPD) over the entirety of Clark County by major source sector.

Source Category	2016 NOx	2023 NOx
Point source	14.6	9.7
Nonpoint source	4.0	4.1
On-road mobile	48.7	20.2
Non-road mobile	42.4	24.5
Airports (commercial & Federal)	12.7	16.6
Locomotives	1.3	1.1
Fires	0.0	0.0
TOTAL	**123.7**	**76.2**

Table 6-5. July weekday average 2016 and 2023 anthropogenic VOC emissions (TPD) over the entirety of Clark County by major source sector.

Source Category	2016 VOC	2023 VOC
Point source	2.1	1.8
Nonpoint source	57.0	60.8
On-road mobile	27.8	17.7
Non-road mobile	29.5	27.6
Airports (commercial & Federal)	2.3	3.1
Locomotives	0.1	0.0
Fires	0.3	0.3
TOTAL	**119.1**	**111.3**

[18] Available at https://gaftp.epa.gov/Air/emismod/2016/v2/reports/county_daily/

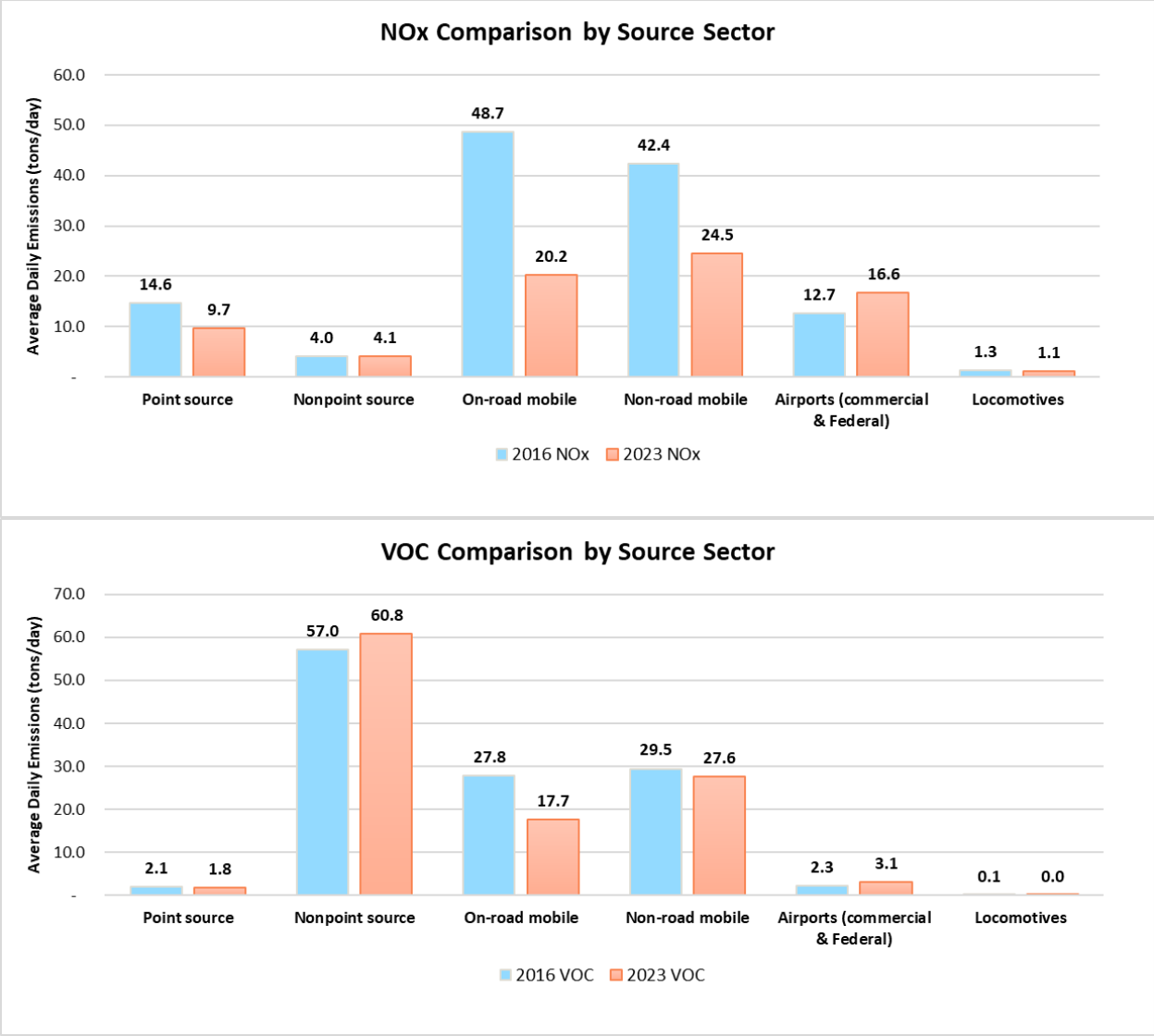

Figure 6-1. Comparison of July weekday average anthropogenic NOx (top) and VOC (bottom) emissions (TPD) between 2016 and 2023 over the entirety of Clark County by major source sector.

Figures 6-2 through 6-6 show the spatial distribution of 2016 NOx and VOC emissions and their differences in 2023. Figure 6-2 displays emissions for the on-road mobile category. The emissions are seen along major roadways, which confirms correct spatial allocation and decline in the future year. Figure 6-3 shows emissions for the non-road category, with most occurring over the populated urban area and a decline in 2023. Figure 6-4 displays emissions for the non-point category with hotspots over the Las Vegas Valley and emission increases for 2023. Figures 6-5 and 6-6 show emissions for airport and locomotive sectors, respectively.

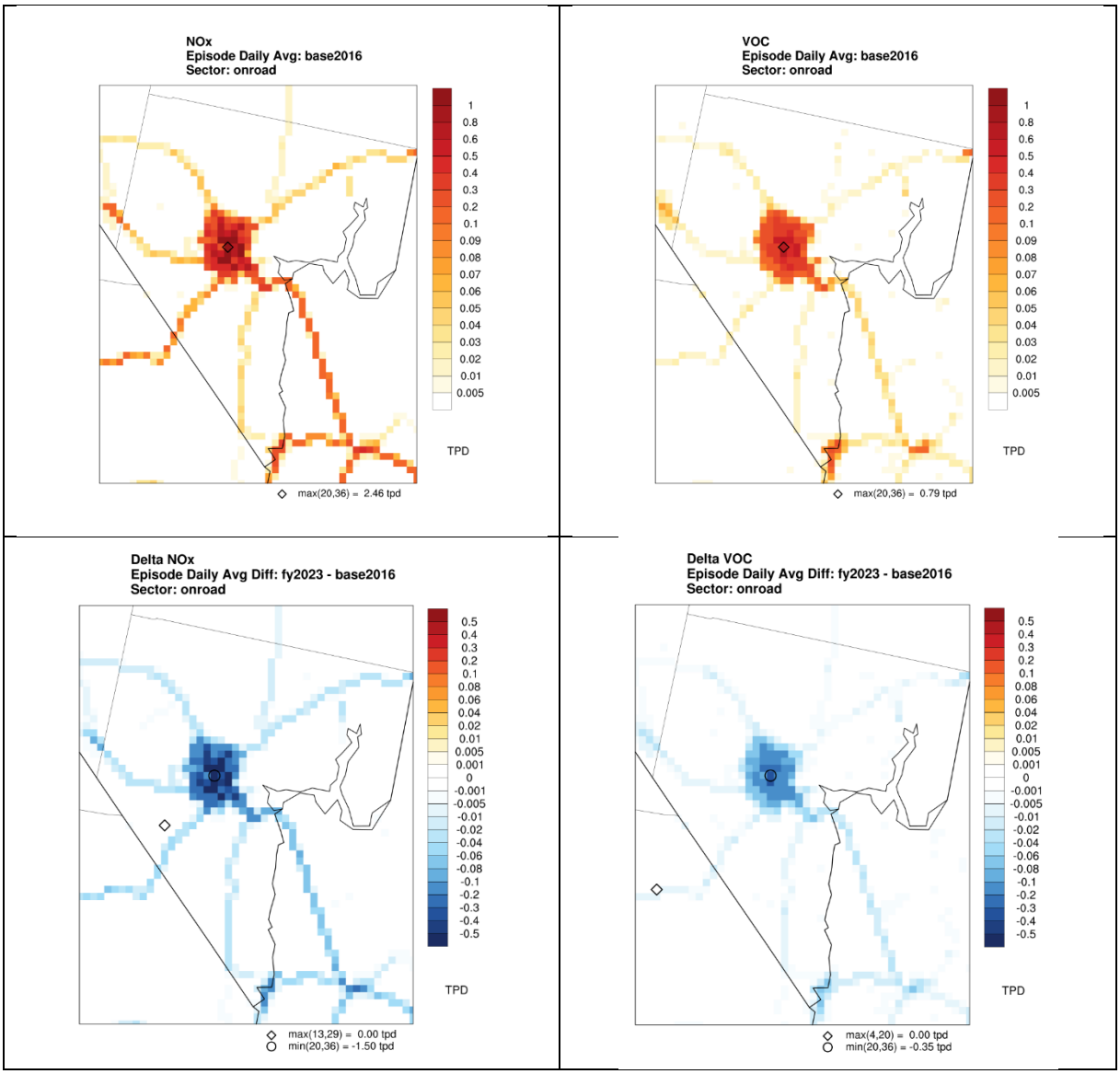

Figure 6-2. Spatial map of daily average NOx (left) and VOC (right) emissions for the on-road mobile category over the CC4c2 grid; 2016 (top) and differences between 2023 and 2016 (2023-2016, bottom).

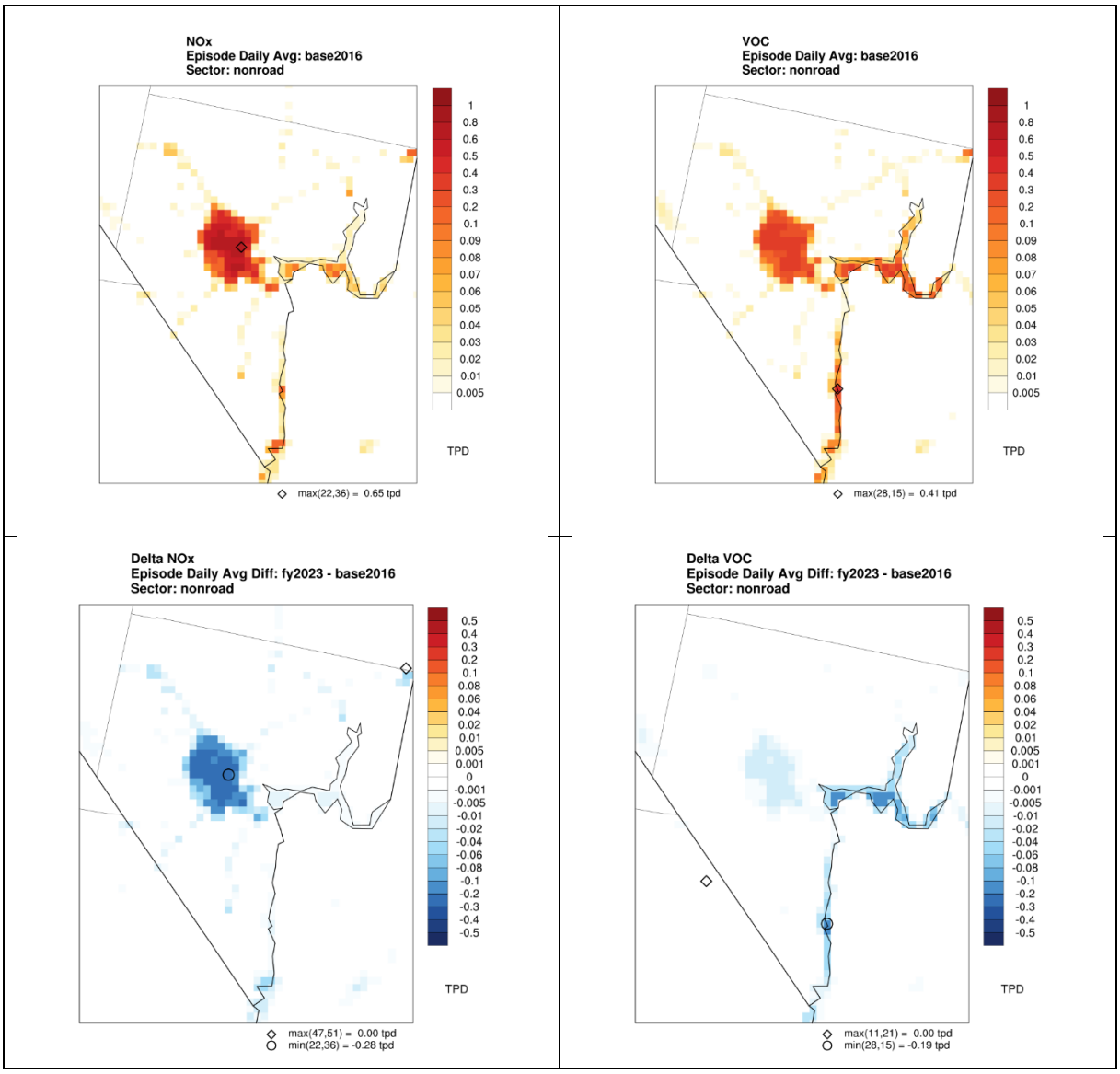

Figure 6-3. Spatial map of daily average NOx (left) and VOC (right) emissions for the non-road category over the CC4c2 grid; 2016 (top) and differences between 2023 and 2016 (2023-2016, bottom).

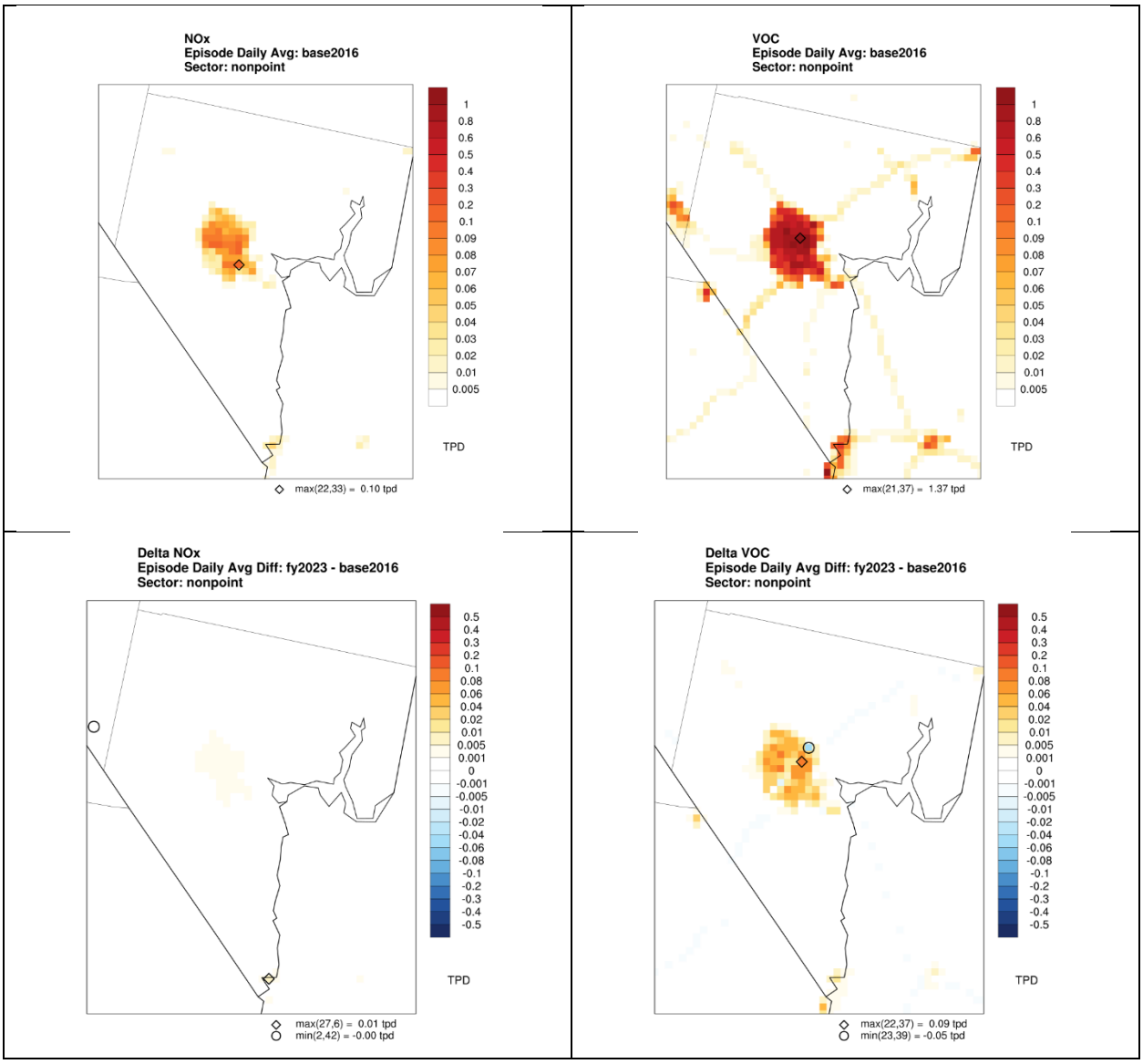

Figure 6-4. Spatial map of daily average NOx (left) and VOC (right) emissions for the non-point category over the CC4c2 grid; 2016 (top) and differences between 2023 and 2016 (2023-2016, bottom).

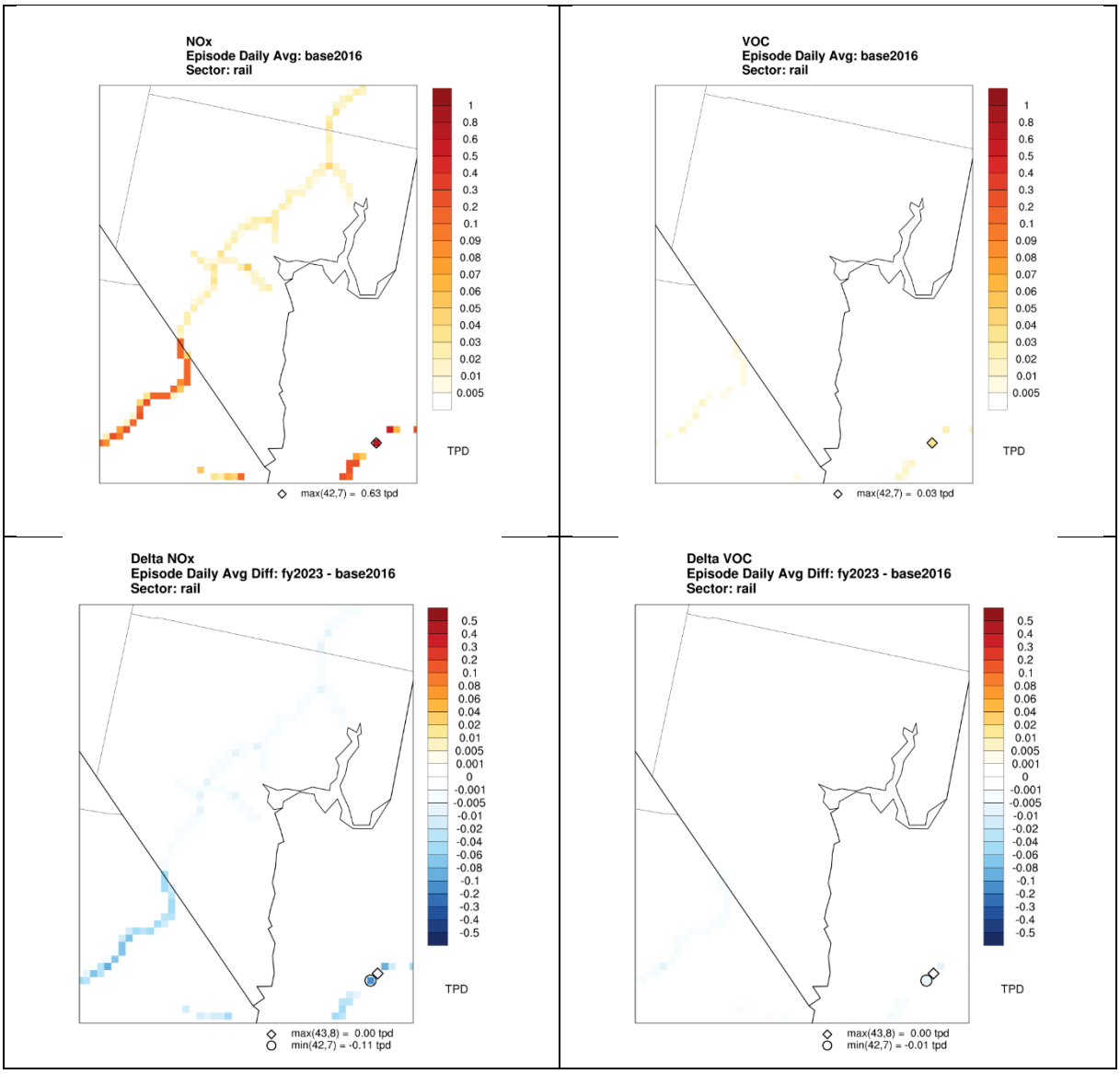

Figure 6-5. Spatial map of daily average NOx (left) and VOC (right) emissions for locomotives over the CC4c2 grid; 2016 (top) and differences between 2023 and 2016 (2023-2016, bottom).

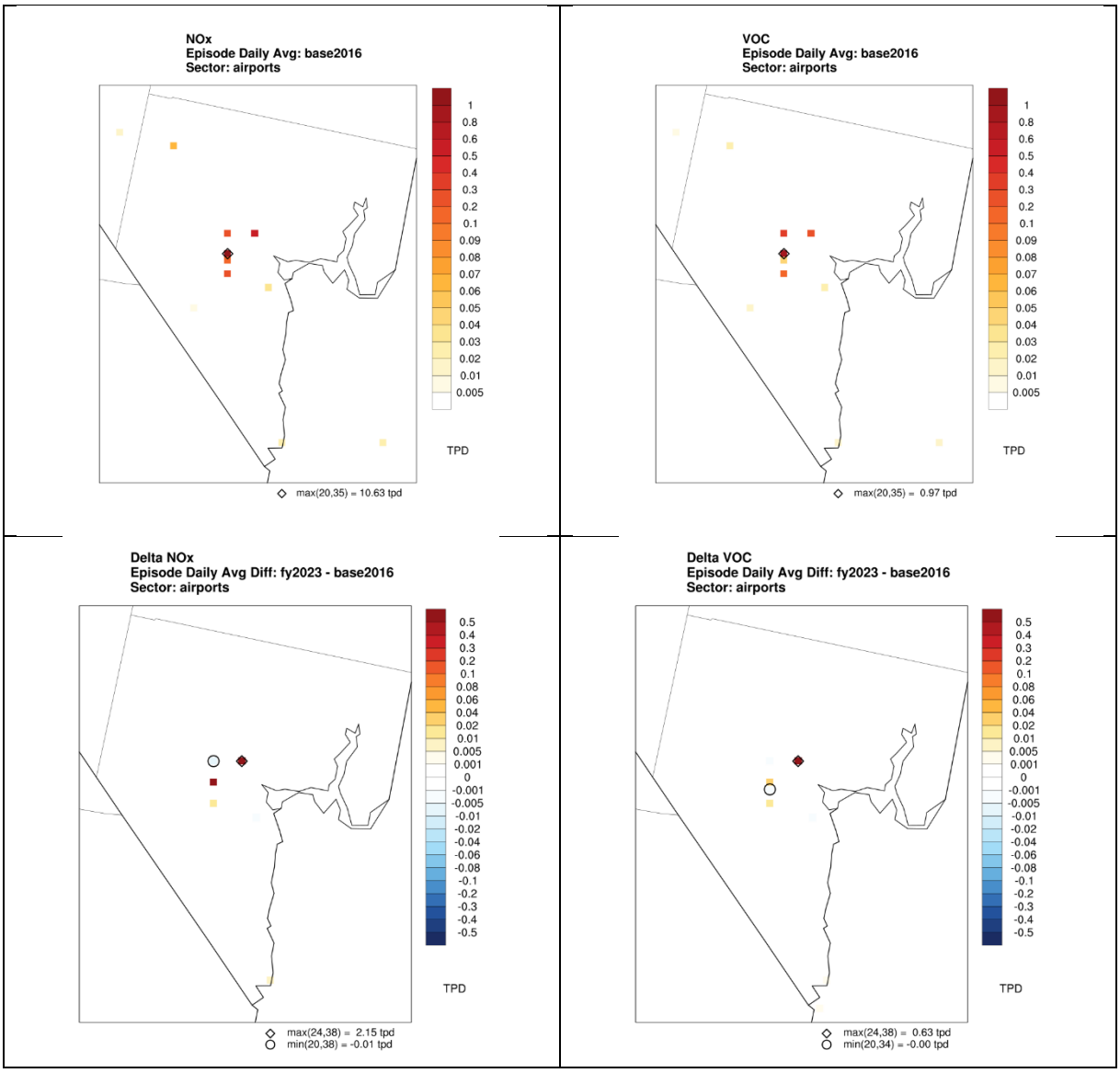

Figure 6-6. Spatial map of daily average NOx (left) and VOC (right) emissions for airports in the CC4c2 domain; 2016 (top) and differences between 2023 and 2016 (2023-2016, bottom).

7.0 OTHER MODEL INPUTS

7.1 CAMx-Ready Meteorological Inputs

As part of the development of the 2016v2 modeling platform, EPA generated CAMx-ready meteorological inputs for the 36US3 and 12US2 grids using WRF v3.8 and WRFCAMx v4.7. Ramboll has reviewed and used these meteorological inputs for several other projects. For this project, we used the most recent version of WRFCAMx (v5.2) to map the 4 km meteorological output data from the large WRF domain (Figure 5-1) onto the CC4c2 domain (Figure 4-2).

WRFCAMx is a program that translates WRF meteorological output fields into the input format required by CAMx. Additionally, WRFCAMx calculates turbulent vertical exchange coefficients (Kv) that define the rate and depth of vertical mixing in CAMx. Finally, WRFCAMx also maps specific fractional land use/landcover (LU/LC) categories from WRF to the categories defined within CAMx. WRFCAMx processing steps include:

- Reading the meteorological model output files and translating from the Coordinated Universal Time (UTC) to local time zones (if specified).
- Extracting (and interpolating as needed) meteorological data to the CAMx modeling domain.
- Aggregating or "collapsing" meteorological data from the WRF vertical layer structure to a coarser CAMx vertical grid (if specified).
- Computing Kv fields, mapping LU/LC, and diagnosing other variables specifically needed by CAMx or its pre-processors.
- Generating the CAMx-ready meteorological fields.

In addition to various updates, a novel aspect of WRFCAMx v5.2 is the ability to produce CAMx-ready meteorology in netCDF format, which is more versatile to manipulate and view than the original Fortran binary format generated with version v4.7. CAMx is able to read a mix of binary and netCDF input files. Table 7-1 summarizes the WRFCAMx option settings used for the CC4c2 domain in this study.

Table 7-1. WRFCAMx settings for Clark County CC4c2 domain.

WRFCAMx Option	Settings
CAMx nested grid	True: automatically adds nested grid buffer cells
Diagnostic fields	True: to support QA/QC and certain emission programs
Sea ice adjustment	False: no sea ice in the domain
KV Method	All: up to 3 methods are allowed depending on the WRF configuration (MYJ, YSU, CMAQ)
Sub-grid Convection	None: diagnoses sub-grid convective cloud cover (usually for grid resolution > 10 km)
Sub-grid stratiform	False: diagnoses sub-grid stratiform cloud cover (usually for grid resolution > 10 km)
Time zone	UTC
Layer mapping	Use all WRF layers, no collapsing

WRFCAMx diagnoses the vertical eddy diffusivity (Kv) values from WRF wind, temperature, and boundary layer parameters when turbulent kinetic energy (TKE) is not available in the WRF output (as is the case in all EPA WRF runs). Often the boundary layer treatments in WRF do not resolve urban landscapes sufficiently or correctly to maintain elevated mixing during the night, therefore another

program is used to address this limitation. The program KVPATCH is a CAMx pre-processor that applies spatially varying minimum Kv profiles near the surface to account for the effects of the urban heat island that can result in enhanced vertical mixing near the surface. KVPATCH first sets a minimum Kv value in the surface layer (layer 1) between 0.1 to 1.0 m^2/s depending on the fraction urban land use present in a grid cell. Then a second treatment diagnoses a minimum vertical Kv profile above that through a user-specified depth, usually 100 to 200 m.

For the 12US2 domain, EPA selected the "YSU" Kv scheme for the 2016v2 CAMx modeling platform with a minimum Kv of 0.1 m^2/s. They applied KVPATCH to reset a minimum Kv profile for urban grid cells within the lowest 200 m of the surface. To be consistent, Ramboll also selected the YSU mixing scheme, however we set the depth of the Kv adjustment to 100 m to reflect stronger nightly inversions in cold, dry air reflective of western US desert environments. Also, as part of our quality assurance and quality control (QA/QC) steps, we found that WRF designates highways as "urban" land use. Since the grid cell areas covered by highways are very small (much less than 1%), KVPATCH was modified to apply the patch only to regions where urban land use is greater than 10% of grid cell area.

KVPATCH also includes an option that enhances Kv profiles through the depth of convective clouds. The purpose of this is to increase afternoon vertical mixing when and where convective clouds occur within the grid. WRF often collapses boundary layer depths during the afternoon under such convection due to surface cooling, when in fact such clouds enhance vertical turbulent exchange. A clear example of this is described below. We configured KVPATCH to bypass this convective mixing patch.

7.2 CMAQ-Ready Meteorological Inputs

WRF output was also processed using MCIP v5.2.1 to generate CMAQ-ready inputs for the CC4c2 domain. These inputs are necessary to develop weather-sensitive on-road and biogenic emissions using SMOKE-MOVES, BEIS and/or MEGAN, respectively. We also conducted QA reviews on the resulting MCIP dataset.

7.3 Quality Assurance

7.3.1 WRFCAMx

We performed a qualitative analysis of the WRFCAMx data from the EPA WRF application (referred to as "run0" in Section 5) for selected days to ensure the results were reasonable and consistent with WRF data. Selected fields such as the surface temperature, 10-meter winds, precipitation, YSU planetary boundary layer (PBL) depth, and total cloud optical depth generated from WRFCAMx were plotted for selected days (July 1 and 2, 2016), a period noted for poor meteorological replication in the LVV. This analysis should not be construed as a meteorological model performance, as there are no comparisons to observed conditions, but rather it served a visual check for obvious numerical or translation problems between WRF and CAMx.

On June 30 simulated precipitation occurred over Lake Mead and Arizona, southeast of Las Vegas, at around 4 PM Pacific Standard Time (PST), which moved south to southeast before leaving the CC4c2 domain at around 10 PM. Figure 7-1 shows the start of this precipitation episode with the wind vector field overlaid. Wind vectors show that surface wind divergence can be attributed in part to the down drafts associated with the precipitation event (Figure 7-1), as well as convergence/divergence patterns associated with terrain-induced flow. Horizontal wind speeds in the LVV affected by downdrafts exceeded 15 m/s. However, during the hours when high ozone concentrations are expected (11 AM to 3 PM), some stagnation occurred in the region.

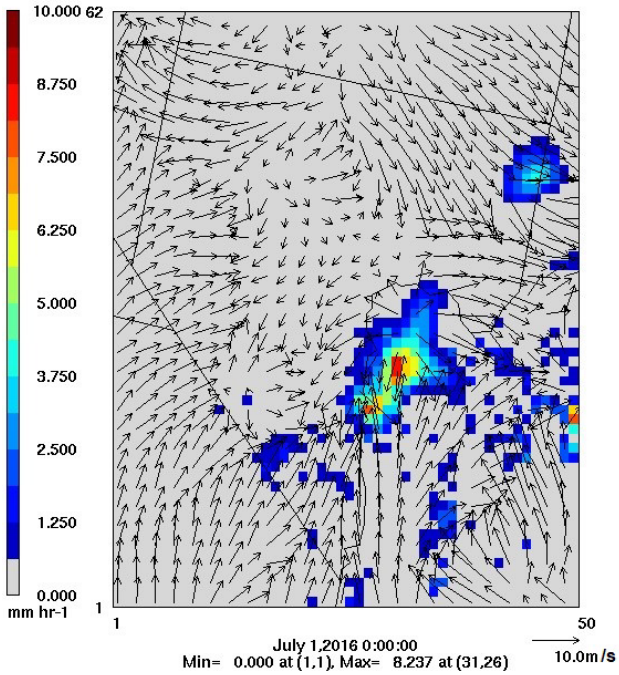

Figure 7-1. Surface precipitation and wind vectors in the CC4c2 domain on July 1, 2016, at 00 UTC (June 30, 2016, at 4 PM PST). Precipitation is shown in units of mm/hr, and wind vectors are in m/s.

A second simulated convective event started at 10-11 AM PST on July 1 near southwest Las Vegas (not shown). This convective area also moved in a southeast direction and left the domain at about 4 PM. On July 2, from 10 AM to 5 PM LST, southerly winds reestablished with the potential to transport air masses from beyond the southern portion of the domain into the LVV. In summary, the wind patterns responding to the precipitation cells are consistent with expectations, and no obvious errors or flaws stemming from WRFCAMx were identified.

In general, the simulated PBL exhibited low values (less than 200 m) at night. During 11 AM to 1 PM, the PBL increased to an excess of 2000 meters. However, on July 1 and July 2, the PBL collapsed dramatically in the middle of the day in apparent response to the development of a convective cell that caused thermal cooling of the surface (Figure 7-2). As suggested earlier in explaining KVPATCH, this suggests a high degree of complexity in the PBL dynamics, and it may be worth examining it as part of CAMx evaluations during ozone events. WRF commonly develop such features during convective events, and no problems associated with WRFCAMx were apparent.

Simulated temperature ranged between 12°C to 48°C (54°F to 118°F) during July 1 and 2, with lower values at night and higher temperatures during the day. On July 1, the maximum temperatures in the LVV occurred around 11 AM PST. Lower temperatures occurred in the higher elevations of the Sheep and Spring Mountains to the west and northwest of the LVV, respectively. WRF appeared to accurately capture the urban heat island effect. On July 1 at midnight, the highest temperatures were simulated in Las Vegas, and this persisted through the overnight hours. Some grid cells along the eastern border of Clark County with Arizona showed constant temperatures around 70° F. These cells are co-located with the Colorado River and Lake Mead, which act as a heat reservoir, explaining the constant temperature. Around Lake Mead temperature gradients can be observed on July 2 at 21 UTC (1 PM PST) when temperatures surrounding the lake were around 118°F and cells within the lake remained around 70°F (Figure 7-3). No problems associated with WRFCAMx were apparent.

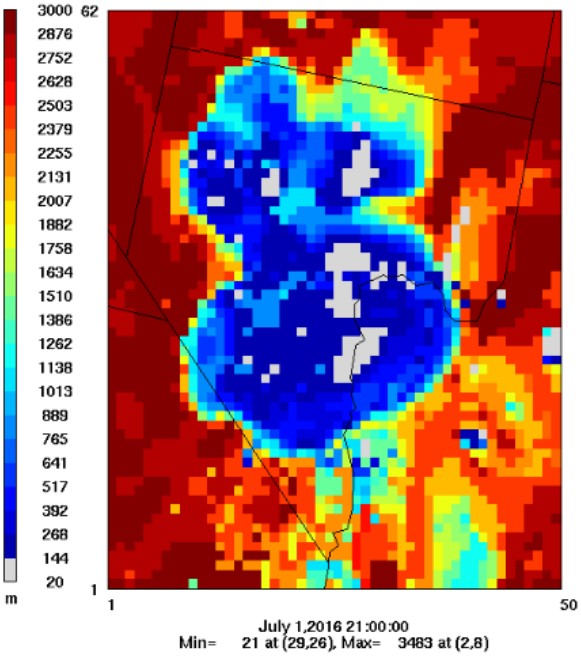

Figure 7-2. Planetary boundary layer (PBL) depth in the CC4c2 domain on July 1, 2016, at 21 UTC (July 1, 2016, at 1 PM PST). PBL is shown in meters (m) above ground.

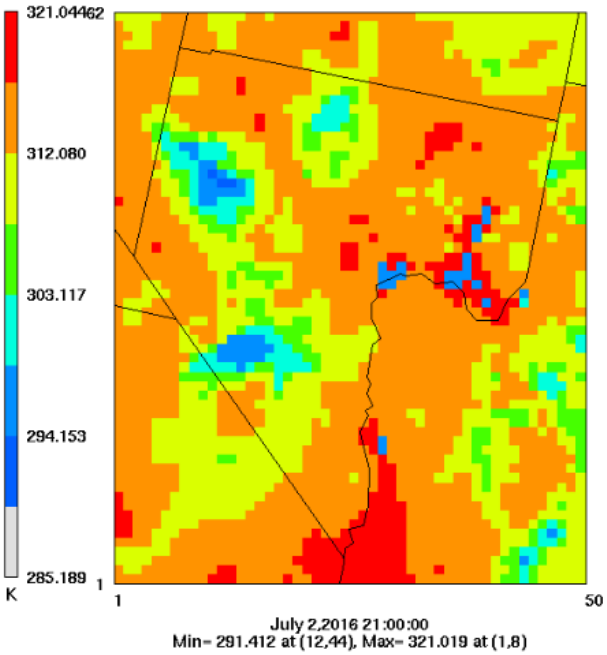

Figure 7-3. Temperature in the CC4c2 domain on July 2, 2016, at 21 UTC (July 2, 2016, at 1 PM PST). Temperature is shown in Kelvin (K).

During July 1 and 2 simulated cloud cover was generally sparse, however large cloud optical depth values were correlated to convective precipitation cells. During the hours of high ozone formation (11 AM to 3 PM) on July 2, spotty cloud cover conditions were simulated over the domain (Figure 7-4). No problems associated with WRFCAMx were apparent. It is highly likely that invoking the sub-grid convective diagnosis in WRFCAMx would have increased the amount of cloudiness during the daytime hours.

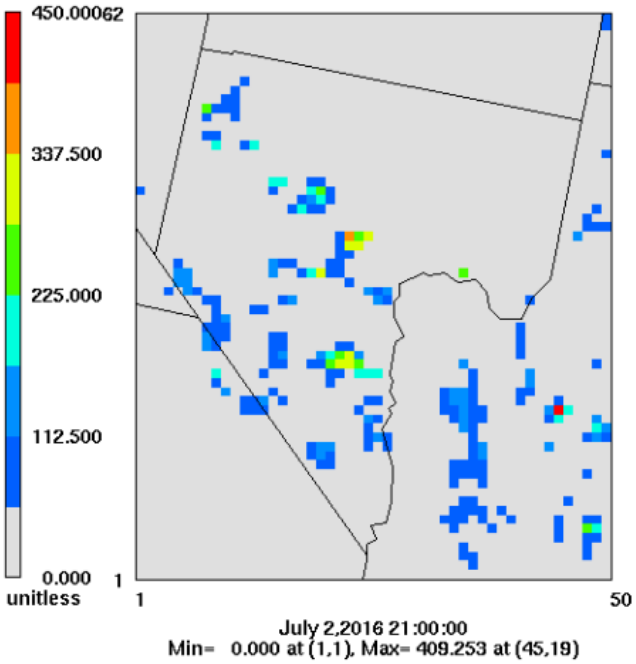

Figure 7-4. Cloud optical depth in the CC4c2 domain on July 2, 2016, at 21 UTC (July 2, 2016, at 1 PM PST).

In addition to CAMx-ready meteorological inputs, WRFCAMx processed the WRF LU/LC dataset to CAMx LU/LC inputs fields with proper mapping to CAMx categories. We conducted QA/QC on the resulting CAMx-ready landcover files to ensure reasonable characterization throughout the CC4c2 domain. LU/LC extractions from WRF were plotted and compared to the topography in Clark County. The largest two elevations in Clark County correspond to the Spring Mountains and Sheep Range. Mountains, urban areas, and vegetative type were consistent with known topography and landcover in the region (Table 7-2). The urban landcover clearly shows Las Vegas and highways. Deciduous shrubs cover most of Clark County and the rest of the CC4c2 domain. Evergreen needleleaf forests cover the mountain ranges in the region (Figures 7-5 through 7-7). No problems associated with WRFCAMx were apparent.

Table 7-2. CAMx LU/LC coverages over the CC4c2 domain.

LU/LC Variables	Description	Coverage
urban	Urban	Shows Las Vegas
dshrub	Deciduous shrub	Covers most of the 4km domain
eneedl	Evergreen needleleaf forest	Covers the Sheep Range and Spring Mountains
water	Water	Follows the Colorado River and Lake Mead
mwood	Mixed woodland	Small to negligible
desert	Desert (barren)	Small to negligible
swamp	Swamp	Small to negligible
cropland	Cropland	Small to negligible
lgrass	Long grass	Small to negligible
tforest	Transitional forest	No values
tundra	Tundra	No values
icrops	Irrigated cropland	No values
cotton	Cotton	No values
maize	Maize	No values
sugar	Sugar	No values
rice	Rice	No values
sgrass	Short grass	No values
tshrub	Thorn shrub	No values
eshrub	Evergreen shrub	No values
ddecid	Drought deciduous trees	No values
tbroad	Tropical broadleaf forest	No values
dbroad	Deciduous broadleaf forest	No values
dneedl	Deciduous needleleaf forest	No values
ebroad	Evergreen broadleaf forest	No values
Lake	Lake	No values
Ice	Ice	No values

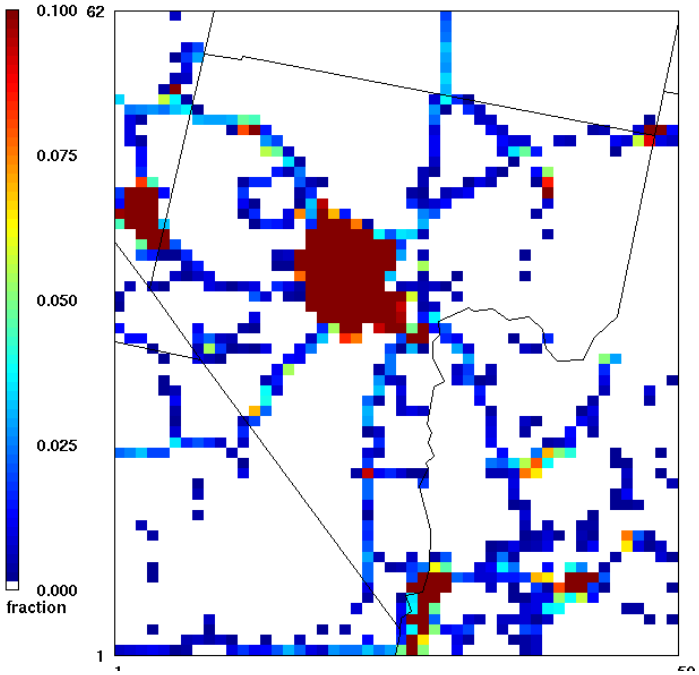

Figure 7-5. Land use categorized as "urban" in the CC4c2 domain.

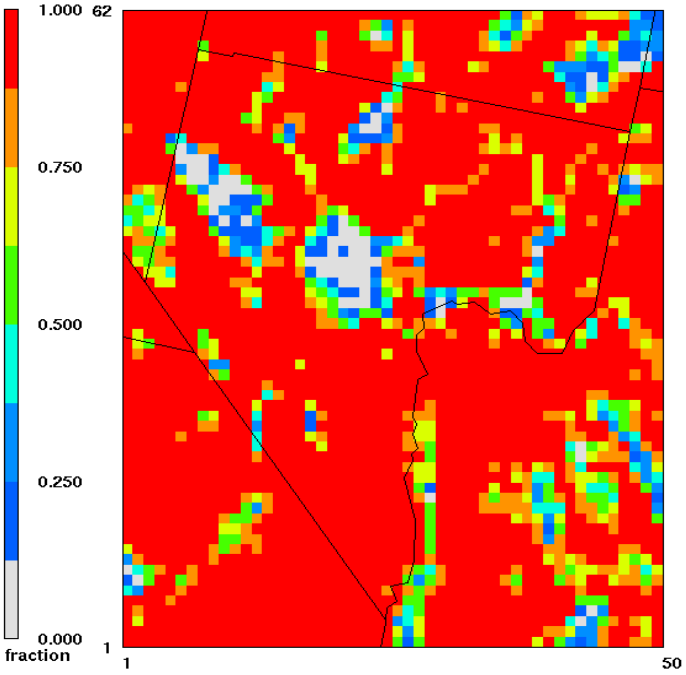

Figure 7-6. Land use categorized as "deciduous shrub" in the CC4c2 domain.

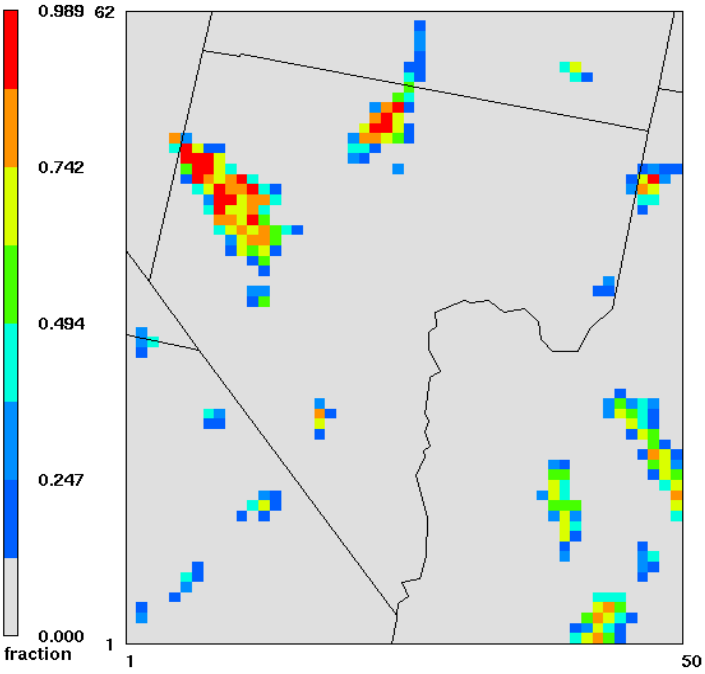

Figure 7-7. Land use categorized as "evergreen needleleaf forest" in the CC4c2 domain.

7.3.2 KVPATCH

Vertical diffusivity (Kv) fields modified with KVPATCH were compared to the original Kv fields from WRFCAMx. Figure 7-8 shows an example of nighttime Kv differences arising from the use of KVPATCH and illustrates that the adjustment was correctly applied to the urban areas around Las Vegas and Fort Mojave Reservation just east of Clark County. Note that only some areas needed an upward adjustment to reflect the minimum Kv profile.

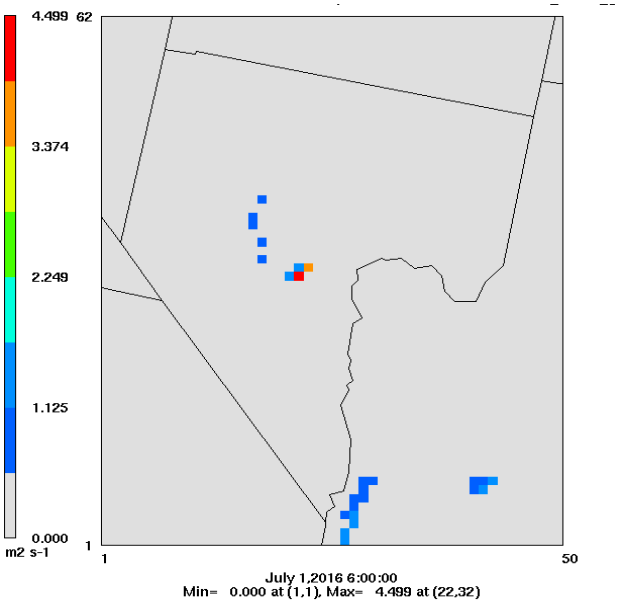

Figure 7-8. Enhancements generated from applying KVPATCH in layer 3 on July 1, 2016, at 6 UTC (June 30, 2016, 10 PM PST)

7.3.3 MCIP

We found that MCIP results were reasonable and similar to WRFCAMx. MCIP results were quality assured by comparing a few meteorological fields such as surface winds and temperature against the corresponding WRFCAMx extraction for selected days. Figure 7-9 shows a comparison between WRFCAMx and MCIP surface temperature on June 30 at 4 PM PST and it illustrates that the spatial variation in both is very similar if not identical, which is expected. Notice that the WRFCAMx domain is larger than the MCIP domain by extra rows and columns around the perimeter because CAMx requires meteorological inputs to include nested grid buffer cells.

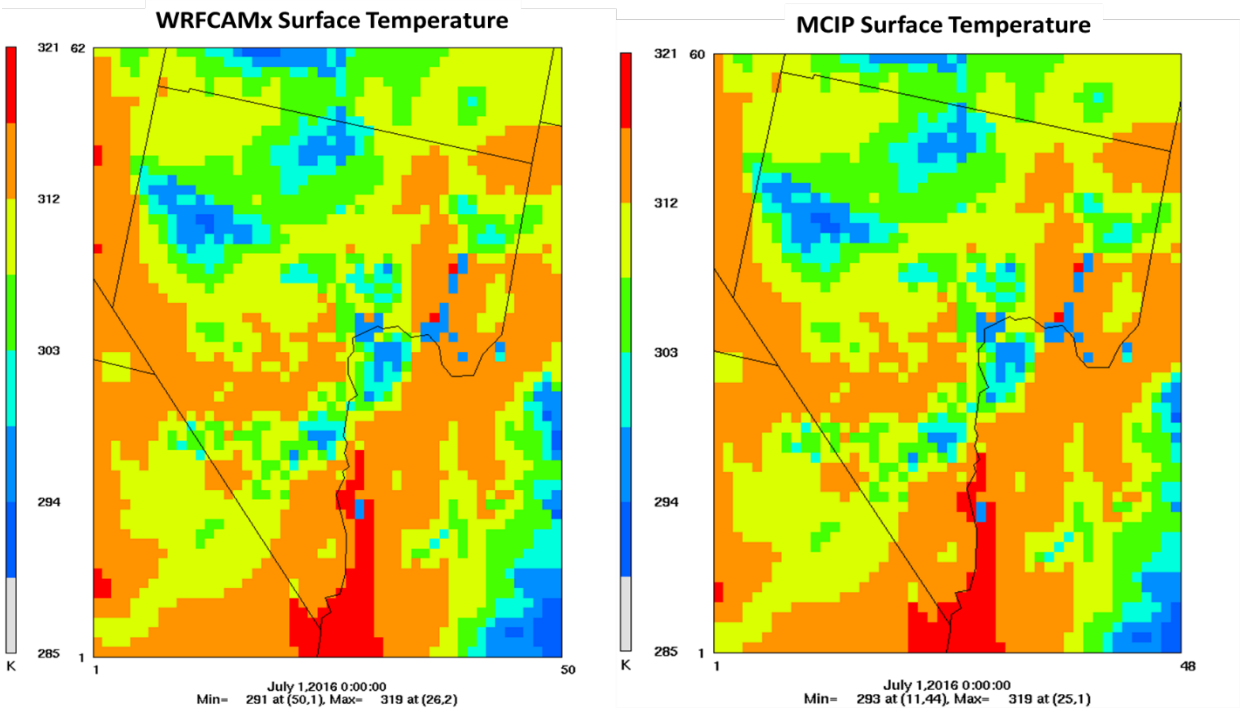

Figure 7-9. WRFCAMx and MCIP surface temperatures for July 1, 2016, at 0 UTC (June 30, 2016, 4 PM PST).

7.4 Initial and Boundary Conditions

Initial and boundary conditions (IC/BC) for the 36US3 and 12US2 domains were obtained from the EPA 2016v2 modeling platform (EPA, 2022a,c). The 36US3 IC/BCs were developed by EPA from version 3.1.1 of the hemispheric version of the Community Multi-scale Air Quality Model (H-CMAQ). The resulting BCs were generated at one-hour intervals. Three-dimensional concentration output fields from EPA's 2016_fj and 2023_fj 36US3 CAMx simulation were then used to generate BCs for the 2016_fj and 2023_fj 12US2 base case scenarios, respectively. Ramboll has reviewed and used these IC/BC inputs for several other projects. Note that alternative sources of BC were tested in CAMx as described in Section 8.4.

7.5 Ozone Column and Photolysis Rates

Total atmospheric ozone column data are needed to derive clear-sky photolysis rate inputs for CAMx. Typically, 24-hour ozone column data retrieved from the Ozone Monitoring Instrument (OMI) aboard the Aura satellite are available on FTP sites supported by the National Aeronautics and Space Administration (NASA, 2022) and used for this purpose. In this project, however, ozone column and

photolysis rate values for the 36US3 and 12US2 domains were obtained from the 2016v2 EPA Modeling platform. Ramboll has reviewed and used these chemical data inputs for several other projects. In 2-way nested grid applications, CAMx interpolates master grid ozone column inputs to all nested grids; i.e., the ozone column dataset prepared by EPA for the 12US2 grid was used for the entire 12US2/CC4c2 grid system. EPA developed photolysis rates for the Carbon Bond version 6, release 4 (CB6r4) photochemical mechanism. For this project, we applied CAMx v7.20 using the latest Carbon Bond mechanism (CB6r5), which is fully compatible with photolysis rates developed for CB6r4.

8.0 BASE YEAR AND SENSITIVITY MODELING

This Section describes the CAMx 2016 base year modeling configuration, initial and sensitivity applications, and model performance evaluation. Seven CAMx runs were conducted:

1. An initial base case running only gas-phase ozone chemistry;
2. Inclusion of aerosol chemistry and an improvement in the spatial characterization of emissions from Harry Reid International Airport;
3. Alternative North American boundary conditions using output from the GEOS-Chem global chemistry model;
4. A series of short tests with modified vertical diffusion coefficients;
5. Replacement of biogenic emissions from BEIS3.7/BELD5 with emissions from BEIS3.6/BELD4;
6. Replacement of biogenic emissions from BEIS3.7/BELD5 with emissions from BEIS4/BELD6;
7. Alternative North American boundary conditions using output from the CAM-Chem global chemistry model.

8.1 CAMx 2016 Modeling Platform

Clark County's photochemical modeling is based on the EPA's 2016v2 MP, which includes CAMx-ready emissions, meteorology, initial/boundary conditions (IC/BC), and other model input datasets. The historical base year is 2016 and the future base planning year is 2023. EPA input datasets are available for two nested grids: 36US3 covering North America and 12US2 covering the conterminous US. A third CC4c2 grid has been added covering the CCNAA, the entirety of Clark County, and portions of surrounding areas in southern Nevada and southeastern California (see Figures 4-1 and 4-2). All grids run with the full 35 layer vertical grid structure (see Table 4-3).

Model simulations were conducted using CAMx v7.2, which was publicly released in May 2022 (Ramboll, 2022b), and employed the Carbon Bond version 6 (CB6) photochemical mechanism to be consistent with the EPA 2016v2 databases. The Clark County modeling period spans from May 1 through August 31, 2016. A one-month spin up period in April is run without the 4 km grid to initialize the model from ICs.

Table 8-1 lists the initial 2016 base case model configuration. This configuration is identical to the EPA 2016v2 MP except for the following:

- The CC4c2 grid is added with associated meteorological and emission inputs.
- The modeling period is May 1 through August 31 (with April spin-up) instead of a full calendar year.
- CB6 gas-phase ozone chemistry is run exclusively without aerosols to shorten CAMx runtimes.
- Vertical advection is solved using the "Piecewise Parabolic Method" (PPM), a new and less numerically diffusive option in CAMx v7.2, instead of the original implicit hybrid method in earlier CAMx versions used by EPA.

Table 8-1. CAMx model configuration for the CCNAA 2016 initial base case simulation.

Model Component	CCNAA Application	Comment
Model Code	CAMx v7.20 - May 2022	
Horizontal Grids		
Map Projection	Lambert Conic Conformal	EPA 2016 MP
36 km (36US3)	172 x 148 cells	EPA 2016 MP (1-way nesting)
12 km (12US2)	396 x 246 cells (no buffer cells)	EPA 2016 MP (2-way nesting)
4 km (CC4c2)	50 x 62 cells (with buffer cells)	CCNAA grid (2-way nesting)
Vertical Grid	35 layers	EPA 2016 MP, defined by WRF
Initial Conditions	30-day spin-up on 12US2 grid from "clean" ICs using 2016 emissions	Start 12US2/CC4c2 2-way nests on May 1
Boundary Conditions	EPA 2016 MP 12US2 BCs	
Time Zone	UTC	EPA 2016 MP
Emissions		
36/12 km Data Sources	EPA 2016v2 MP	
4 km Data Sources	EPA 2016v2 MP + Clark County Data	
Models/Processing Tools	SMOKE, MOVES3, SMOKE-MOVES, BEIS3.7/BELD5	CCNAA grid
Plume-in-Grid	Off	No large point sources in high-resolution CCNAA grid
In-line Ix emissions	On	Oceanic halogens
Chemistry		
Gas Phase Chemistry	CB6r5	Latest mechanism available
Aerosol Chemistry	None	Gas phase only
Meteorological Interface	WRFCAMx v5.2	
Horizontal Diffusion	Smagorinsky	Spatially variant K-theory
Vertical Diffusion	YSU Kv formulation	Minimum Kv 0.1 to 1.0 m^2/s
ACM2	Off	Boundary layer convection
Sub-grid Cloud Convection	Off	
Deposition		
Dry Deposition	Zhang03	
Wet Deposition	On	rain/snow/graupel
Surface Chemistry Model	Off	
Bi-directional Ammonia	Off	For aerosol chemistry
Numeric Solvers		
Gas Phase Solver	Euler Backward Iterative(EBI)	Default fast and accurate solver
Vertical Advection	Piecewise Parabolic Method (PPM)	Default
Horizontal Advection	Piecewise Parabolic Method (PPM)	Default
Integration Time Step	Wind speed dependent	~0.5-1 min (4 km), 1-5 min (12 km), 5-15 min (36 km)
Super Stepping	On	Maximizes time step selection

8.2 Evaluation Approach

The CAMx performance evaluation followed procedures recommended by EPA (2018a). An important purpose of the evaluation is to judge the reliability of the model in predicting ozone and related compounds and to establish a level of confidence that modeled ozone responses to changes in emissions within the CCNAA are sufficiently accurate and reliable. The CAMx 2016 results were compared against observed ambient ozone and precursor concentrations, as available, to establish the extent to which the model is capable of reproducing conditions that actually occurred. The model performance evaluation included many types of graphical and statistical comparisons between predicted and observed concentrations, as documented in the Modeling Protocol (Ramboll, 2022a). Following the evaluation, diagnostic tests were undertaken to investigate model sensitivity to key inputs, such as emissions, meteorology, chemistry, and boundary conditions, and to improve model performance in replicated observed conditions.

Statistical metrics involved comparing simulated surface ozone and NO_2 concentrations paired in space and time with measurements archived in EPA's Air Quality System (AQS) database[19]. Figure 8-1 shows the location of AQS sites operating within central Clark County during the summer of 2016.

Figure 8-1. Map of air quality monitoring sites that operated within central Clark County during the summer of 2016. Ozone sites are noted in green, the high elevation site in the Spring Mountains is noted in yellow, and NOx monitoring sites are noted in blue (which are co-located with ozone sites at Jerome Mack and Joe Neal). Additional sites not contained within the image include: Jean to the southwest, Indian Springs to the Northwest, and Mesquite far to the northeast.

[19] http://www.epa.gov/air/data/.

The Atmospheric Model Evaluation Tool (AMET[20,21]; EPA, 2022f) is a suite of software designed to facilitate the analysis and evaluation of model predictions against observations. AMET matches model output from grid cells with observations from monitoring sites operating within one or more networks. AMET also maps individual modeled species to corresponding compounds reported in the observation database. Model and observation data pairings are then used to analyze the model's performance using a variety of statistical and graphical techniques. AMET v1.5 is the latest version, released in August 2022.

EPA has deemphasized the use of statistical goals because of a historical tendency to focus on achieving such goals in lieu of assessing whether a model properly simulates atmospheric processes. Models may often look correct but for the wrong reasons, a result of compensatory errors. However, model performance goals are still useful for interpreting model performance and putting the performance into context. Building off the work of Simon et al. (2012), Emery et al. (2016) developed a set of performance goals and criteria based on the variability in past US photochemical modeling exercises. "Goals" indicate statistical values that the top one-third of applications have met and should be viewed as the best a model can be expected to achieve. "Criteria" indicate statistical values that about two thirds of past applications have met and should be viewed as a performance level that models should be able to achieve. Statistical results outside the criteria indicate that the model performs poorly. We compared CAMx 2016 ozone performance statistics for normalized mean bias (NMB), normalized mean error (NME) and correlation coefficient (r) against the goals and criteria proposed by Emery et al. (2016), as listed in Table 8-2.

Table 8-2. Recommended benchmarks for ozone statistical performance (Emery et al., 2016). These goals apply in cases with and without the use of an observed minimum cutoff concentration (e.g., 60 ppb).

Statistic	Goal	Criteria
NMB	<±5%	<±15%
NME	<15%	<25%
R	>0.75	>0.50

8.3 Initial Base Case Model Performance Evaluation

The initial base case evaluation focused on statistical comparisons involving maximum daily 8-hour average (MDA8) ozone and hourly NOx in the CCNAA to assess overall predictive skill in reproducing day-to-day variability of observed air quality at key monitors and to identify any fatal flaws that required corrective action. The evaluation also included an ozone performance evaluation across the Mojave desert region to assess transport from California.

8.3.1 Summary of Results

Results from the evaluation of the initial 2016 base case simulation are summarized below:

- MDA8 ozone was under predicted for most months and most Clark County sites, but generally remained within statistical benchmark criteria.
  - Model bias transitioned from large under predictions in May to near zero bias by August;
  - Performance was reflective of the inputs provided by the EPA 12US2 2016v2 database, and not surprisingly EPA results showed similar performance;
  - Under prediction bias was relatively larger on high observed ozone days (>60 ppb);

[20] https://www.cmascenter.org/amet/.

[21] https://www.epa.gov/cmaq/atmospheric-model-evaluation-tool.

  - Regional upwind performance in southern California followed similar patterns, with generally larger under prediction bias than in Clark County.
- NO_2 concentrations in Las Vegas transitioned from over prediction to under prediction from May to August.
  - This was an opposite trend from ozone and presented an early indication that NOx reductions may lead to ozone increases (a so-called "NOx-disbenefit");
  - The predicted hourly diurnal NO_2 pattern was overestimated at all hours and "neighborhood" monitors that were not directly sited near freeways.
  - Predictions indicated either too much NOx emissions, improper temporal or spatial allocation, and/or insufficient vertical mixing especially during commute hours.
  - Animations of ozone spatial patterns indicated lower ozone in central Las Vegas and much higher ozone in outlying areas, further suggesting NOx-rich conditions in central Las Vegas that inhibited ozone formation and may lead to NOx-disbenefits.

8.3.2 MDA8 Ozone Bias and Error Performance Statistics

Table 8-3a lists monthly NMB and NME statistical performance for MDA8 ozone over all days and all ozone monitoring sites within the CC4c2 domain. The table compares results from the Clark County initial base case and EPA's 2016v2 12US2 simulation (EPA, 2022c). NMB and NME are color coded for visual reference to statistical goals and criteria benchmarks.

Performance results between the base case and EPA simulation were very similar, showing a consistent and systematic negative bias over all months. A rather large negative bias outside of the criteria benchmark occurred in May, followed by a transition to smaller bias through August well within the statistical goal. The large bias in May also led to higher gross error than other months in both models, while June through August exhibited consistent gross error of just above 10%, which is well within the statistical goal.

Table 8-3a. Monthly model performance statistics for MDA8 ozone over all days and all ozone monitoring sites within the CC4c2 domain that operated during the summer of 2016. Normalized mean bias (NMB) and normalized mean unsigned error (NME, also referred to as gross error) are shown with color coding indicating statistics outside performance criteria (red), between goals and criteria (yellow) and within goals (green). Results from the Clark County initial base case and EPA's 2016v2 12US2 simulation are compared.

Month	MDA8 Ozone (no cutoff)			
	NMB (%)		NME (%)	
	CC4c2	EPA 12US2	CC4c2	EPA 12US2
May	-17.9	-15.9	18.3	16.1
June	-9.2	-6.5	11.2	9.0
July	-8.2	-7.9	11.1	10.7
Aug	0.1	-0.6	10.7	11.5
May-Aug	-8.8	-7.7	12.8	11.8

Table 8-3b presents the same information but limited to sites and days when observed MDA8 ozone exceeded 60 ppb. Similar patterns are evident on high ozone days, but there was a tendency toward larger negative bias even though gross error remained in the low teens during June through August.

Table 8-3b. As in Table 8-3a, but for all sites and days when monitored MDA8 ozone exceeded 60 ppb.

Month	MDA8 Ozone (60 ppb cutoff)			
	NMB (%)		NME (%)	
	CC4c2	EPA 12US2	CC4c2	EPA 12US2
May	-21.5	-19.7	21.5	19.7
June	-11.3	-9.2	12.7	9.6
July	-11.7	-12.0	12.7	12.6
Aug	-4.3	-5.6	11.4	11.8
May-Aug	-11.5	-11.1	13.9	12.8

Table 8-4 breaks out monthly NMB and NME over all days (i.e., no 60 ppb cutoff) at each monitoring site within the CC4c2 domain. Similar color shading is used to visually characterize values relative to goal and criteria benchmarks. The under prediction patterns were consistent across all sites, so there was no single site that influenced the statistics in Table 8-3a. The consistently worst performing site was in California, upstream of Clark County, which monitors air that often arrives directly from the Los Angeles basin. The best performance throughout the modeling period was achieved at Mesquite, far to the northeast of Las Vegas. Within the LVV, Joe Neal and JD Smith were the worst performing sites during May through July.

Table 8-4. Monthly model performance statistics for MDA8 ozone over all days at each monitoring site within the CC4c2 domain that operated during the summer of 2016. Normalized mean bias (NME) and normalized mean unsigned error (NME) are shown with color coding indicating statistics outside performance criteria (red), between goals and criteria (yellow) and within goals (green).

		May		June		July		Aug	
Site_ID	Name	NMB	NME	NMB	NME	NMB	NME	NMB	NME
060711001	California	-24.7	24.7	-17.3	17.3	-17.0	17.9	-11.8	12.4
320030022	Apex	-18.7	18.8	-9.6	9.9	-8.6	11.5	1.5	9.8
320030023	Mesquite	-12.3	13.4	-2.7	7.1	0.4	6.7	12.9	22.9
320030043	Paul Meyer	-18.2	18.4	-10.3	12.0	-9.0	10.9	-2.4	9.5
320030071	Walter Johnson	-17.8	18.0	-8.9	11.4	-8.7	10.8	-0.5	9.4
320030073	Palo Verde	-15.0	16.0	-7.1	10.5	-7.3	10.5	0.3	9.9
320030075	Joe Neal	-20.0	20.1	-11.3	13.2	-11.1	12.1	0.6	9.1
320030298	Green Valley	-15.6	16.6	-10.0	11.4	-6.1	10.2	2.0	11.8
320030540	Jerome Mack-NCORE	-19.5	19.6	-9.6	11.7	-9.4	11.9	-1.1	10.0
320030601	Boulder City	-16.0	16.2	-7.2	8.0	-3.0	10.1	-3.8	10.9
320031019	Jean	-16.5	16.7	-7.9	9.3	-6.9	9.0	-1.6	8.9
320032002	J.D. Smith	-20.9	21.1	-13.4	14.5	-10.6	12.5	-0.7	9.6
320037771	SM Youth Camp	-19.7	19.7	-9.2	11.3	-9.2	10.1	1.6	9.7
320037772	Indian Springs	-15.9	16.6	-5.4	10.6	-4.6	10.0	3.8	10.2
320038000	LV Paiute	-17.3	17.5	-10.0	11.5	-9.3	10.4	4.3	9.7

These results indicated that the model performed poorly in May, marginally well during June, typically well during July, but notably well during August. The systematic under prediction tendency suggested a consistent source of error. Additional graphical and day-specific comparisons described below were analyzed to identify patterns that might uncover or direct further investigation into the source of error. Additionally, sensitivity tests were conducted to assess the influence from different model configuration options and inputs.

8.3.3 Graphical Analyses of Model Performance

Figure 8-2 displays a spatial map of site-specific monthly NMB patterns for MDA8 ozone across the CC4c2 domain. In this case, NMB was determined from all days without the 60 ppb cutoff applied, so the maps are consistent with the data in Table 8-4. These plots show the systematic negative bias in May and the progressive improvement through August. Again, the consistent bias among all LVV core sites is notable.

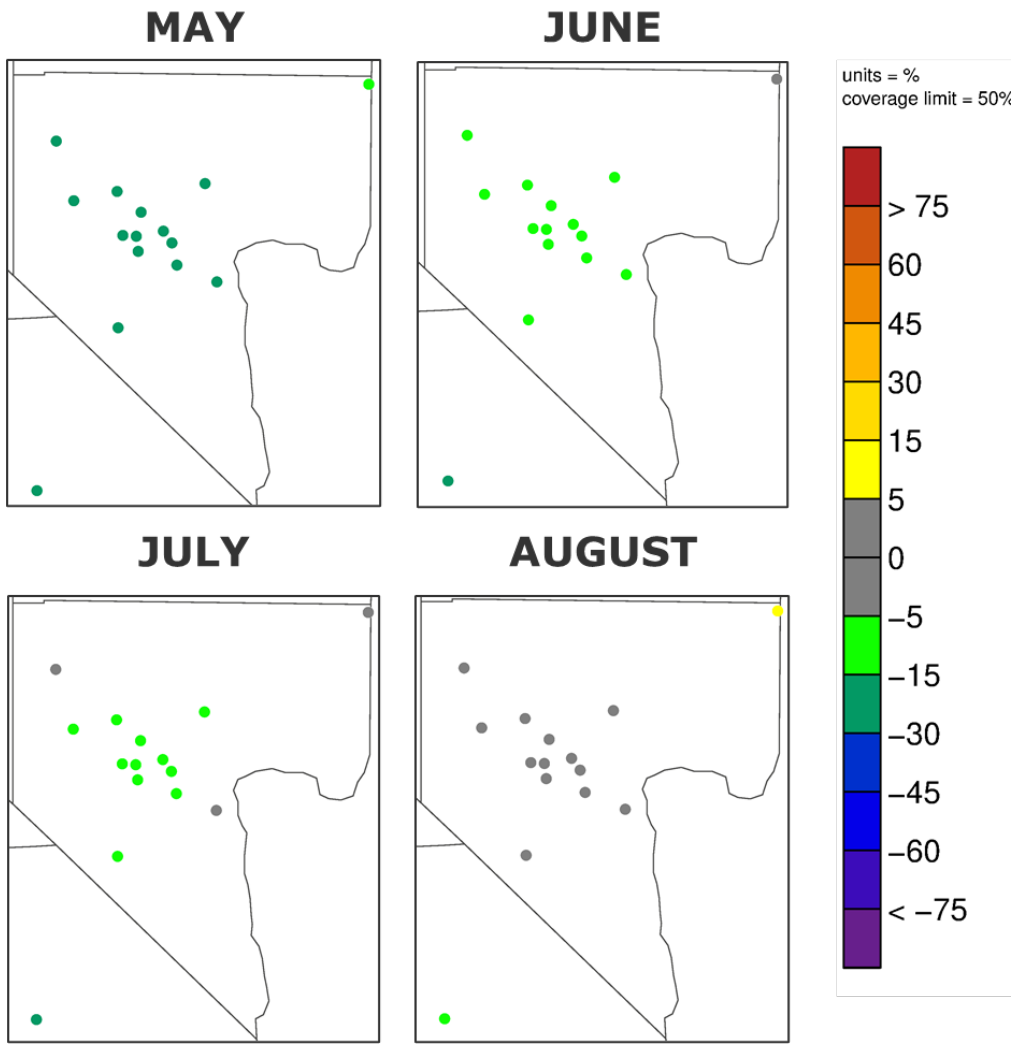

Figure 8-2. Map of site-specific monthly normalized mean bias (NMB) patterns for MDA8 ozone within the CC4c2 domain.

Figure 8-3 presents a similar spatial map of site-specific monthly NMB, but for selected monitoring sites across the Mojave Desert of Southern California. These sites monitor the air mass that is often transported between the Los Angeles basin and the LVV. Simulated MDA8 ozone for these statistics were taken from the 12US2 grid. The plots show the same general pattern of systematic negative bias and month-by-month improvement through August. While performance was fairly consistent among all desert sites, the under prediction bias was much larger than the LVV sites. This implicated a lack of regional ozone and associated transport as a likely contributor to poor performance in the LVV. Such performance issues were previously reported in EPA's 2016v2 model performance evaluation (EPA, 2022c).

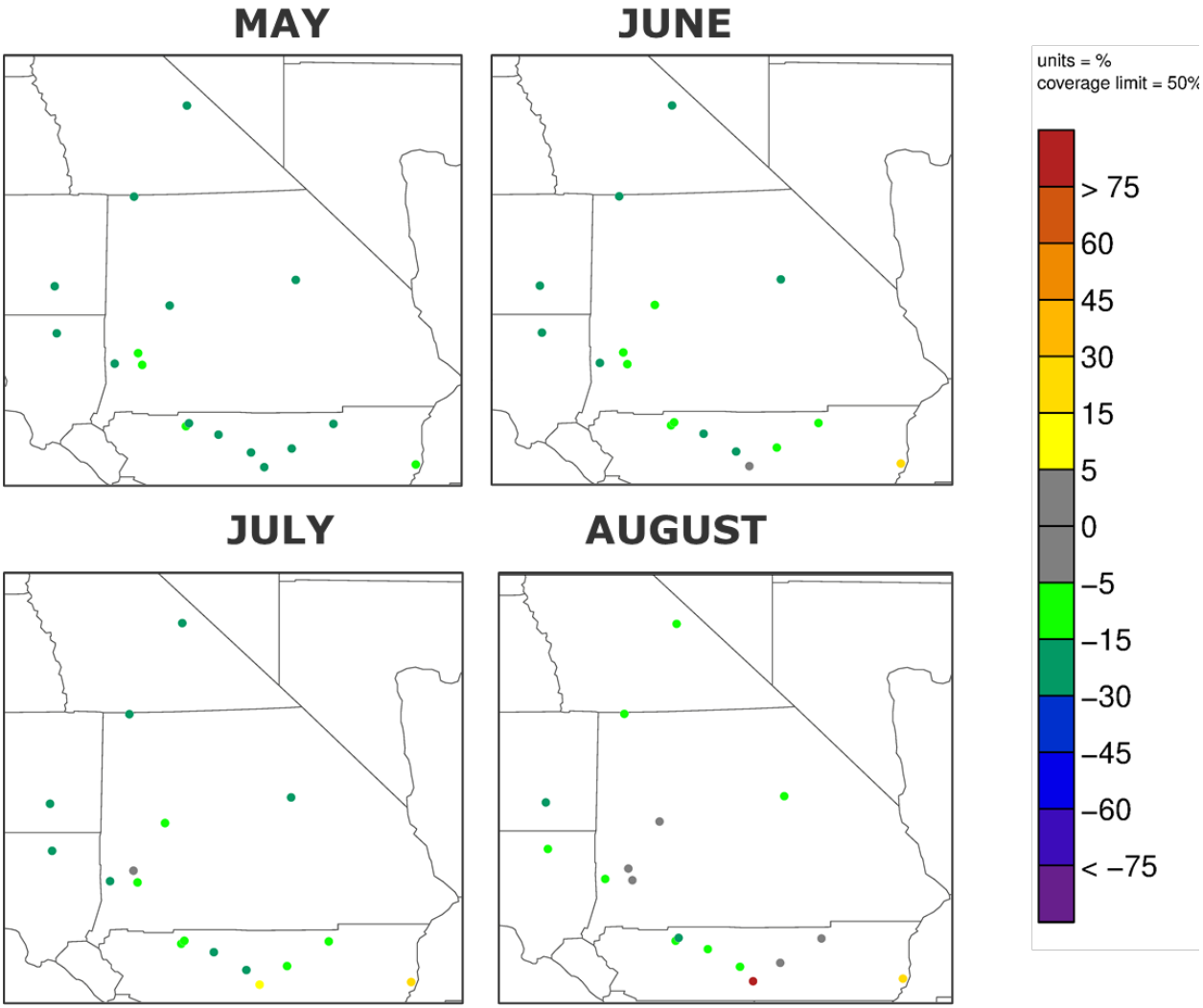

Figure 8-3. Map of site-specific monthly normalized mean bias (NMB) patterns for MDA8 ozone across the Mojave Desert of the southern California portion of the 12US2 domain.

Figure 8-4 presents time series of observed and simulated MDA8 ozone during the May through August modeling period at two representative monitoring sites. Whereas the model performed rather similarly over all LVV sites, Joe Neal (top panel) represents a site where the model performed more poorly during May through July, while Palo Verde (bottom panel) represents a site where the model performed better, though differences are subtle. The trend toward improving model-observation

agreement from May to August is notable. Yet performance in replicating the highest peak days was not skillful in any month, and the model occasionally over predicted non-event dates in August (we revisit this issue later in this Section).

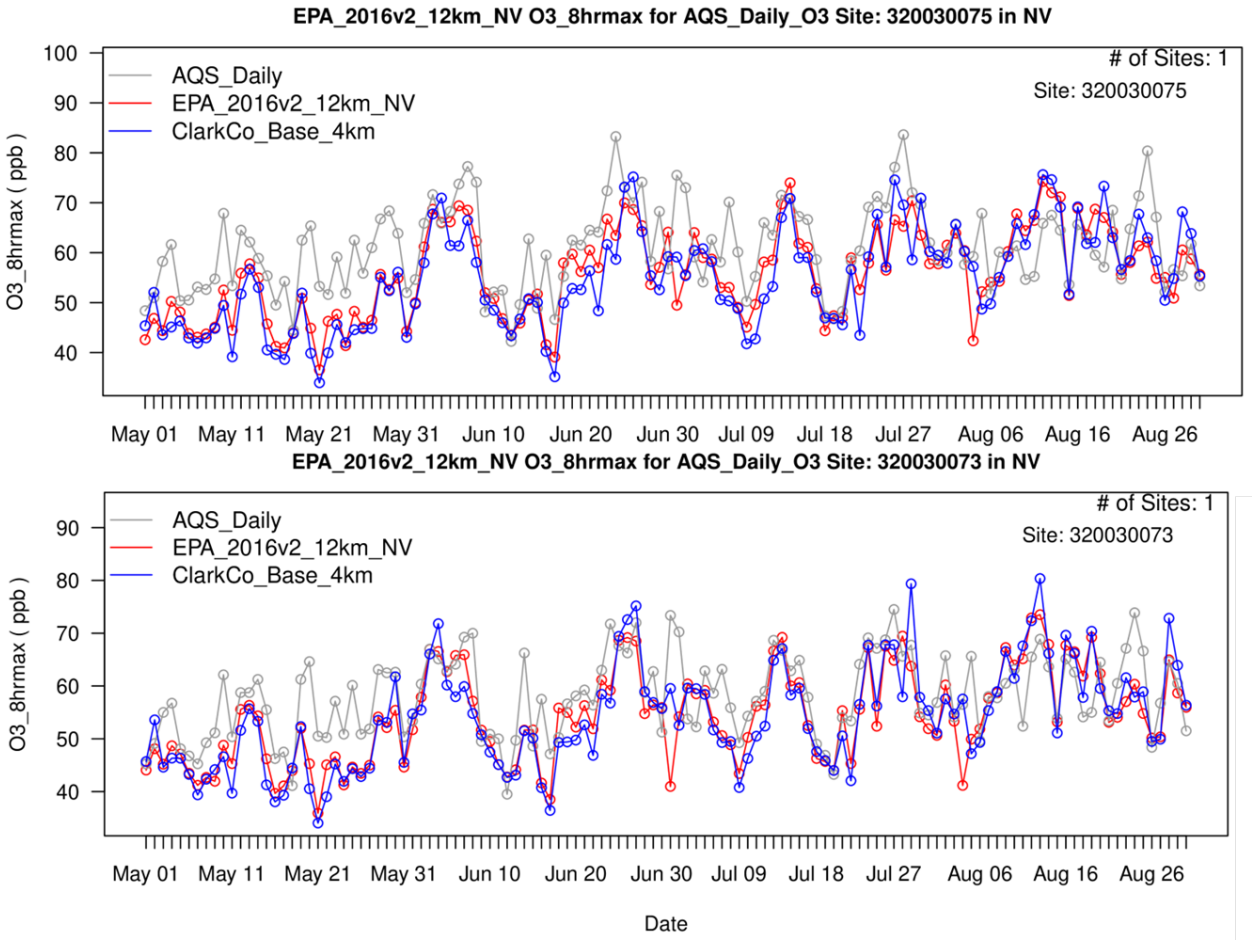

Figure 8-4. Time series of MDA8 ozone over the entire modeling period at the Joe Neal (top) and Palo Verde (bottom) monitoring sites. Daily AQS measurements are shown in grey, the modeled base case CC4c2 results are shown in blue, and EPA's results taken from their 2016v2 simulation on the 12US2 domain (EPA, 2022c) are shown in red.

Comparisons between the initial base case and the EPA 2016v2 12US2 results show that the current simulation tracked EPA's results very closely. This demonstrates that the introduction of the CC4c2 grid with its own emissions and meteorology had a minor influence on overall results. It further suggests that simulated ozone in the LVV were heavily influenced by a poor replication of regional ozone and transport into the LVV on the 12US2 grid (the inputs for which are identical to EPA's 2016v2 MP).

Scatter plots provide a way to visualize model-observation agreement over all days and sites. Figure 8-5 shows MDA8 ozone scatter plots separated by month for all sites within the CC4c2 grid. Again, the transition from under predictions in May to more balanced performance in August is evident. NMB characterizes the relative average difference between all points within the cloud and the 1:1 line that represent a perfect simulation. NME (unsigned error), R^2 (variance, or correlation R), and root mean square error (RMSE) are measures of the degree of scatter of the cloud. The amount of scatter was

consistent from June through August and was consistent with or better than typical ozone model performance reported by Emery et al. (2016).

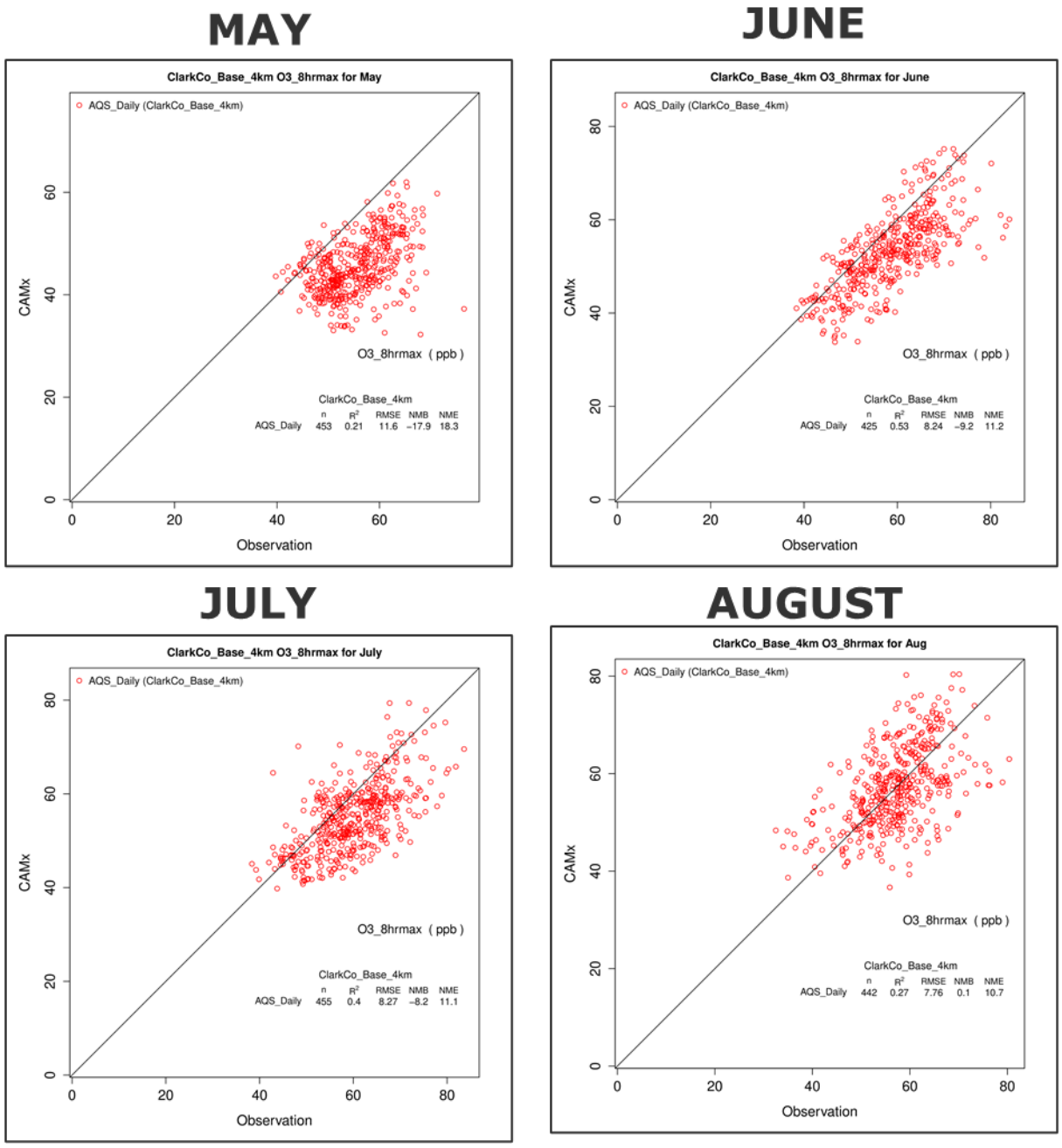

Figure 8-5. Monthly scatter plots of MDA8 ozone over all sites in the CC4c2 domain. Monthly statistics are also indicated on each plot and are described in the text.

Local ozone production depends on the amount of NO_2 available for photolysis and so it is important to assess simulated NO_2 performance against measurements. Figure 8-6 presents scatter plots of 1-hour NO_2 for all hours of the day and all 5 NO_2 monitoring sites within the LVV, arranged similarly to Figure 8-5 (see Figure 8-1 for the location of NOx monitors). The scatter plots show that NO_2 tended to be

over predicted in May but transitioned to more under predictions from July through August. As will be shown below, the net bias represents a balance between large under predictions near roadway sites and large over predictions at other "neighborhood" sites. Nevertheless, the NO_2 downward bias trend is opposite from the upward ozone bias trend over the season. This suggests that modeled ozone production in the LVV increases with local NOx reductions (i.e., a NOx-disbenefit).

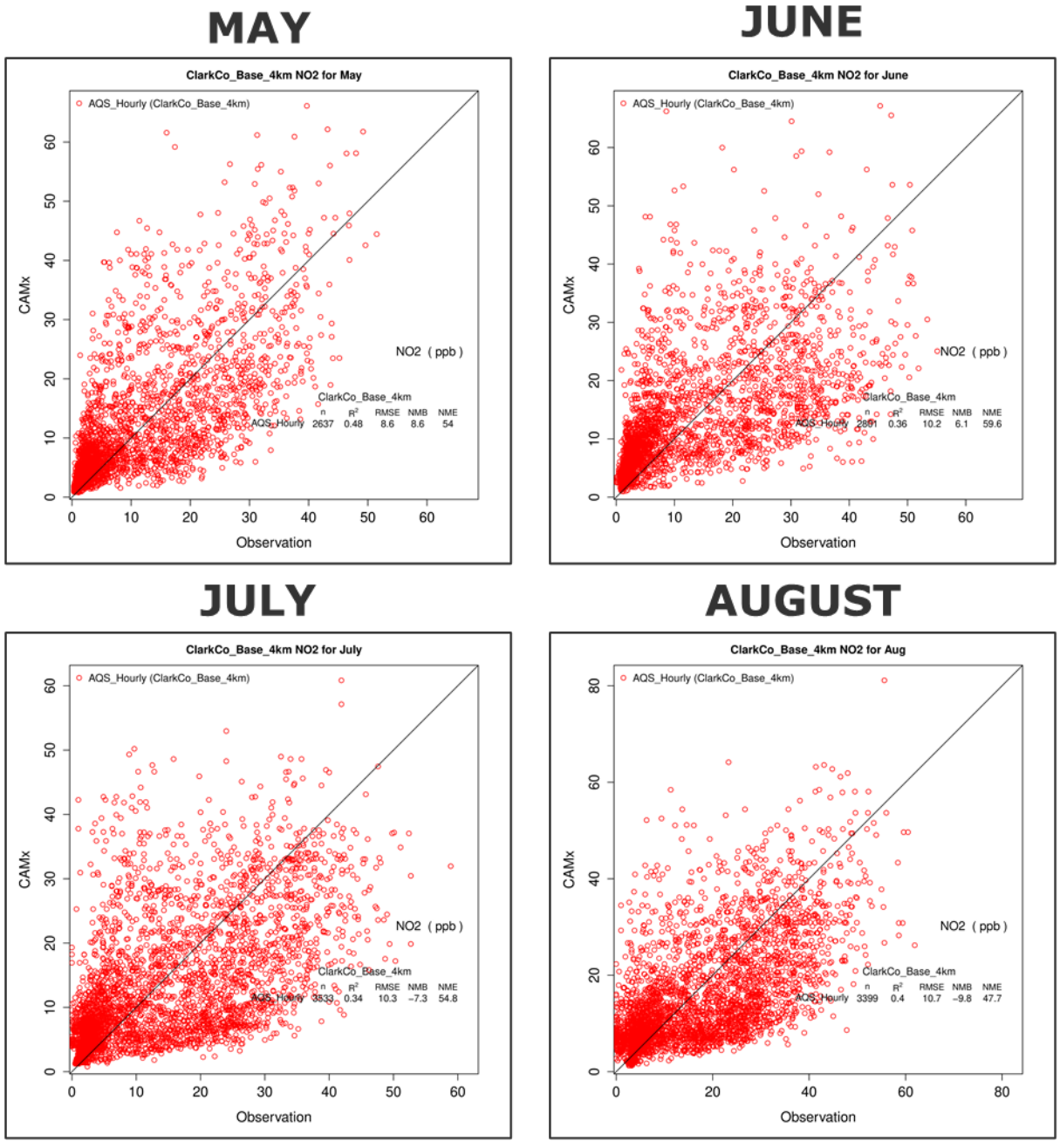

Figure 8-6. Monthly scatter plots of 1-hour NO_2 over all sites within the Las Vegas Valley. Monthly statistics are also indicated on each plot and are described in the text.

The degree of scatter, as visually evident and represented by the statistics on each plot, was rather large and NME consistently ranged from 50% to 60% over the period. This is typical of photochemical model performance for two reasons: (1) the model grid cannot spatially resolve primary NOx emissions at small sub-grid scales that monitors directly sense (near roads, point sources, etc.); (2) secondary NO_2 is derived from NO titration by ozone and local radical production, and so just like ozone, many processes involving emissions, chemistry, and meteorology must be properly simulated to achieve good NO_2 performance. It is therefore difficult to get good performance over all hours of the day, and especially at night when NOx concentrations peak in the stable, low mixing environment. The dependency of NOx performance on grid resolution is one particularly strong reason why no generalized and meaningful model performance benchmarks have been developed for NOx.

Observed time series of hourly NO_2 possess a high degree of noise from local influences, so model performance is difficult to visually interpret in that format. Instead, we used an AMET function to generate "box plots" of observed and predicted NO_2 concentrations that compare period-average and range for each hour of the day (Figure 8-7). The two sites in the top row of Figure 8-7 are located near freeways in central Las Vegas (see Figure 8-1). Here we would expect to see under predictions of NO_2, which was generally the case. The other three sites in Figure 8-7 show consistently large over predictions and ranges over all hours of the day, especially during morning and evening commute hours when emissions peak and the boundary layer is shallow. These features indicate either too much mobile source emissions allocated to commute hours and/or insufficient mixing depths, both of which are common issues seen in many other photochemical modeling exercises. Predicted NO_2 concentrations of 20 to 40 ppb during the early evening indicate ozone suppression via NO titration toward the end of the daily maximum 8-hour averaging period. Perhaps a more concerning issue is the very large over predictions during midday hours, when observations away from major roadways ranged over a few ppb while predicted NO_2 ranged closer to 10 ppb. This further suggests that the model was NOx-rich and inhibited daytime ozone production.

8.3.4 Analysis of Highest Observed Ozone Days

Table 8-5 ranks the highest observed ozone days exceeding 70 ppb during summer 2016 according to peak site concentrations in the LVV. Site- and date-paired model predictions are also listed for comparison. The table notes which days are expected to be influenced by regional wildfires versus local production and regional anthropogenic transport, according to previous analyses conducted by DES/DAQ.

Table 8-5 shows that most exceedance days were not well replicated, with typical under predictions of around 10 ppb. On only 8 of the 26 days listed, model-observation differences were within 5 ppb at these peak sites. Considering all days, the average peak observation was 75.4 ppb versus the average paired prediction of 64.7 ppb (absolute and normalized bias of -10.6 ppb and -14%, respectively). Results are similar when considering only days expected to be influenced by local production and regional transport. On those 9 days, the average peak observation was 75.1 ppb versus the average paired prediction of 63.4 ppb (absolute and normalized bias of -11.7 ppb and -16%, respectively).

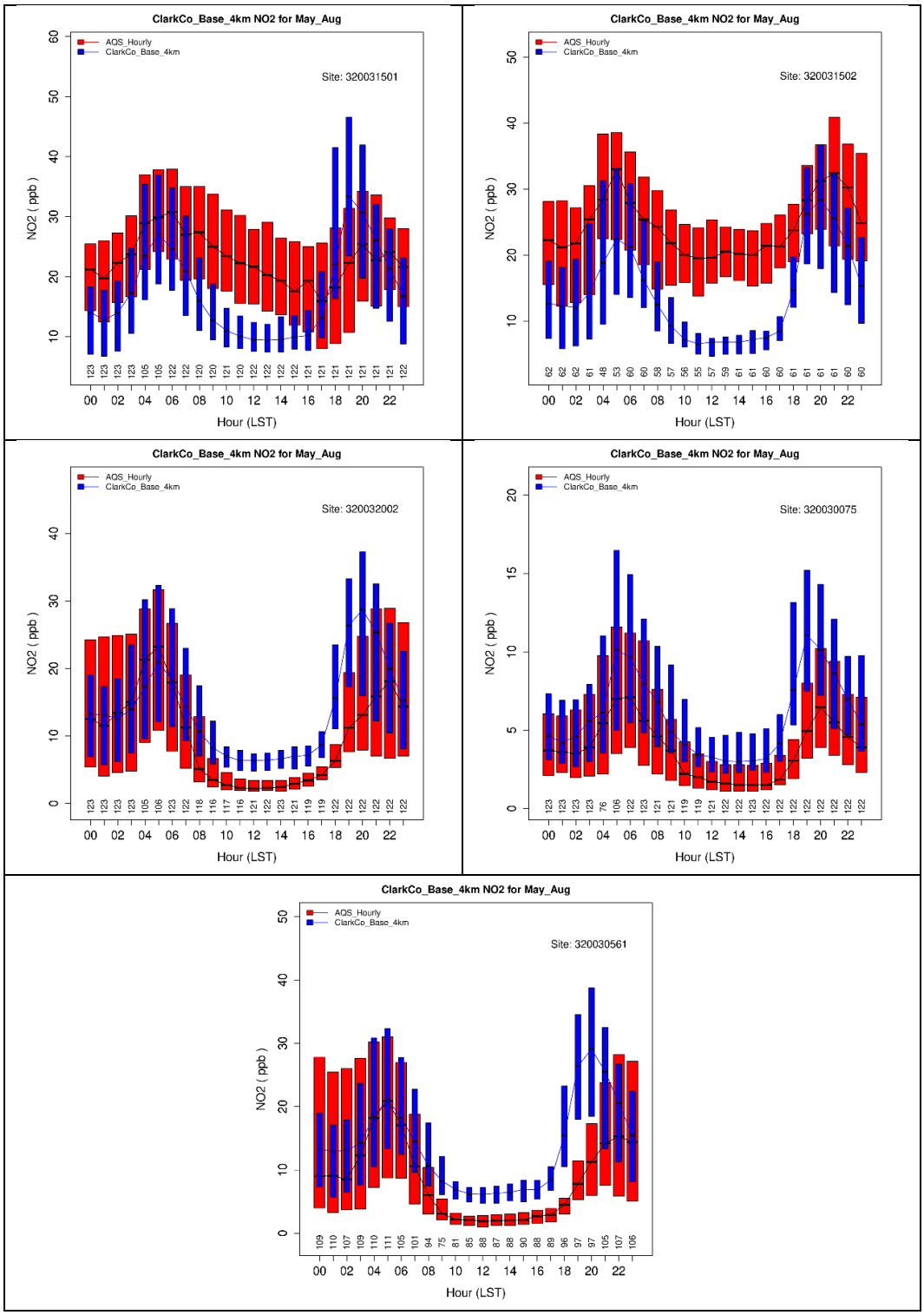

Figure 8-7. Diurnal box plots for observed (red) and predicted (blue) NO_2 at each hour of the day. Averages and ranges are determined over the entire May through August modeling period. "Near-Road" #1 and #2 sites (top row), J.D. Smith (left center), Joe Neal (right center), Sunrise Acres (bottom).

Table 8-5. Observed and predicted MDA8 ozone on days when at least one site monitored an exceedance above 70 ppb. The table shows the observed ozone at the peak site each day, ranked from highest to lowest, and the paired predicted values. Dates noted in red are expected to be influenced by regional wildfires. Dates noted in blue are expected to be caused mainly by local production and upwind transport from anthropogenic sources. Dates noted in black have not been assessed with respect to likely causes.

Site Name	Site ID	Date	Observed	Predicted	Difference
Apex	3200300221	6/24/2016	84.0	60.1	-23.9
Joe Neal	3200300751	7/27/2016	83.6	69.6	-14.1
Joe Neal	3200300751	8/24/2016	80.4	63.0	-17.4
LV Paiute	3200380001	7/1/2016	80.3	65.2	-15.0
LV Paiute	3200380001	6/7/2016	80.1	72.1	-8.1
LV Paiute	3200380001	7/26/2016	79.6	75.2	-4.4
LV Paiute	3200380001	6/8/2016	76.8	60.2	-16.5
SM Youth Camp	3200377714	5/20/2016	76.5	37.2	-39.3
LV Paiute	3200380001	8/23/2016	75.9	71.5	-4.4
Paul Meyer	3200300431	7/29/2016	75.5	77.9	2.4
LV Paiute	3200380001	7/2/2016	75.4	56.2	-19.2
LV Paiute	3200380001	6/25/2016	74.3	73.8	-0.5
Joe Neal	3200300751	6/27/2016	74.1	64.2	-9.9
LV Paiute	3200380001	6/3/2016	74.1	72.4	-1.7
Indian Springs	3200377721	7/25/2016	73.9	61.2	-12.7
Joe Neal	3200300751	6/6/2016	73.8	61.4	-12.4
SM Youth Camp	3200377714	8/25/2016	73.4	61.8	-11.5
Apex	3200320021	7/28/2016	73.0	59.7	-13.3
LV Paiute	3200380001	7/13/2016	73.0	71.3	-1.7
Joe Neal	3200300751	6/23/2016	72.4	61.6	-10.7
LV Paiute	3200380001	6/26/2016	72.4	73.9	1.5
LV Paiute	3200380001	7/14/2016	72.4	72.6	0.3
LV Paiute	3200380001	7/24/2016	72.3	62.2	-10.1
SM Youth Camp	3200377714	6/14/2016	71.5	50.7	-20.8
Paul Meyer	3200300431	8/13/2016	70.8	77.2	6.4
Joe Neal	3200300751	7/7/2016	70.1	50.3	-19.8

8.4 Sensitivity/Diagnostic Tests

These simulations involved assessing ozone impacts from modifying key inputs such as certain emission sectors, meteorological parameters, and chemistry inputs (i.e., mechanisms definitions, boundary conditions, etc.). Such tests help to elucidate sources of poor base case model performance as well as likely influences from future emission changes.

Six sensitivity tests were run that modified the initial 2016 base case configuration:

1. Include aerosols and associated chemical interactions, and elevate landing/takeoff operation (LTO) emissions from Harry Reid International Airport along typical 3-D departure and approach paths (SENS1);
2. Use results from a 2016 GEOS-Chem global chemistry model run (Ramboll, 2022c) to replace EPA's 2016 MP boundary conditions for the 36US3 domain, and run the 36US3 domain alone to develop alternative boundary conditions for the 12US2/CC4c2 domain (SENS2; otherwise, same as SENS1);

3. Conduct a series of short runs over June 20-27, a period of high observed ozone with mixed model performance, in which vertical diffusivity coefficient (Kv) profiles were altered to reduce and increase the rate of mixing at various times of the day (SENS3; otherwise, same as SENS1);
4. Use BEIS3.6/BELD4 biogenic emissions from the 2016v1 MP on the 12US2 domain (without the CC4c2 grid) to investigate LVV ozone sensitivity (SENS4; otherwise, same as the initial base case);
5. Use the latest BEIS4/BELD6 biogenic emissions on the 12US2/CC4c2 grids to investigate LVV ozone sensitivity (SENS5; otherwise, same as SENS1);
6. Use results from a 2016 CAM-Chem global chemistry model run (NCAR, 2022) to replace EPA's 2016 MP boundary conditions for the 36US3 domain, and run the 36US3 domain alone to develop alternative boundary conditions for the 12US2/CC4c2 domain (SENS6; otherwise, same as SENS5).

8.4.1 SENS1 Approach

Independent CAMx testing previously conducted by Ramboll indicated that inclusion of aerosols in the photochemical simulation impacts ozone concentrations to varying degrees depending on many factors, but typically the effect remains within 3-5 ppb regionally. Aerosols influence photolysis rates by altering the scattering and absorption of solar radiation. Additionally, aerosols play an important role in the chemical processing of nitrogen oxides and their products (i.e., "NOz"), a portion of which ultimately feeds back to ozone production at regional scales. Given that EPA ran their 2016v2 MP with aerosols, we decided in SENS1 to test the impact of including aerosols on ozone model performance in the LVV.

The base case model performance evaluation described above showed a tendency to over predict NOx (as NO_2) in the central LVV. The 2016 base year emissions processing placed all airport sector emissions into the single surface grid cell that each airport occupies. While most Clark County airports are not major emission sources, Harry Reid (formally McCarran) International Airport is a major source situated near central Las Vegas. Total 2017 emissions from Reid Airport were estimated to be: 2371 TPY CO, 403 TPY VOC, and 3618 TPY NOx. Of these totals, LTOs comprised 19% CO, 14% VOC, and 68% NOx (2443 TPY). Expecting that the large amount of LTO NOx within a single surface grid cell contributed to overestimates at the central LVV NOx monitors, we developed a program to elevate model-ready LTO emissions to higher model layers along assumed typical departure and approach paths, resulting in a vertical "V" shaped emissions profile centered on the Reid Airport surface grid cell. As a result, this modification removed 7.5 TPD NOx from the Reid Airport cell during a typical summer weekday.

Separate vertical profiles were determined for departure and approach segments. For departure, we applied a typical average climb rate of 2250 feet/minute (i.e., between 2000 and 2500 feet/minute) at 250 knots. We assumed a straight-out departure from runway 26R through 10,000 feet (~3 km – roughly the depth of the maximum afternoon boundary layer). For approach, we applied a typical average decent rate of 1000 ft per 3 nautical miles (1388 feet/minute at 250 knots). We also assumed a straight-in final approach to runway 26L from 10,000 feet. Certain details in our approach deviate from the actual Reid Airport flight pattern, but the purpose of the exercise was to remove LTO emissions from the single 20 m deep grid cell and distribute them three-dimensionally in an arguably realistic manner. A program was constructed that allocates fractions of total model-ready hourly, speciated LTO emissions to each cell along the V-shaped pattern. Resulting emissions were written to a CAMx 3-D emissions input file.

8.4.2 SENS2 Approach

SENS2 was conducted to assess how the source of global boundary conditions influence simulated ozone in the LVV. The EPA developed boundary conditions for their 36US3 domain from a 2016 hemispheric application of the Community Multiscale Air Quality (CMAQ) photochemical model (EPA, 2022a). EPA ran the 36US3 domain separately, then extracted resulting 3-D concentrations for all chemical species to generate boundary conditions for the 12US domain, which EPA ran for all of their subsequent analyses. For SENS2, Ramboll developed a new set of 36US3 boundary conditions from a preexisting 2016 GEOS-Chem dataset generated during our projects supporting the Denver ozone SIP (Ramboll, 2022c). Following EPA's approach, we ran the 36US3 with the alternative boundary conditions, then extracted new 12US2 boundary conditions for the April-August modeling period. The 12US2/CC4c2 grid system was then rerun to complete SENS2. Otherwise, SENS2 was configured the same as SENS1.

8.4.3 SENS3 Approach

SENS3 involved several short tests during late June 2016 in which Kv vertical profiles were altered to reduce the rate of daytime mixing through the boundary layer without altering the depth of mixing. According to aerosol backscatter profiles measured during a summer 2021 field study (NOAA, 2022), the deep afternoon boundary layer is not uniformly well mixed, but instead consistently exhibits vertical pollutant gradients. We postulated that WRF-derived Kv profiles are perhaps too large, over mixing the boundary layer, rapidly resulting in uniform ozone and precursor profiles, and thereby contributing to under predictions of surface ozone. In each test, varying amounts of Kv reductions were applied within the daytime boundary layer. In a separate test, we raised the minimum boundary layer depth during nighttime and morning hours to 300 m in an attempt to reduce the degree of NOx over predictions during commute hours and to assess impacts on ozone production rates. Otherwise, all SENS3 tests were configured the same as SENS1.

8.4.4 SENS4 Approach

SENS4 replaced BEIS3.7/BELD5 biogenic emissions from the 2016v2 MP with BEIS3.6/BELD4 biogenic emissions from the 2016v1 MP. Results from the initial base case indicated that simulated isoprene concentrations often exceeded 1 ppb within the LVV during the daytime. These represent large over predictions relative to 2021 field study measurements (NOAA, 2022) that indicate isoprene should range over a few tenths of a ppb. EPA's analyses undertaken for Denver (Ramboll, 2022c) showed that western statewide biogenic isoprene emissions from BEIS3.6 are about twice as high as BEIS3.7 but urban emissions are lower. Only the 12US2 domain was run for this test as BEIS3.6/BELD4 biogenic emissions from the 2016v1 MP were readily available on that grid. Otherwise, SENS4 was configured the same as the initial base case, with no aerosols and no adjustment to Reid Airport LTO emissions since that was applied only on the CC4c2 grid.

8.4.5 SENS5 Approach

SENS5 replaced BEIS3.7/BELD5 biogenic emissions with the latest BEIS4/BELD6 biogenic emissions platform. Reports from EPA's early testing for the western US (Ramboll, 2022c) indicated that BEIS4 resulted in lower biogenic emissions than BEIS3.6. EPA graciously processed BELD6 vegetative cover datasets for the 12US2 and CC4c2 grids for our use with BEIS4. Ramboll processed BEIS4 biogenic emissions on the 36US3/12US2/CC4c2 grid system for the entirety of the April-August modeling period and ran CAMx with the same configuration as SENS1.

8.4.6 SENS6 Approach

SENS6 was conducted to assess another alternative source of global model boundary conditions. The Community Atmosphere Model with Chemistry (CAM-chem) is a component of the NCAR Community

Earth System Model (CESM) and is used for simulations of global tropospheric and stratospheric atmospheric composition (NCAR, 2022). CAM-chem uses the MOZART chemical mechanism, with various choices of complexity for tropospheric and stratospheric chemistry. CESM2, including CAM6-chem, is the current version. NCAR has run CAM-Chem and archives 6-hourly output on a ~1 degree resolution global grid from January 1, 2001 to December 31, 2020. Portions of the grid can be downloaded from NCAR for chemical model downscaling to support regional applications (Buchholz et al., 2019).

Ramboll developed a new set of 36US3 boundary conditions from existing 2016 CAM-Chem datasets archived at NCAR (NCAR, 2022). We developed graphical comparisons of ozone fields across North America and at several altitude from GEOS-Chem and CAM-Chem and noted that the latter simulated much higher ozone patterns throughout the mid- and upper-troposphere (3-8 km) over the western US. Anticipating that this additional mid-level ozone may help to alleviate large regional ozone under predictions across the western US, we ran the 36US3 grid with the alternative boundary conditions, then extracted new 12US2 boundary conditions for the April-August modeling period. The 12US2/CC4c2 grid system was then rerun to complete SENS6. Otherwise, SENS6 was configured the same as SENS1 and SENS5 using BEIS4 on all three grids.

8.4.7 Summary of Results

Results from the 2016 sensitivity cases are summarized below:

- In SENS1 and SENS2, MDA8 ozone continued to be under predicted for most sites and months, and performance statistics showed successively worse performance in both tests.
  - Both sensitivity runs had little influence on basin-wide and regional ozone.
  - SENS1 with elevated Reid Airport emissions showed filling of a local ozone hole in that area caused by high NOx emissions.
  - SENS1 with aerosols resulted in consistent 1-3 ppb decreases in background concentrations entering the LVV.
  - SENS2 with alternative 36US3 boundary conditions showed generally lower background concentrations entering the LVV relative to both the initial base case and SENS1.
  - Under prediction bias continued to be relatively larger on high observed ozone days (>60 ppb).
- In SENS1 and SENS2, NO_2 continued to transition to lower ambient concentrations from May to August.
  - Elevating Reid Airport emissions in SENS1 reduced surface NO_2, resulting in a near zero bias in May to -18% bias in August, which was more expected given the inability of the grid to resolve local NOx emissions.
  - The SENS1 impact to diurnal NO_2 concentrations was substantial during certain hours of the day with largest reductions at sites closest to Reid Airport, especially during the daytime and evening commute hours.
  - Elevating Reid Airport LTO emissions away from the surface grid cell was appropriate.
- All SENS3 tests with reduced rates of vertical mixing usually resulted in substantially lower regional and local ozone.
  - Lower Kv resulted in a clear inhibition of local ozone production due to enhancing near-surface buildup of NOx concentrations in the central LVV.
  - Lower Kv resulted in a widespread reduction in downward mixing of higher regional ozone concentrations aloft.

- A SENS3 test that raised Kv such that that the boundary layer depth would never decrease below 300 m during the night and morning hours resulted in no effects to NOx or ozone during daylight hours when vertical mixing far exceeded the 300 m minimum.
  - Deeper mixing between 8 PM and 6 AM reduced NOx concentrations in the central LVV substantially, but those reductions had no impact on morning or daytime NO_2 or ozone production.
- Use of BEIS3.6/BELD4 biogenic emissions on the 12US2 grid in SENS4 greatly increased ozone in the LVV and improved statistical performance during June-August to within benchmark goals.
  - BEIS3.6/BELD4 generated higher rural biogenic isoprene emissions but lower urban emissions that better agree with 2021 field measurements in central Las Vegas.
  - However, the regional under prediction bias across the California transport corridor was not as dramatically affected, perhaps because of the NOx-limited, VOC-lean conditions there. Biogenic isoprene also can react with and destroy ozone, balancing the low ozone production rates in rural areas.
  - Given the much higher rural VOC emissions, use of coarse resolution, and some large MDA8 ozone over predictions during June-August, we were concerned that the much higher ozone resulting from BEIS3.6/BELD4 led to a model that performs better but for the wrong reason.
- Use of BEIS4/BELD6 biogenic emissions in SENS5 did not markedly change ozone performance in the LVV or over the wider region relative to SENS1 and led to under predictions of isoprene in the LVV.
  - BEIS4/BELD6 generated much lower rural and urban biogenic isoprene emissions than both BEIS3.6 and BEIS3.7.
  - The lack of regional impact across the California transport corridor was again most likely a result of NOx-limited, VOC-lean conditions there.
- The use of CAM-Chem BCs in SENS6 led to markedly improved regional and urban ozone performance during May and June, but similar performance to SENS5 during July and August.
  - Under prediction bias continued to be relatively larger on high observed ozone days (>60 ppb) but most months were within statistical benchmarks.
- Overall, the evaluation of initial base year model performance indicates:
  - A lack of regional ozone buildup and transport into the LVV that is ameliorated during the spring and early summer by the use of alternative boundary conditions representing North American background ozone;
  - A strong sensitivity to rural rather than urban biogenic VOC emissions;
  - Local NOx-heavy chemistry (ozone inhibition and potential NOx disbenefit);
  - Relative quantities of ozone and NOx change over the summer, leading to better performance for both compounds in August.

8.4.8 Results from Sensitivity Tests 1 and 2

Table 8-6a lists monthly NMB and NME statistical performance for MDA8 ozone over all days and all ozone monitoring sites within the CC4c2 domain. The table compares results from the Clark County base case and both sensitivity runs. NMB and NME are color coded for visual reference to statistical goals and criteria benchmarks.

Performance among all simulations was very similar, showing a consistent and systematic negative bias over all months. A rather large negative bias outside of the criteria benchmark occurred in May, followed by a transition to smaller bias through August well within the statistical goal. The sensitivity tests resulted in a progressively larger bias and error relative to the initial base case.

Table 8-6. Monthly model performance statistics for MDA8 ozone over all days and all ozone monitoring sites within the CC4c2 domain that operated during the summer of 2016. Normalized mean bias (NMB) and normalized mean unsigned error (NME) are shown with color coding indicating statistics outside performance criteria (red), between goals and criteria (yellow) and within goals (green). Results from the Clark County initial base case and two sensitivity cases are compared.

Month	MDA8 Ozone (no cutoff)					
	NMB (%)			NME (%)		
	BASE	SENS1	SENS2	BASE	SENS1	SENS2
May	-17.9	-19.5	-18.5	18.3	19.6	18.7
June	-9.2	-9.4	-12.1	11.2	11.2	13.3
July	-8.2	-8.6	-11.6	11.1	11.2	13.5
Aug	0.1	-1.2	-4.6	10.7	10.9	9.6
May-Aug	-8.8	-9.7	-11.7	12.8	13.2	13.8

Table 8-6b presents the same information but limited to sites and days when observed MDA8 ozone exceeded 60 ppb. Similar patterns are evident on high ozone days, with again progressively worse performance in the sensitivity tests. The overall monthly statistical results shown in these tables apply consistently across all CCNAA monitoring sites, with no single sites indicating substantially worse or better statistical performance than the initial base case.

Table 8-6b. As in Table 8-6a, but for all sites and days when monitored MDA8 ozone exceeded 60 ppb.

Month	MDA8 Ozone (60 ppb cutoff)					
	NMB (%)			NME (%)		
	BASE	SENS1	SENS2	BASE	SENS1	SENS2
May	-21.5	-22.5	-21.6	21.5	22.5	21.6
June	-11.3	-11.4	-12.9	12.7	12.7	13.9
July	-11.7	-12.0	-14.7	12.7	12.8	15.3
Aug	-4.3	-5.3	-8.8	11.4	12.0	11.0
May-Aug	-11.5	-12.1	-14.0	13.9	14.2	15.0

Figures 8-8 and 8-9 present spatial maps of site-specific monthly NMB from the SENS1 and SENS2 cases, respectively, for selected monitoring sites across the Mojave Desert of Southern California. The plots show the same general pattern of systematic negative bias and month-by-month improvement through August as the initial base case (Figure 8-3). The under prediction bias remained much larger than the LVV sites and slightly larger than the initial base case. This continued to implicate a lack of regional ozone and associated transport as a likely contributor to poor performance in the LVV, despite the use of alternative boundary conditions. Therefore, model performance across Southern California and within the LVV was not sensitive to the inclusion of aerosol chemistry or the use of GEOS-Chem as the source of global background as represented by boundary conditions.

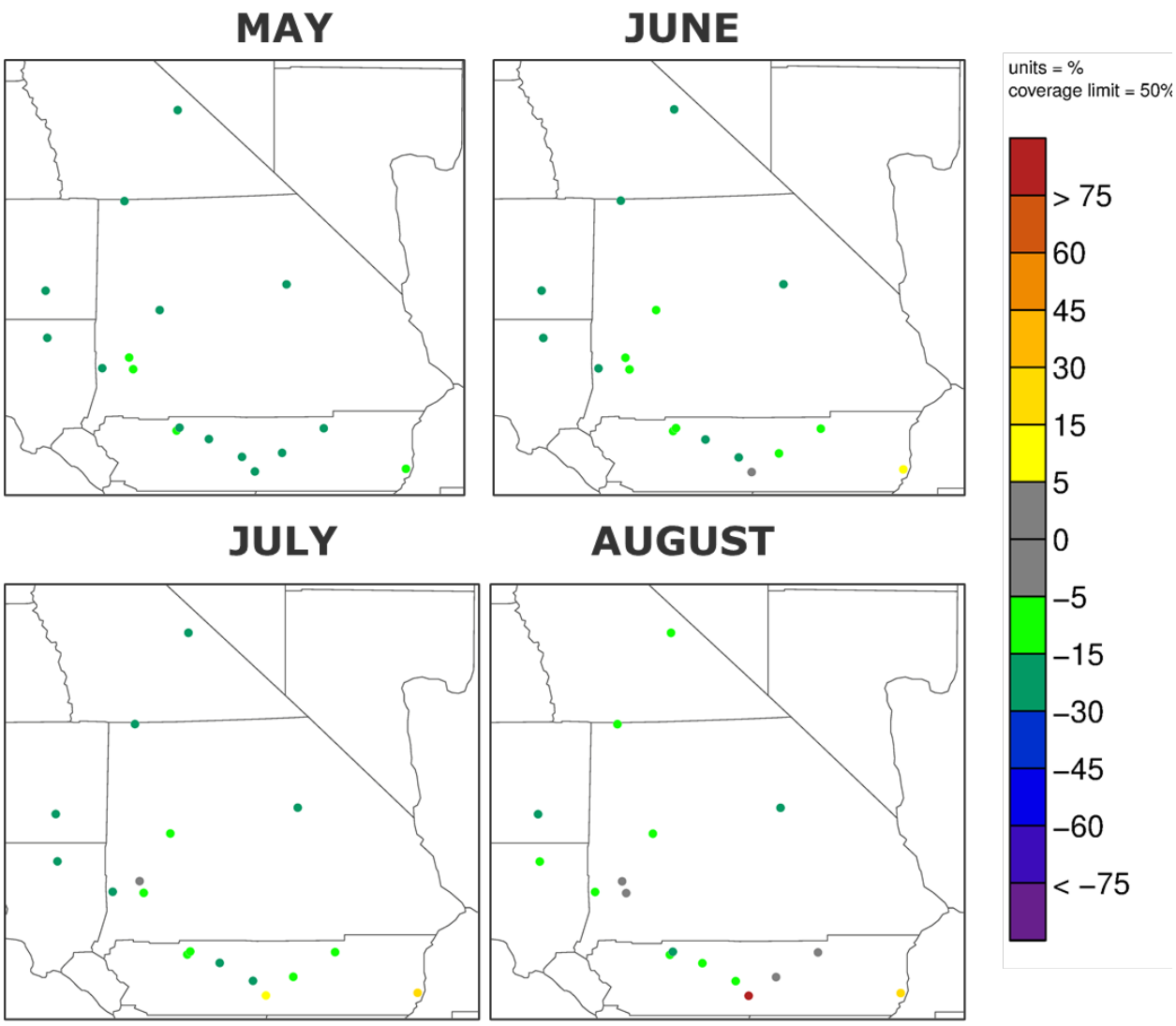

Figure 8-8. Map of site-specific monthly normalized mean bias (NMB) patterns for MDA8 ozone in the SENS1 case across the Mojave Desert of the southern California portion of the 12US2 domain.

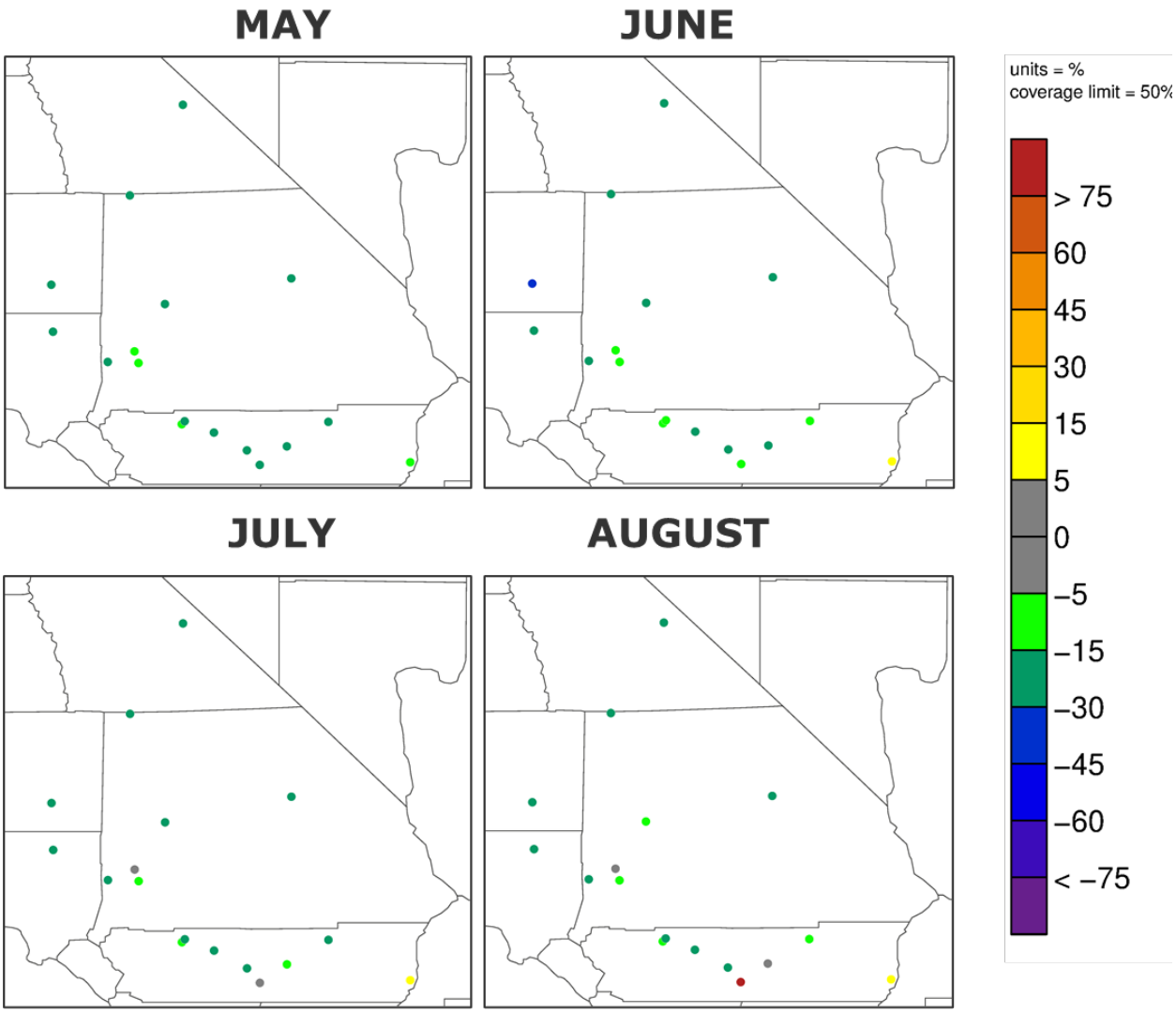

Figure 8-9. Map of site-specific monthly normalized mean bias (NMB) patterns for MDA8 ozone in the SENS2 case across the Mojave Desert of the southern California portion of the 12US2 domain.

Figure 8-10 presents time series of observed and simulated MDA8 ozone during the May through August modeling period at the Joe Neal monitoring site. The initial base case is shown in blue and the sensitivity cases are shown in red (SENS1 in top panel, SENS2 in bottom panel). The base case and SENS1 predicted nearly identical ozone results, with periods when SENS1 was slightly lower. SENS2 resulted in consistently lower ozone throughout the summer due to alternative boundary conditions and lower regional ozone. Figure 8-11 shows time series at the Palo Verde site with very similar results.

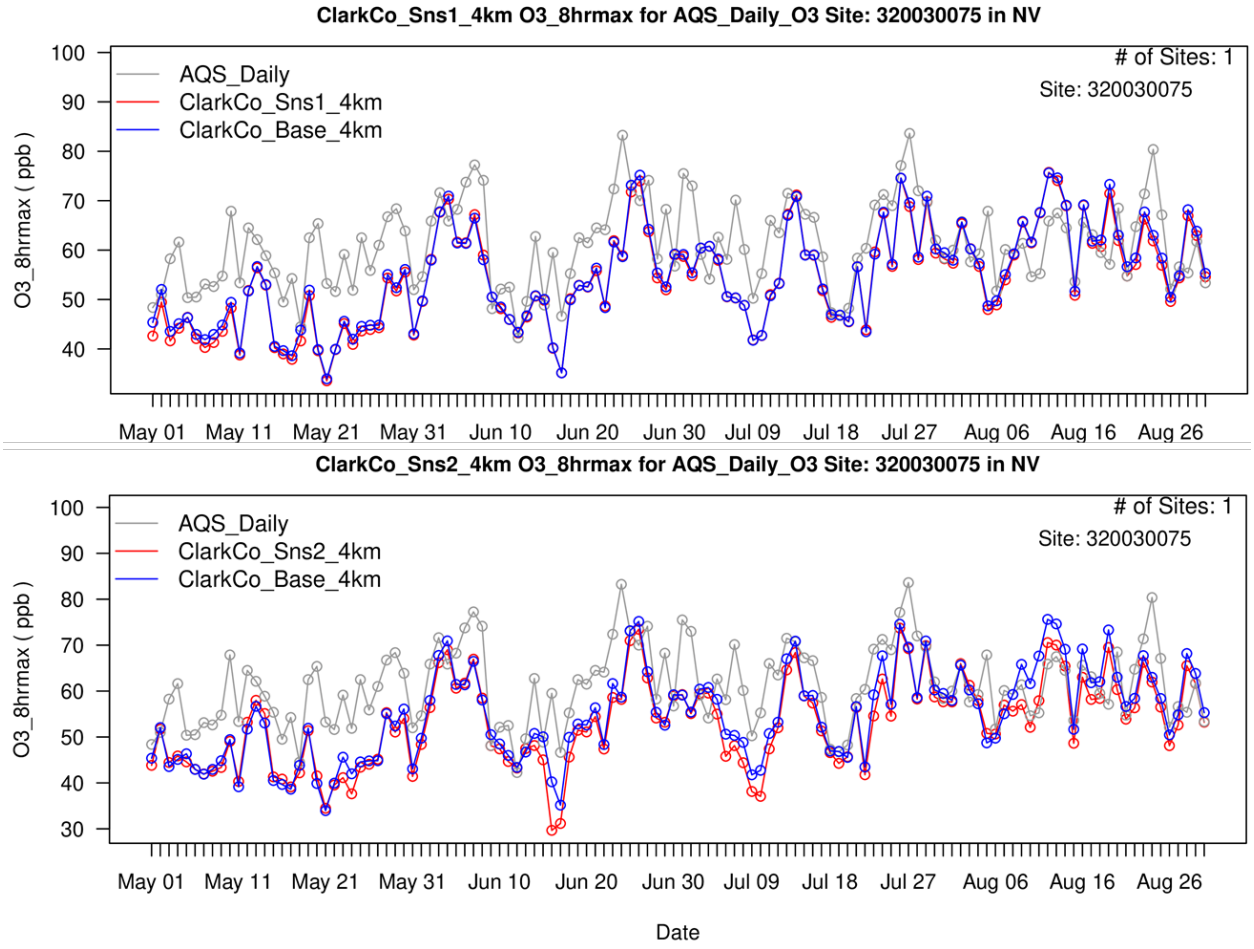

Figure 8-10. Time series of MDA8 ozone over the entire modeling period at the Joe Neal monitoring site. Daily AQS measurements are shown in grey, the modeled base case results are shown in blue, and the SENS1 (top) and SENS2 (bottom) results are shown in red.

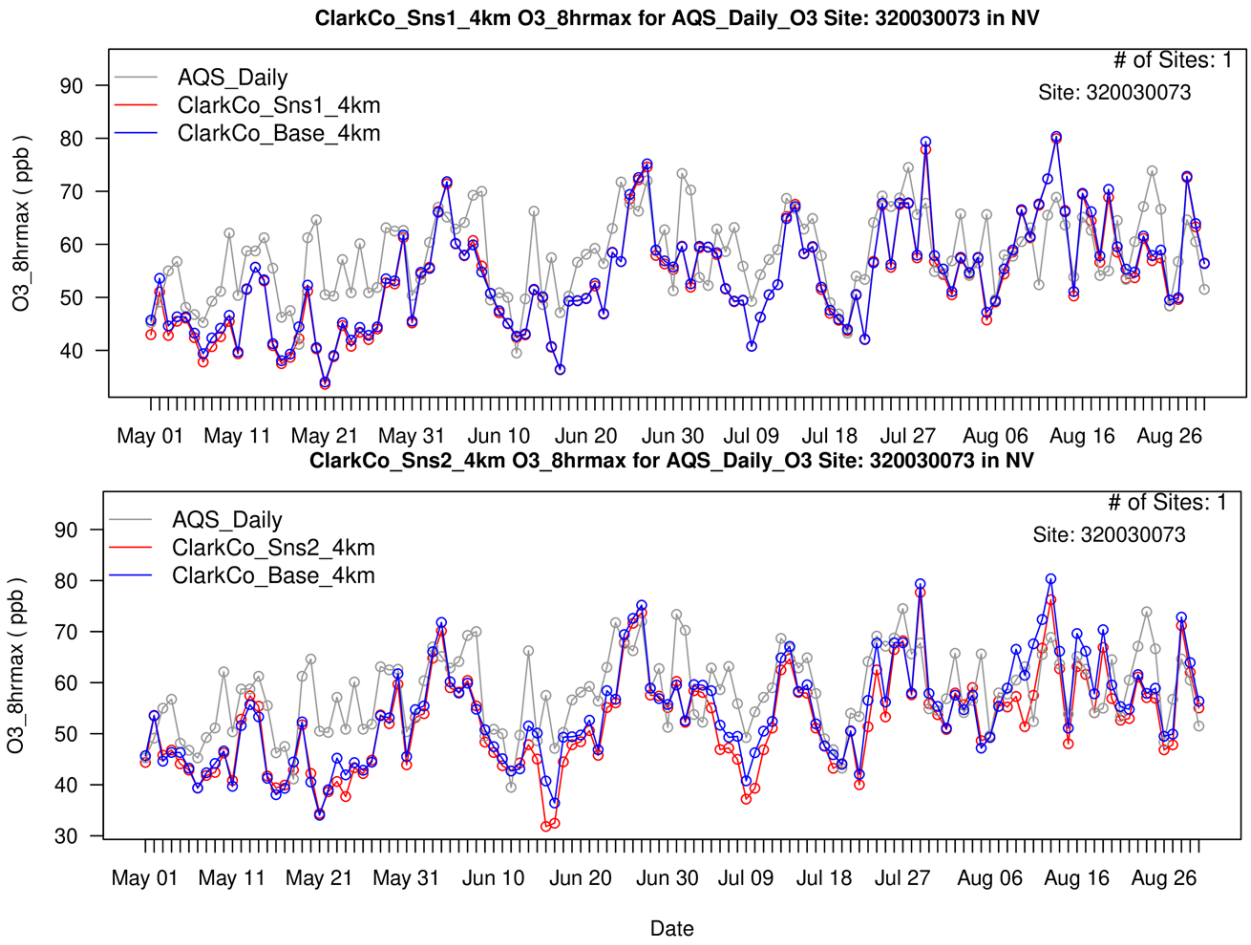

Figure 8-11. Time series of MDA8 ozone over the entire modeling period at the Palo Verde monitoring site. Daily AQS measurements are shown in grey, the modeled base case results are shown in blue, and the SENS1 (top) and SENS2 (bottom) results are shown in red.

Scatter plots of 1-hour NO_2 from the SENS1 case (not shown) show the same general patterns as the initial base case, but the largest over predictions were reduced 10-20 ppb in SENS1 due to the elevation of LTO emissions. The lower NO_2 concentrations resulted in a bias transition from about zero in May to -18% in August. We expected a tendency for consistent under predictions given the inability of the grid to resolve local NOx emissions, so these results conformed to expectations. Normalized errors (degree of scatter) remained in the range of 50% to 60% and correlations remained low for the period.

Figure 8-12 shows box plots of observed and predicted diurnal NO_2 concentrations in the SENS1 case, arranged similarly to Figure 8-7 that displays initial base case results (note different concentration scales among these plots). Diurnal prediction patterns were similar to the base case, but NO_2 reductions were notable at sites nearest Reid Airport (near-road sites and Sunrise Acres). At these sites, the largest reductions occurred during the evening commute hours, and midday NO_2 concentrations decreased from near 10 ppb to closer to 5 ppb.

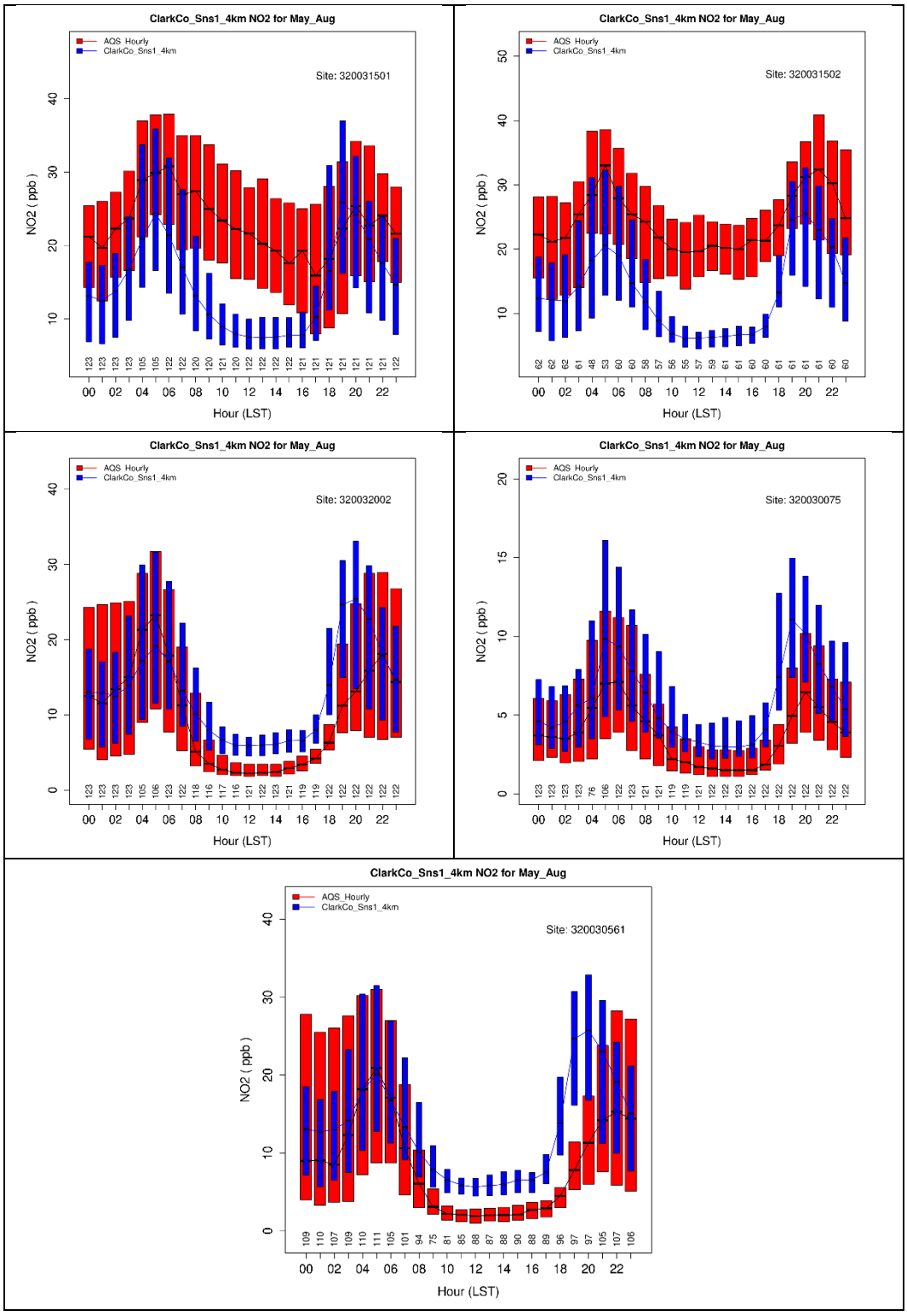

Figure 8-12. Diurnal box plots for observed (red) and SENS1 predicted (blue) NO_2 at each hour of the day. Averages and ranges are determined over the entire May through August modeling period. "Near-Road" #1 and #2 sites (top row), J.D. Smith (left center), Joe Neal (right center), Sunrise Acres (bottom).

However, there continued to be a strong tendency to over predict at sites not situated near major roadways, especially during evening commute hours. Continued over predicted NOx concentrations of 20 to 30 ppb during the evening likely suppressed ozone toward the end of the daily maximum 8-hour averaging period. These features continued to indicate problems with the characterization of mobile source emissions and/or perhaps insufficient mixing depths. However, these results confirmed that elevating Reid Airport LTO emissions away from the surface grid cell was appropriate.

8.4.9 Sensitivity to Vertical Mixing

Figure 8-13 shows an example of Doppler lidar aerosol backscatter and turbulence intensity above North Las Vegas airport in August 2021 reported by NOAA (2022). These types of plots provide valuable qualitative information about the structure of the summer daytime boundary layer. The diagnosed boundary layer height extended above 3 km, in agreement with WRF results used in this study. Measurements showed that the daytime boundary layer was not uniformly well mixed, but instead it consistently exhibited gradients in vertical pollutant profiles (left) and turbulent mixing rates (right).

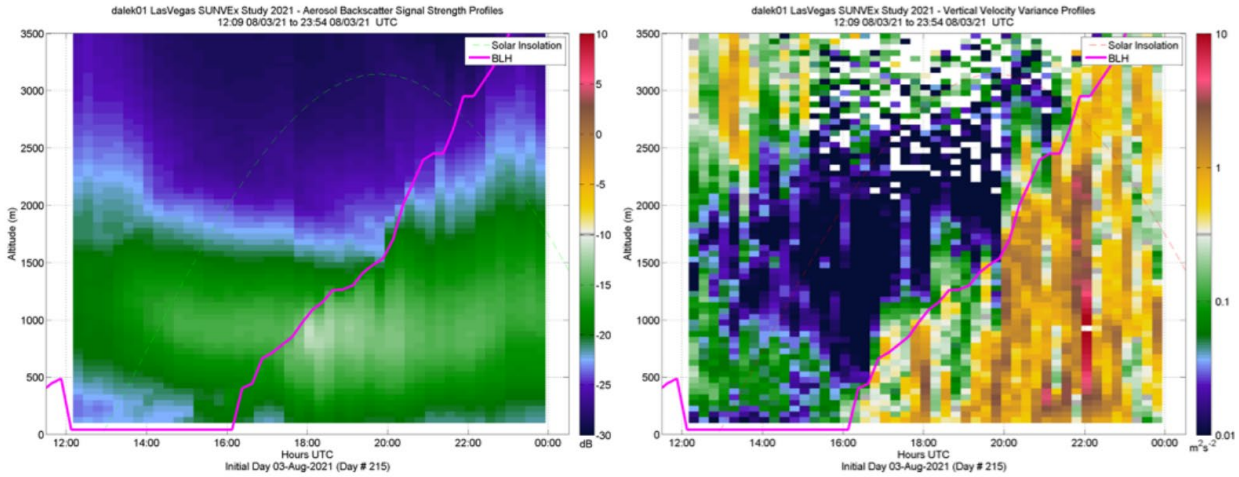

Figure 8-13. Example 15-minute time-height cross sections from Doppler lidar profiles of aerosol backscatter (dB, left) and turbulent intensity (m^2/s^2, right) on an August day in 2021. An estimate of the boundary layer height is shown as the magenta line (taken from NOAA, 2022).

In each of four diffusivity tests conducted under SENS3, we applied varying amounts of Kv reduction within the daytime boundary layer. Yet all tests resulted in substantially lower regional and local ozone. Reduced Kv rates resulted in a clear inhibition of local ozone production due to the near-surface buildup of NOx concentrations in the central LVV. Reduced Kv rates also resulted in a widespread reduction in downward mixing of higher regional ozone concentrations aloft. Therefore, we provide only one example of SENS3 results below for illustrative purposes.

Figure 8-14 shows the spatial pattern of MDA8 ozone on June 24, a day with peak observed MDA8 ozone of 84 ppb at Apex to the northeast of Las Vegas but very low predicted ozone across the LVV. The effects from reduced Kv on this day were typical of all other days and tests: regional ozone was substantially lower than the base case, and the base case ozone hole over central Las Vegas was larger and deeper. Since these tests disproved our hypothesis that reduced Kv might increase surface ozone by limiting mixing rates, and effectively reducing the net mixing volume, we did not pursue our investigation further.

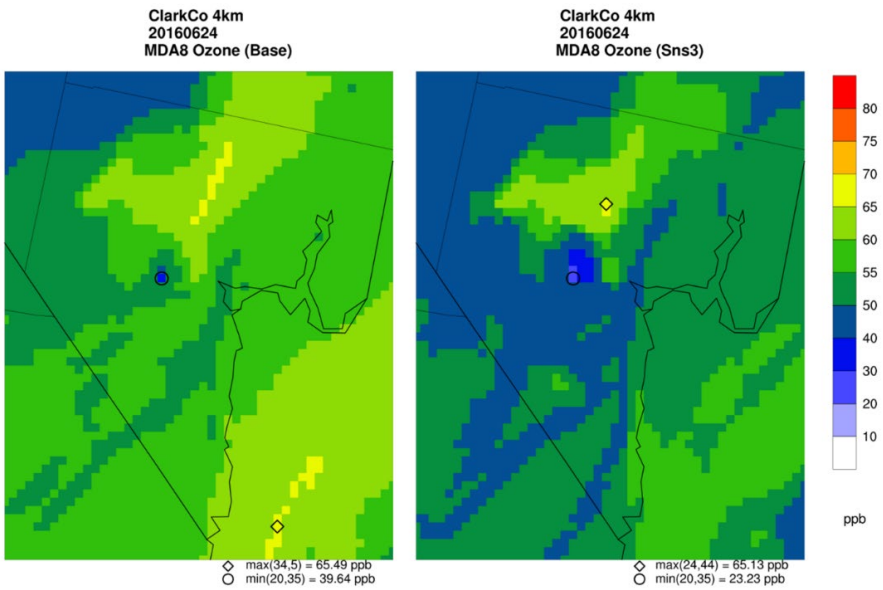

Figure 8-14. Spatial distribution of MDA8 ozone on June 24, 2016 from the base case (left) and from a SENS3 Kv reduction case (right).

Another Kv sensitivity test was performed in which we configured the diffusivity inputs in such a way that boundary layer depth would never decrease below 300 m during the night and morning hours. This test investigated the role of vertical mixing in over predicting NOx concentrations during commute periods. No effects to NOx or ozone were seen during daylight hours when vertical mixing far exceeded the 300 m minimum. Between 8 PM and 6 AM, however, the deeper mixing depths were effective at reducing NOx concentrations in the central LVV substantially, but those reduction had no impact on morning or daytime NO_2 or ozone production. By 6-7 AM, NOx and ozone concentrations were identical to the base case, indicating a very rapid growth of deep mixing above 300 m early each day. Therefore, this Kv modification was not carried into additional CAMx simulations.

8.4.10 Sensitivity to Biogenic Emissions

8.4.10.1 BEIS3.6/BELD4 on the 12US2 Grid

SENS4 replaced BEIS3.7/BELD5 biogenic emissions on the 12US2 domain with BEIS3.6/BELD4 biogenic emissions from the 2016v1 MP. Only the 12US2 domain was run for this test, without the CC4c2 grid, as BEIS3.6/BELD4 biogenic emissions were readily available on that grid. Otherwise SENS4 was configured the same as the base case.

Table 8-7a lists monthly NMB and NME statistical performance for MDA8 ozone over all days and all ozone monitoring sites within the CC4c2 domain. The table compares results from the SENS4 and EPA's 2016v2 12US2 simulation to maximize consistency for the evaluation. NMB and NME are color coded for visual reference to statistical goals and criteria benchmarks. Performance results in SENS4 were remarkably improved over the EPA simulation, despite the continuing large negative bias outside of the criteria benchmark in May. Bias and gross error were within or very near the goals in June through August, with a slight over prediction in August. Overall statistical performance over the entire May through August period was also within goals.

Table 8-7a. Monthly model performance statistics for MDA8 ozone over all days and all ozone monitoring sites within the CC4c2 domain that operated during the summer of 2016. Normalized mean bias (NMB) and normalized mean unsigned error (NME, also referred to as gross error) are shown with color coding indicating statistics outside performance criteria (red), between goals and criteria (yellow) and within goals (green). Results from the SENS4 case and EPA's 2016v2 12US2 simulation are compared.

Month	MDA8 Ozone (no cutoff)			
	NMB (%)		NME (%)	
	SENS4	EPA 12US2	SENS4	EPA 12US2
May	-14.4	-15.9	15.3	16.1
June	-2.6	-6.5	8.4	9.0
July	-2.2	-7.9	10.2	10.7
Aug	5.4	-0.6	12.6	11.5
May-Aug	-3.4	-7.7	11.6	11.8

Table 8-7b presents the same information but limited to sites and days when observed MDA8 ozone exceeded 60 ppb. Similar improvements were evident on high ozone days, with just slightly more negative bias.

Table 8-7b. As in Table 8-7a, but for all sites and days when monitored MDA8 ozone exceeded 60 ppb.

Month	MDA8 Ozone (60 ppb cutoff)			
	NMB (%)		NME (%)	
	SENS4	EPA 12US2	SENS4	EPA 12US2
May	-18.2	-19.7	18.2	19.7
June	-3.8	-9.2	8.5	9.6
July	-5.0	-12.0	11.1	12.6
Aug	0.4	-5.6	11.6	11.8
May-Aug	-5.6	-11.1	11.7	12.8

Figure 8-15 displays a spatial map of site-specific monthly NMB patterns for MDA8 ozone across the CC4c2 portion of the 12US2 domain. In this case, NMB was determined from all days without the 60 ppb cutoff applied, so the maps are consistent with the data in Table 8-7a. These plots again show dramatic improvements in bias in June and July relative to the base case (Figure 4), and the change to slight over predictions throughout much of the LVV in August.

Figure 8-16 presents a similar spatial map of site-specific monthly NMB, but for selected monitoring sites across the Mojave Desert of Southern California. The plots indicate some improvement in overall negative bias patterns relative to the base case (Figure 8-3), but the differences are more subtle than for sites within the LVV. Therefore, the regional under prediction bias over the California transport corridor remained an issue.

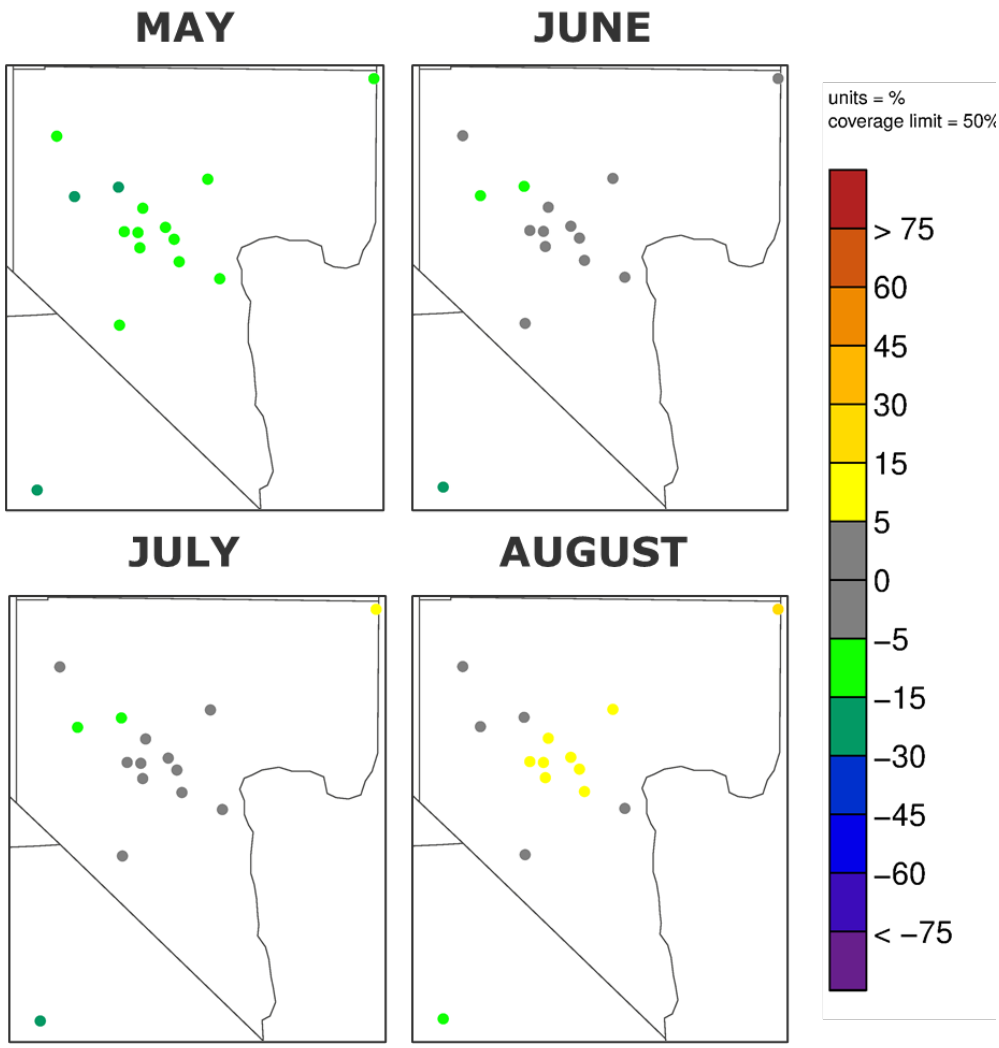

Figure 8-15. Map of site-specific monthly normalized mean bias (NMB) patterns for MDA8 ozone from SENS4 within the CC4c2 portion of the 12US2 domain.

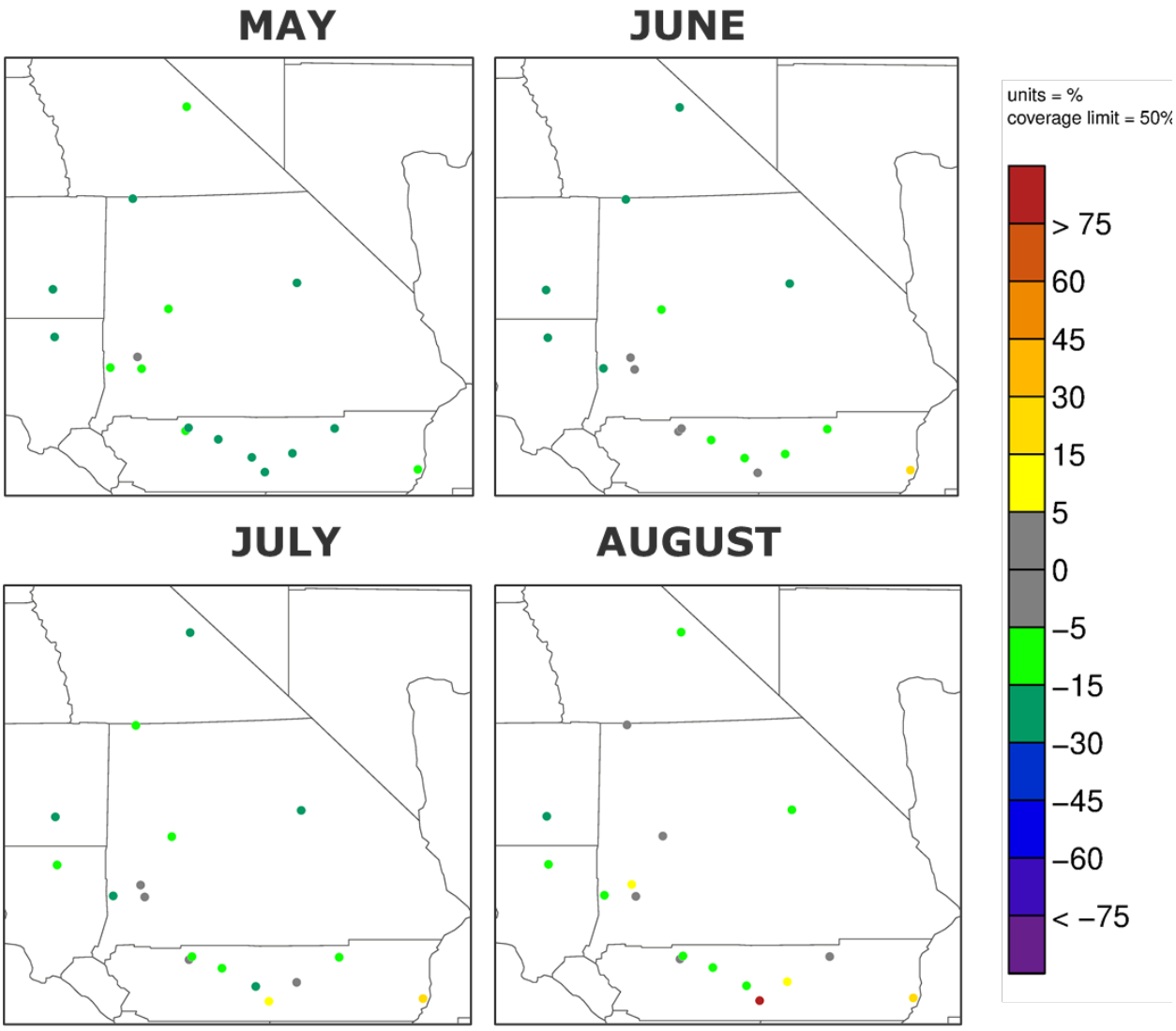

Figure 8-16. Map of site-specific monthly normalized mean bias (NMB) patterns for MDA8 ozone from SENS4 across the Mojave Desert of the southern California portion of the 12US2 domain.

Figure 8-17 presents time series of observed and simulated MDA8 ozone during the May through August modeling period at two representative monitoring sites. The use of BEIS3.6/BELD4 biogenic emissions in SENS4 led to a substantial increase in simulated ozone at these two sites, as well as all other LVV sites as shown above. There was a clear tendency to over predict daily ozone in August, but the SENS4 simulation in June and July was markedly better than EPA's 2016v2 results, and by extension better than the initial base case simulation on the CC4c2 grid.

These results showed improved model performance when choosing the alternative source of biogenic emissions. BEIS3.6/BELD4 generated higher rural biogenic isoprene emissions but lower urban biogenic emissions relative to BEIS3.7. In this sensitivity run, lower urban biogenic emissions resulted in isoprene concentrations of roughly 0.25 ppb compared to more than 1 ppb in the base case. Therefore, isoprene from BEIS3.6 better agreed with 2021 field measurements in central Las Vegas (NOAA, 2022).

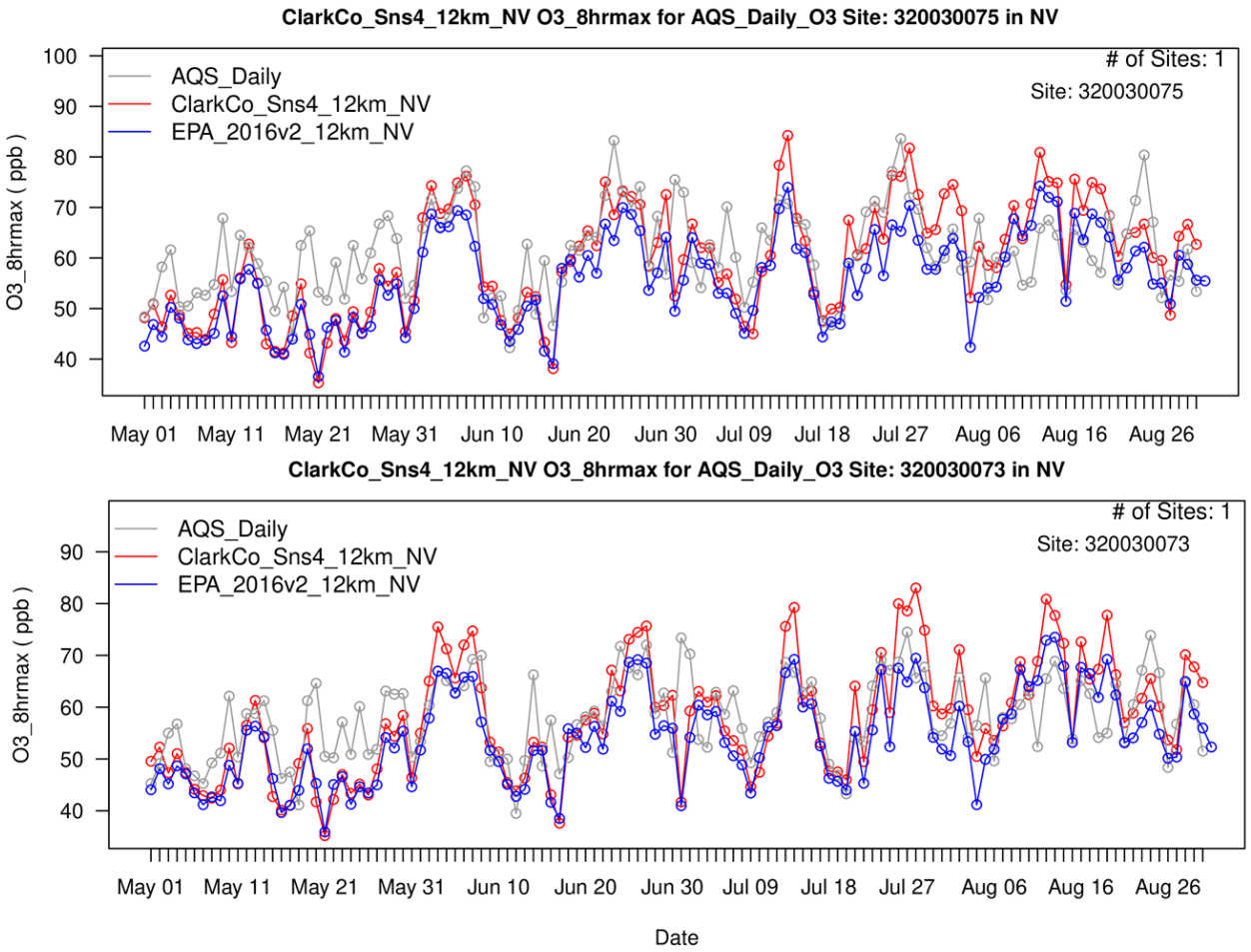

Figure 8-17. Time series of MDA8 ozone over the entire modeling period at the Joe Neal (top) and Palo Verde (bottom) monitoring sites. Daily AQS measurements are shown in grey, the modeled SENS4 results are shown in red, and EPA's results taken from their 2016v2 simulation on the 12US2 domain are shown in blue.

Higher levels of rural biogenics entering the basin generated more ozone in the NOx-rich conditions. The use of 12-km resolution may have played some role in increasing ozone production rates in the LVV as rural biogenics and urban NOx more readily mixed at this coarse resolution. Given the much higher rural VOC emissions, use of course resolution, and some large MDA8 ozone over predictions during June-August, we were concerned that the much higher ozone resulting from BEIS3.6/BELD4 led to a model that performed better but for the wrong reason.

In the Mojave Desert, however, much less ozone sensitivity to biogenic emissions was evident perhaps because of the NOx-lean (i.e., NOx-limited) conditions there. Biogenic isoprene also can react with and destroy ozone, resulting in lower ozone production rates in rural areas.

8.4.10.2 BEIS4/BELD6 on the 12US2/CC4c2 Grids

Table 8-8 lists 2016 summer monthly average biogenic emissions on the CC4c2 grid as determined from four different biogenic emission platforms (note that for completeness the table includes BEIS3.6/BELD4 estimates on the CC4c2 grid that we generated after SENS4 was completed).

Table 8-8. 2016 summer monthly biogenic emissions (TPD) estimated for the CC4c2 modeling domain from four biogenic modeling systems.

Biogenic Model	May	June	July	August	Average
	NOx				
BEIS3.6/BELD4 (2016v1)	6	9	9	9	8
BEIS3.7/BELD5 (2016v2)	5	7	8	7	7
BEIS4/BELD6	5	7	8	7	7
MEGAN3.2	17	32	30	27	27
Biogenic Model	**VOC**				
BEIS3.6/BELD4 (2016v1)	850	1,936	2,128	1,737	1,663
BEIS3.7/BELD5 (2016v2)	288	654	717	586	561
BEIS4/BELD6	71	154	167	139	133
MEGAN3.2	2	3	15	26	12
Biogenic Model	**Isoprene**				
BEIS3.6/BELD4 (2016v1)	145	294	304	258	250
BEIS3.7/BELD5 (2016v2)	57	114	118	101	97
BEIS4/BELD6	13	23	22	20	19
MEGAN3.2	1	1	7	2	3
Biogenic Model	**Terpene**				
BEIS3.6/BELD4 (2016v1)	253	582	653	534	505
BEIS3.7/BELD5 (2016v2)	64	148	165	135	128
BEIS4/BELD6	16	36	40	33	31
MEGAN3.2	1	1	4	2	2

Figures 8-18a and b show plots of season-average NOx and VOC emissions, respectively, for each of the four models. While modeled NOx and VOC emission rates trended downward with succeeding biogenic emission models, the huge range of emission rates among these versions is stunning and illustrates the remaining uncertainty in desert biogenic emission estimates and related vegetative characterization over just the last few years. Most notably, VOC emissions vary by nearly 1000-fold between BEIS3.6 and the latest Model of Emissions of Gases and Aerosols from Nature (MEGAN), version 3.2 (UCI, 2022).

The rather large VOC estimates from BEIS3.6/BELD4 confirmed our suspicion of that model's tendency to over predict regional VOC emissions and resulting ozone production in the LVV, despite the lower urban isoprene levels in the LVV in agreement with 2021 measurements. BEIS3.7/BELD5, on the other hand, was a complete inversion of isoprene emission patterns from its predecessor, with much smaller rural rates but larger urban rates that led to isoprene overestimates in the LVV yet much lower ozone. The latest version, BEIS4/BELD6, reduced both rural and urban isoprene emissions below both of its predecessors. Sensitivity results from using this version are described below. MEGAN3.2 indicated practically zero biogenic VOC within the CC4c2 domain, which appeared to be far too low relative to evidence from 2021 LVV measurements. However, MEGAN estimated the largest amount of biogenic NOx emissions among all four models by factors of 3 to 4. Given its very different and very low VOC emission profiles, we dropped MEGAN3.2 from further consideration.

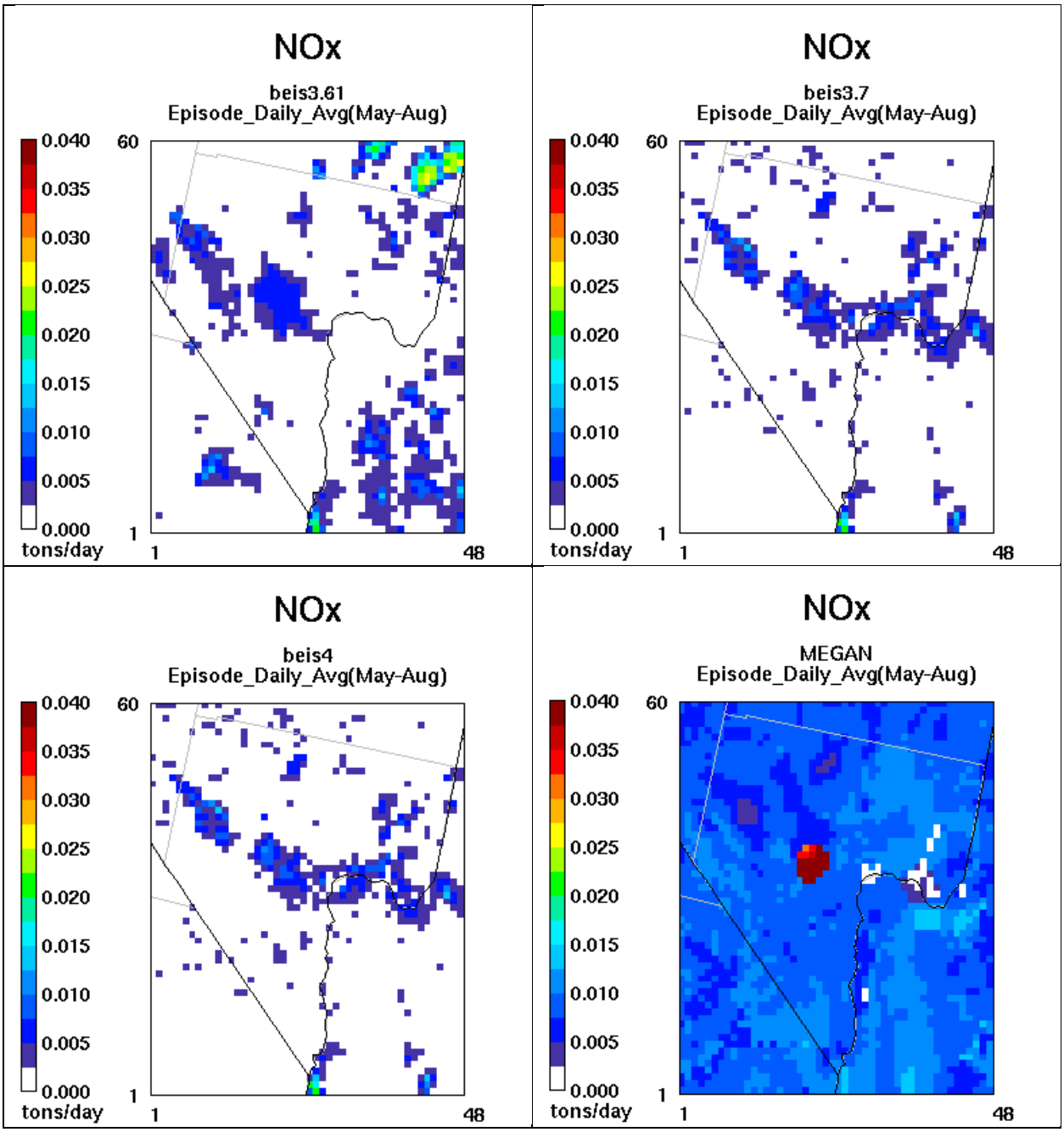

Figure 8-18a. Spatial plots of season-average NOx emissions (tons per day) from four biogenic models: BEIS3.6/BELD4 (top left); BEIS3.7/BELD5 (top right); BEIS4/BELD6 (bottom left); MEGAN3.2 (bottom right).

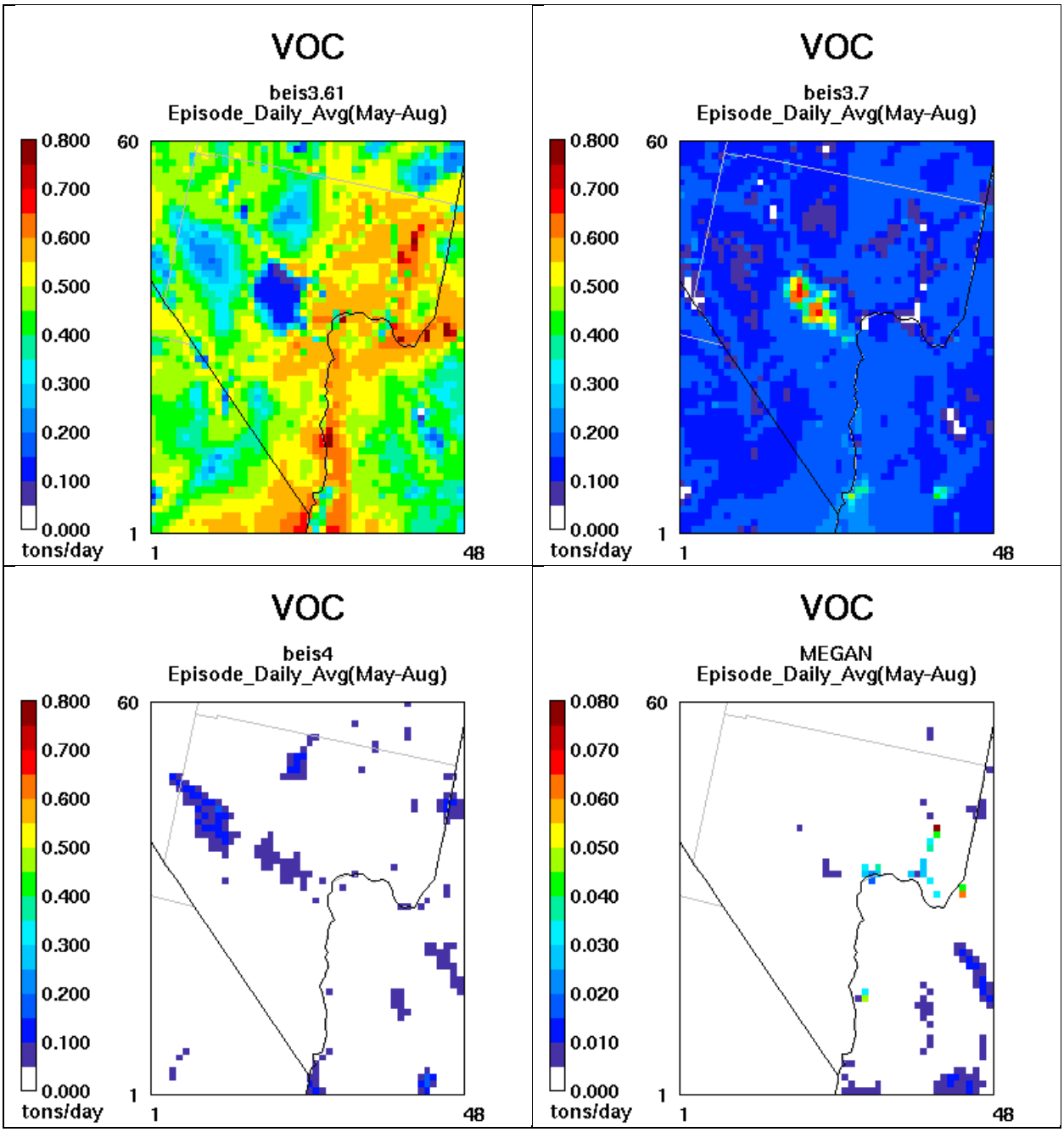

Figure 8-18b. Spatial plots of season-average VOC emissions (tons per day) from four biogenic models: BEIS3.6/BELD4 (top left); BEIS3.7/BELD5 (top right); BEIS4/BELD6 (bottom left); MEGAN3.2 (bottom right). Note that the scale for MEGAN3.2 is ten times smaller than for all BEIS versions.

SENS5 replaced BEIS3.7/BELD5 biogenic emissions on the 12US2 and CC4c2 domains with estimates from the new BEIS4/BELD6 biogenic emissions model. The 12US2/CC4c2 domains were rerun with the model configuration from SENS1. Table 8-9a lists monthly NMB and NME statistical performance for MDA8 ozone over all days and all ozone monitoring sites within the CC4c2 domain. The table compares results from the SENS1 and SENS5 simulations. NMB and NME are color coded for visual reference to statistical goals and criteria benchmarks. Performance results in SENS5 were very similar to SENS1 indicating little sensitivity in using BEIS4 over BEIS3.7. Table 8-9b presents the same information but limited to sites and days when observed MDA8 ozone exceeded 60 ppb. Similar results were also evident on high ozone days, with just slightly more negative bias.

Table 8-9a. Monthly model performance statistics for MDA8 ozone over all days and all ozone monitoring sites within the CC4c2 domain that operated during the summer of 2016. Normalized mean bias (NMB) and normalized mean unsigned error (NME, also referred to as gross error) are shown with color coding indicating statistics outside performance criteria (red), between goals and criteria (yellow) and within goals (green). Results from the SENS1 and SENS5 cases are compared.

Month	MDA8 Ozone (no cutoff)			
	NMB (%)		NME (%)	
	SENS1	SENS5	SENS1	SENS5
May	-19.5	-19.2	19.6	19.3
June	-9.4	-9.9	11.2	11.6
July	-8.6	-7.9	11.2	11.0
Aug	-1.2	-1.3	10.9	10.3
May-Aug	-9.7	-9.5	13.2	13.0

Table 8-9b. As in Table 8-9a, but for all sites and days when monitored MDA8 ozone exceeded 60 ppb.

Month	MDA8 Ozone (60 ppb cutoff)			
	NMB (%)		NME (%)	
	SENS1	SENS5	SENS1	SENS5
May	-22.5	-22.5	22.5	22.5
June	-11.4	-12.8	12.7	13.3
July	-12.0	-11.8	12.8	12.6
Aug	-5.3	-6.4	12.0	10.8
May-Aug	-12.1	-12.7	14.2	14.1

Figure 8-19 presents spatial maps of site-specific monthly NMB for selected monitoring sites across the Mojave Desert of Southern California. The plots indicate very similar performance relative to SENS1 (Figure 8-8). Therefore, the regional under prediction bias over the California transport corridor remained an issue.

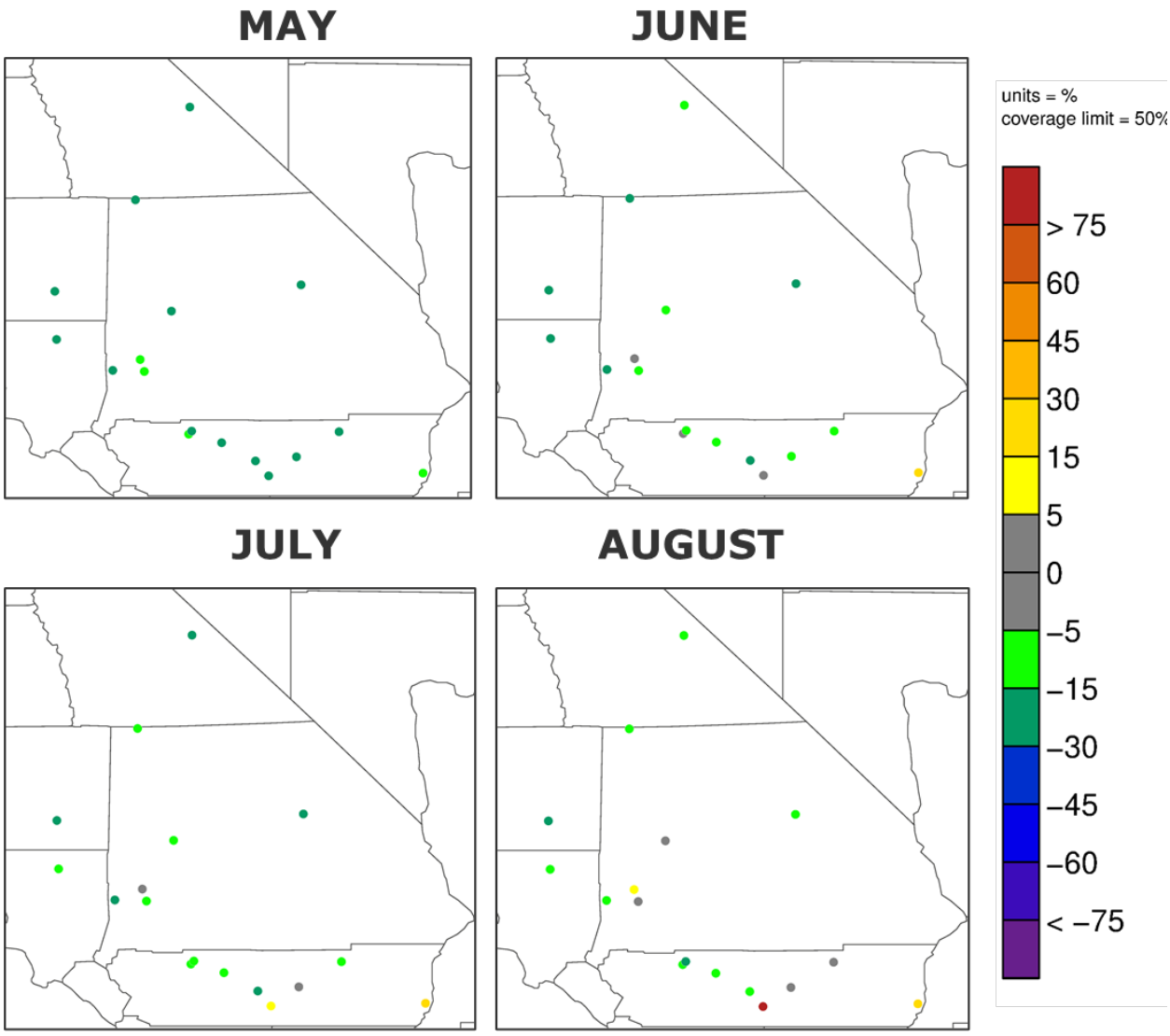

Figure 8-19. Map of site-specific monthly normalized mean bias (NMB) patterns for MDA8 ozone from SENS5 across the Mojave Desert of the southern California portion of the 12US2 domain.

Figure 8-20 presents time series of observed and simulated MDA8 ozone during the May through August modeling period at two representative monitoring sites. The use of BEIS4/BELD6 biogenic emissions in SENS5 resulted in very similar results as SENS1, yet slightly degraded ozone model performance toward a larger under prediction tendency. BEIS4/BELD6 generated much lower rural and urban biogenic isoprene emissions. In this sensitivity run, lower urban biogenic emissions resulted in isoprene concentrations of roughly 0.01 ppb, which is about 10-20 times lower than 2021 field measurements in central Las Vegas (NOAA, 2022).

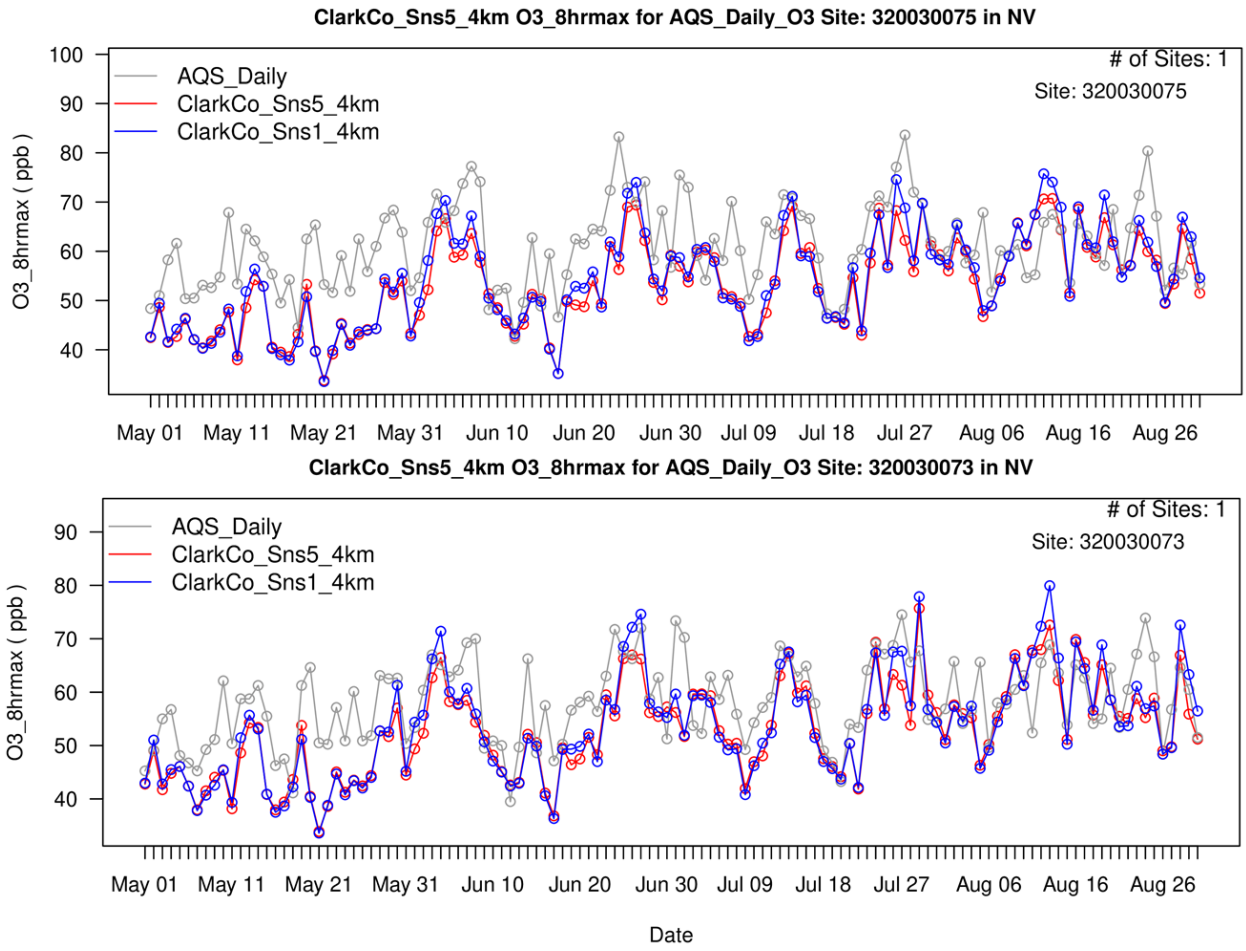

Figure 8-20. Time series of MDA8 ozone over the entire modeling period at the Joe Neal (top) and Palo Verde (bottom) monitoring sites. Daily AQS measurements are shown in grey, the modeled SENS5 results are shown in red, and SENS1 results are shown in blue.

8.4.11 Sensitivity to CAM-Chem Boundary Conditions

8.4.11.1 Global Model Intercomparison

Prior to conducting the second sensitivity test involving the source of continental boundary conditions, we graphically compared simulated ozone fields from two global models, GEOS-Chem and CAM-Chem, at several altitudes. We also compared model results to routine vertical ozone profile data recorded by NOAA ozonesondes launched from Trinidad Head, California. The purpose of this comparison was to identify any consistent biases among the two global models, and to assess whether a single model consistently best characterized mid- and upper-tropospheric ozone patterns and thus has the best chance to positively impact regional surface ozone across the western US.

Figure 8-21 compares GEOS-Chem and CAM-Chem ozone fields, extracted to the CAMx 36US3 modeling grid, at several altitudes on May 1, 2016 at 00 UTC (4 PM Pacific Standard Time). Figure 8-22 shows similar comparisons on May 20, 2016 when high ozone was measured at the mountaintop monitor at Spring Mountain Youth Camp northwest of the LVV. In both cases, and throughout the modeling period, CAM-Chem consistently simulated higher ozone in mid-tropospheric tendrils by as much as 20-50 ppb.

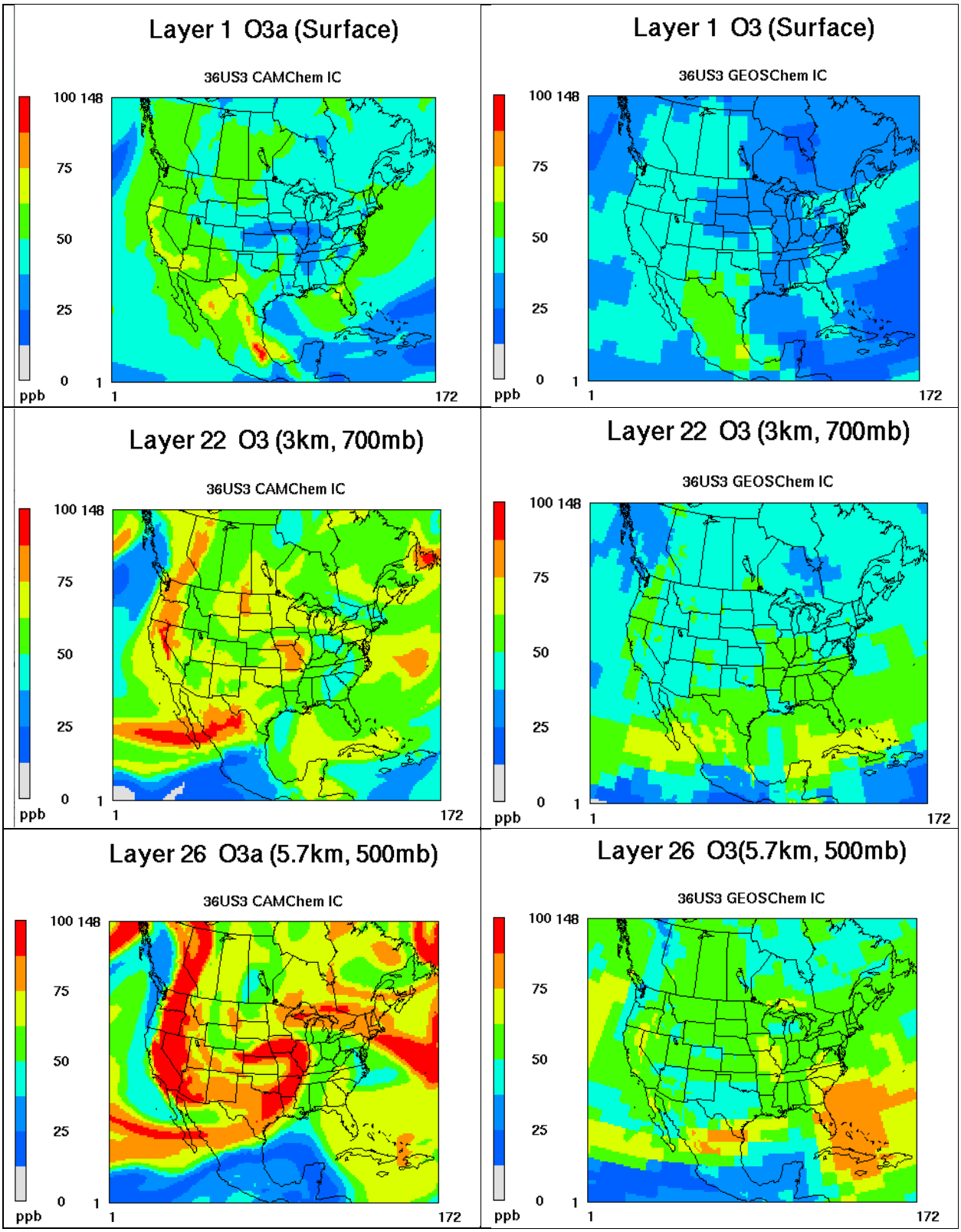

Figure 8-21. CAM-Chem (left) and GEOS-Chem (right) ozone fields extracted to the CAMx 36US3 modeling grid at three altitudes on May 1, 2016, 00 UTC (4 PM PST).

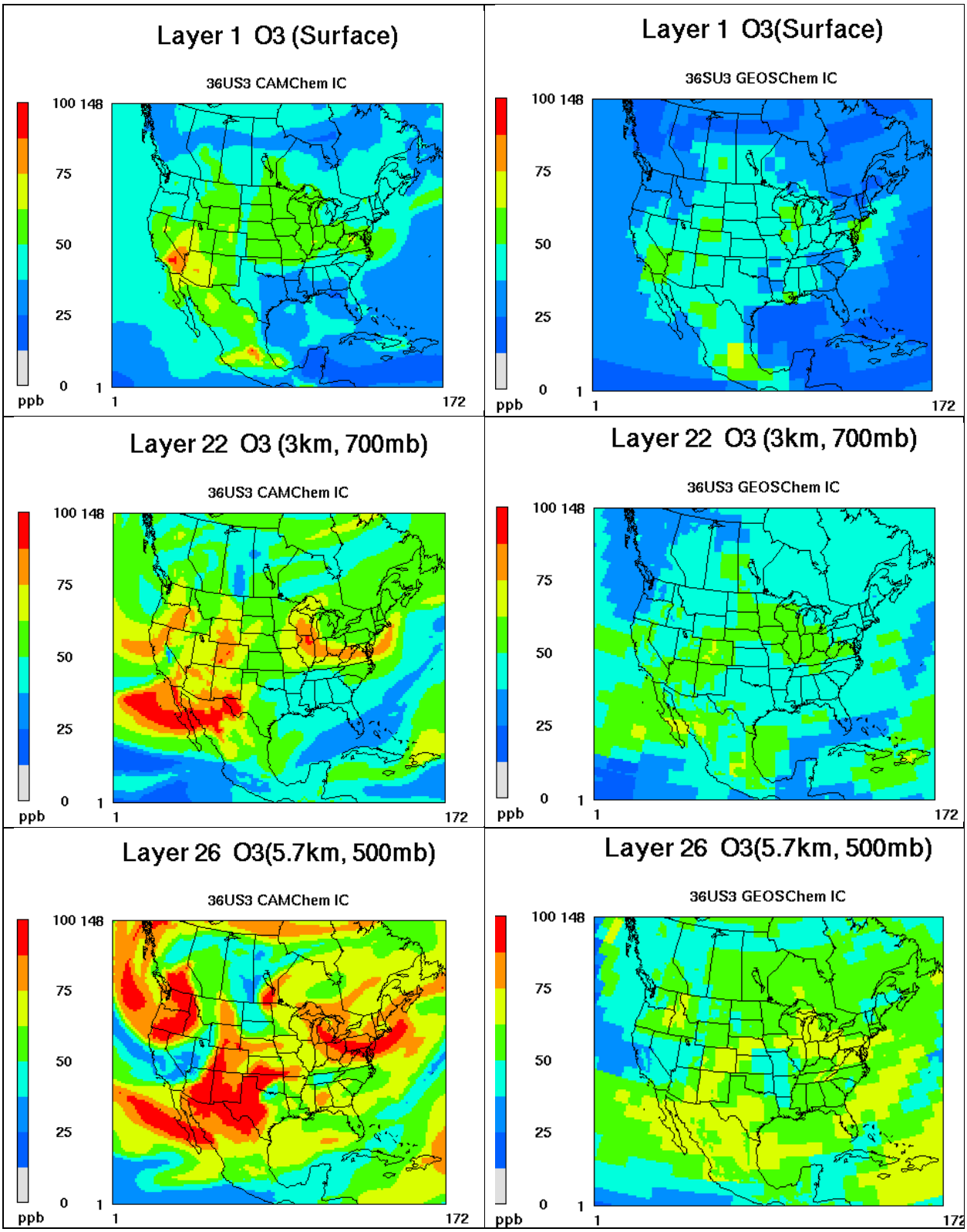

Figure 8-22. CAM-Chem (left) and GEOS-Chem (right) ozone fields extracted to the CAMx 36US3 modeling grid at three altitudes on May 20, 2016, 00 UTC (4 PM PST).

The value of ~75 ppb at 3 km over southern Nevada on May 20 agrees well with the 79 ppb measured at Spring Mountain Youth Camp on that date.

Figure 8-23 presents graphical comparisons of summer-season average ozone profiles observed at Trinidad Head, California and simulated by CAM-Chem and GEOS-Chem. Figure 8-24 compares profiles for each day when observations were recorded during the modeling period. Results confirm that the higher mid- and upper-tropospheric ozone concentrations simulated by CAM-Chem consistently tended to replicate observed profiles much better than GEOS-Chem. However, CAM-Chem suffered from a consistent low bias in the tropopause height and this led to large over estimates of stratospheric ozone relative to GEOS-Chem, which performed much better in that respect.

The higher mid-tropospheric ozone generated by CAM-Chem was nevertheless an intriguing feature that conceivably would lead to higher surface ozone across the western US mountains and deserts during deep afternoon mixing. Therefore, we chose to run CAMx with 36US3 BCs extracted from the 6-hourly CAM-Chem output fields. For this sensitivity case, we scaled back the CAM-Chem ozone results above 9 km (layers 30-35) by a uniform season-averaged factor of 0.56 to better replicate the stratospheric ozone profile. Resulting ozone profiles are shown in Figures 8-25 and 8-26 and confirm improved agreement.

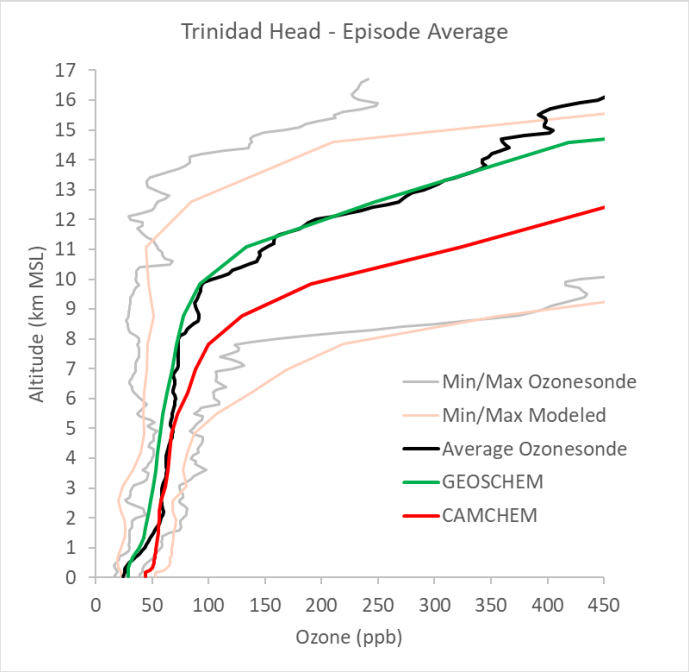

Figure 8-23. 2016 summer season-average ozone profiles observed at the NOAA Trinidad Head ozonesonde launch site (black) and simulated by GEOS-Chem (green) and CAM-Chem (red). Season-maximum and minimum observed profiles (grey) and simulated profiles among both models (orange) are also plotted.

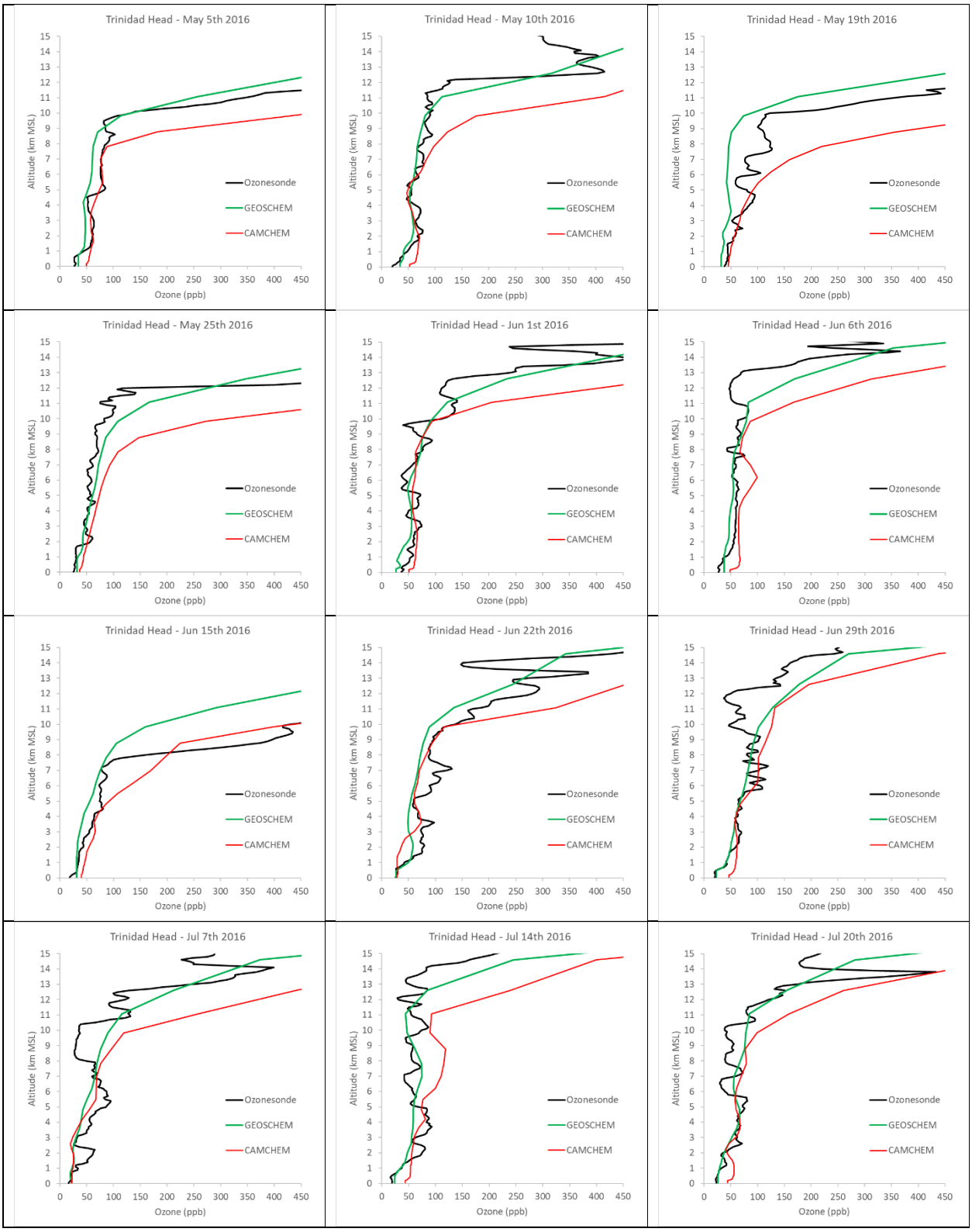

Figure 8-24. Ozone profiles during summer 2016 observed at the NOAA Trinidad Head ozonesonde launch site (black) and simulated by GEOS-Chem (green) and CAM-Chem (red).

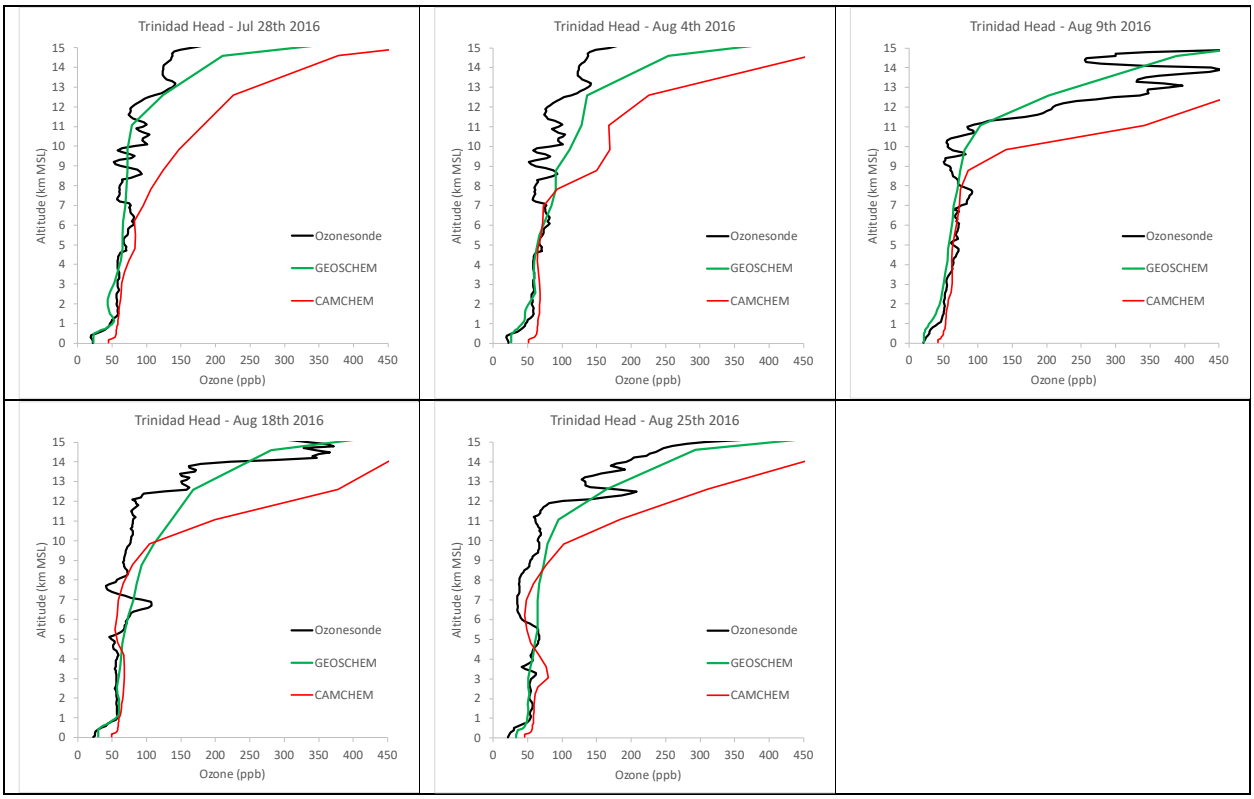

Figure 8-24 (concluded).

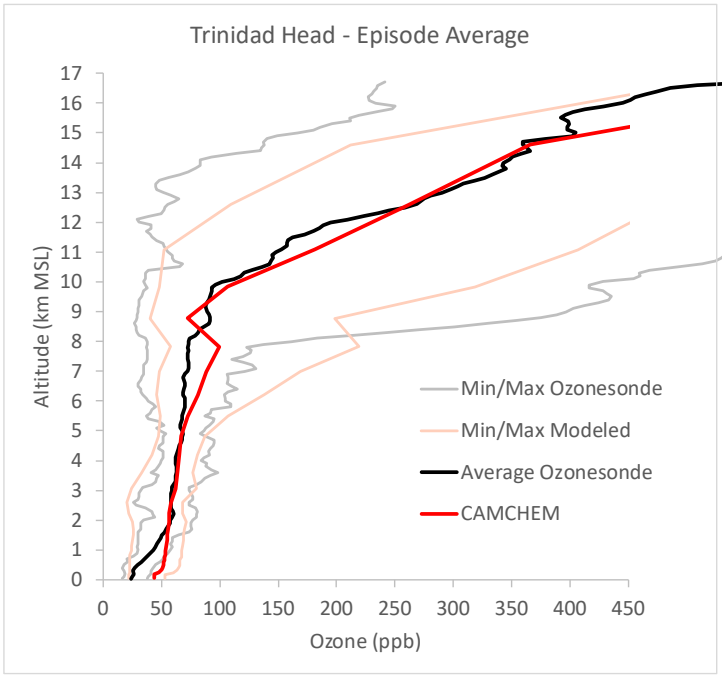

Figure 8-25. 2016 summer season-average ozone profiles observed at the NOAA Trinidad Head ozonesonde launch site (black) and simulated by CAM-Chem where ozone above 9 km was scaled by 0.56 (red). Season-maximum and minimum observed profiles (grey) and CAM-Chem simulated profiles with scaling (orange) are also plotted.

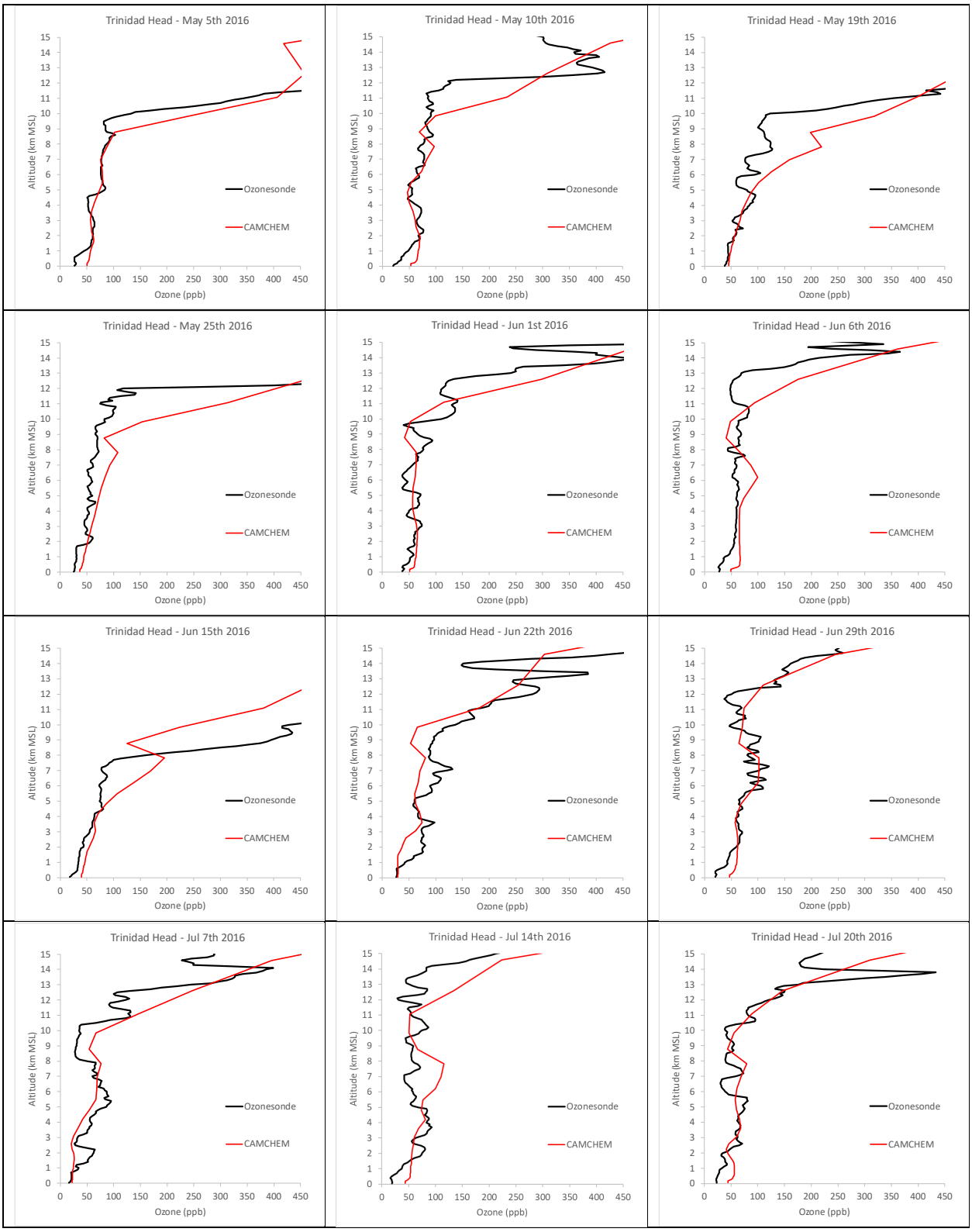

Figure 8-26. Ozone profiles during summer 2016 observed at the NOAA Trinidad Head ozonesonde launch site (black) and simulated by CAM-Chem where ozone above 9 km was scaled by 0.56 (red).

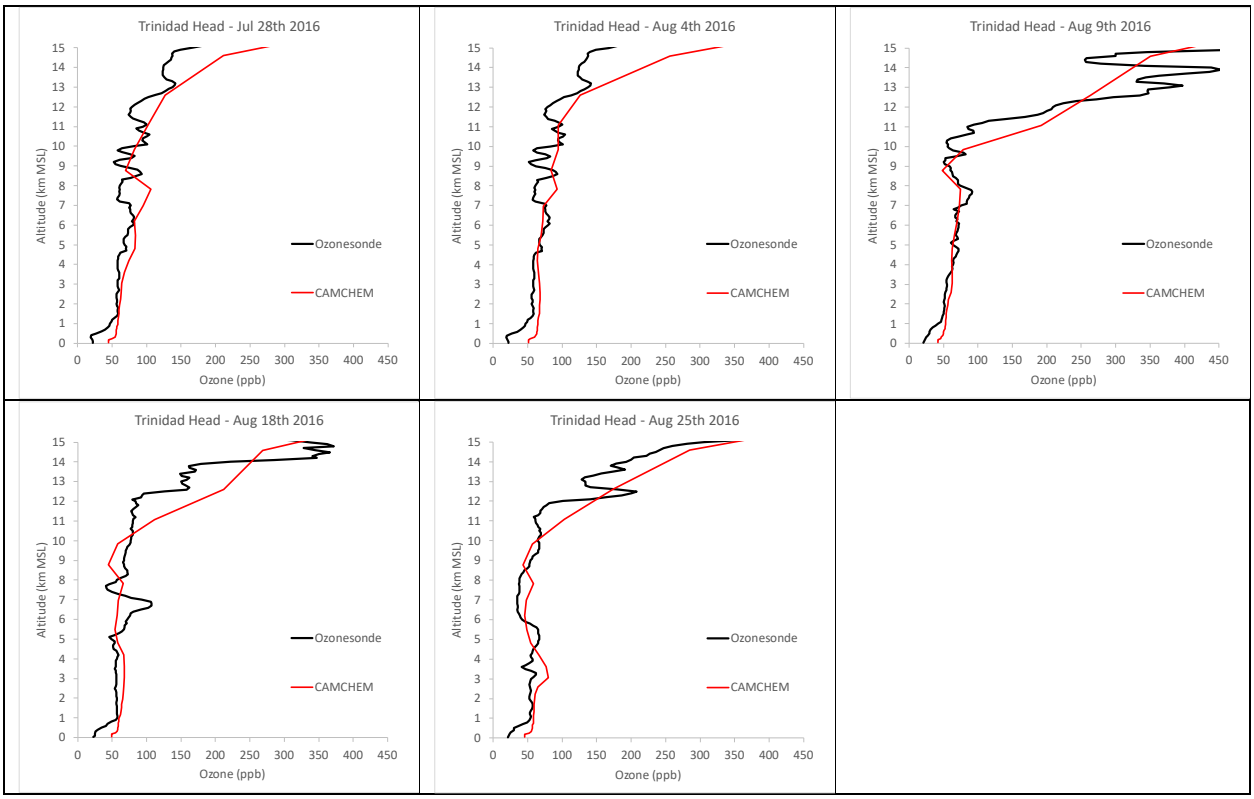

Figure 8-26 (concluded).

8.4.11.2 CAM-Chem Sensitivity Results

SENS6 used CAM-Chem to define lateral BCs on the 36US3 grid, and resulting three-dimensional output fields were downscaled to provide BCs for the 12US2/CC4c2 grids. Otherwise, CAMx was run with same configuration as SENS5 (BEIS4/BELD6) and SENS1 (elevated airport emissions, includes aerosols).

Table 8-10a lists monthly NMB and NME statistical performance for MDA8 ozone over all days and all ozone monitoring sites within the CC4c2 domain. The table compares results from the SENS5 and SENS6 simulations. NMB and NME are color coded for visual reference to statistical goals and criteria benchmarks. Performance results in SENS6 were significantly improved during May-June, but statistical performance during July-August was similar to SENS5, indicating progressively less influence from North American background as represented by CAM-Chem as the summer progressed. Table 8-10b presents the same information but limited to sites and days when observed MDA8 ozone exceeded 60 ppb. Similar results were also evident on high ozone days, with just slightly more negative bias.

Figure 8-27 presents spatial maps of site-specific monthly NMB for selected monitoring sites across the Mojave Desert of Southern California. The plots indicate improvements in NMB for several sites during May-June yet similar results as SENS5 during July-August (Figure 8-19). Therefore, the regional under prediction bias over the California transport corridor was improved substantially during the months when they were largest.

Table 8-10a. Monthly model performance statistics for MDA8 ozone over all days and all ozone monitoring sites within the CC4c2 domain that operated during the summer of 2016. Normalized mean bias (NMB) and normalized mean unsigned error (NME, also referred to as gross error) are shown with color coding indicating statistics outside performance criteria (red), between goals and criteria (yellow) and within goals (green). Results from the SENS5 and SENS6 cases are compared.

Month	MDA8 Ozone (no cutoff)			
	NMB (%)		NME (%)	
	SENS5	SENS6	SENS5	SENS6
May	-19.2	-5.0	19.3	8.5
June	-9.9	-4.8	11.6	9.9
July	-7.9	-7.1	11.0	10.5
Aug	-1.3	-1.7	10.3	10.5
May-Aug	-9.5	-4.7	13.0	9.9

Table 8-10b. As in Table 8-10a, but for all sites and days when monitored MDA8 ozone exceeded 60 ppb.

Month	MDA8 Ozone (60 ppb cutoff)			
	NMB (%)		NME (%)	
	SENS5	SENS6	SENS5	SENS6
May	-22.5	-11.2	22.5	11.4
June	-12.8	-9.4	13.3	10.9
July	-11.8	-11.7	12.6	12.7
Aug	-6.4	-8.8	10.8	10.6
May-Aug	-12.7	-10.3	14.1	11.5

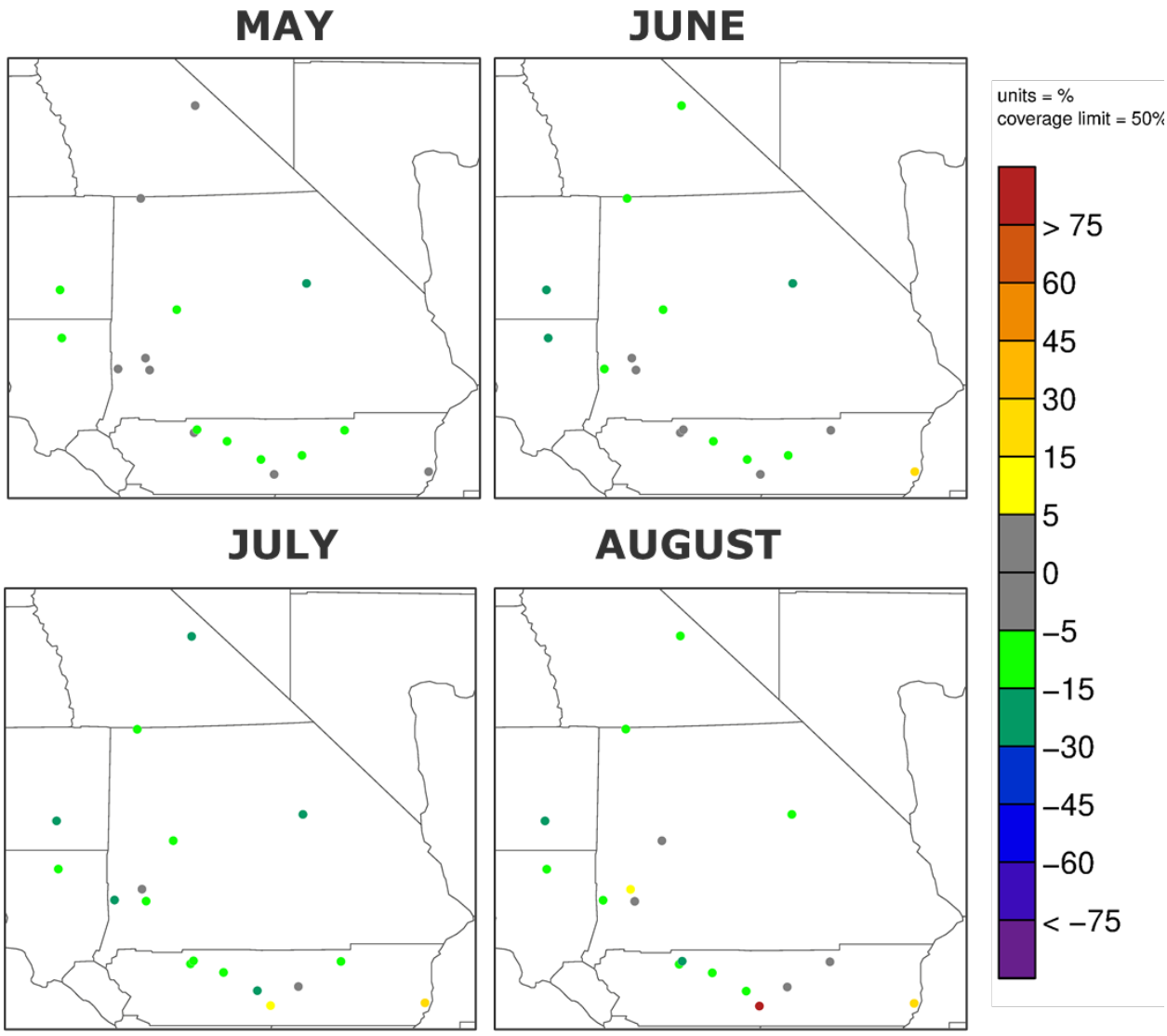

Figure 8-27. Map of site-specific monthly normalized mean bias (NMB) patterns for MDA8 ozone from SENS6 across the Mojave Desert of the southern California portion of the 12US2 domain.

Figure 8-28 presents time series of observed and simulated MDA8 ozone during the May through August modeling period at two representative monitoring sites. The ozone improvements during May-June from the use of CAM-Chem boundary conditions are clear. During July-August, however, the model settled into the same patterns that were seen from SENS1 and SENS5, with perhaps a small incremental deterioration in the under prediction bias.

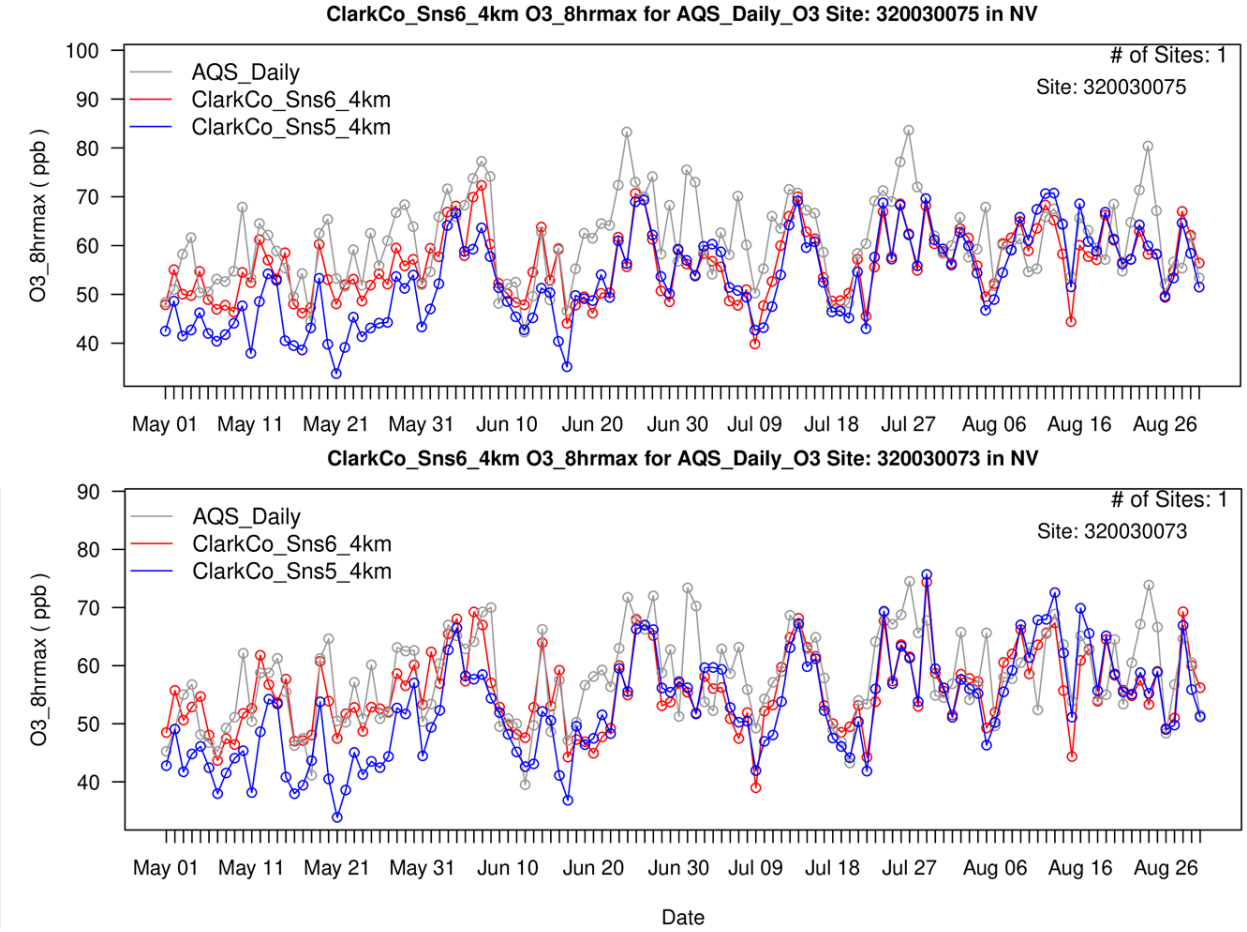

Figure 8-28. Time series of MDA8 ozone over the entire modeling period at the Joe Neal (top) and Palo Verde (bottom) monitoring sites. Daily AQS measurements are shown in grey, the modeled SENS6 results are shown in red, and SENS5 results are shown in blue.

8.5 Final Base Case Configuration and Results

Based on results from the initial CAMx 2016 base case simulation, model performance was insufficient to support regulatory analyses for the CCNAA SIP. However, from 6 sets of sensitivity tests we identified specific updates that improved model results and we incorporated these into the final 2016 base case configuration:

- Apply elevated LTO emissions from Harry Reid International Airport to reduce the large NOx burden in central Las Vegas;
- Include aerosols and related chemistry so that the full effect from wildfires and large urban pollution plumes are properly characterized throughout the modeling domain, although this was shown to have little impact on ozone results;
- Apply biogenic emissions derived from the latest BEIS4/BELD6 model on the 36US3, 12US2 and CC4c2 grids to replace the original BEIS3.7/BELD5 biogenic emissions from the 2016v2 MP;
- Apply an alternative set of 36US3 initial/boundary conditions derived from NCAR's 2016 CAM-chem global chemistry model results.

This configuration was identical to SENS6, and so that sensitivity configuration was used as the final base case (Table 8-11). In this section we provide a more detailed analysis of SENS6 results and compare them to statistical results from the original base case to affirm the performance improvements. We then analyze the top 10 predicted MDA8 ozone days at each official DV monitor within the CCNAA, which were used in the 2023 DV projections, and note the number and type of observed high ozone days that were captured.

8.5.1 Summary

The final 2016 base case is referred to as "Base2" in plots and tables below. Results from the model performance evaluation are summarized below with comparisons back to the initial base case:

- Model performance in replicating observed MDA8 ozone patterns was significantly improved during May-June, while performance during July-August was similar to the initial base case.
- Model bias and error statistics for MDA8 ozone remained consistent across all sites in the final base case simulation, so there was no single site that influenced statistical results.
- Results indicated that the final base case performed typically well for ozone during May through June and continued to perform notably well during August.
  - The remaining systematic under prediction tendency continued to implicate a lack of regional ozone and associated transport into the LVV.
- Performance in replicating the highest peak ozone days was not especially skillful in any month, but the final base case reduced occasional over predictions on non-event dates in August.
  - All days when peak observed MDA8 ozone exceeded 70 ppb remained under predicted in the final base case by an average of 10 ppb, regardless of influences by local emissions or wildfires.
- The top 10 modeled days at each of 6 key (exceedance) monitoring sites within the CCNAA were all above 60 ppb.
  - All sites included a similar set of dates in different orders and matched up with 7 or 8 observed days that exceed 70 ppb with small bias within a few percent and gross error of typically 5%.
- Elevating Reid Airport emissions reduced the overall surface NO_2 over prediction bias but did not ameliorate it entirely at neighborhood monitors.
  - The impact to diurnal NO_2 concentrations was substantial during certain hours of the day especially at sites closest to Reid Airport during commute hours.
  - The NOx reduction in central Las Vegas raised simulated ozone there in better agreement with nearby ozone measurements, indicating a NOx disbenefit response.
- Ozone production from the dearth of biogenic emissions in the desert environment was likely minimal given very low isoprene concentrations measured during the 2021 field study.
  - The initial base case using BEIS3.7 clearly over predicted morning isoprene concentrations within the urban area at 1-2 ppb relative to 2021 measurements of a few tenths of a ppb.
  - BEIS4 resulted in large urban isoprene under predictions of around 0.01 ppb.
  - We conclude that there is far too much uncertainty in the biogenic models to know whether any of them appropriately estimate rural and urban VOC emissions in the desert environment of the southwestern US.

Table 8-11. CAMx model configuration for the CCNAA 2016 final base case simulation. Changes from the initial base case are noted in red.

Model Component	CCNAA Application	Comment
Model Code	CAMx v7.20 - May 2022	
Horizontal Grids		
Map Projection	Lambert Conic Conformal	EPA 2016 MP
36 km (36US3)	172 x 148 cells	EPA 2016 MP (1-way nesting)
12 km (12US2)	396 x 246 cells (no buffer cells)	EPA 2016 MP (2-way nesting)
4 km (CC4c2)	50 x 62 cells (with buffer cells)	CCNAA grid (2-way nesting)
Vertical Grid	35 layers	EPA 2016 MP, defined by WRF
Initial Conditions	36US3 IC April 1 from CAM-Chem, 12US2/CC4c2 IC May 1 from 36US3	
Boundary Conditions	36US3 BC from CAM-Chem, 12US2 BC from 36US3	
Time Zone	UTC	EPA 2016 MP
Emissions		
36/12 km Data Sources	EPA 2016v2 MP	
4 km Data Sources	EPA 2016v2 MP + Clark County Data, elevated Reid LTO emissions	
Models/Processing Tools	SMOKE, MOVES3, SMOKE-MOVES, BEIS4/BELD6	CCNAA grid
Plume-in-Grid	Off	No large point sources in high-resolution CCNAA grid
In-line Ix emissions	On	Oceanic halogens
Chemistry		
Gas Phase Chemistry	CB6r5	Latest mechanism available
Aerosol Chemistry	None	Gas phase only
Meteorological Interface	WRFCAMx v5.2	
Horizontal Diffusion	Smagorinsky	Spatially variant K-theory
Vertical Diffusion	YSU Kv formulation	Minimum Kv 0.1 to 1.0 m^2/s
ACM2	Off	Non-local boundary layer convection
Sub-grid Cloud Convection	Off	
Deposition		
Dry Deposition	Zhang03	
Wet Deposition	On	rain/snow/graupel
Surface Chemistry Model	Off	
Bi-directional Ammonia	Off	For aerosol chemistry
Numeric Solvers		
Gas Phase Solver	Euler Backward Iterative (EBI)	Default fast and accurate solver
Vertical Advection	Piecewise Parabolic Method (PPM)	Default
Horizontal Advection	Piecewise Parabolic Method (PPM)	Default
Integration Time Step	Wind speed dependent	~0.5-1 min (4 km), 1-5 min (12 km), 5-15 min (36 km)
Super Stepping	On	Maximizes time step selection

8.5.2 MDA8 Ozone Bias and Error Performance Statistics

Table 8-12a lists monthly NMB and NME statistical performance for MDA8 ozone over all days and all ozone monitoring sites within the CC4c2 domain. The table compares results from the Clark County initial and final base case simulation. NMB and NME are color coded for visual reference to statistical goals and criteria benchmarks. As seen in results from SENS6, statistical performance was significantly improved during May-June, while statistical performance during July-August was similar to the initial base case. Table 8-12b presents the same information but limited to sites and days when observed MDA8 ozone exceeded 60 ppb. Similar results were also evident on high ozone days, just with more negative bias in most months relative to Table 8-12a, but a noticeable increase in negative bias during August in the final base case.

Table 8-12a. Monthly model performance statistics for MDA8 ozone over all days and all ozone monitoring sites within the CC4c2 domain that operated during the summer of 2016. Normalized mean bias (NMB) and normalized mean unsigned error (NME, also referred to as gross error) are shown with color coding indicating statistics outside performance criteria (red), between goals and criteria (yellow) and within goals (green). Results from the Clark County initial and final base case simulations are compared.

Month	MDA8 Ozone (no cutoff)			
	NMB (%)		NME (%)	
	Base2	Base	Base2	Base
May	-5.0	-17.9	8.5	18.3
June	-4.8	-9.2	9.9	11.2
July	-7.1	-8.2	10.5	11.1
Aug	-1.7	0.1	10.5	10.7
May-Aug	-4.7	-8.8	9.9	12.8

Table 8-12b. As in Table 8-12a, but for all sites and days when monitored MDA8 ozone exceeded 60 ppb.

Month	MDA8 Ozone (60 ppb cutoff)			
	NMB (%)		NME (%)	
	Base2	Base	Base2	Base
May	-11.2	-21.5	11.4	21.5
June	-9.4	-11.3	10.9	12.7
July	-11.7	-11.7	12.7	12.7
Aug	-8.8	-4.3	10.6	11.4
May-Aug	-10.3	-11.5	11.5	13.9

Table 8-13 breaks out monthly NMB and NME over all days (i.e., no 60 ppb cutoff) at each monitoring site within the CC4c2 domain and compares results from the initial and base cases. Similar color shading is used to visually characterize values relative to goal and criteria benchmarks. Statistical results remained consistent across all sites in the final base case simulation, so there was no single site that influenced the statistics in Table 8-12a. The consistently worst performing site was in California, upstream of Clark County, which monitors air that often arrives directly from the Los Angeles basin. Again, dramatic improvements in bias and error are noted in May and June, with more similar results in July and August.

Table 8-13. Monthly model performance statistics for MDA8 ozone over all days at each monitoring site within the CC4c2 domain that operated during the summer of 2016. Normalized mean bias (NME) and normalized mean unsigned error (NME) are shown with color coding indicating statistics outside performance criteria (red), between goals and criteria (yellow) and within goals (green). Results from the Clark County initial and final base case simulations are compared.

	May				June				July				Aug			
	NMB		NME		NMB		NME		NMB		NME		NMB		NME	
Site Name	Base2	Base	Base2	Base	Base2	Base	Base2	Base	Base2	Base	Base2	Base	Base2	Base	Base2	Base
California	-13.2	-24.7	13.2	24.7	-13.2	-17.3	14.3	17.3	-14.6	-17.0	15.3	17.9	-11.0	-11.8	12.0	12.4
Apex	-5.9	-18.7	8.4	18.8	-4.4	-9.6	8.1	9.9	-7.5	-8.6	11.0	11.5	0.5	1.5	9.3	9.8
Mesquite	2.0	-12.3	7.6	13.4	3.2	-2.7	7.7	7.1	2.4	0.4	7.4	6.7	15.0	12.9	22.1	22.9
Paul Meyer	-6.2	-18.2	7.9	18.4	-6.7	-10.3	11.2	12.0	-8.5	-9.0	11.0	10.9	-4.7	-2.4	10.0	9.5
Walter Johnson	-6.0	-17.8	8.0	18.0	-6.4	-8.9	11.3	11.4	-8.7	-8.7	10.9	10.8	-3.9	-0.5	9.0	9.4
Palo Verde	-2.3	-15.0	7.0	16.0	-4.3	-7.1	9.3	10.5	-7.0	-7.3	10.3	10.5	-3.3	0.3	9.2	9.9
Joe Neal	-8.0	-20.0	9.7	20.1	-9.1	-11.3	12.2	13.2	-11.6	-11.1	12.5	12.1	-3.6	0.6	9.2	9.1
Green Valley	-2.3	-15.6	7.2	16.6	-5.7	-10.0	9.1	11.4	-5.7	-6.1	9.9	10.2	-0.1	2.0	11.0	11.8
Jerome Mack-NCORE	-7.3	-19.5	8.7	19.6	-5.9	-9.6	9.7	11.7	-9.2	-9.4	10.8	11.9	-3.9	-1.1	10.2	10.0
Boulder City	-2.4	-16.0	6.5	16.2	-0.7	-7.2	7.9	8.0	-0.8	-3.0	9.3	10.1	-2.9	-3.8	11.0	10.9
Jean	-3.2	-16.5	6.7	16.7	-0.3	-7.9	7.8	9.3	-4.5	-6.9	8.5	9.0	-0.3	-1.6	9.9	8.9
J.D. Smith	-8.7	-20.9	9.8	21.1	-9.5	-13.4	12.2	14.5	-10.4	-10.6	11.6	12.5	-3.8	-0.7	9.9	9.6
SM Youth Camp	-5.1	-19.7	9.5	19.7	-4.3	-9.2	9.1	11.3	-6.0	-9.2	8.7	10.1	-0.1	1.6	9.1	9.7
Indian Springs	-0.8	-15.9	9.5	16.6	0.5	-5.4	9.6	10.6	-2.4	-4.6	9.3	10.0	2.0	3.8	9.6	10.2
LV Paiute	-4.5	-17.3	8.1	17.5	-6.6	-10.0	10.8	11.5	-8.8	-9.3	10.3	10.4	1.2	4.3	9.0	9.7

These results indicate that the final base case performed typically well during May through June and continued to perform notably well during August. The remaining systematic under prediction tendency, while much smaller than the initial base case, continued to suggest a consistent source of error.

Figure 8-29 displays spatial maps of site-specific monthly NMB patterns for MDA8 ozone across the CC4c2 domain, for both the initial and final base case simulations. In this figure, NMB was determined from all days without the 60 ppb cutoff applied, so the maps are consistent with the data in Table 8-13. These plots show the systematic negative bias throughout the summer with the progressive improvement through August. Again, the statistical improvement in bias in May and June is notable.

Tables 8-14a and 14b list monthly NMB and NME statistical performance for MDA8 ozone for selected monitoring sites across the Mojave Desert of Southern California. These sites monitor the air mass that is often transported between the Los Angeles basin and the LVV. Simulated MDA8 ozone for these statistics were taken from the 12US2 grid. While slightly larger biases are evident than for LVV sites in both initial and final base cases, these results also showed a substantial improvement during May and June in the final base case statistics.

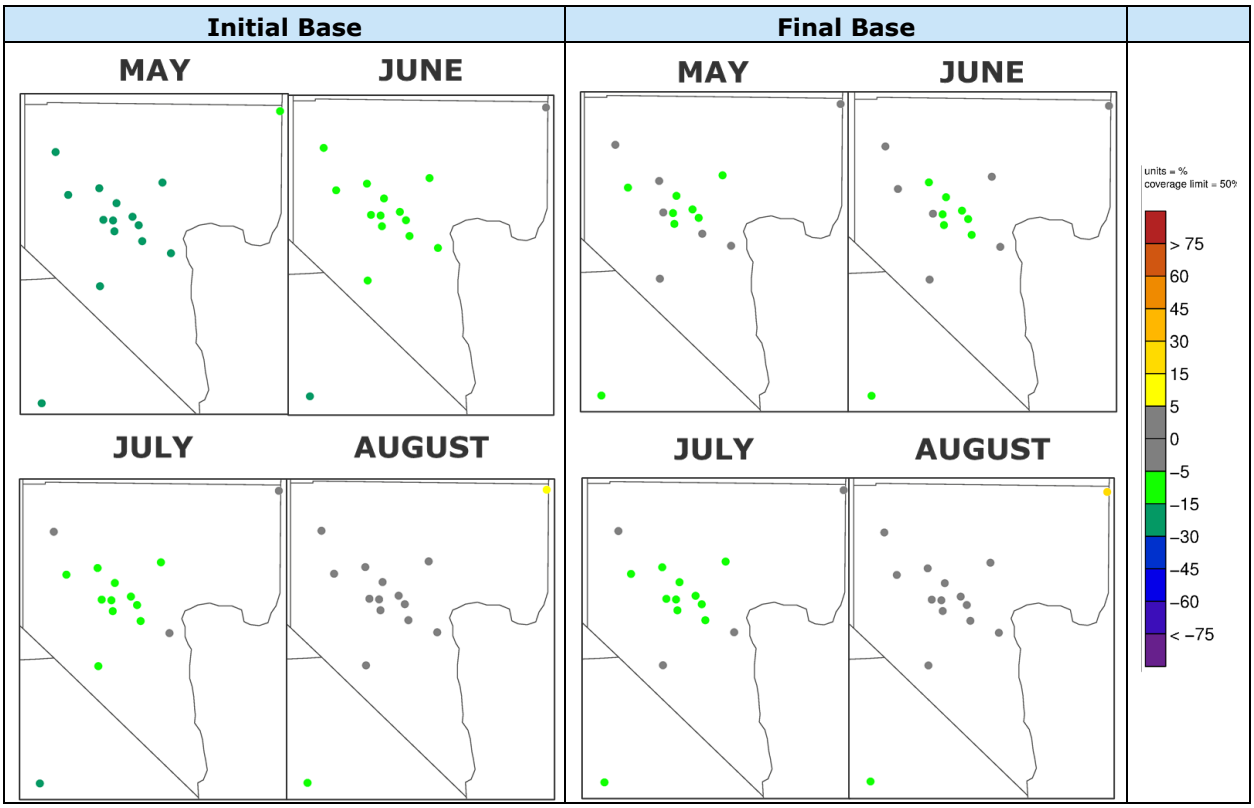

Figure 8-29. Map of site-specific monthly normalized mean bias (NMB) patterns for MDA8 ozone within the CC4c2 domain. Initial base case (left) and final base case (right).

Table 8-14a. Monthly model performance statistics for MDA8 ozone over all days and for selected monitoring sites across the Mojave Desert of Southern California. Normalized mean bias (NMB) and normalized mean unsigned error (NME, also referred to as gross error) are shown with color coding indicating statistics outside performance criteria (red), between goals and criteria (yellow) and within goals (green). Results from the Clark County initial and final base case simulations are compared.

Month	MDA8 Ozone (no cutoff)			
	NMB (%)		NME (%)	
	Base2	Base	Base2	Base
May	-6.0	-17.5	9.5	18.0
June	-6.4	-13.3	13.2	17.2
July	-10.0	-12.2	14.9	16.3
Aug	-5.4	-6.0	14.6	15.1
May-Aug	-7.0	-12.1	13.1	16.6

Table 8-14b. As in Table 8-14a, but for all sites and days when monitored MDA8 ozone exceeded 60 ppb.

Month	MDA8 Ozone (60 ppb cutoff)			
	NMB (%)		NME (%)	
	Base2	Base	Base2	Base
May	-10.9	-19.3	11.6	19.4
June	-10.0	-16.5	13.1	18.0
July	-14.3	-16.4	15.3	17.1
Aug	-11.1	-11.5	13.4	14.2
May-Aug	-11.7	-15.5	13.6	16.9

Figure 8-30 presents spatial maps of site-specific monthly NMB for the same selected monitoring sites across the Mojave Desert, for both the initial and final base case simulations. In this figure, NMB was determined from all days without the 60 ppb cutoff applied, so the maps are consistent with the data in Table 14a. The plots show the general pattern of systematic negative bias across the region and the improvements achieved in May and June in the final base case results. The remaining bias continued to implicate a lack of regional ozone and associated transport into the LVV.

Figure 8-31 presents time series of observed and simulated MDA8 ozone during the May through August modeling period at two representative monitoring sites. Results from the initial and final base cases are compared. Again, the improvements in the final base case during May and early June from the use of alternative boundary conditions from CAM-Chem are evident, while the two simulations tracked each other more closely in July and August. Performance in replicating the highest peak days was not especially skillful in any month, but the final base case tended to reduce occasional over predictions on non-event dates in August.

8.5.3 Analysis of Ozone Precursors

As described above, the final base case included the modified spatial allocation of NOx emissions from LTO cycles at Reid Airport consistent with the SENS1 sensitivity test. Comparisons to NO_2 observations at five central LVV monitoring sites, and effects to local ozone patterns, are documented in the section describing SENS1 results. To recap those results, elevating Reid Airport emissions reduced the overall surface NO_2 over prediction bias but did not ameliorate it entirely at neighborhood monitors. The impact to diurnal NO_2 concentrations was substantial during certain hours of the day with largest reductions at sites closest to Reid Airport, especially during the daytime and evening commute hours. No additional NOx emission modifications were applied in the final base case. Therefore, the detailed NOx performance evaluation is not repeated here.

As described above, our analyses and sensitivity tests involving alternative biogenic emission models helped to bracket the ozone impacts from biogenic VOC within the LVV. Ultimately, we ascertained that ozone production from the dearth of biogenic emissions in the desert environment is likely minimal given very low isoprene concentrations measured during the 2021 field study. Figure 8-32 compares predicted isoprene concentrations on a specific summer day among the different biogenic emission tests conducted in this study. Given similar meteorological conditions day-to-day, the examples in Figure 8-32 were consistent with other days of the modeling period. The choice of 10 AM PST in these plots was typically the hour during which predicted isoprene was maximum before deep boundary layer mixing and chemistry reduced concentrations substantially. Isoprene is not emitted during nighttime hours.

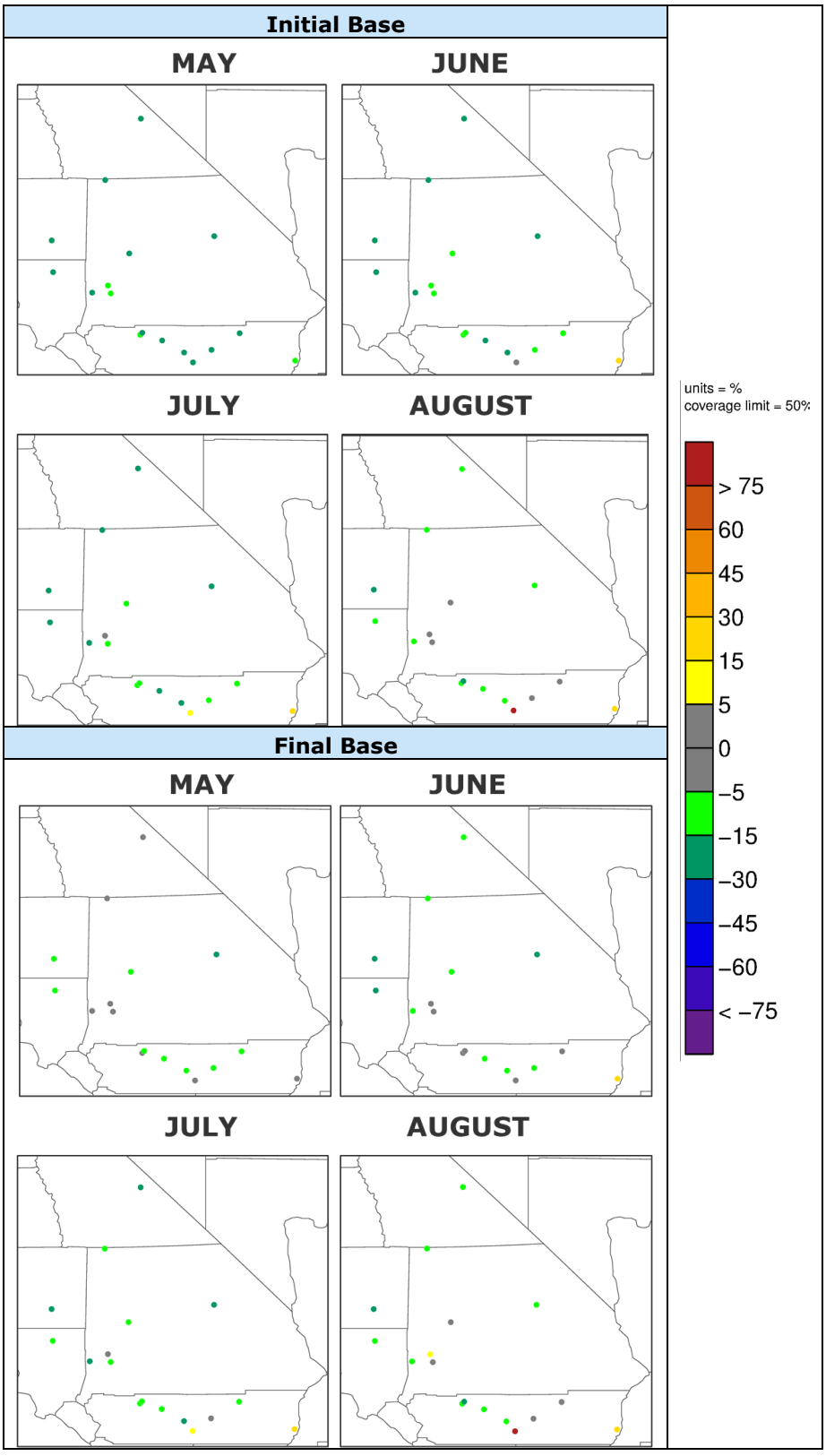

Figure 8-30. Map of site-specific monthly normalized mean bias (NMB) patterns for MDA8 ozone across the Mojave Desert of the southern California portion of the 12US2 domain. Initial base case (top) and final base case (bottom).

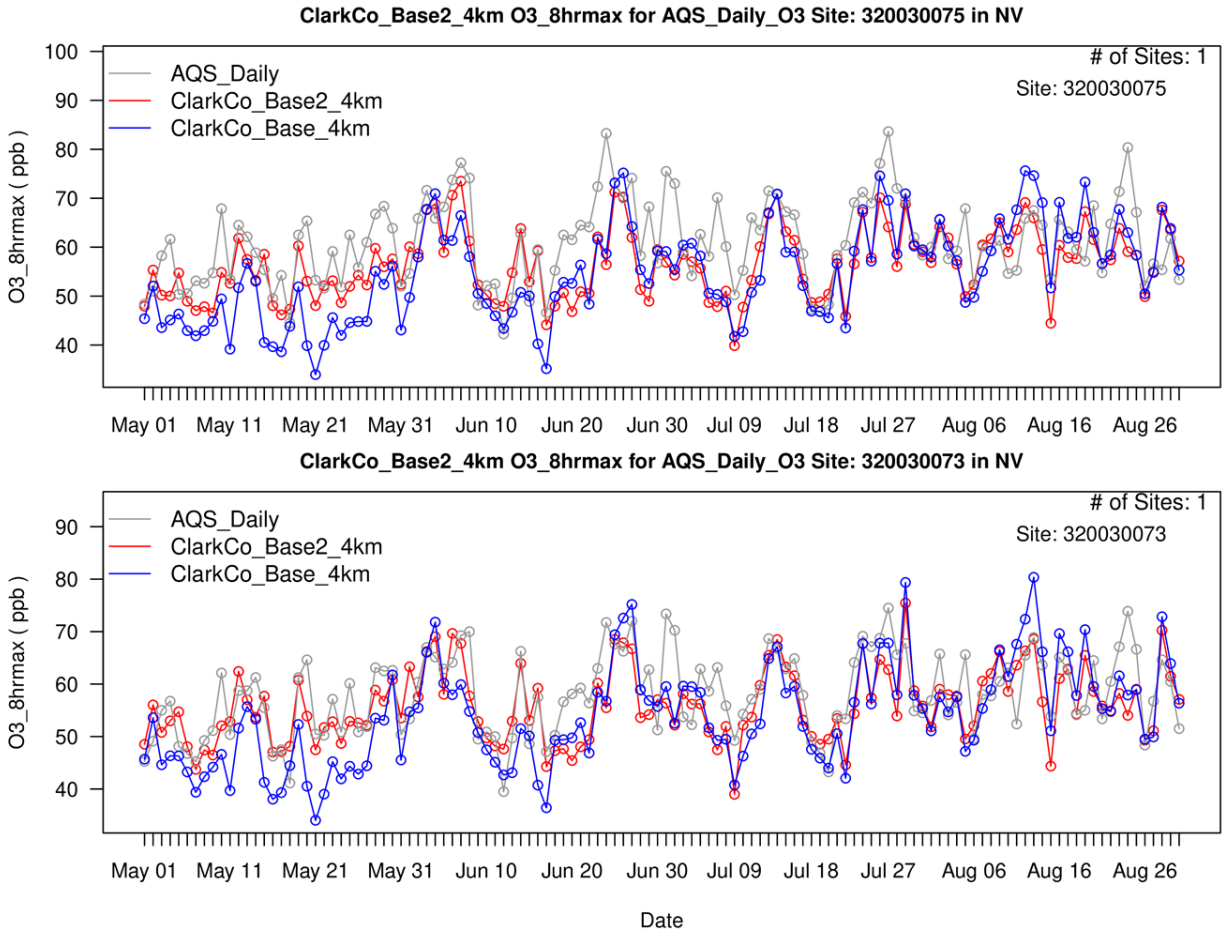

Figure 8-31. Time series of MDA8 ozone over the entire modeling period at the Joe Neal (top) and Palo Verde (bottom) monitoring sites. Daily AQS measurements are shown in grey, the modeled final base case results are shown in red, and the initial base case results are shown in blue.

The initial base case clearly over predicted morning isoprene concentrations within the urban area at 1-2 ppb whereas 2021 measurements ranged over a few tenths of a ppb. BEIS4 resulted in large urban isoprene under predictions of around 0.01 ppb, while BEIS3.6 resulted in the best agreement (0.25 ppb) but led to ozone over predictions in August. However, BEIS3.6 resulted in rural isoprene concentrations of 1 ppb or more, which were massively over predicted relative to 2021 isoprene measurements of <0.01 ppb measured outside of Las Vegas. We believe that the urban 0.25 ppb isoprene achieved in SENS4 (BEIS3.6) and the resulting ozone over predictions were caused by the very high rural biogenic emission transported into the NOx-rich urban area. At this point we conclude that there is far too much uncertainty in the biogenic models to know whether any of them appropriately estimate rural and urban VOC emissions in the desert environment of the southwestern US.

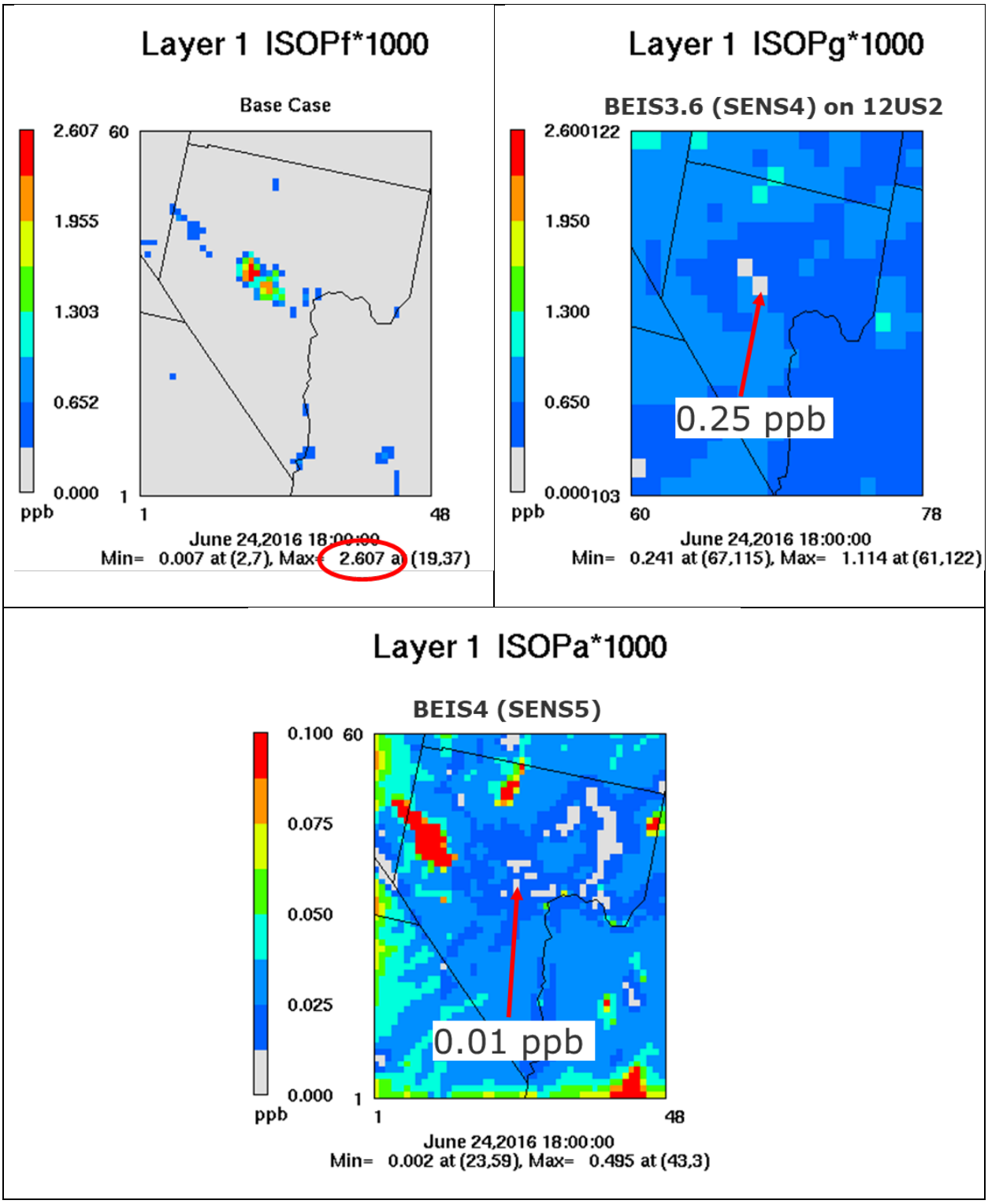

Figure 8-32. Predicted isoprene concentrations at 10 AM PST, June 24 2016, from three CAMx simulations using different versions of the BEIS biogenic emissions model. Measured isoprene concentrations in Las Vegas during 2021 ranged over a few tenths of a ppb (NOAA, 2022) but rural isoprene was measured below 0.01 ppb. The initial base case used BEIS3.7 whereas the final base case used BEIS4. See text for details about each simulation.

8.5.4 Analysis of Highest Observed Ozone Days

Table 8-15 ranks the 26 highest observed ozone days exceeding 70 ppb during summer 2016 according to peak site concentrations in the LVV. Site- and date-paired model predictions from the initial and final base cases are also listed for comparison. The table notes which days are expected to be influenced by regional wildfires versus local production and regional anthropogenic transport, according to previous analyses conducted by DES/DAQ.

Results show that all days remained under predicted, with 8 of 26 days within 5 ppb and average under predictions of around 10 ppb. Considering all days, the average peak observation was 75.4 ppb versus the average paired prediction of 64.7 ppb in the initial base case (absolute and normalized bias of -10.7 ppb and -14%, respectively) and 64.2 ppb in the final base case (absolute and normalized bias of -11.2 ppb and -15%, respectively). Results were similar when considering only days not influenced by wildfires. On those 15 days, the average peak observation was 74.2 ppb versus the average paired prediction of 64.4 ppb in the final base case (absolute and normalized bias of -9.8 ppb and -13%, respectively).

Figure 8-33 shows spatial plots of MDA8 ozone on each of the 26 high ozone dates with observations overlaid as colored circles to visually aid in prediction-observation comparisons. Based solely on visual inspection, well performing dates included: June 3, 6, 7, 25, and 26; July 13, 14 and 29; August 13. June 6 exhibited an over prediction tendency, but all other dates displayed in Figure 8-33 exhibited under predictions at nearly all sites.

Table 8-15. Observed and predicted MDA8 ozone on days when at least one site monitored an exceedance above 70 ppb. The table shows the observed ozone at the peak site each day, ranked from highest to lowest, and the paired predicted values. Dates noted in red are expected to be influenced by regional wildfires. Dates noted in blue are expected to be caused mainly by local production and upwind transport from anthropogenic sources. Dates noted in black have not been assessed with respect to likely causes. Orange highlighted predictions are under predicted by more than 5 ppb, bold predictions in the final base case are higher than the initial base case.

Site Name	Site ID	Date	Observed	Base	Base2
Apex	3200300221	6/24/2016	84.0	60.1	58.9
Joe Neal	3200300751	7/27/2016	83.6	69.6	62.4
Joe Neal	3200300751	8/24/2016	80.4	63.0	58.2
LV Paiute	3200380001	7/1/2016	80.3	65.2	61.9
LV Paiute	3200380001	6/7/2016	80.1	72.1	**78.1**
LV Paiute	3200380001	7/26/2016	79.6	75.2	71.5
LV Paiute	3200380001	6/8/2016	76.8	60.2	**62.7**
SM Youth Camp	3200377714	5/20/2016	76.5	37.2	**52.7**
LV Paiute	3200380001	8/23/2016	75.9	71.5	66.5
Paul Meyer	3200300431	7/29/2016	75.5	77.9	71.8
LV Paiute	3200380001	7/2/2016	75.4	56.2	55.3
LV Paiute	3200380001	6/25/2016	74.3	73.8	72.0
Joe Neal	3200300751	6/27/2016	74.1	64.2	61.3
LV Paiute	3200380001	6/3/2016	74.1	72.4	71.9
Indian Springs	3200377721	7/25/2016	73.9	61.2	61.1
Joe Neal	3200300751	6/6/2016	73.8	61.4	**69.9**
SM Youth Camp	3200377714	8/25/2016	73.4	61.8	**62.8**
Apex	3200320021	7/28/2016	73.0	59.7	55.7
LV Paiute	3200380001	7/13/2016	73.0	71.3	70.7
Joe Neal	3200300751	6/23/2016	72.4	61.6	**61.7**
LV Paiute	3200380001	6/26/2016	72.4	73.9	70.3
LV Paiute	3200380001	7/14/2016	72.4	72.6	72.2
LV Paiute	3200380001	7/24/2016	72.3	62.2	**62.7**
SM Youth Camp	3200377714	6/14/2016	71.5	50.7	**62.8**
Paul Meyer	3200300431	8/13/2016	70.8	77.2	65.5
Joe Neal	3200300751	7/7/2016	70.1	50.3	47.8

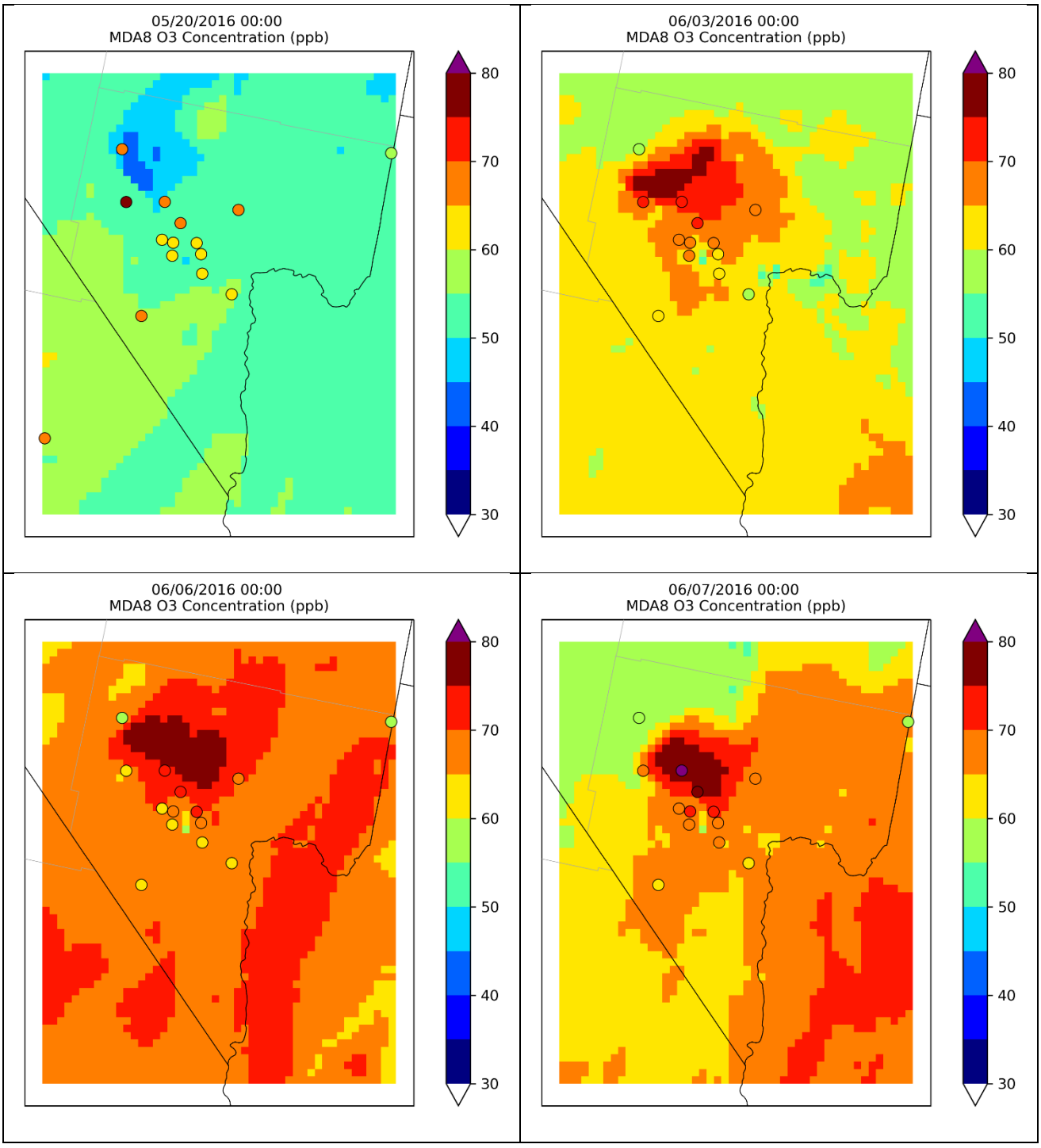

Figure 8-33. Spatial plots of predicted MDA8 ozone on 26 high ozone dates in 2016 when at least one peak measurement exceeded 70 ppb. Observations are overlaid as colored circles.

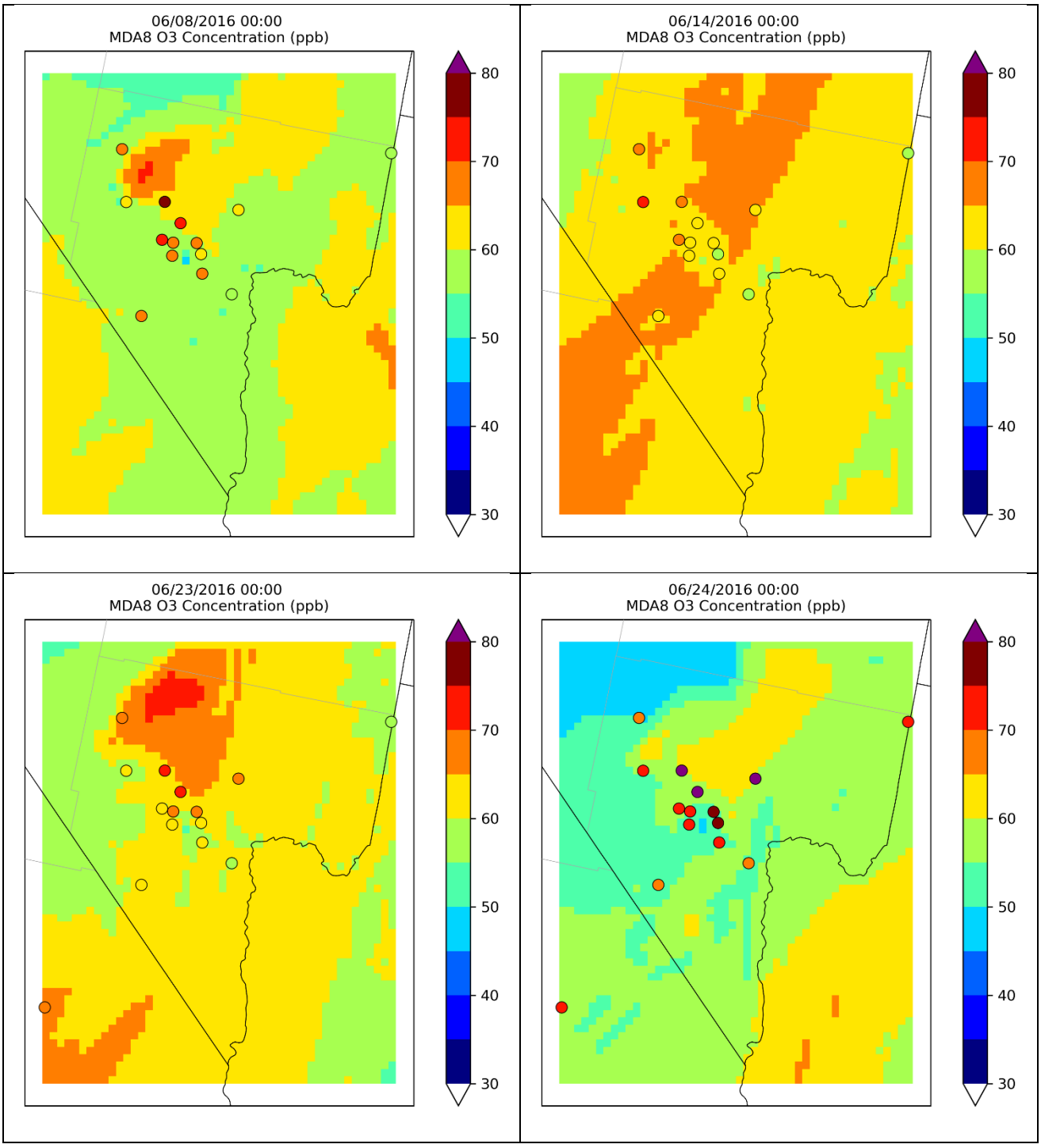

Figure 8-33 (continued).

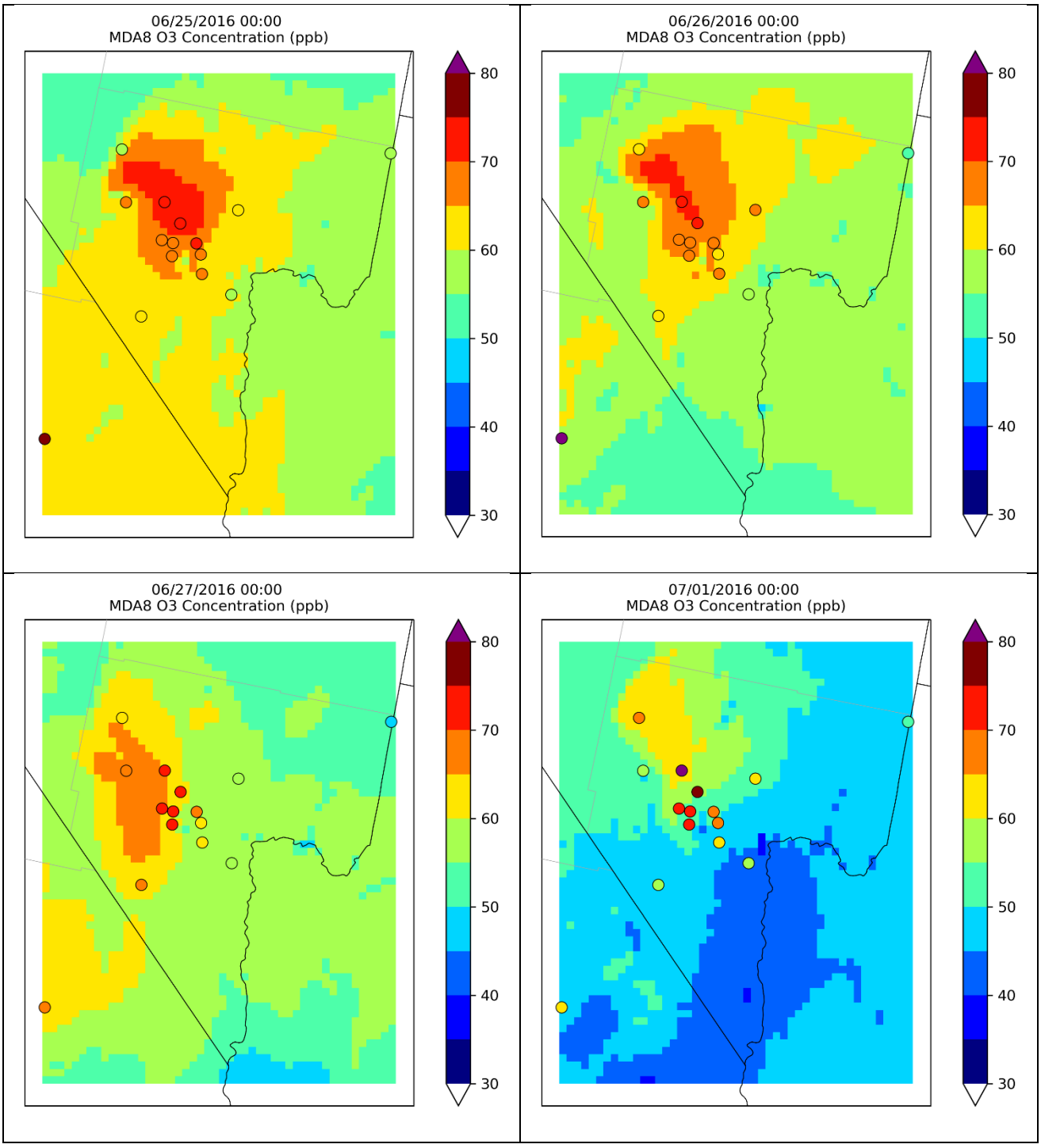

Figure 8-33 (continued).

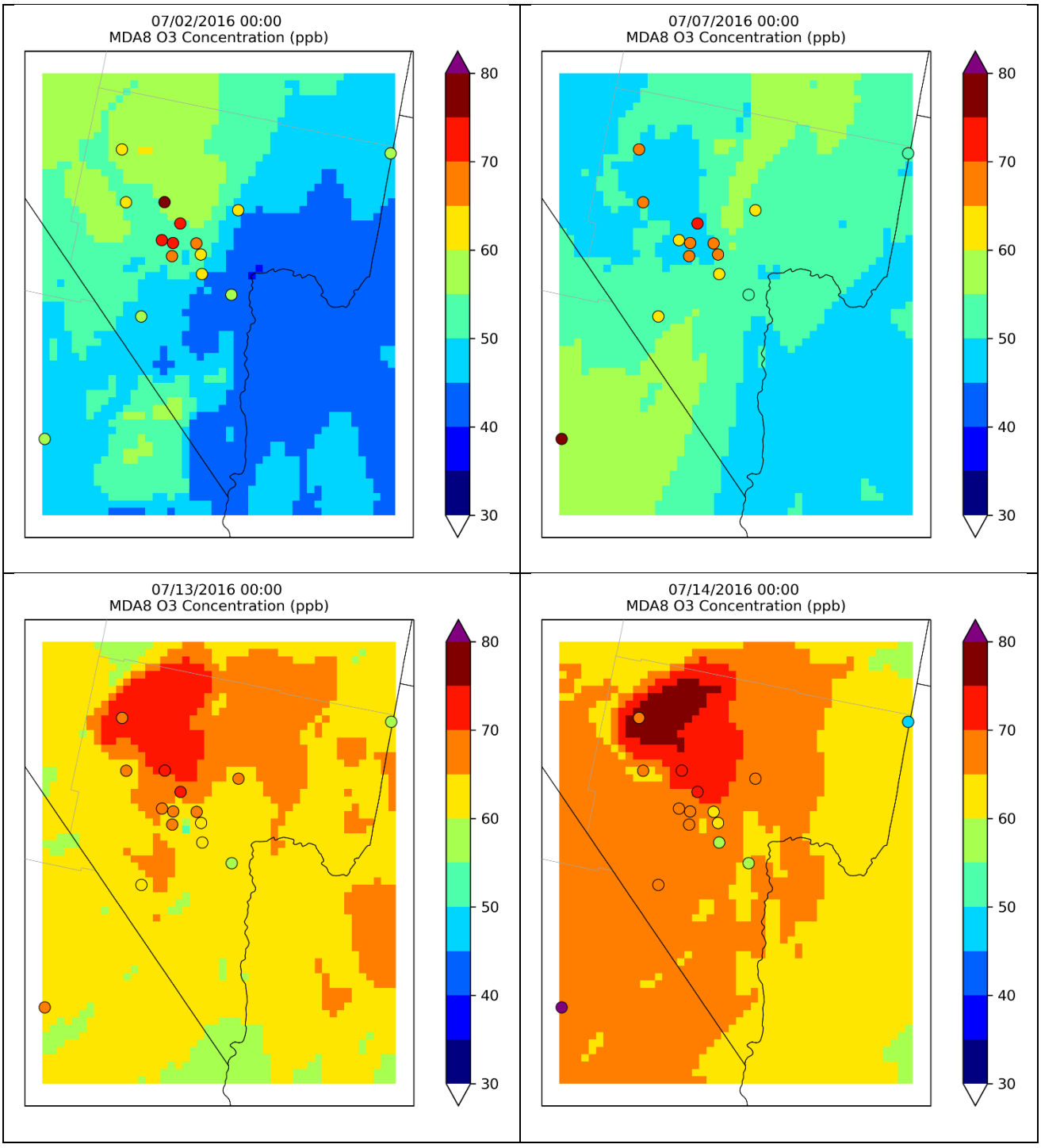

Figure 8-33 (continued).

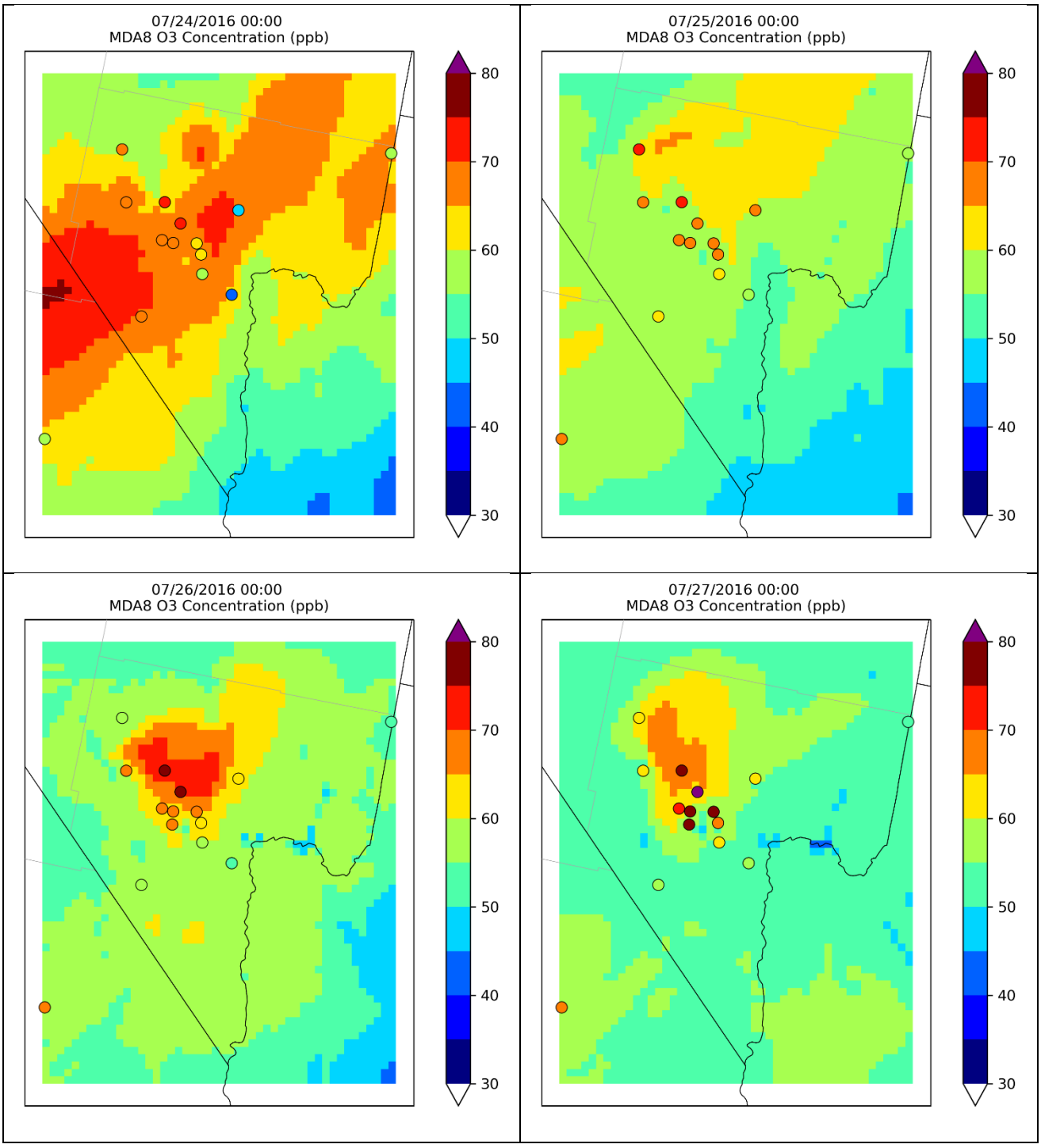

Figure 8-33 (continued).

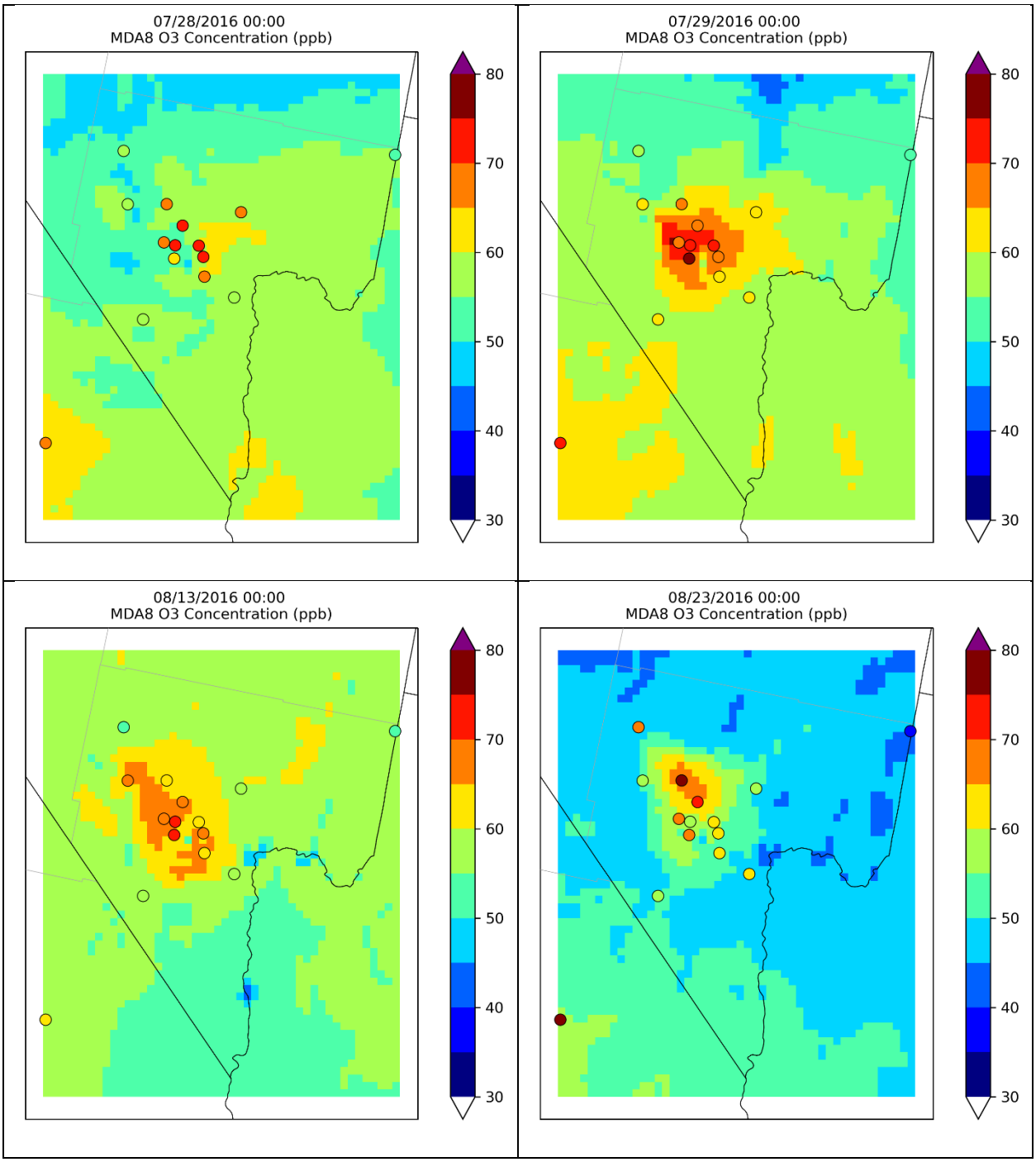

Figure 8-33 (continued).

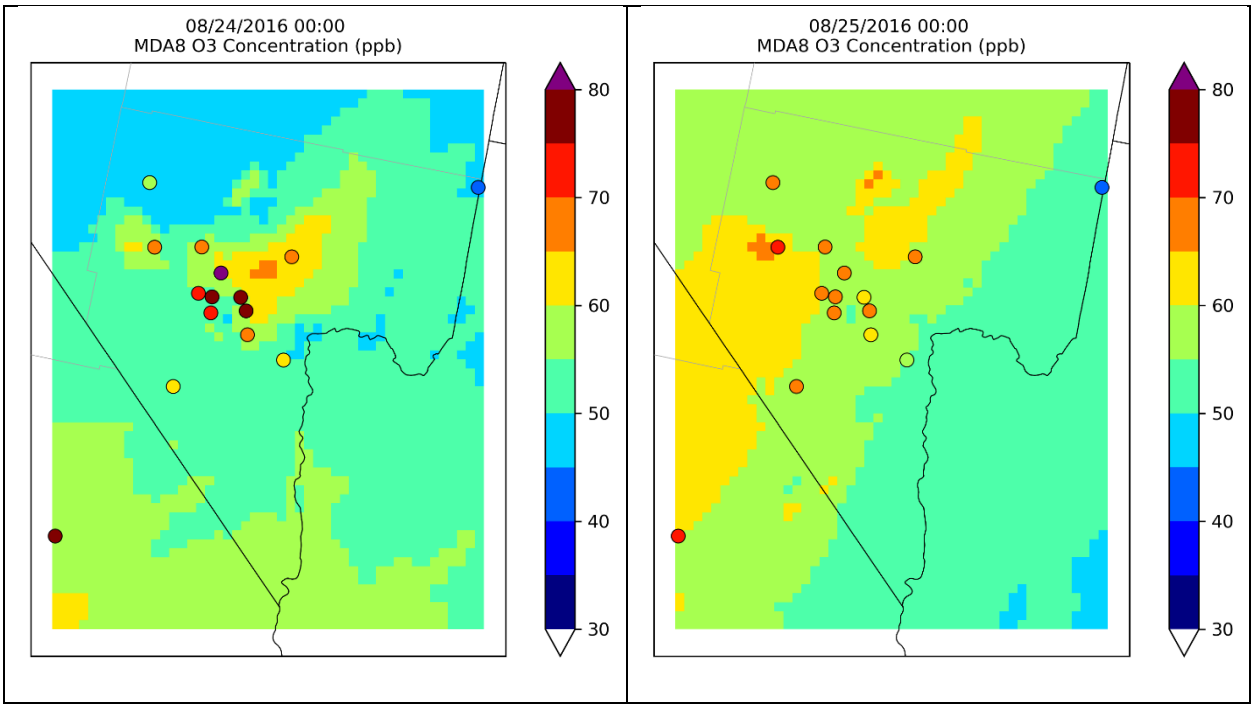

Figure 8-33 (concluded).

8.5.5 Analysis of Highest Predicted Ozone Days

EPA (2018a) modeling guidance provides detailed procedures on using base and future year modeling results to project future year ozone DVs – referred to as a "modeled attainment test". EPA has developed the Software for Model Attainment Test - Community Edition (SMAT-CE; EPA, 2022g) that codifies the recommended procedures. Modeling output for the base and future year is used in a relative sense to scale the observed base year ozone DV to a future year ozone DV at each monitoring site. The model-derived Relative Response Factor at each site is defined as the ratio of the average modeled MDA8 future ozone concentration to the average modeled MDA8 base ozone concentrations. The averages are determined for the 10 days with the highest modeled base year MDA8 ozone concentrations near the monitor (i.e., within a 3x3 array of grid cells), provided those values are all ≥60 ppb and regardless of observed conditions on those days. If there are less than 10 modeled days meeting this criterion, then only the days meeting this criterion are used in the average, provided there are at least 5 days available for the RRF calculation. If there are less than 5 days meeting this criterion, EPA recommends that RRFs not be calculated for the given site and the regional EPA office should be consulted if the site is an important high DV site.

EPA guidance allows some flexibility to exclude "exceptional event like" days (i.e., days that might not qualify as official exceptional events such as wildfire influences) from the DV projections with appropriate justification. There are two approaches to account for exceptional event like days in the attainment year DVF projection: (1) remove such days from the base year DVB calculation so that the DV more faithfully reflects local to regional anthropogenic ozone conditions and patterns; (2) remove such days from the list of modeled highest 10 base year ozone days in the RRF calculation so that the projection more faithfully reflects impacts from local to regional emission reductions.

In this section we analyze the top 10 modeled days at each of the 6 monitoring sites within the CCNAA that reported 2018-2020 DVs (Figure 8-34). We also note the number of days in each list that

correspond to observed days that exceeded 70 ppb (Table 8-15, Figure 8-33) along with current expectations for their cause.

Figure 8-34 shows the spatial distribution of 2018-2020 DVs reported at ozone monitoring sites within and immediately surrounding the CCNAA. Sites shown in grey did not report ozone DVs, including LV Paiute and J.D. Smith. Thus only 6 sites recorded DVs within the CCNAA while 8 ozone monitoring sites reported ozone measurements in 2016. Four sites within Las Vegas and near Henderson exceeded the 2015 ozone NAAQS, as shown in dark blue (Joe Neal, 74 ppb; Walter Johnson, 73 ppb; Paul Meyer, 73 ppb, Green Valley, 72 ppb). These 4 sites are critical in the 2023 SMAT-CE DV projections.

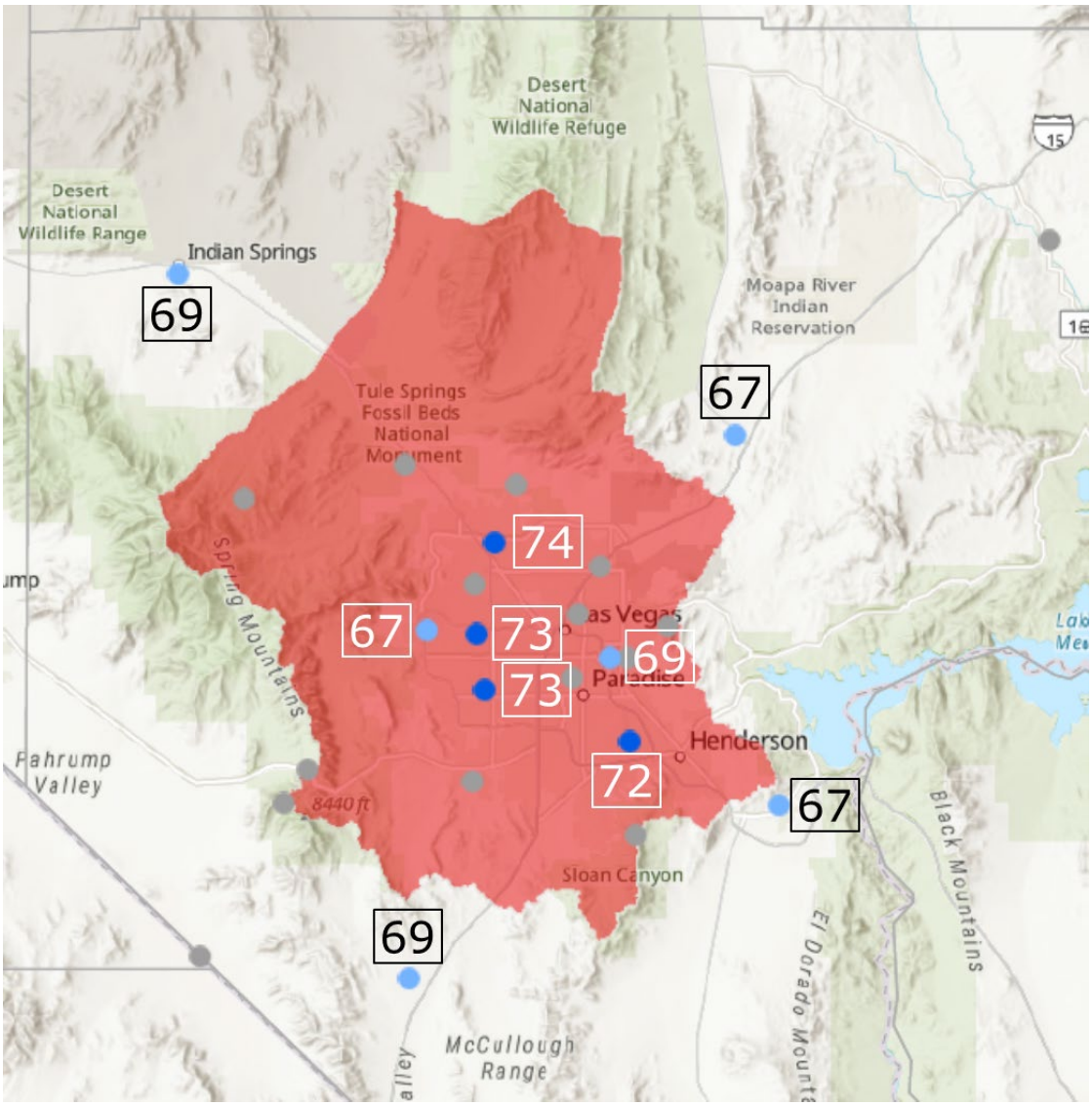

Figure 8-34. Spatial distribution of 2020 design values at 10 ozone monitoring sites within and immediately surrounding the CCNAA (depicted by orange shading). Sites shown in grey did not measure or report ozone design values. Background image from https://epa.maps.arcgis.com/apps/MapSeries/index.html?appid=bc6f3a961ea14013afb2e0d0e450b0d1.

Tables 8-16 through 8-21 present the top 10 modeled ozone days in the final base case scenario at each of 6 CCNAA monitors. All sites include 10 modeled days above 60 ppb, and all tend to include a similar set of dates in different orders. Results are summarized below.

Joe Neal: 7 observed exceedance days in the top 10 list (3 fire-influenced days, 2 local/transport days, 2 undetermined days).

Average observation / prediction: 69.9 / 69.2 ppb
Bias absolute / normalized: -0.6 ppb / -0.9%
Error absolute / normalized: 3.9 ppb / 5.6%

Table 8-16. Top 10 modeled MDA8 ozone days in the final base case scenario at the Joe Neal monitoring site, and date-paired observed MDA8 ozone. Exceedance dates noted in red are expected to be influenced by regional wildfires. Exceedance dates noted in blue are expected to be caused mainly by local production and upwind transport from anthropogenic sources. Exceedance dates noted in bold have not been assessed with respect to likely causes. Remaining dates did not exceed 70 ppb at any monitoring site in 2016.

Date	Observed	Predicted	Difference
6/7/2016	77.3	72.3	-4.9
6/25/2016	73.0	70.7	-2.3
7/14/2016	70.8	70.0	-0.7
6/6/2016	73.8	69.9	-3.8
6/26/2016	70.0	69.3	-0.7
7/26/2016	77.1	68.6	-8.6
8/12/2016	65.9	68.3	2.4
7/29/2016	69.6	68.2	-1.5
6/4/2016	65.9	68.1	2.2
8/28/2016	55.4	67.0	11.6

Palo Verde: 8 observed exceedance days in the top 10 list: (3 fire-influenced days, 2 local/transport days, 3 undetermined days).

Average observation / prediction: 67.0 / 68.6 ppb
Bias absolute / normalized: 1.7 ppb / 2.5%
Error absolute / normalized: 2.7 ppb / 4.0%

Table 8-17. As in Table 8-16, but at the Palo Verde monitoring site.

Date	Observed	Predicted	Difference
7/29/2016	67.8	74.4	6.6
8/28/2016	64.6	69.3	4.6
6/6/2016	64.1	69.2	5.1
7/14/2016	66.8	68.1	1.4
6/4/2016	65.1	68.0	2.9
6/25/2016	67.6	68.0	0.3
7/24/2016	69.1	67.7	-1.4
8/13/2016	68.9	67.4	-1.5
6/7/2016	69.3	67.0	-2.3
6/26/2016	66.3	67.0	0.7

Walter Johnson: 8 observed exceedance days in the top 10 list (3 fire-influenced days, 2 local/transport days, 3 undetermined days).

Average observation / prediction: 68.0 / 68.1 ppb
Bias absolute / normalized: 0.1 ppb / 0.1%
Error absolute / normalized: 2.4 ppb / 3.5%

Table 8-18. As in Table 8-16, but at the Walter Johnson monitoring site.

Date	Observed	Predicted	Difference
7/29/2016	71.9	73.9	2.0
6/6/2016	65.6	68.8	3.2
7/24/2016	69.1	68.5	-0.6
7/14/2016	67.4	68.0	0.6
8/28/2016	64.1	67.8	3.7
6/25/2016	69.5	67.2	-2.3
6/4/2016	63.9	66.8	2.9
6/7/2016	70.4	66.6	-3.7
8/13/2016	70.1	66.5	-3.6
6/26/2016	67.6	66.4	-1.3

Paul Meyer: 7 observed exceedance days in the top 10 list (2 fire-influenced days, 2 local/transport days, 3 undetermined days).

Average observation / prediction: 67.1 / 66.6 ppb
Bias absolute / normalized: -0.5 ppb / -0.7%
Error absolute / normalized: 2.8 ppb / 4.2%

Table 8-19. As in Table 8-16, but at the Paul Meyer monitoring site.

Date	Observed	Predicted	Difference
7/29/2016	75.5	71.8	-3.7
6/6/2016	64.8	68.0	3.3
8/28/2016	64.5	66.7	2.2
7/14/2016	65.8	66.7	0.9
6/25/2016	68.1	65.9	-2.2
6/7/2016	69.0	65.9	-3.1
6/4/2016	64.9	65.6	0.7
8/13/2016	70.8	65.5	-5.3
6/26/2016	67.8	65.3	-2.4
8/9/2016	60.1	64.7	4.6

Jerome Mack: 7 observed exceedance days in the top 10 list (3 fire-influenced days, 2 local/transport days, 2 undetermined days).

Average observation / prediction: 64.1 / 65.8 ppb
Bias absolute / normalized: 1.7 ppb / 2.7%
Error absolute / normalized: 3.4 ppb / 5.3%

Table 8-20. As in Table 8-16, but at the Jerome Mack monitoring site.

Date	Observed	Predicted	Difference
7/24/2016	61.1	68.0	6.9
6/7/2016	67.9	67.4	-0.5
6/6/2016	67.0	67.0	0.0
7/14/2016	62.8	66.8	4.0
7/29/2016	67.9	66.1	-1.8
8/12/2016	67.9	65.0	-2.9
8/9/2016	57.3	64.9	7.7
6/25/2016	67.5	64.3	-3.2
6/26/2016	63.1	64.2	1.1
6/4/2016	58.1	63.9	5.8

Green Valley: 7 observed exceedance days in the top 10 list (2 fire-influenced days, 2 local/transport days, 3 undetermined days).

Average observation / prediction: 61.8 / 65.4 ppb
Bias absolute / normalized: 3.6 ppb / 5.8%
Error absolute / normalized: 4.4 ppb / 7.1%

Table 8-21. As in Table 8-16, but at the Green Valley monitoring site.

Date	Observed	Predicted	Difference
7/24/2016	57.1	69.1	12.0
7/14/2016	59.4	66.2	6.8
8/13/2016	62.3	65.8	3.6
6/6/2016	64.0	65.7	1.7
7/15/2016	64.9	65.6	0.8
7/16/2016	62.6	64.8	2.2
6/14/2016	61.9	64.3	2.4
8/9/2016	54.6	64.3	9.7
7/29/2016	63.3	64.3	1.0
6/7/2016	68.0	64.0	-4.0

9.0 FUTURE YEAR MODELING

This Section describes the CAMx 2023 future year base case modeling configuration, the methods to apply the modeled attainment test that projects the 2016-2018 average DV to the 2023 future year, and DV projection results. The methodology closely followed the approach described in EPA modeling guidance (EPA, 2018a) and in the Modeling Protocol developed during the early phases of this project (Ramboll, 2022a).

9.1 Summary of Results

The 2023 future base case was used in combination with the final 2016 base case to project 2016-2018 DVs to 2023 at each monitoring site in the basin, based on relative scaling factors that were developed from ozone concentration ratios between the two model runs. Results from the modeled attainment test are summarized below:

- According to the method codified by EPA (2022g), no exceedances were projected in 2023 based on the 2023 future base CAMx simulation. The peak 3-year average projected 2023 DV was 69 ppb at Joe Neal.
- Comparison of the modeled 2016 ozone against the 2016-2018 average DV at each site shows that the modeled spatial pattern of high and low ozone was well represented in the CAMx results. This adds some weight to the argument that the model adequately replicated the processes that form and disperse ozone throughout the basin, and in turn the spatial distribution of the respective RRFs was reasonably represented as well.
- The amount of predicted regional ozone streaming into the CCNAA from southern California was an important component in the 2023 projection. The accuracy of the 2023 projection depends in large measure on the accuracy of the regional anthropogenic emission inventory, wildfire influences, and the chemistry and dispersion/transport patterns characterized in the CAMx simulations.

9.2 Future Year Model Configuration

The CCNAA is currently classified as a Moderate Nonattainment Area under the 2015 ozone NAAQS because 2018-2020 ozone DVs failed to attain the standard by the August 3, 2021 attainment date for Marginal areas (Figure 8-34). Moderate areas must attain the NAAQS by August 3, 2024 based on the 2021-2023 DV, or risk further bump-up to Severe. Thus, attainment demonstration modeling was conducted for the 2023 future year.

The final 2016 base case CAMx configuration was repeated but using 2023 base case anthropogenic emission inputs for each of the three modeling domains (36US3, 12US2, CC4c2). All other inputs were the same as the final 2016 base case simulation, including meteorology, natural emissions, 36US3 boundary conditions, and photolysis inputs. This model configuration was otherwise identical to the final 2016 sensitivity run called "SENS6" (Table 9-1).

The following natural emission sources remained unchanged from the 2016 base year:

- Biogenic emissions from the EPA BEIS4/BELD6 model;
- Lighting NOx emissions;
- Open Land Fires (Wildfires, Prescribed Burns and Agricultural Burning)

As described in Section 6, the EPA 2016v2 MP provided all of the 2023 model-ready anthropogenic emission estimates for the 36US3 and 12US2 modeling grids (EPA, 2022b). A combination of 2016v2 emissions and Clark County data were used to process 2023 model-ready anthropogenic emissions on

the CC4c2 grid. The 2023 emissions inventory reflect local, state, and national rules that are currently known and "on-the-books." The 2023 future base case therefore does not include any additional control measures that are either planned or promulgated to begin during or after 2023.

9.3 Ozone Attainment Demonstration

EPA (2018a) modeling guidance includes detailed procedures on using base and future year modeling results to project future year ozone DVs – referred to as a "modeled attainment test". EPA has developed the Software for Model Attainment Test - Community Edition (SMAT-CE; EPA, 2022g) that codifies the recommended procedures.

9.3.1 Modeled Attainment Test

The SMAT-CE procedure is outlined in Chapter 4 of EPA's modeling guidance (EPA, 2018a, pages 99-110). PGM output for the base and future year is used in a relative sense to scale the base year ozone DV (DVB) to the future year ozone DV (DVF) at each monitoring site. The model-derived Relative Response Factor (RRF) is defined individually at each monitoring site as the ratio of average future MDA8 ozone concentration ($O3_{FY}$) to the average base MDA8 ozone concentrations ($O3_{BY}$), where the average is over the same set of several modeled high ozone days. This is expressed mathematically below:

$$DVF = DVB \times RRF$$

$$RRF = \sum(O3_{FY}) / \sum(O3_{BY})$$

The site-specific DVB is defined as the three-year average ozone DV centered on the base modeling year. As each year's DV is itself defined as the three-year average of the 4th highest MDA8 ozone concentration each year (H4MDA8), the DVB is thus based on 5 years of H4MDA8 ozone concentrations centered on the base year, such that the central year is weighted by a factor of 3/5, the 2nd and 4th years are weighted by a factor of 2/5, and the 1st and 5th years are weighted by a factor of 1/5. This approach is EPA's way to account for interannual variability affecting DVs in and around the base year.

The CCNAA modeled base year is 2016 so the DVB at each site is defined from three years of ozone DVs as follows:

$$DVB_{2016} = (DV_{2014\text{-}2016} + DV_{2015\text{-}2017} + DV_{2016\text{-}2018}) / 3$$

or

$$DVB_{2016} = (H4MDA8_{2014} + 2xH4MDA8_{2015} + 3xH4MDA8_{2016} + 2xH4MDA8_{2017} + H4MDA8_{2018}) / 5$$

Table 9-1. CAMx model configuration for the CCNAA 2023 future base case simulation. Changes from the final 2016 base case are noted in red.

Model Component	CCNAA Application	Comment
Model Code	CAMx v7.20 - May 2022	
Modeling Period	May 1 – August 31, 2016	
Horizontal Grids		
Map Projection	Lambert Conic Conformal	EPA 2016 MP
36 km (36US3)	172 x 148 cells	EPA 2016 MP (1-way nesting)
12 km (12US2)	396 x 246 cells (no buffer cells)	EPA 2016 MP (2-way nesting)
4 km (CC4c2)	50 x 62 cells (with buffer cells)	CCNAA grid (2-way nesting)
Vertical Grid	35 layers	EPA 2016 MP, defined by WRF
Initial Conditions	36US3 IC April 1 from CAM-Chem, 12US2/CC4c2 IC May 1 from 36US3	
Boundary Conditions	36US3 BC from CAM-Chem, 12US2 BC from 36US3	
Time Zone	UTC	EPA 2016 MP
Emissions		
36/12 km Data Sources	EPA 2023fj from 2016v2 MP	
4 km Data Sources	EPA 2023fj from 2016v2 MP + 2023 Clark County Data, elevated Reid LTO emissions	
Models/Processing Tools	SMOKE, MOVES3, SMOKE-MOVES, BEIS4/BELD6	CCNAA grid
Plume-in-Grid	Off	No large point sources in high-resolution CCNAA grid
In-line Ix emissions	On	Oceanic halogens
Chemistry		
Gas Phase Chemistry	CB6r5	Latest mechanism available
Aerosol Chemistry	Active	Gas phase only
Meteorological Interface	WRFCAMx v5.2	
Horizontal Diffusion	Smagorinsky	Spatially variant K-theory
Vertical Diffusion	YSU Kv formulation + KVPATCH	Minimum Kv 0.1 to 1.0 m^2/s
ACM2	Off	Non-local boundary layer convection
Sub-grid Cloud Convection	Off	
Deposition		
Dry Deposition	Zhang03	
Wet Deposition	On	rain/snow/graupel
Surface Chemistry Model	Off	
Bi-directional Ammonia	Off	For aerosol chemistry
Numeric Solvers		
Gas Phase Solver	Euler Backward Iterative (EBI)	Default fast and accurate solver
Vertical Advection	Piecewise Parabolic Method (PPM)	Default
Horizontal Advection	Piecewise Parabolic Method (PPM)	Default
Integration Time Step	Wind speed dependent	~0.5-1 min (4 km), 1-5 min (12 km), 5-15 min (36 km)
Super Stepping	On	Maximizes time step selection

The RRF is determined from maximum MDA8 ozone concentrations near each monitor, averaged over 10 days with the highest base year modeled MDA8 ozone concentrations.

Near the Monitor: This means that the highest modeled base year MDA8 ozone is selected from one of a 3x3 array of grid cells centered on the monitor. The future year MDA8 ozone is selected from the same grid cell of the 3x3 array.

10 Highest Base Year MDA8 Ozone Days: Modeled MDA8 ozone concentrations are averaged over 10 days with the highest base year modeled ozone concentrations near the monitor, provided MDA8 ozone on the chosen days are each ≥60 ppb. If there are less than 10 days meeting this criterion, then only the days meeting this criterion are used in the average, provided there are at least 5 days available for the RRF calculation. If there are less than 5 days meeting this criterion, EPA recommends that RRFs not be calculated for the given site and the regional EPA office should be consulted if the site is an important high DV site.

9.3.2 Flexibility in RRF Calculations

EPA's guidance includes some flexibility to modify the recommended ozone DV projection procedure. There may be good reason why certain grid cells within the 3x3 array centered on the monitor may not be representative of conditions at the monitor; for example, if portions of the 3x3 array have different atmospheric conditions (over water) or the monitor is in an area with sharp terrain gradients.

Another consideration is to account for "exceptional event like" days (i.e., days that might not qualify as official exceptional events) such as wildfires. EPA (2019c) includes provisions for excluding such days with appropriate justification. There are two approaches to account for exceptional event like days in the attainment year DVF projection: (1) remove such days from the base year DVB calculation so that the DV more faithfully reflects local to regional anthropogenic ozone conditions and patterns; (2) remove such days from the list of modeled highest 10 base year ozone days in the RRF calculation so that the projection more faithfully reflects impacts from local to regional emission reductions. As described in the Modeling Protocol (Ramboll, 2022a) several days of 2016 may warrant exclusion, but it would be problematic to exclude a large number.

In the CCNAA attainment demonstration, any deviations in the modeled attainment test from EPA's recommended procedures have been documented and justified. The standard EPA method was always calculated as one of the projection approaches analyzed.

9.3.3 SMAT-CE Configuration

We applied SMAT-CE v2.1 (8/26/22) with the most current monitoring database from EPA containing 2002-2020 4th high MDA8 ozone for all official sites operating in Clark County. The SMAT-CE configuration involved defining the 2016-2018 3-year DV period for base monitored ozone (2014-2018 4th highs), choosing the maximum ozone within a 3x3 grid cell matrix around each monitor, and projecting DVs using the 3-year average DV and 3-year maximum DV at each monitor. The average is used for the standard attainment test, while maxima are used to identify any future maintenance monitors.

Figure 9-1 presents the settings reported in the SMAT-CE configuration file for the application described here. These settings are presented simply as a reference for documentation purposes; we refer the reader to the SMAT-CE User's Guide (EPA, 2022g) for additional information on each parameter setting. In general, our approach was to use default or standard settings throughout the

setup menu. We made no special modifications to monitored data or specific selection of modeled days for the RRF calculation.

```
RunType=RunOzone
OutputFileDir=C:\Users\Documents\My SMAT-CE Files\Result\Output
OutputFileName=ClarkCo_O3SIP.cfg
scenarioName=ClarkCo_O3SIP
doPointEstimatesForecast=1
doQuarterlyModelData=1
doSpatialFieldEstimates=1
doBaseOnlyVNA=0
doFutureOnlyVNA=0
doSpatialFieldEstimatesGradAdj=1
doBaseOnlyEVNA=0
doFutureOnlyEVNA=0
doNeighborFileSpatial=1
doAutomaticallyExtract=1
doDesignValuePeriods=1
doMaxDesignValuePeriods=1
ozoneMonitorDataFile=C:\Users\Documents\My SMAT-CE Files\Data\SampleData\Monitor_data\
SMAT_OZONE_MAX4DV_STD70_2002_2020.CSV
doInputfromCmaq=0
baselineModelDataFile=C:\Users\ Documents\My SMAT-CE Files\Result\CSV\ClarkCo_O3SIP\ camxv720_cb6r5.May-
Aug.12US2.35.clark.sns6.MDA8.4km.SMAT.csv
forecastModelDataFile=C:\Users\ Documents\My SMAT-CE Files\Result\CSV\ClarkCo_O3SIP\ camxv720_cb6r5.May-
Aug.12US2.35.clark.fy2023.MDA8.4km.SMAT.csv
temporalAdjustmentAtMonitorGrid=3x3
temporalAdjustmentType=Maximum-paired in space
ozoneStartYear=2014-2016
ozoneEndYear=2016-2018
minNumDV=1
requiredDVPeriods=None selected
defaultInterpolationMethod=Inverse Distance Weights
doCheckToSetMaxDistance=0
maxDistance=100
useInitialThresholdValue=0
initialThresholdValue=85
minNumofDaysAtorAboveThreshold=10
topXmodeledozonedays=10
minAllowableThresholdValue=60
minNumDaysAtorAboveMinAllowableThreshold=5
doBackstop=0
backstopMinThresholdforSpatialField=0
subrangeFirstDay=1
subrangeLastDay=123
doPairDays=0
SRF_StartValue=1
SRF_EndValue=5
```

Figure 9-1. SMAT-CE settings applied for the 2023 future base DV projections.

9.3.4 Results at Monitoring Sites

Table 9-2 shows base and projected DV results. According to SMAT-CE, no exceedances were projected in 2023 based on the 2023 future base CAMx simulation. The peak average projected DV was 69 ppb at Joe Neal.

Figure 8-34 shows the spatial distribution of monitored 2020 DVs reported at sites within and immediately surrounding the CCNAA. Four sites within Las Vegas and near Henderson exceeded the 2015 ozone NAAQS, as shown in dark blue (Joe Neal, 74 ppb; Walter Johnson, 73 ppb; Paul Meyer, 73 ppb, Green Valley, 72 ppb). These 4 sites resulted in the bump-up from Marginal to Moderate nonattainment in 2021.

Table 9-2. 2016-2018 monitored and 2023 projected DVs at each monitoring site within the LVV according to SMAT-CE calculations using the 2016 base and 2023 future base CAMx simulations. Red values indicate exceedances of the 2015 ozone NAAQS, green indicate values below the NAAQS. Sites noted with an asterisk continued to exceed the ozone NAAQS in 2020, leading to the bump up from Marginal to Moderate nonattainment status (Figure 8-34).

Site ID	Site Name	2016-2018 DV Avg 3x3	2023 DV Avg 3x3
320030022	Apex	70.3	65.2
320030023	Mesquite	61.3	57.2
320030043	Paul Meyer*	72.0	67.7
320030071	Walter Johnson*	72.3	67.9
320030073	Palo Verde	72.3	67.2
320030075	Joe Neal*	75.0	69.0
320030298	Green Valley*	71.0	67.3
320030540	Jerome Mack	68.7	64.1
320030601	Boulder City	66.0	61.5
320031019	Jean	68.3	63.9
320032002	J.D. Smith	72.5	67.3
320037772	Indian Springs	68.5	62.3

Figure 9-2 shows a scatter plot comparing, at each monitoring site in Table 9-2, the average of modeled top 10 MDA8 ozone in 2016 as reported by SMAT-CE against the historical 2016-2018 average DV. The plot confirms that the model under predicted 2016-2018 DV levels consistently, but perhaps more importantly, the linear correlation was rather good (R^2 = 0.83). This shows that the 2016 modeled spatial patterns of high and low ozone represented the historical DV patterns well. It further adds some weight to the argument that the model adequately replicated the spatial distribution of the processes that form and disperse ozone throughout the basin, and so in turn the spatial distribution of the respective RRFs should be reasonably represented as well. Certainly, the same could not be said if the comparison in Figure 9-2 exhibited low correlation (large scatter) with high predicted ozone where low ozone was monitored and vice versa.

The amount of predicted regional ozone streaming into the CCNAA from southern California is an important component in the 2023 projection. The accuracy of the 2023 DVF projection depends in large measure on the accuracy of the regional anthropogenic emission inventory, wildfire influences, and the chemistry and dispersion/transport patterns characterized in the CAMx simulations.

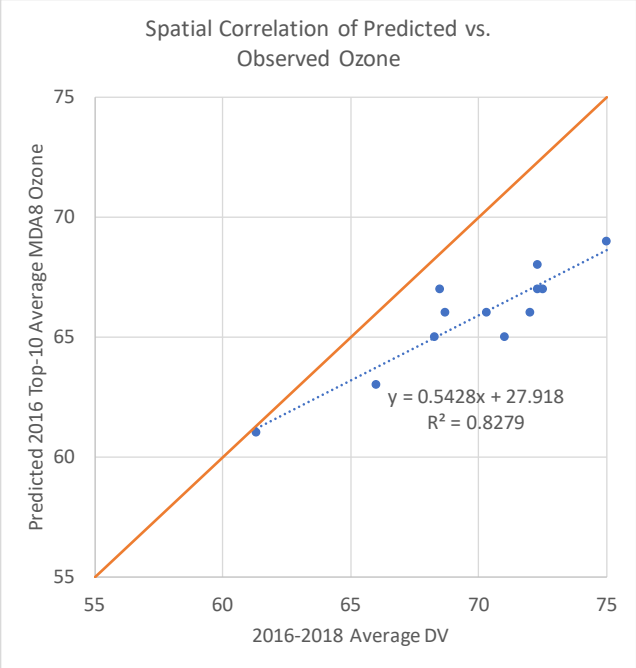

Figure 9-2. Comparison at each monitoring site (blue dots) between the average modeled top 10 MDA8 ozone in 2016 as reported by SMAT-CE and the historical 2016-2018 average DV.

10.0 FUTURE YEAR CONTROL MEASURE SIMULATIONS

This Section describes the CAMx future year control measure modeling scenarios and results from applying the modeled attainment test to project the 2016-2018 average DV to the 2023 future year. The methodology closely follows the approach described in EPA modeling guidance (EPA, 2018a) and in the Modeling Protocol developed during the early phases of this project (Ramboll, 2022a).

10.1 Summary of Results

We developed a 2023 future year emission inventory that reflects 6 control measures representing the CCNAA 15% VOC Rate of Progress (ROP) Plan as originally developed and documented by Ramboll (2023a). The control measures reduced VOC emissions only from the nonpoint solvent sector of the 2023fj platform emissions inventory. [Note that the ROP has since been substantially revised (Ramboll, 2024a,b) to reflect a different set of control measures extending to 2026 in response to discussions with EPA.]

- Projected 2023 DVs were all well below the ozone NAAQS but only 0-0.4 ppb lower than the DV projections from the 2023 future base case (Section 9). The peak average projected DV was 68.8 ppb at Joe Neal.

We developed a 2023 CCNAA future year conformity budget emission inventory that reflects an additional 2 TPD NOx and VOC margin above CCNAA 2023 base case on-road mobile source emissions (Ramboll, 2023b), as well as increased point source NOx and VOC to account for emissions currently contained within Clark County Emissions Reduction Credit (ERC) program.

- Projected 2023 DVs were all well below the ozone NAAQS and 0-0.3 ppb higher than the DV projections from the 2023 future base case. The peak projected DV was 69.3 ppb at Joe Neal.

10.2 15% VOC Rate of Progress Plan

Clean Air Act Section 182(b)(1) requires moderate ozone nonattainment areas to reduce VOC emissions by 15% over 6 years following the baseline year (2017 in the case of the CCNAA). This requirement is known as the Rate of Progress (ROP) plan. Ramboll (2023a) developed a technical support document that identified and quantified several control measures that, along with specific Reasonably Available Control Technology (RACT) measures developed by the DES/DAQ, would achieve a 15% VOC reduction relative to the 2017 CCNAA emission inventory.

10.2.1 Control Measures

Table 10-1 is repeated from Ramboll (2023a) and presents the 2017 baseline and 2023 future year CCNAA emission inventories, estimated 2023 emission reductions for each RACT and planned local control measure, and net total 2023 emissions and reductions. Net emission reductions from 2017 to 2023 are 19.53 TPD or 18.1%, indicating that the 15% ROP requirement can be met through the implementation of the RACT and planned local control measures. [Note that the ROP has since been substantially revised (Ramboll, 2024a,b) to reflect a different set of control measures extending to 2026 in response to discussions with EPA.]

Table 10-1. CCNAA 2017 and 2023 VOC emissions (TPD) by sector, emission reductions by control measure, and net change in CCNAA emissions from 2017 to 2023 for the 15% ROP scenario as documented by Ramboll (2023a).

Description	2017	2023	Difference	Percent Difference
VOC Emissions by Sector				
Point source	1.25	1.32	0.07	5.6%
Nonpoint source	56.05	58.29	2.24	4.0%
Onroad mobile	24.43	17.01	-7.42	-30.4%
Nonroad mobile	24.03	24.17	0.14	0.6%
Airports (commercial & Federal)	1.94	2.62	0.68	35.1%
Locomotives	0.04	0.03	-0.01	-25.0%
Subtotals	**107.73**	**103.44**	**-4.29**	**-4.0%**
RACT VOC Emission Reductions				
Solvent Metal Cleaning (Degreasers)		0.66		
Graphic Arts		1.43		
Cutback Asphalt		0.78		
Industrial Cleaning Solvents		2.82		
Subtotals		**5.69**		
VOC Emission Reductions for Planned Local Control Measures				
Consumer Products OTC Model Rules Phase IV		6.74		
AIM Coatings OTC Model Rules Phase II		2.70		
Subtotals		**9.44**		
Net VOC Emissions				
Totals	**107.73**	**88.31**	**-19.42**	**-18.0%**

10.2.2 Emissions Processing

We prepared SMOKE control packets for each control measure listed in Table 10-1. The control packets specify control factors at the source category code (SCC) level, as shown in Table 10-2. The control factors were applied to 2023fj Clark County inventories from the 2016v2 Modeling Platform (EPA, 2022b) to develop emissions for the 15% ROP control scenario. Both RACT and planned local control measures reduced VOC emissions only from the nonpoint solvent sector of the 2023fj platform emissions inventory.

The RACT measures were applied only to the CCNAA, while the two planned local control measures (AIM coatings and Consumer products) were applied to the whole county. To develop CAMx-ready emissions, we created an adjusted emission inventory by applying SCC-level control factors from the SMOKE control packets and processed resulting emissions through SMOKE. First, the adjusted emission inventory with VOC reductions from both the planned local control measures and RACT measures was processed through SMOKE for the CCNAA portion of Clark County (HA 212 domain). Next, the adjusted inventory with VOC reductions from just the planned local control measures was processed for the full CC4c2 modeling domain. Finally, the emissions generated for the CCNAA were merged into the CC4c2 domain to develop the final merged CAMx-ready emissions.

Table 10-2. SCC-level VOC control efficiency (%) by control measure for 15% ROP scenario.

SCC	SCC Description	VOC Control Efficiency (%)
RACT Control Measures		
Degreasing		
2460200000*	All Household Products	5.5%
2460290000*	Household Products: Miscellaneous Household Products	5.5%
Graphical Arts		
2425000000	Solvent - Graphic Arts	56.3%
Cutback Asphalt		
2461021000	Cutback Asphalt	100%
Industrial Cleaning Solvent		
2402000000	Chemical Strippers	76.0%
Planned Local Control Measures		
Consumer Products		
2460100000	Solvent - All Personal Care Products	23.9%
2460110000	Personal Care Products: Hair Care Products	23.9%
2460190000	Personal Care Products: Miscellaneous Personal Care Products	23.9%
2460200000*	All Household Products	21.3%
2460290000*	Household Products: Miscellaneous Household Products	21.3%
2460500000	All Coatings and Related Products	23.9%
2460600000	All Adhesives and Sealants	23.9%
2460900000	Solvent - Miscellaneous Products (Not Otherwise Covered)	23.9%
Architectural and Industrial Maintenance (AIM) Coatings		
2401001000	Architectural Coatings	40.7%
2401100000	Industrial Maintenance Coatings	40.7%

* Control measures are additive when the same SCC is controlled by more than one control measure.

Table 10-3 summarizes the 2023 VOC emissions by SCC before and after applying control measures selected for the 15% ROP scenario. The comparison of VOC control efficiency for each SCC in Table 10-2 and the corresponding percent reduction in Table 10-3 confirm that the control factors were applied correctly during emission processing to produce CAMx-ready emissions for the 15% ROP control scenario.

Table 10-3. Annual VOC emissions inventory before and after applying control factors.

SCC	SCC Desc	2023 VOC Emissions (TPY)	VOC Emissions with 15% ROP Controls (TPY)	Difference (%)
2461021000	Cutback Asphalt	303	0	100%
2460200000	All Household Products	456	334	27%
2460290000	Household Products: Miscellaneous Household Products	3,995	2,924	27%
2460110000	Personal Care Products: Hair Care Products	4,076	3,102	24%
2460190000	Personal Care Products: Miscellaneous Personal Care Products	118	90	24%
2460600000	All Adhesives and Sealants	1,742	1,325	24%
2401001000	Architectural Coatings	1,683	998	41%
2460500000	All Coatings and Related Products	524	399	24%
2402000000	Chemical Strippers	1,359	326	76%
2401100000	Industrial Maintenance Coatings	826	490	41%
2425000000	Solvent - Graphic Arts	934	408	56%
2460900000	Solvent - Miscellaneous Products (Not Otherwise Covered)	44	33	24%
2460100000	Solvent - All Personal Care Products	52	40	24%
Total		**16,112**	**10,469**	**35%**

Table 10-4 summarizes the model-ready VOC emissions over the entirety of Clark County by major anthropogenic categories for the 2023 future base case and 15% ROP scenarios. As noted previously, the 15% ROP control scenario only affects the solvent sector of the nonpoint source category. Figure 10-1 shows the spatial distribution of May-August average day 2023 VOC emissions and differences when the 15% ROP reductions are applied. The reductions occur mostly over the CCNAA with the largest average reduction of 0.31 tons/day.

Table 10-4. July weekday average 2023 future base case and 2023 15% ROP emissions (TPD) over the entirety of Clark County by major source category.

Source Category	2023 VOC	2023 15% ROP
Point source	1.8	1.8
Nonpoint source	60.8	50.9
On-road mobile	17.7	17.7
Non-road mobile	27.6	27.6
Airports (commercial & Federal)	3.1	3.1
Locomotives	0.0	0.0
Fires	0.3	0.3
TOTAL	**111.3**	**101.4**

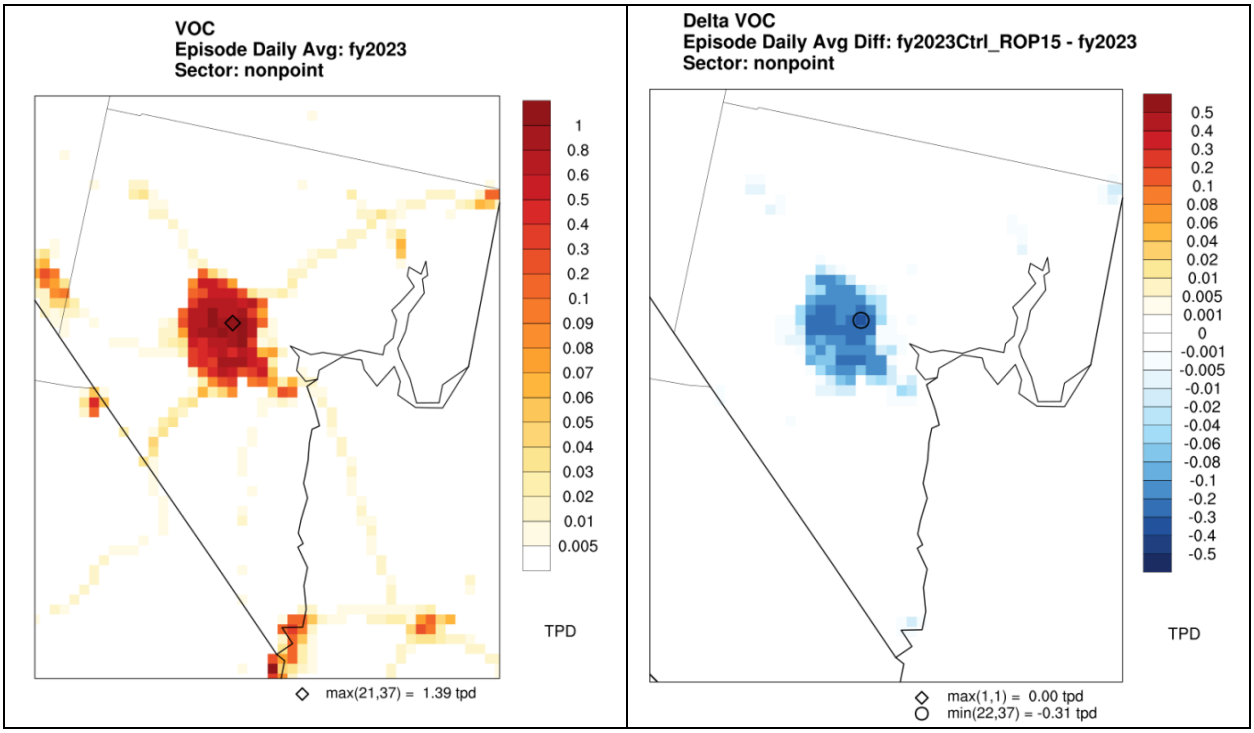

Figure 10-1. Spatial map of May-August average daily VOC emissions (TPD) for the nonpoint source category over the CC4c2 grid; 2023 future base case (left) and differences when 15% ROP reductions are applied.

10.2.3 CAMx Modeling

The 2023 future year base case CAMx run (Section 5) was repeated but replacing 2023 solvent sector emissions on the CC4c2 grid with revised emissions reflecting 15% VOC ROP control measures as described above. All other inputs were not modified (Table 10-5), and only the 12US2/CC4c2 2-way

nested grids were run using the 2023 12US2 future base case boundary conditions extracted from the 36US3 grid.

10.2.3.1 SMAT-CE Configuration

We applied SMAT-CE identically to the original 2023 future base case scenario, specifying 2016-2018 3-year DV period for base monitored ozone (2014-2018 4th highs centered on 2016). All other configuration options remained the same as the original SMAT-CE run, which employed default or standard settings throughout the setup menu. We made no special modifications to monitored data or specific selection of modeled days for the RRF calculation.

10.2.3.2 Results at Monitoring Sites

Table 10-6 shows projected DV results at monitoring sites that reported sufficient data during the 2016-2018 base year DV period. Projected DVs were all well below the ozone NAAQS but only 0-0.4 ppb lower than the DV projections from the 2023 future base case. This is a relatively small decrease given 18% reductions in CCNAA VOC emissions relative to the 2023 future base case. The peak average projected DV was 68.8 ppb at Joe Neal.

Table 10-5. CAMx model configuration for the CCNAA 2023 15% VOC ROP scenario. Changes from the 2023 future base case are noted in red.

Model Component	CCNAA Application	Comment
Model Code	CAMx v7.20 - May 2022	
Modeling Period	May 1 – August 31, 2016	
Horizontal Grids		
Map Projection	Lambert Conic Conformal	EPA 2016 MP
36 km (36US3)	172 x 148 cells	Not run
12 km (12US2)	396 x 246 cells (no buffer cells)	EPA 2016 MP (2-way nesting)
4 km (CC4c2)	50 x 62 cells (with buffer cells)	CCNAA grid (2-way nesting)
Vertical Grid	35 layers	EPA 2016 MP, defined by WRF
Initial Conditions	12US2/CC4c2 IC May 1 from 36US3	2023 future year base case
Boundary Conditions	12US2 BC from 36US3	2023 future year base case
Time Zone	UTC	EPA 2016 MP
Emissions		
36/12 km Data Sources	EPA 2023fj from 2016v2 MP	
4 km Data Sources	EPA 2023fj from 2016v2 MP + 2023 Clark County Data, elevated Reid LTO emissions	15% VOC ROP reductions applied to solvent sector
Models/Processing Tools	SMOKE, MOVES3, SMOKE-MOVES, BEIS4/BELD6	CCNAA grid
Plume-in-Grid	Off	No large point sources in high-resolution CCNAA grid
In-line Ix emissions	On	Oceanic halogens
Chemistry		
Gas Phase Chemistry	CB6r5	Latest mechanism available
Aerosol Chemistry	Active	Gas phase only
Meteorological Interface	WRFCAMx v5.2	
Horizontal Diffusion	Smagorinsky	Spatially variant K-theory
Vertical Diffusion	YSU Kv formulation + KVPATCH	Minimum Kv 0.1 to 1.0 m^2/s
ACM2	Off	Non-local boundary layer convection
Sub-grid Cloud Convection	Off	
Deposition		
Dry Deposition	Zhang03	
Wet Deposition	On	rain/snow/graupel
Surface Chemistry Model	Off	
Bi-directional Ammonia	Off	For aerosol chemistry
Numeric Solvers		
Gas Phase Solver	Euler Backward Iterative (EBI)	Default fast and accurate solver
Vertical Advection	Piecewise Parabolic Method (PPM)	Default
Horizontal Advection	Piecewise Parabolic Method (PPM)	Default
Integration Time Step	Wind speed dependent	~0.5-1 min (4 km), 1-5 min (12 km), 5-15 min (36 km)
Super Stepping	On	Maximizes time step selection

Table 10-6. 2023 projected DVs at each monitoring site within the LVV according to SMAT-CE calculations using the 2016-2018 average base year DVs. Projected DVs are listed for the original 2023 future base case and for the 2023 15% VOC ROP scenario. Green indicates values below the NAAQS while sites noted with an asterisk continued to exceed the ozone NAAQS in 2020, leading to the bump up from Marginal to Moderate nonattainment status.

Site ID	Site Name	2023 Future Base DV	2023 15% VOC ROP	Differences
		Avg 3x3	Avg 3x3	Avg
320030022	Apex	65.2	65.2	0.0
320030023	Mesquite	57.2	57.2	0.0
320030043	Paul Meyer*	67.7	67.5	-0.2
320030071	Walter Johnson*	67.9	67.5	-0.4
320030073	Palo Verde	67.2	66.9	-0.3
320030075	Joe Neal*	69.0	68.8	-0.2
320030298	Green Valley*	67.3	67.1	-0.2
320030540	Jerome Mack	64.1	64.0	-0.1
320030601	Boulder City	61.5	61.5	0.0
320031019	Jean	63.9	63.9	0.0
320032002	J.D. Smith	67.3	67.1	-0.2
320037772	Indian Springs	62.3	62.2	-0.1

10.3 Conformity Budget

Working from the 2023 CCNAA base year emission inventory (Ramboll, 2023b), the DES/DAQ defined the 2023 CCNAA conformity budget to include: (1) a safety margin for the on-road mobile sector, and (2) all banked stationary source ERC. Modeling using the 2023 base year inventory demonstrated attainment of the ozone NAAQS (Section 9) without additional reductions associated with the 15% VOC Rate of Progress (ROP) Plan (Section 10.2). Therefore, the 2023 conformity budget builds from the 2023 base year inventory. Specifically, the 2023 conformity budget adds 2 TPD of both NOx and VOC to on-road mobile source emissions within the CCNAA, and adds current ERC NOx and VOC to point source emissions within the CCNAA. Tables 10-7 and 10-8 summarize the 2023 CCNAA VOC and NOx emission inventories, respectively, for the 2023 base and conformity scenarios.

Table 10-7. 2023 CCNAA base and conformity VOC emission inventories.

Source Category	2023 Base (TPD)	2023 Conformity (TPD)	Change (TPD)	Change (%)
Point source	1.32	**1.37**	0.05	3.8%
Nonpoint source	58.29	58.29		
On-road mobile	17.01	**19.01**	2.00	11.8%
Non-road mobile	24.17	24.17		
Airports (commercial & Federal)	2.62	2.62		
Locomotives	0.03	0.03		
ERC	0.05	**0.00**	-0.05	-100%
Total	**103.49**	**105.49**	2.00	1.9%

Table 10-8. 2023 CCNAA base and conformity NOx emission inventories.

Source Category	2023 Base (TPD)	2023 Conformity (TPD)	Change (TPD)	Change (%)
Point source	3.23	**4.15**	0.92	27.6%
Nonpoint source	4.01	4.01		
On-road mobile	19.15	**21.15**	2.00	10.4%
Non-road mobile	22.98	22.98		
Airports (commercial & Federal)	15.52	15.52		
Locomotives	0.66	0.66		
ERC	0.92	**0.00**	-0.92	-100%
Total	**66.47**	**68.47**	2.00	3.0%

The CCNAA emission inventories in Tables 10-7 and 10-8 reflect typical July weekday conditions consistent with the emissions budget reported in the SIP Inventory report (Ramboll, 2023b). To transfer this information to CAMx-ready hourly May-August emission inputs over the CC4c2 grid, it was necessary to adjust the 2023 base year model-ready on-road and point source emission files in a manner that faithfully replicates the incremental NOx and VOC changes noted in the tables above. This was done by developing and applying scaling factors to all NOx and VOC species for all point sources and all on-road sources within the grid cells covering only the CCNAA.

We developed a grid cell mask defining the CCNAA domain for emissions processing, which comprises a sub-set of 4 km grid cells covering the CCNAA with some overlap. We then summed emissions over that area and developed a single set of seasonal scaling factors for on-road and point sources. For on-road sources, the scaling factor was based on May-August average emissions to account for meteorological variations throughout the summer. For point sources, the scaling factor was based on July weekday average emissions to yield the respective NOx and VOC TPD increases defined in Tables 10-7 and 10-8. Note that this approach resulted in applying ERC increments to all point sources located within the CCNAA domain relative to their respective individual emission rates (i.e., sources with higher emission rates received a larger fraction of the ERC credit total). Scaling was applied to all point sources within two groups of model-ready files: electric generating units (EGU or IPM) and all others (non-IPM). As a quality assurance step, resulting on-road and point source emissions were

plotted to review the spatial differences between the 2023 base and conformity input files. We confirmed that NOx and VOC emissions were increased only within the CCNA portion of the CC4c2 modeling grid. Base and conformity model-ready emissions were then summed over the CCNAA and averaged over July weekdays to ensure absolute average increases in on-road and point source sectors were consistent with the CCNAA inventory increments (Tables 10-9 and 10-10).

Table 10-9. 2023 CCNAA model-ready July weekday average base and conformity VOC emissions (TPD).

Source Category	2023 Base	2023 Conformity	Change	Change (%)
Point source	0.58	**0.63**	0.05	8.7%
On-road mobile	16.21	**18.50**	2.29	14.1%

Table 10-10. 2023 CCNAA model-ready July weekday average base and conformity NOx emissions.

Source Category	2023 Base	2023 Conformity	Change	Change (%)
Point source	2.85	**3.77**	0.92	32.3%
On-road mobile	18.60	**20.87**	2.27	12.2%

Note that 2023 model-ready emissions in the SMOKE CCNAA domain differ slightly from the 2023 CCNAA emission inventory in Tables 10-7 and 10-8. We attribute on-road emission differences to the use of EPA's 2023fj MOVES3 emission factors and use of hourly- and day-specific meteorology to estimate gridded emission rates. The additional on-road emissions for conformity are slightly higher than 2 TPD due to the application of scaling factors based on May-August average emissions. Point source emission differences from Tables 10-7 and 10-8 result from the use of EPA's 2023fj Clark County point source emissions for modeling.

10.3.1 CAMx Modeling

The 2023 future year base case CAMx run (Section 9) was repeated but replacing emissions on the CC4c2 grid with the revised on-road and point emissions described above. All other inputs were not modified (Table 10-11), and only the 12US2/CC4c2 2-way nested grids were run using the 2023 12US2 future base case boundary conditions extracted from the 36US3 grid.

Table 10-11. CAMx model configuration for the CCNAA 2023 conformity emissions budget scenario. Changes from the 2023 future base case are noted in red.

Model Component	CCNAA Application	Comment
Model Code	CAMx v7.20 - May 2022	
Modeling Period	May 1 – August 31, 2016	
Horizontal Grids		
Map Projection	Lambert Conic Conformal	EPA 2016 MP
36 km (36US3)	172 x 148 cells	Not run
12 km (12US2)	396 x 246 cells (no buffer cells)	EPA 2016 MP (2-way nesting)
4 km (CC4c2)	50 x 62 cells (with buffer cells)	CCNAA grid (2-way nesting)
Vertical Grid	35 layers	EPA 2016 MP, defined by WRF
Initial Conditions	12US2/CC4c2 IC May 1 from 36US3	2023 future year base case
Boundary Conditions	12US2 BC from 36US3	2023 future year base case
Time Zone	UTC	EPA 2016 MP
Emissions		
36/12 km Data Sources	EPA 2023fj from 2016v2 MP	
4 km Data Sources	EPA 2023fj from 2016v2 MP + 2023 Clark County Data, elevated Reid LTO emissions	2 TPD NOx and VOC margins added to the on-road sector, ERC NOx and VOC added to point sources
Models/Processing Tools	SMOKE, MOVES3, SMOKE-MOVES, BEIS4/BELD6	CCNAA grid
Plume-in-Grid	Off	No large point sources in high-resolution CCNAA grid
In-line Ix emissions	On	Oceanic halogens
Chemistry		
Gas Phase Chemistry	CB6r5	Latest mechanism available
Aerosol Chemistry	Active	Gas phase only
Meteorological Interface	WRFCAMx v5.2	
Horizontal Diffusion	Smagorinsky	Spatially variant K-theory
Vertical Diffusion	YSU Kv formulation + KVPATCH	Minimum Kv 0.1 to 1.0 m^2/s
ACM2	Off	Non-local boundary layer convection
Sub-grid Cloud Convection	Off	
Deposition		
Dry Deposition	Zhang03	
Wet Deposition	On	rain/snow/graupel
Surface Chemistry Model	Off	
Bi-directional Ammonia	Off	For aerosol chemistry
Numeric Solvers		
Gas Phase Solver	Euler Backward Iterative (EBI)	Default fast and accurate solver
Vertical Advection	Piecewise Parabolic Method (PPM)	Default
Horizontal Advection	Piecewise Parabolic Method (PPM)	Default
Integration Time Step	Wind speed dependent	~0.5-1 min (4 km), 1-5 min (12 km), 5-15 min (36 km)
Super Stepping	On	Maximizes time step selection

10.3.1.1 SMAT-CE Configuration

We applied SMAT-CE identically to the original 2023 future base case scenario, specifying 2016-2018 3-year DV period for base monitored ozone (2014-2018 4th highs centered on 2016). All other configuration options remained the same as the original SMAT-CE run, which employed default or standard settings throughout the setup menu. We made no special modifications to monitored data or specific selection of modeled days for the RRF calculation.

10.3.1.2 Results at Monitoring Sites

Table 10-12 shows projected DV results at monitoring sites that reported sufficient data during the 2016-2018 base year DV period. Projected DVs were all well below the ozone NAAQS and 0-0.3 ppb higher than the DV projections from the 2023 future base case. The peak projected DV was 69.3 ppb at Joe Neal.

Table 10-12. 2023 projected DVs at each monitoring site within the LVV according to SMAT-CE calculations using the 2016-2018 average base year DVs. Projected DVs are listed for the original 2023 future base case and for the 2023 conformity budget scenario. Green indicates values below the NAAQS while sites noted with an asterisk continued to exceed the ozone NAAQS in 2020, leading to the bump up from Marginal to Moderate nonattainment status.

Site ID	Site Name	2023 Future Base DV Avg 3x3	2023 Conformity DV Avg 3x3	Differences Avg
320030022	Apex	65.2	65.3	0.1
320030023	Mesquite	57.2	57.2	0.0
320030043	Paul Meyer*	67.7	67.8	0.1
320030071	Walter Johnson*	67.9	68.0	0.1
320030073	Palo Verde	67.2	67.3	0.1
320030075	Joe Neal*	69.0	69.3	0.3
320030298	Green Valley*	67.3	67.3	0.0
320030540	Jerome Mack	64.1	64.2	0.1
320030601	Boulder City	61.5	61.5	0.0
320031019	Jean	63.9	63.9	0.0
320032002	J.D. Smith	67.3	67.5	0.2
320037772	Indian Springs	62.3	62.5	0.2

11.0 OZONE SOURCE APPORTIONMENT

CAMx Source Apportionment (SA) was run for the 2023 future year base scenario (Section 9) to quantify and rank ozone contributions from specific source sectors and regions that contribute to high ozone in the CCNAA. This included tagging contributions from other states, international anthropogenic emissions, and regional wildfires to assess culpability of upstream and international contributions to support toward the weight of evidence (Section 12). SA also provided insights into NOx and VOC sensitivity in space and time, which can be used to assess the direction of emission reduction strategies. An initial SA design document was developed and discussed with DES/DAQ (Ramboll, 2022e) and certain configuration changes were subsequently adopted in light of technical needs and schedule constraints.

The SA configuration strikes a balance among three technical needs: (1) quantifying local source contributions among source sectors within the CCNAA; (2) quantifying upwind state and international contributions to identify states subject to Clean Air Act §110 Good Neighbor provisions and to support a possible §179B demonstration on the impacts from international anthropogenic emissions (IAE); (3) characterizing local ozone chemical regimes to determine VOC-limited versus NOx-limited conditions.

11.1 Summary of Results

- Contributions to model-projected 2023 DV at Joe Neal are consistent with EPA's two interstate source apportionment analyses.
- Natural and non-US ozone concentrations comprise the majority of ozone at 49 ppb (71% of the 69 ppb DV), California anthropogenic emissions contribute an average of 7 ppb (11%), Clark County contributes 11 ppb (16%), fires within the North American modeling domain contribute 2.4 ppb (4%), and the rest of the US contributes 1.7 ppb (3%).
- The modeled contributions to the 2023 DV at Joe Neal from all global international anthropogenic emissions are 13 ppb at Joe Neal, a value that is consistent throughout the entire inter-mountain western US and consistent with many previous studies.
- Of the total 11 ppb contributed by Clark County anthropogenic sources to the 2023 DV, non-road and onroad emissions contribute most (45% and 28%, respectively), followed by non-point area sources (9%), solvent area sources (10%), and point sources (5%).
- Of the total 7 ppb contributed by California anthropogenic sources to the 2023 DV, non-road and onroad sectors also dominate (34% each), with smaller contributions from non-point, solvent, and point sources. However, natural and fire sources contribute substantial ozone, averaging 1.4 and 2.1 ppb, respectively.
- Clark County emissions result in a relatively balanced mix of NOx and VOC sensitive ozone production over the top 10 simulated days at Joe Neal, with some substantial variations day-to-day. This is typical of a locally "transitional" regime where ozone would respond to both NOx and VOC changes.
- Spatially, ozone formation in areas outside the CCNAA is dominantly NOx-limited at nearly 100%, while ozone in the LVV represents a more balanced mix within the urban area.

11.2 CAMx Ozone Source Apportionment Tools

There are two ozone source apportionment options in CAMx:

Ozone Source Apportionment Technology (OSAT): The original apportionment method uses 10 reactive tracers for each source sector/region (i), which include emitted VOC and NOx, several

intermediate NOz and odd-oxygen products that track NOx recycling, and ozone formed under VOC-limited (O3Vi) and NOx-limited (O3Ni) conditions. When an increment of ozone (ΔO3) is formed under VOC-limited conditions, the ΔO3 is allocated to the O3Vi tracers based on the relative contribution of VOC from sector/region i to total VOC. A similar approach is used to allocate ΔO3 to the O3Ni tracers under NOx-limited conditions. The ratio of the production rates of hydrogen peroxide (H_2O_2) and nitric acid (HNO_3) is the indicator used to classify ozone formation as being instantaneously limited by NOx or VOC at a particular grid cell and time. Ozone formation is classified as being NOx-limited when $P(H_2O_2)/P(HNO_3) > 0.35$ (Sillman, 1995). Thus, ΣO3Vi and ΣO3Ni over all i indicate how much ozone was formed under VOC-limited versus NOx-limited conditions, respectively, during transport to a particular grid cell.

Anthropogenic Precursor Culpability Assessment (APCA): The only difference between APCA and OSAT is the algorithm used to allocate ozone production under VOC-limited or NOx-limited conditions. APCA recognizes that certain emission sectors are not controllable (e.g., biogenic) and that apportioning ozone production to these categories does not provide information relevant to control strategies. In certain situations where OSAT would attribute ozone production to non-controllable emissions, APCA instead allocates that ozone production to the controllable precursors that participated. For example, when biogenic VOC and anthropogenic NOx form ozone under VOC-limited conditions (a situation where OSAT would attribute ozone production to biogenic VOC), APCA attributes ozone production to the anthropogenic NOx. Thus, APCA results in more ozone formation attributed to anthropogenic NOx and less ozone formation attributed to biogenic VOC. As a result, the O3Vi and O3Ni tracers may not provide reliable information on how much ozone is actually formed under VOC-limited versus NOx-limited conditions. APCA approaches the OSAT method when biogenic VOC are low (as in the CCNAA) and/or as ozone formation becomes more NOx-limited, either because of direct NOx reductions, downstream dilution of the urban plume, or in NOx-lean conditions (e.g., rural areas).

Note that neither of the options above are able to determine whether NOx disbenefits occur (i.e., when NOx emission reductions result in ozone increases). However, a large amount of VOC-limited ozone could suggest that NOx disbenefits might occur. The proper approach to analyze the possibility and magnitude of NOx disbenefits requires a sensitivity method, either by modeling a so-called "brute force" emission reduction or by employing the Decoupled Direct Method (DDM) sensitivity tool.

11.3 Identifying Key Source Regions

The selection of source regions to track in SA was guided by EPA's interstate ozone transport analyses for the 2015 ozone NAAQS (EPA, 2022d; 2023a). EPA estimated 2023 DV contributions from individual states, biogenic emissions, fires, foreign/offshore sources, and boundary conditions (BC). We analyzed EPA's results to determine which upwind sources have the most potential to contribute to ozone DVs in the CCNAA. As is typical for ozone, EPA found that BCs representing global background contributions from natural and IAE sources comprise the vast majority (~70%) of ozone in Clark County. California anthropogenic emissions contribute roughly the same amount of ozone as Nevada's own contribution when averaged over CCNAA sites. Contributions from Canada and Mexico, wildfires, and biogenic emissions comprise the majority of the balance, with other States contributing fractions of one ppb (much less than 1%).

11.4 CAMx Source Apportionment Configuration

The SA application was designed to address both regional/international transport and local contributions within Clark County. The APCA method was invoked to chemically attribute NOx and VOC precursors to ozone formation. Analysis of results focused on contributions to ozone within the CCNAA. The source region and sector splits are defined below.

The 2023 SA simulation divided the 36US3/12US2/CC4c2 modeling domains into 6 source regions (Figure 11-1):

1) All of Clark County including the CCNAA
2) Remaining areas of Nevada
3) California
4) Remaining areas of the US, including the 200 mile US coastal zone
5) Mexico
6) Other international, including Canada and outside the 200 nautical mile US coastal zone

The 2023 SA simulation tracked ozone contributions from the following 7 source sectors within the 12US2/CC4c2 2-way modeling grids:

1) Natural (biogenic, lightning NOx, oceanic)
2) Open Land Fires (all wildfires, prescribed and agricultural fires)
3) On road sources
4) Non-road sources (including airports, rail, commercial marine vessels)
5) Point sources
6) Non-point solvent sector
7) Remaining non-point sectors

In the 36US3 grid, 3 source sectors were tracked along with global BCs:

1) Natural (biogenic, lightning NOx, oceanic)
2) Open Land Fires (all wildfires, prescribed and agricultural fires)
3) All anthropogenic sources

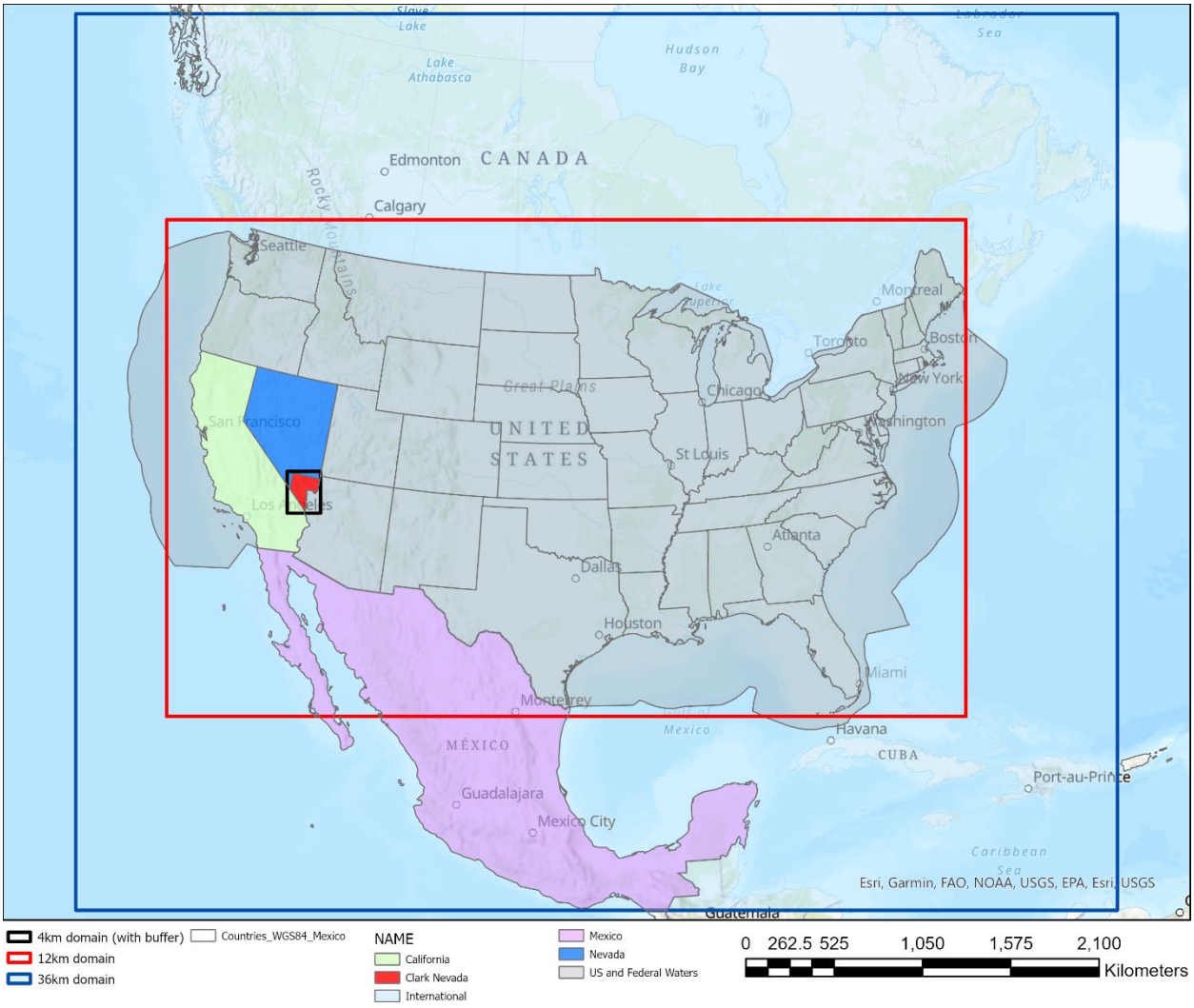

Figure 11-1. Source apportionment regions for the 2023 SA run.

Tracer concentrations for these 3 categories by 6 regions, along with a set of 2 global BCs (IAE and natural) and one set of ICs were transferred to the 12US2/CC4c2 grids via SA tracer BCs. Details are described below.

11.5 Preparing Boundary Conditions Representing International Emissions

On the 36US3 grid, SA tracked initial conditions (IC) and BC tracers. Two separate sets of BC tracers tracked global IAE and remaining natural emissions as defined by two sets of global model output. It is important that the sum of BC tracers for a given chemical species (e.g., ozone) add to the total BC concentration used for the core model at each hour and boundary grid cell to maintain consistency. The final CAMx configuration for the Clark County ozone SIP employed BCs developed from the publicly available CAM-Chem global model output datasets provided by (NCAR). CAM-Chem includes all global anthropogenic and natural precursor emissions and stratospheric ozone. Therefore, another source of global model output was needed to define the IAE contribution, which is normally determined from a "zero out rest of world" (ZROW) or natural-only scenario from the same global model. No such data were available from CAM-Chem. However, both total and ZROW scenarios were available from EPA's 2016 H-CMAQ applications, which were developed specifically for the 2016v2

modeling platform and have pedigree of prior use for similar purposes. Specifically, H-CMAQ BCs have been used by EPA (2022d) for their preliminary interstate transport modeling, and by the State of Utah to support their §179B demonstration (UDAQ, 2021).

Under normal situations, where both total and ZROW cases are generated by a single model, we use a pre-processor that differences output concentrations from the two runs and maps those differences to two sets of BC tracers:

BC1: Total global model output

BC2: ZROW (natural-only) global model output

Tracer Group 1: BC1-BC2 = IAE (all precursors and ozone)

Tracer Group 2: BC2 = ZROW (all precursors and ozone)

In the current situation, where the total was from CAM-Chem and ZROW was from H-CMAQ, it was imperative to account for the vastly different ozone patterns generated by the two models, which we previously found to be especially apparent in the low to mid-troposphere over the eastern Pacific and western US (Section 8.4.11). Approaches to derive the IAE portion could involve either relative scaling of the CAM-Chem output or calculating absolute differences between the two models. Relative scaling was not preferred because conceptually the IAE simulated by H-CMAQ would be scaled significantly higher or lower by the vastly different ozone concentrations generated by CAM-Chem.

We considered two approaches using absolute differences. We preferred subtracting a small portion (IAE) from the total to yield ZROW, as opposed to subtracting a large portion (ZROW) from the total to yield IAE. The second approach would likely result in negative IAE values (trapped at zero) as well as frequent unrealistically large IAE values that conceivably could reach 30-40 ppb based on the differences seen between CAM-Chem and H-CMAQ ozone patterns. The first approach better constrained the IAE contribution because it was determined from the self-consistent H-CMAQ results, but it required additional pre-processing steps:

First step:

BC1: Total global model output from H-CMAQ

BC2: ZROW (natural-only) global model output from H-CMAQ

BC3: BC1-BC2 = IAE

Second step:

BC4: Total global model output from CAM-Chem

BC3: IAE (from Step 1)

Tracer Group 1: BC4-BC3 = ZROW (natural-only) CAM-Chem surrogate

Tracer Group 2: BC3 = IAE

11.6 CAMx Source Apportionment Size and Runtime

The 36US3 grid tracked 21 sets of SA tracers (3 categories x 6 regions + natural BC + IAE BC + total IC). This resulted in 210 total chemical tracers (21 x 10 ozone, precursor and intermediate species classes). Like the standard CAMx run for the 2023 future year base case, the 36US3 grid was run

alone from April 1 (ICs) through August 31. SA tracer concentrations were output as 3-D arrays so that each of the 210 tracers could be passed to the 12US2/CC4c2 grid system as BCs for the separate 2-way nested SA run. This SA configuration resulted in a run time of 6 days (4% real time) and produced 3.0 TB of output. The 36US3 SA was run on 24 cores using 8 MPI nodes by 3 OMP threads on a x86_64 Intel® Xeon® ES-2690 chipset at 2.60 GHz.

The 12US2/CC4c2 grids tracked 65 sets of SA tracers (7 categories x 6 regions + 21 BC from 36US3 + top BC + IC for 12US2/CC4c2). This resulted in 650 total chemical tracers for ozone, precursor and intermediate species classes. The SA simulation for these 2-way nested grids was also run from April 1 (ICs) through August 31 in order for IC tracers among the 3 grids to be self-consistent. SA tracer concentrations were output as 2-D surface arrays. This large SA configuration resulted in a run time of 45 days (30% real time) and produced 3.3 TB of output. The 12US2/CC4c2 SA was run on 48 cores using 16 MPI nodes by 3 OMP threads on a x86_64 Intel® Xeon® ES-2690 chipset at 2.60 GHz.

11.7 2023 Ozone Source Apportionment Results

Raw hourly ozone SA tracer data were post-processed to represent contributions to total MDA8 ozone each day; i.e., the unique 8-hour period defining total MDA8 ozone at each grid cell on each day was used to time-average all ozone tracers. Results were then compiled into an Excel "dashboard" to facilitate interactive analyses in a way that maximizes choices by monitoring site, combinations of sectors, and combinations of regions. However, this dashboard combined ozone tracers generated from NOx- and VOC-sensitive chemistry to reduce the dimensionality of the dataset. A separate Excel dashboard was created to support assessment of sector-specific NOx- and VOC-sensitive chemistry. Examples of each type of plot generated by these dashboards are presented below.

Figure 11-2 presents a "landscape" time series (as a stacked area plot) of regional contributions to 2023 MDA8 ozone at the Joe Neal monitoring site over the May-August modeling period. Our analyses focus on Joe Neal as that is the controlling ozone DV monitor in the CCNAA. The contributions in Figure 11-2 start at the bottom with all global and in-domain natural sources combined, then add fires, IAE, and Mexico to yield the total uncontrollable non-US ozone concentrations. Then contributions from US, California, and Nevada anthropogenic emissions are added. Finally, Clark County anthropogenic contributions are added at the very top to yield the total MDA8 ozone at Joe Neal.

Figure 11-3 shows the global/regional contributions to the model-projected 2023 DV at Joe Neal. This is accomplished by averaging MDA8 ozone contributions at Joe Neal over the top 10 simulated days in the 2023 future base case, determining the "Relative Contribution Factors" (i.e., 10-day average percent contributions), and applying those percentages to the 2023 DV. Natural and non-US ozone concentrations comprise the majority of ozone at Joe Neal at 49 ppb (71% of the 69 ppb DV). California anthropogenic emissions contribute an average of 7 ppb (11%), while Clark County contributes 11 ppb (16%). Fires within the North American modeling domain contribute 2.4 ppb (4%), the rest of the US contributes 1.7 ppb (3%), while the rest of Nevada contributes negligibly (0.1 ppb). These results are consistent with EPA's two interstate source apportionment analyses (EPA, 2022a,b; 2023).

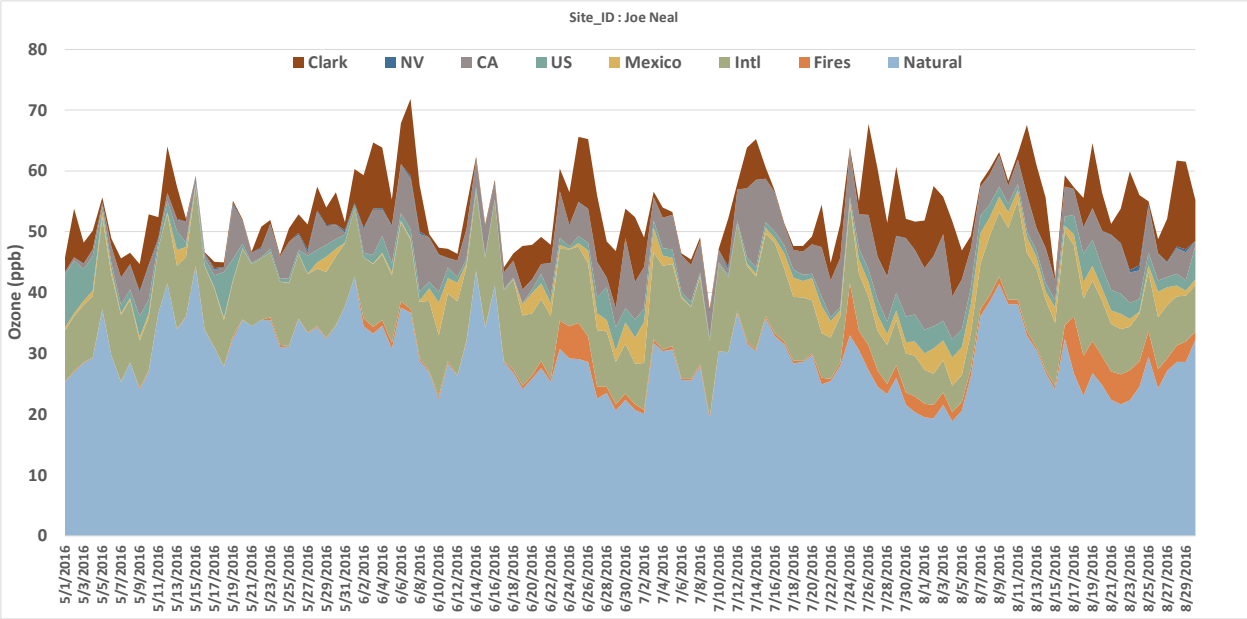

Figure 11-2. Time series of regional contributions to 2023 MDA8 ozone at Joe Neal over the May-August modeling period.

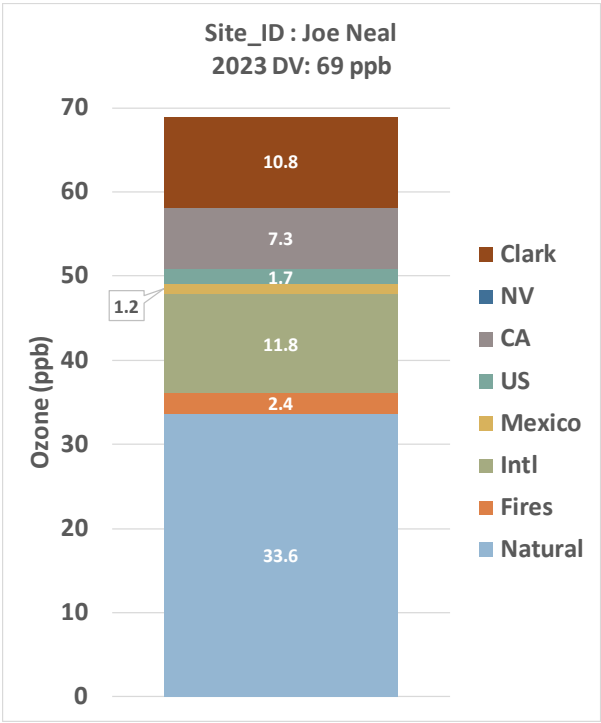

Figure 11-3. Regional contributions to the projected 2023 DV at Joe Neal.

The modeled MDA8 ozone contributions from Mexico and other IAE total 12.5 ppb at Joe Neal over the 10-day averaging period (which is scaled to 13 ppb for the 2023 DV shown in Figure 11-3). Figure 11-4 presents the spatial distribution of 10-day average modeled MDA8 ozone contributions from all IAE (including Mexico) over the entire 12US2 modeling domain. IAE contributions range 10-14 ppb

throughout the entire inter-mountain western US over the averaging period, including southern Nevada. Large ozone plumes from northern Baja California and Imperial County are evident, yet the average Mexico contribution at Joe Neal over the 10 days is 1.2 ppb. Clearly, the IAE pattern over the western US is instead more consistently dominated by global anthropogenic contributions. Further, the IAE pattern in Figure 11-4 is consistent with many previous studies (e.g., EPA, 2015, 2019d; Jaffe et al., 2018; Ramboll, 2021b; Lanford et al., 2015, 2022; Zheng et al., 2020; and numerous references therein) that have shown how mountainous terrain and deep circulation patterns enhance downward mixing of mid- and upper-level tropospheric global ozone to the surface.

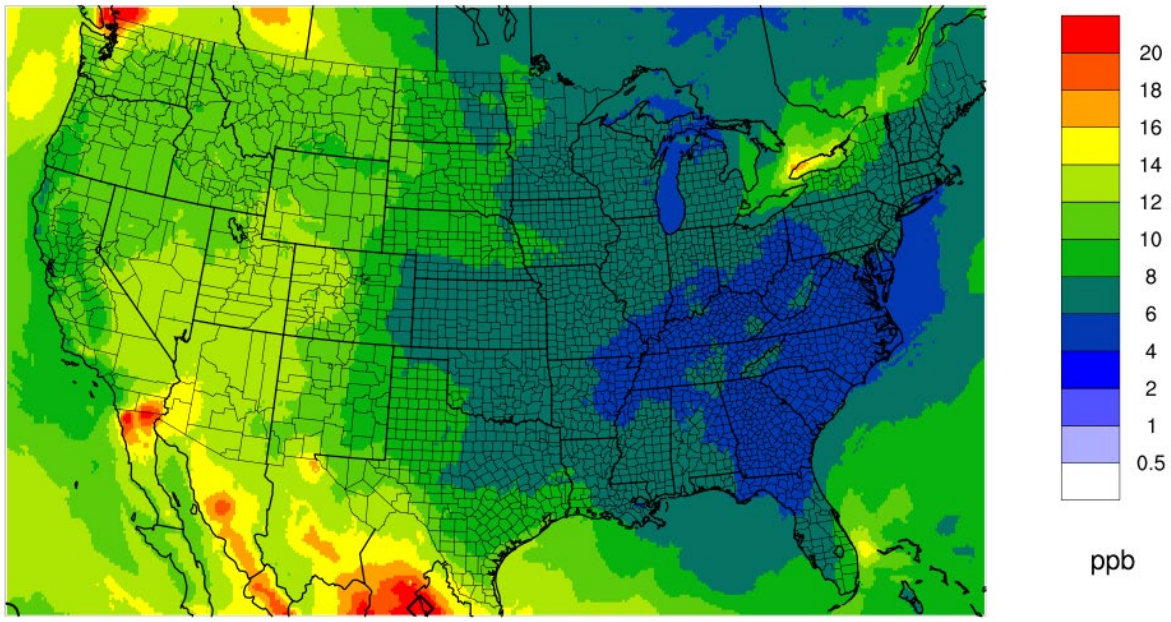

Figure 11-4. Spatial distribution of modeled MDA8 ozone contributions from all IAE (including Mexico) over the entire 12US2 modeling domain, averaged over the top 10 high ozone days at the Joe Neal monitoring site.

Figure 11-5 shows a stacked bar chart of anthropogenic source category contributions from Clark County to the 2023 DV at Joe Neal. Figure 11-6 presents similar information but for all Clark County sectors on each of the top 10 simulated days. Of the total 10.8 ppb contributed by Clark County anthropogenic sources to the 2023 DV, non-road and onroad emissions contribute most (46% and 29%, respectively), followed by non-point area sources (10%), solvent area sources (10%), and point sources (5%). Local natural sources and fires are rather minor contributors. Note that the smallest and most negligible contributor, "Anthro", represents ozone from Clark County that exited the 12US2 domain and recirculated back into Clark County (via 12US2 BCs). This tracer is necessary to account for the full apportioned mass budget across the entire 36US3 and 12US2/CC4c2 modeling domains.

Figures 11-7 and 11-8 show the same information, but for source category contributions from California. In this case, a larger mix of source sectors affects ozone in Clark County. Of the total 7.3 ppb contributed by California anthropogenic sources to the 2023 DV, non-road and onroad sectors also dominate (34% each), with smaller contributions from non-point, solvent, and point sources. However, natural and fire sources contribute substantial ozone over the top 10 simulated days, averaging 1.4 and 2.1 ppb, respectively. Note that recirculated "Anthro" from California is higher than Clark County's, but still negligible.

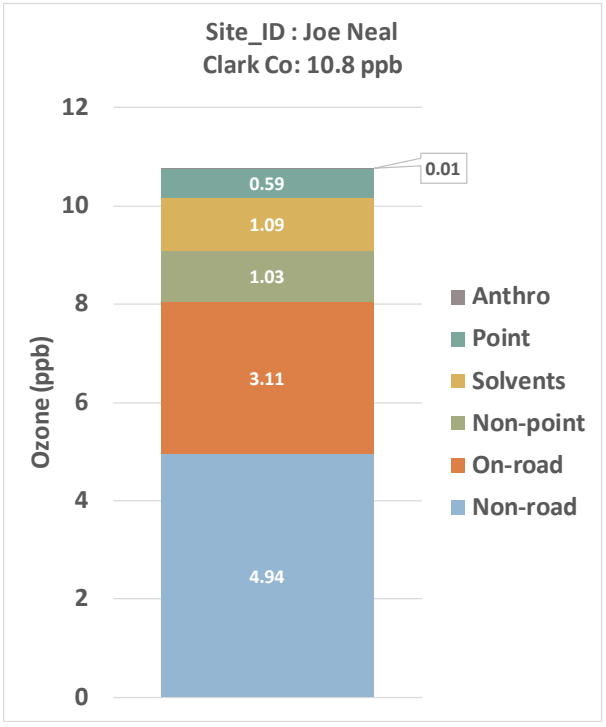

Figure 11-5. Anthropogenic source category contributions from Clark County to the 2023 DV at Joe Neal.

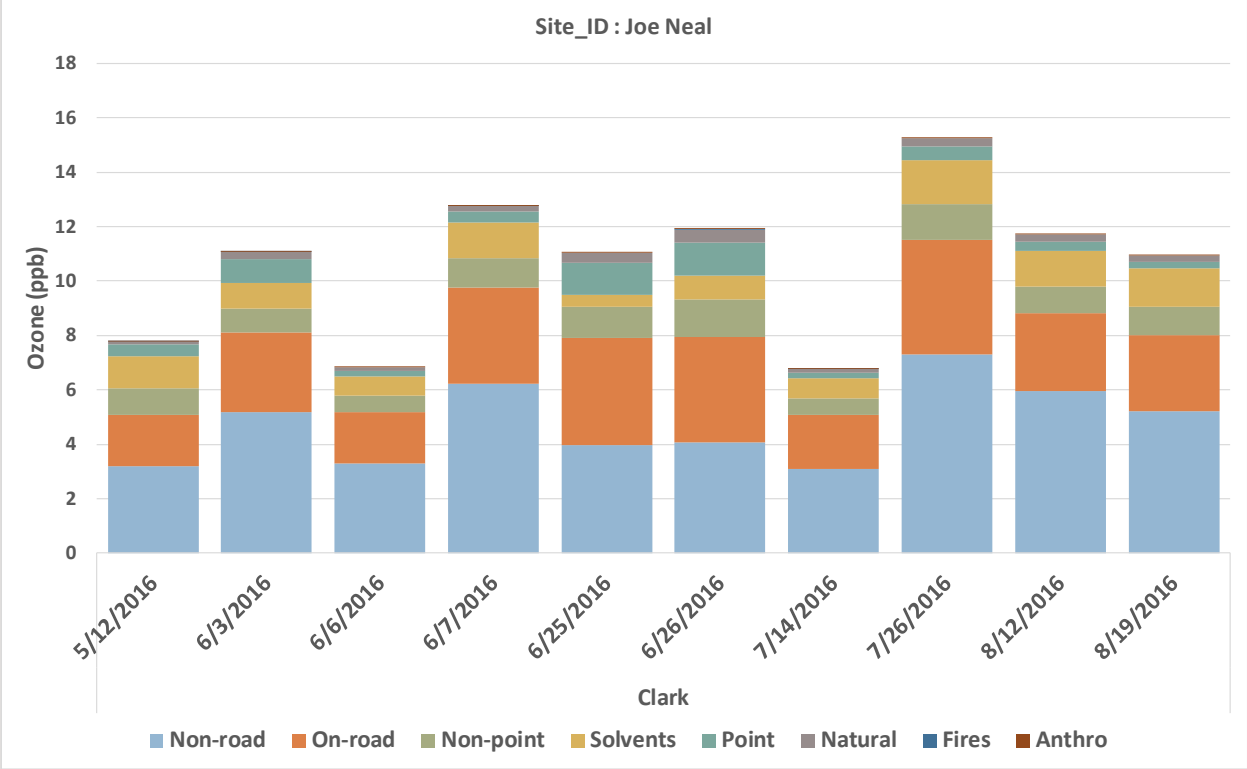

Figure 11-6. Source category contributions from Clark County to simulated MDA8 ozone at Joe Neal on each of the top 10 simulated days.

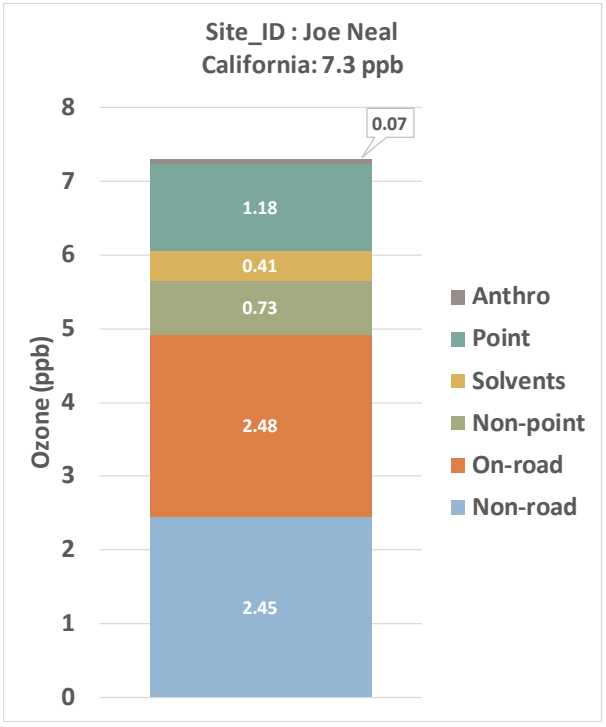

Figure 11-7. Anthropogenic source category contributions from California to the 2023 DV at Joe Neal.

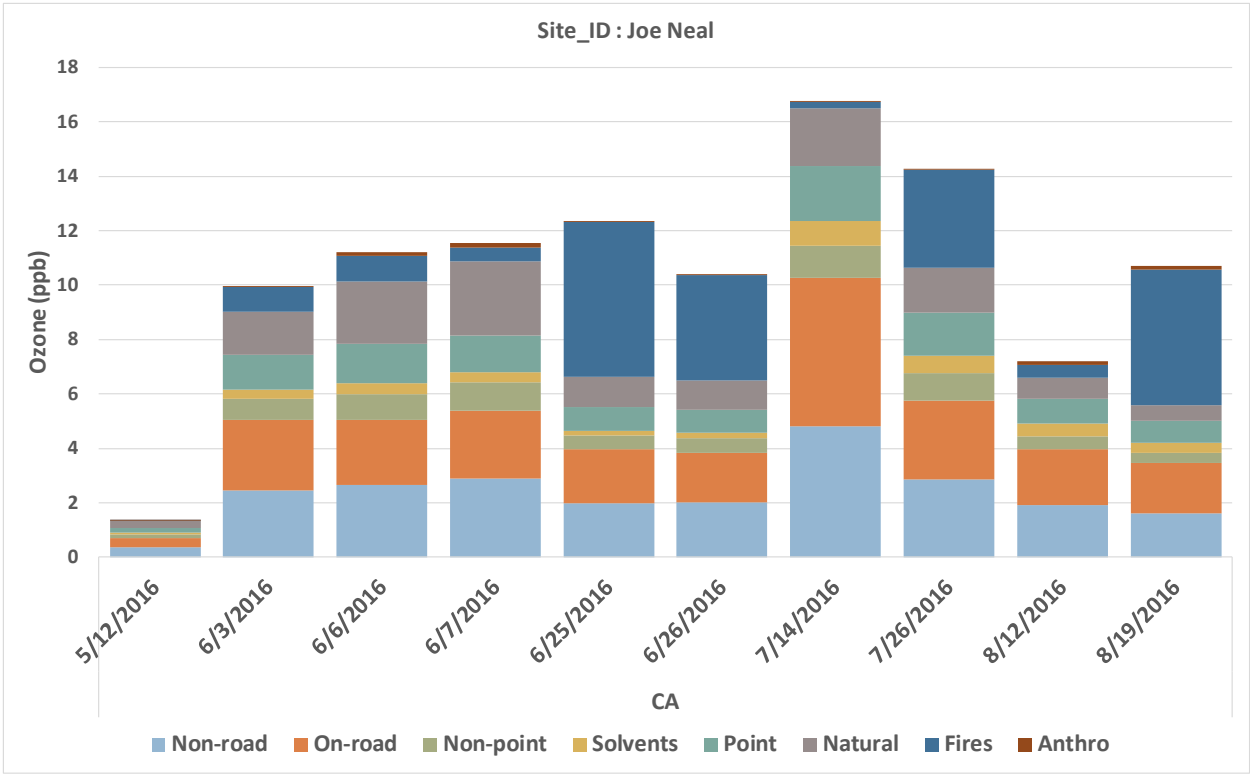

Figure 11-8. Source category contributions from California to MDA8 ozone at Joe Neal on each of the top 10 simulated days.

It is important to understand whether ozone attributed to specific sources forms via NOx-limited or VOC-limited chemistry, as that can help determine directions for control strategies. SA results can provide insights as we show below. Strictly speaking, SA is not equivalent to a "sensitivity analysis" with which to estimate effects of emission reductions on ozone concentrations. This is because ozone chemistry responds non-linearly to emission changes. Rather, SA reports an estimate of attribution under the specific environmental and emission conditions that are given to the model. When those conditions change (e.g., to simulate impacts from a control measure), attribution can change non-linearly, either positively or negatively. However, the ozone response approaches linearity with decreases in emission changes or ozone attribution.

Figures 11-9 and 11-10 present similar stacked bar plots as Figure 11-6 (Clark County contributions) and Figure 11-8 (California contributions) at Joe Neal, but for total anthropogenic emission contributions to NOx and VOC sensitive MDA8 ozone chemistry. Clark County emissions result in a relatively balanced mix of NOx and VOC sensitive ozone production over the top 10 simulated days, with some substantial variations day-to-day. This is typical of a locally "transitional" regime where ozone would respond to both NOx and VOC changes. With a dearth of biogenic VOC emissions within Clark County, the region perhaps exhibits a stronger tendency toward VOC-limited ozone production than other nonattainment areas in the western US. Conversely, ozone contributions from California are dominantly NOx-sensitive. This is likely a result of applying APCA, but is also consistent with conceptual models of ozone production from urban areas in Southern California, in which ozone production transitions from VOC-limited within the South Coast basin to NOx-limited conditions as the air mass exits the basin and crosses the Mojave Desert. Additionally, ozone from biogenic-rich rural areas in California forms in NOx-limited conditions.

Figure 11-11 shows spatial plots of NOx- and VOC-limited MDA8 ozone contributions from Clark County anthropogenic emission sectors within the CC4C2 domain. These results have been averaged over the top 10 simulated ozone days. Figure 11-11(a) includes the average total MDA8 ozone pattern for reference and shows a local ozone plume with maximum concentrations in the northwestern LVV. The other panels in Figure 11-11(a) show the 10-day average fraction of NOx- and VOC-limited ozone from Clark County anthropogenic emissions. In agreement with our conceptual model, ozone in areas outside the CCNAA is dominantly NOx-limited at nearly 100%, while ozone in the LVV represents a more balanced mix within the urban area. Average contributions from Clark County emission sectors are shown in descending order in Figure 11-11(b) through 11-11(f). The largest contribution from non-road emissions (Figure 11-11[b]) produces an ozone plume from NOx-limited chemistry in the northwest LVV, while smaller contributions from VOC-limited chemistry occur toward central Las Vegas. A similar but slightly lower contribution pattern is seen for onroad sources. Ozone generated by point sources is nearly all NOx-limited in a plume extending northeast of the LVV, which is most likely related to their emissions mix and locations relative to the urbanized area of the LVV. As expected, ozone from solvent emissions is entirely from VOC-limited chemistry in the NOx-rich central LVV. Non-point (area) sector contributions are smallest yet fairly balanced among NOx and VOC limited chemistry.

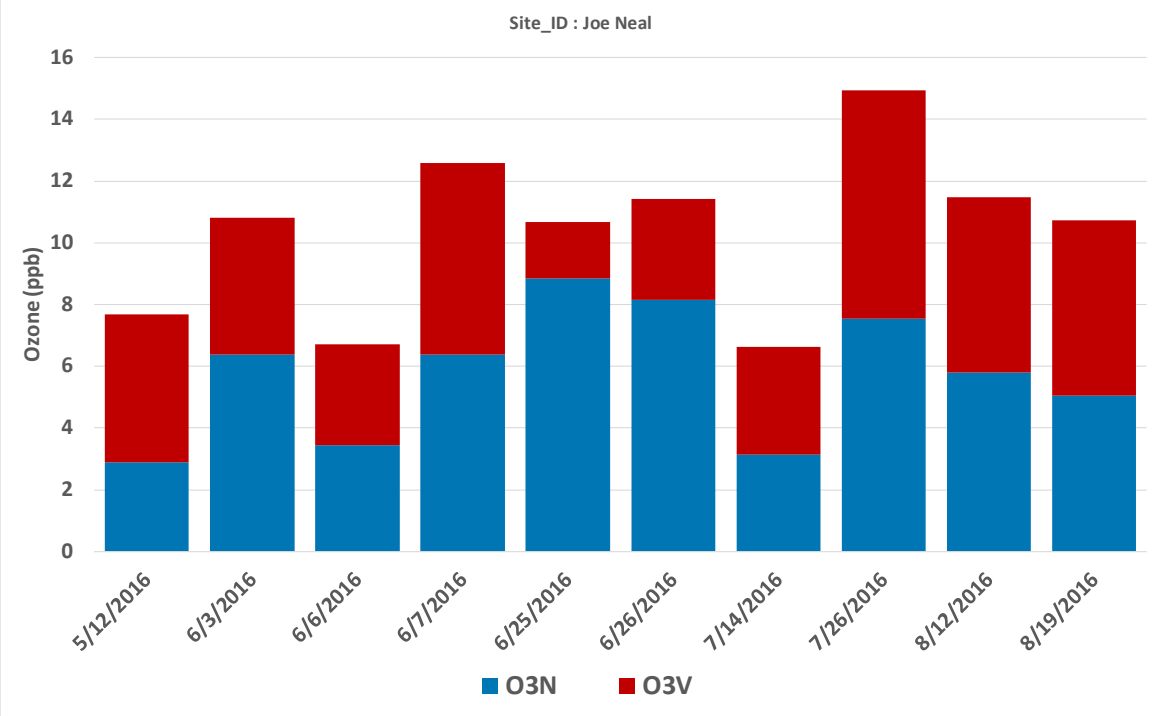

Figure 11-9. Total anthropogenic emission contributions from Clark County to NOx and VOC sensitive MDA8 ozone chemistry at Joe Neal on each of the top 10 simulated days.

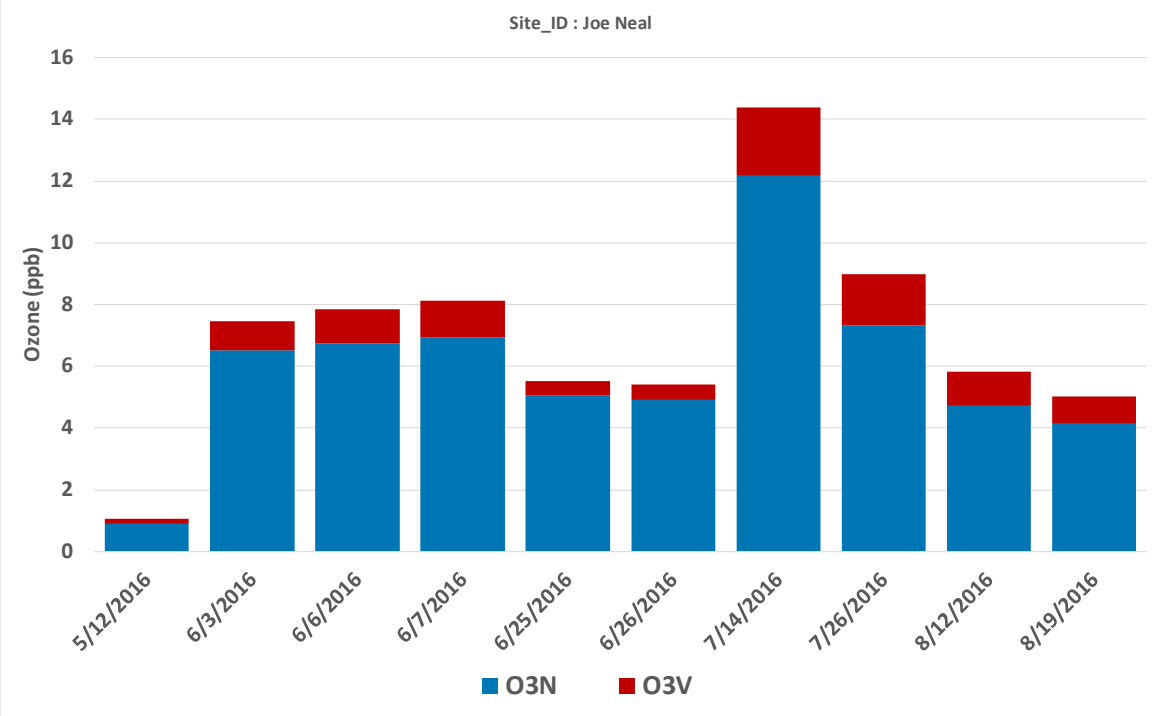

Figure 11-10. Total anthropogenic emission contributions from California to NOx and VOC sensitive MDA8 ozone chemistry at Joe Neal on each of the top 10 simulated days.

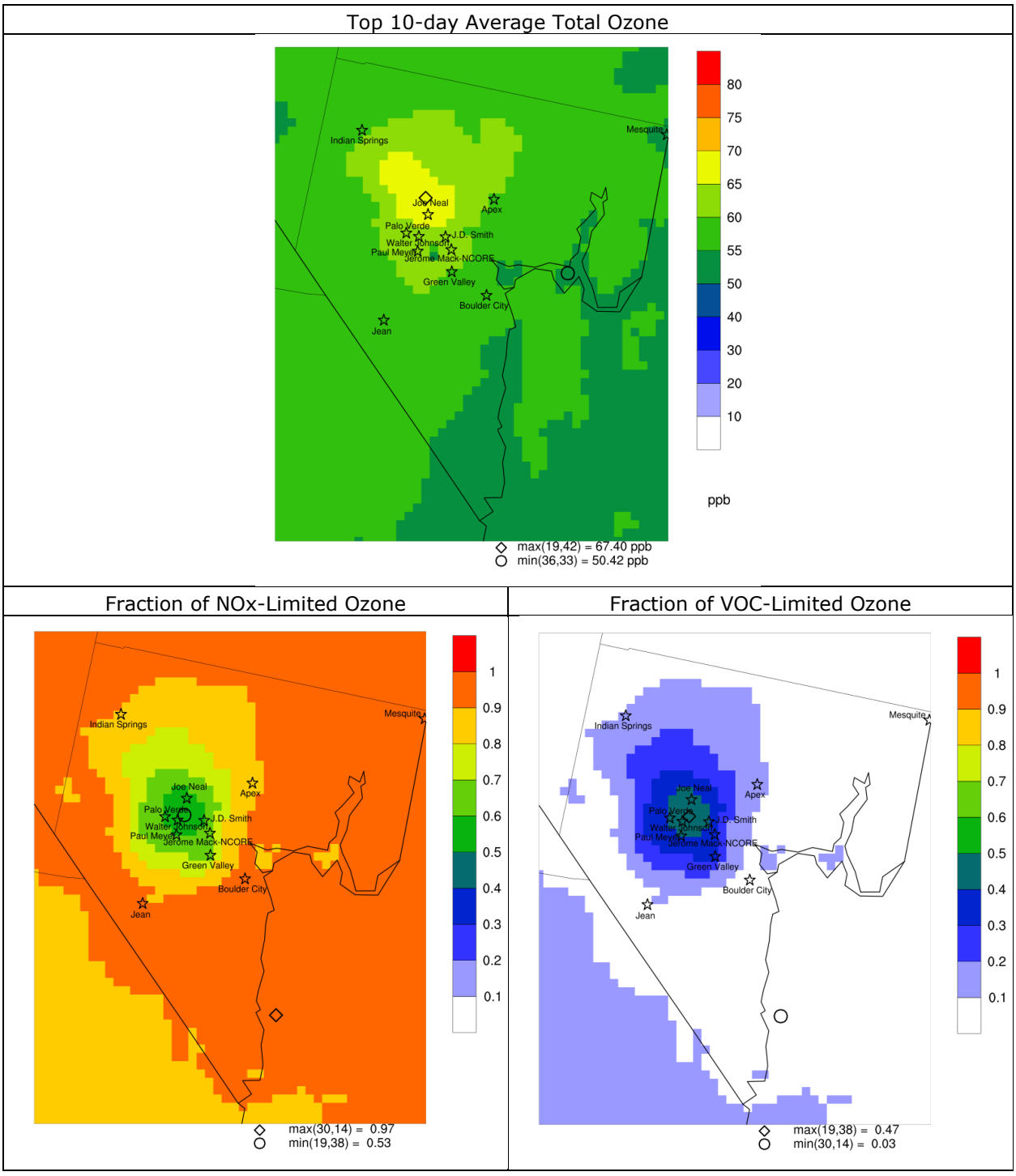

Figure 11-11(a). Top panel: total MDA8 ozone pattern within the CC4C2 domain averaged over the top 10 simulated ozone days. Bottom panels: 10-day average fraction of NOx-limited (left) and VOC-limited (right) MDA8 ozone from Clark County anthropogenic emissions.

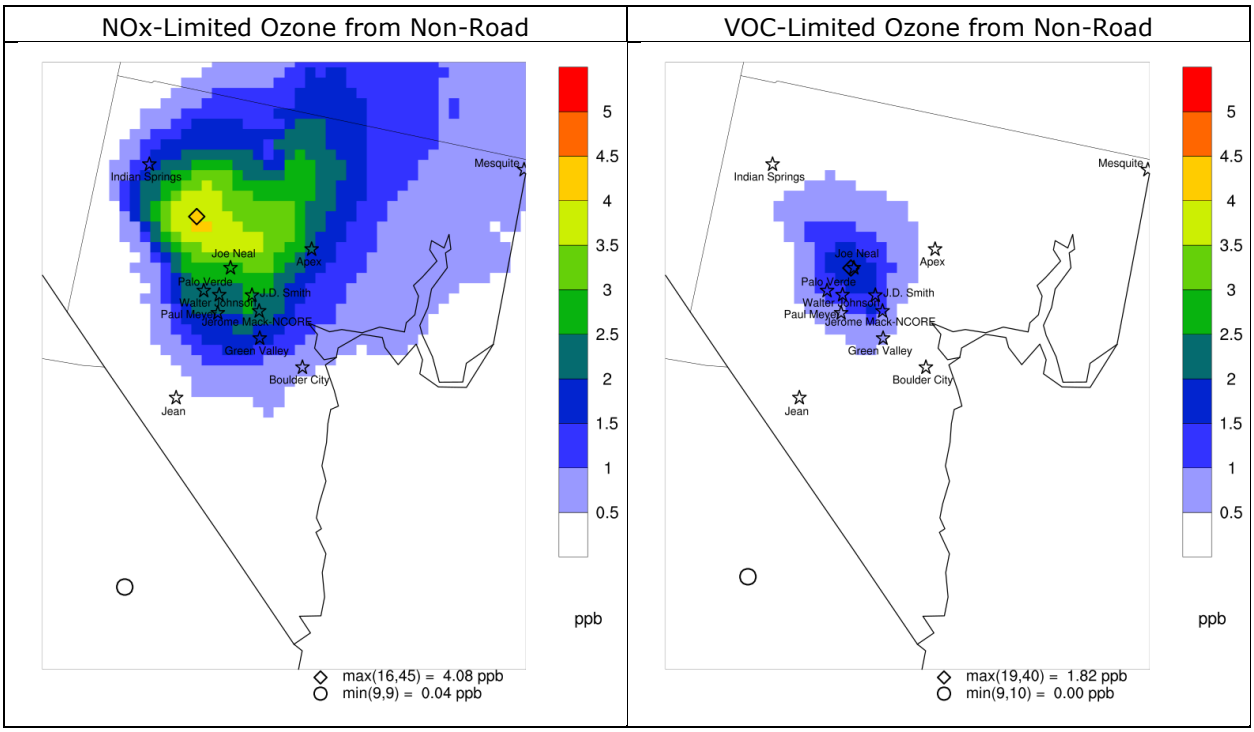

Figure 11-11(b). NOx- and VOC-limited MDA8 ozone contributions from Clark County non-road emissions averaged over the top 10 simulated ozone days.

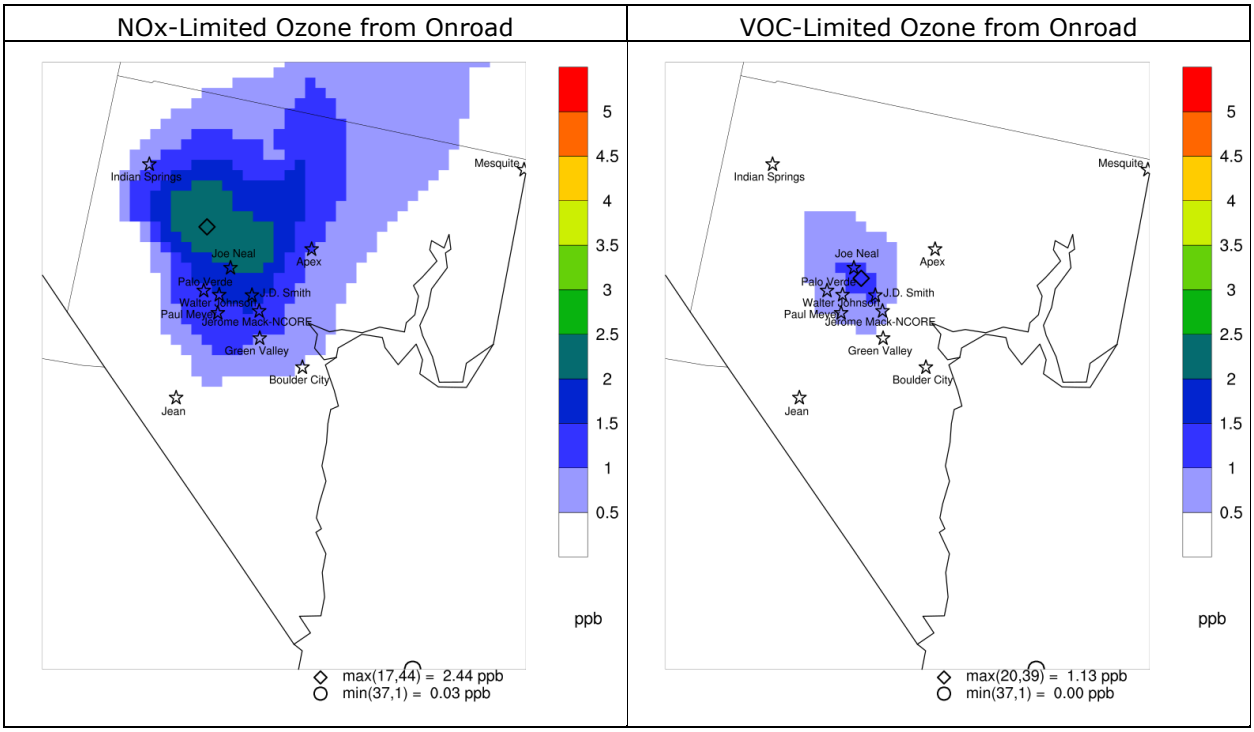

Figure 11-11(c). NOx- and VOC-limited MDA8 ozone contributions from Clark County onroad emissions averaged over the top 10 simulated ozone days.

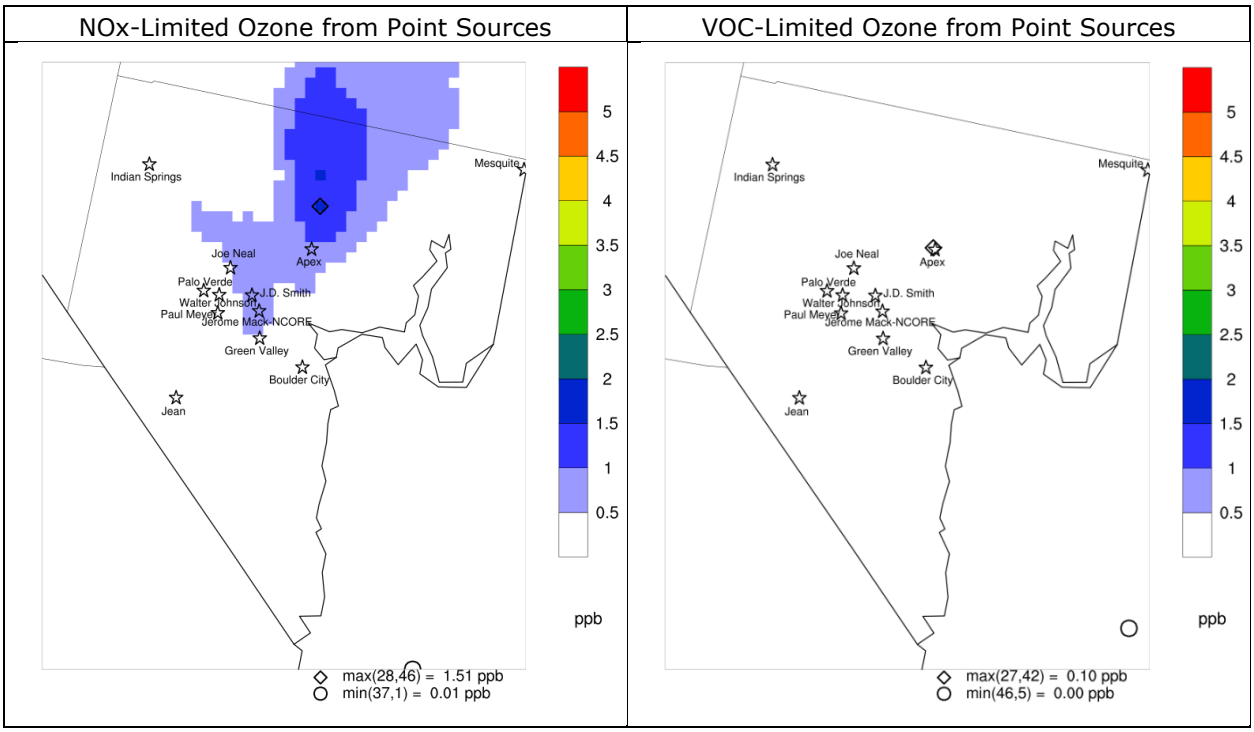

Figure 11-11(d). NOx- and VOC-limited MDA8 ozone contributions from Clark County point source emissions averaged over the top 10 simulated ozone days.

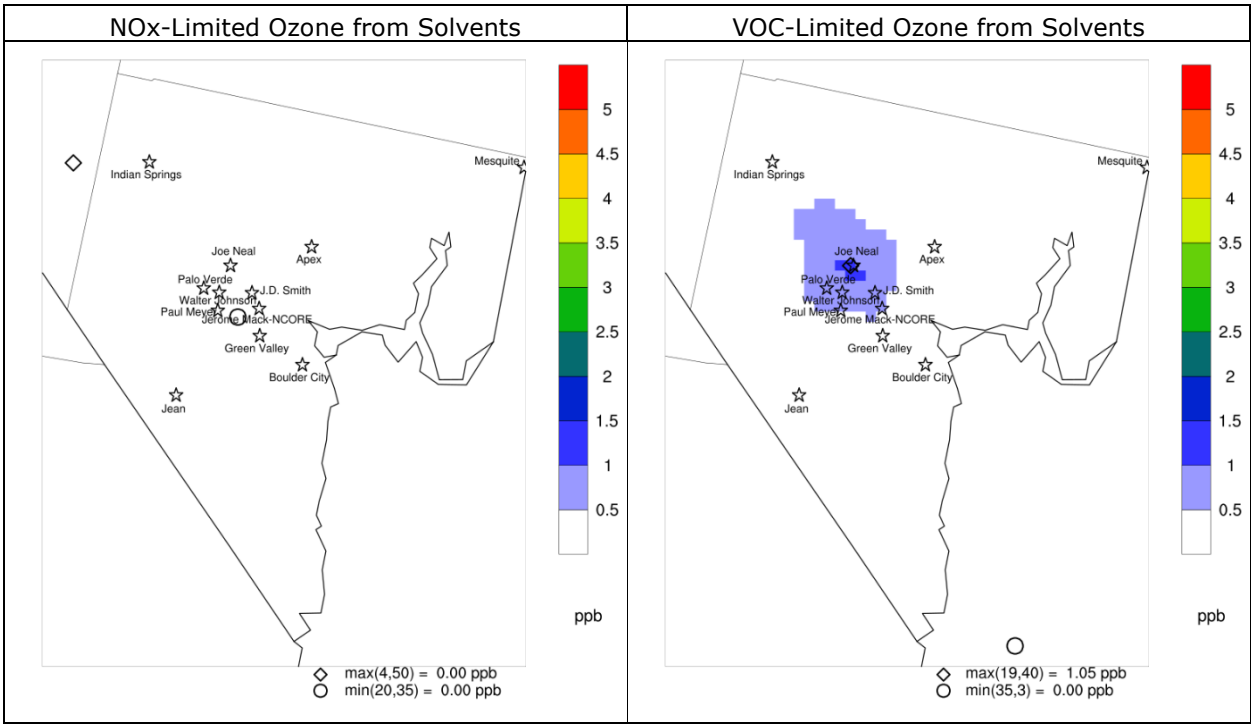

Figure 11-11(e). NOx- and VOC-limited MDA8 ozone contributions from Clark County solvent emissions averaged over the top 10 simulated ozone days.

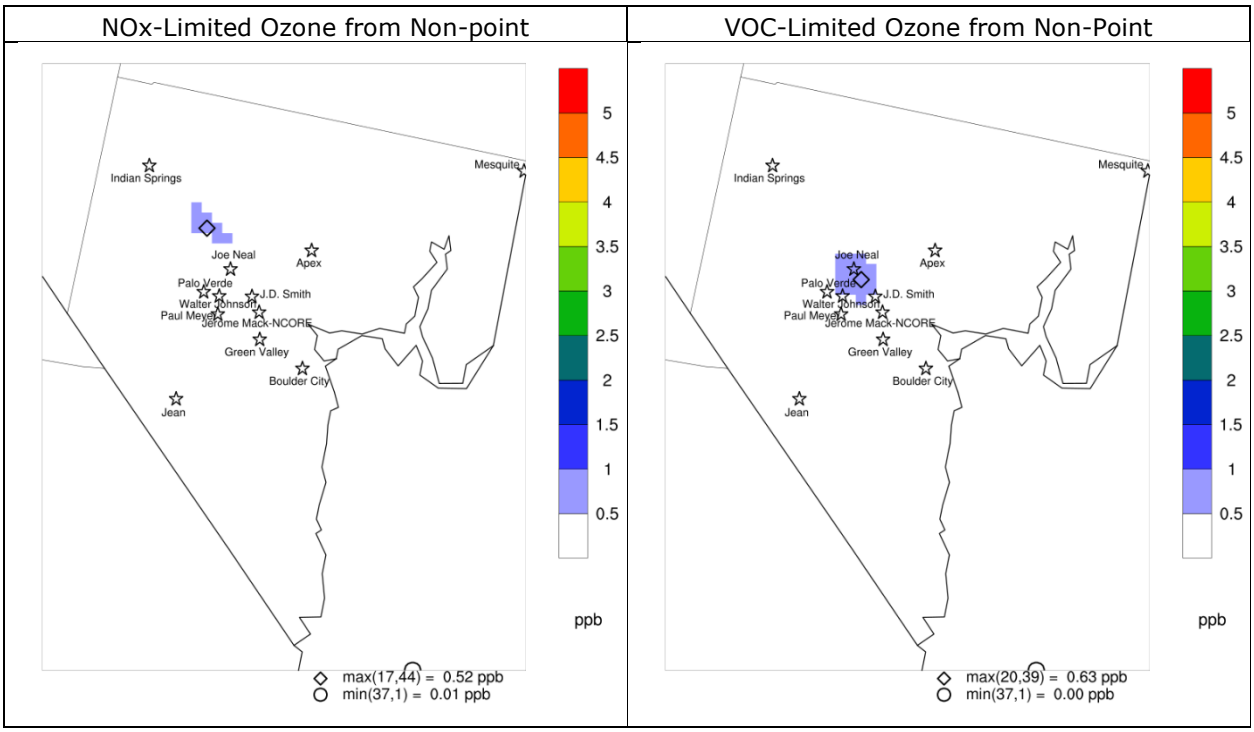

Figure 11-11(f). NOx- and VOC-limited MDA8 ozone contributions from Clark County non-point (area) emissions averaged over the top 10 simulated ozone days.

12.0 WEIGHT OF EVIDENCE ANALYSES

This Section describes the weight of evidence (WOE) component of the project. The purpose of the WOE is to present additional data analyses and modeling results, beyond the standard modeled attainment test, that add additional support to the overall attainment demonstration. The specific types of selected analyses follow from EPA modeling guidance (EPA, 2018a) and the Modeling Protocol developed during the early phases of this project (Ramboll, 2022a).

12.1 Approach

Ramboll performed 7 individual WOE analyses, grouped under the three general areas recommended by EPA (2018):

1) Additional modeling analyses (independent regional/national modeling, other local modeling/research, modeled source apportionment and sensitivity analysis, alternative SMAT configurations and approaches)

   - We summarized EPA's initial and final interstate transport modeling using their 2016v2 and 2016v3 Modeling Platforms (EPA, 2022d; 2023a).
   - We re-ran SMAT for an alternative base year DV period centered on 2017 rather than 2016 (4th high MDA8 ozone days from 2015 through 2019).
   - We re-ran SMAT for the standard 2016-2018 base year DV period but with annual 4th high MDA8 ozone values during 2014-2018 recalculated by removing fire-influenced days (as identified by DES/DAQ) from the monitored annual MDA8 ozone database.
   - We ran a CAMx source apportionment application (Section 11) tracking international, US, and local source category contributions to ozone in Clark County, as well as NOx- and VOC-limited chemistry patterns.

2) Trends in emissions and air quality measurements

   - We assessed Clark County historical and projected future NOx and VOC emission trends over 2008-2033 using a combination of Clark County Inventories.
   - Using EPA's statistical software package and data sets to meteorologically adjust ambient ozone trends (EPA, 2023b; Wells et al., 2021), we developed a set of meteorologically adjusted 2000-2022 ozone trends reflecting the removal of fire-influenced or "EE-like" days (as identified by DES/DAQ).

3) Additional emission controls/reductions

   - We ran CAMx for the 2023 future base case with all wildfire emissions removed and noted impacts to the 2023 projected DVs.

Appendix A describes results from additional 2023 future year emissions sensitivity tests.

12.2 Conclusions

The weight of evidence presented here, according to additional modeling, analyses of precursor emissions and ambient ozone trends, and removal of wildfires from measurements and modeling, all support the results from the photochemical modeling demonstration that the Clark County Moderate Ozone Nonattainment Area will attain the 2015 ozone NAAQS by the attainment year of 2023. Results supporting this conclusion are summarized below, and details of our analyses are presented in the remainder of this report.

12.2.1 Summary of Results

- EPA's initial and final interstate transport modeling:
  - In agreement with our 2023 future base case modeling results, both of EPA's modeling platforms consistently show that the CCNAA will attain the 2015 ozone NAAQS in 2023.
  - EPA source apportionment modeling consistently shows that California and fires together contribute about as much to Clark County 2023 DVs as Nevada's own contribution.

- 2023 SMAT DV projections using a base year DV period centered on 2017:
  - Projected DVs at monitoring sites were consistent with and slightly lower than using a base year DV period centered on 2016, reflecting the slightly lower base year DV. SMAT-CE indicated no exceedances in 2023 in either case.

- 2023 SMAT DV projections using a base year DV period centered on 2016 but with fire-influenced days removed from the observed MDA8 ozone database:
  - Reductions in 2016-2018 DVs of 0 to 2 ppb resulted from the removal of fire-influence days, and 2023 projected DVs were similarly lower with no exceedances among any monitoring site.

- Ozone source apportionment results (Section 11):
  - Contributions to model-projected 2023 DV at Joe Neal are consistent with EPA's two interstate source apportionment analyses.
  - Natural and non-US ozone concentrations comprise the majority of ozone at 49 ppb (71% of the 69 ppb DV), California anthropogenic emissions contribute an average of 7 ppb (11%), Clark County contributes 11 ppb (16%), fires within the North American modeling domain contribute 2.4 ppb (4%), and the rest of the US contributes 1.7 ppb (3%).
  - The modeled contributions to the 2023 DV at Joe Neal from all global international anthropogenic emissions are 13 ppb at Joe Neal, a value that is consistent throughout the entire inter-mountain western US and consistent with many previous studies.

- Clark County 2008-2033 NOx and VOC emission trends:
  - A substantial 56% NOx reduction has occurred between 2008 and 2023 and continued reductions are projected out to 2033 with an overall 2011-2033 reduction of 64%. NOx reductions are driven by large decreases among the on-road and nonroad motor vehicle sectors.
  - VOC emissions have generally decreased over the 2008-2023 period by 25% and a continued net reduction of 26% is projected out to 2033. VOC decreases are driven by on-road and nonroad sectors but curbed by increases in the nonpoint sector because of burgeoning population and commercial activity.
  - Growth in airport emissions over the 2008-2033 period contribute to increasing NOx and VOC.
  - The area is expected to continue its evolution from a transitional NOx- and VOC-sensitive environment toward a relatively more NOx-sensitive environment out to 2033. Therefore, after a period of some NOx-disbenefits in certain areas, continued NOx reductions will be effective in lowering ozone into the future while VOC reductions will be increasingly less effective.

- Meteorologically adjusted 2000-2022 ozone trends with fire-influenced days removed, based on the 97th percentile that better represents 4th highest MDA8 ozone during the May-September ozone season:

  - The MDA8 ozone trends have tended to flatten over the past 10 years, with a substantial degree of remaining interannual variability after filtering for weather. It is likely that this remaining variability is related to other western regional influences, particularly wildfire activity.
  - The flattened trends are in sharp contrast to large anthropogenic emission reductions achieved across the region during this time, further suggesting influences from uncontrollable sources.
  - The no-fire trendlines without the meteorological adjustment correctly show reduced 97th percentile MDA8 ozone only in the years when fire-influenced days were removed, by typically 2 to 3 ppb but as much as 5.5 ppb in 2020 at Joe Neal.
  - The meteorologically adjusted no-fire 97th percentile trendlines exhibit similar interannual variability as the original trendlines but a substantial reduction in recent ozone levels at all sites.
  - 2023 extrapolations for the meteorologically adjusted 97th percentile trendline using all days range from 68.1 to 72.3 ppb.
  - 2023 extrapolations for the meteorologically adjusted 97th percentile trendline without fire-influenced days range from 66.7 to 71.0 ppb.

- CAMx 2023 future base case simulation with all wildfire emissions removed:
  - Projected DVs at monitoring sites were all well below the ozone NAAQS and were 1-3 ppb lower than the DV projections that include the wildfire emissions in the 2023 future base case.
  - The modeled wildfire contribution of 1-3 ppb agreed with EPA's source apportionment estimates from their 2016 MPs (EPA, 2022d, 2023a).

12.3 EPA Interstate Transport Modeling

In January 2022, EPA released the 2016v2 Modeling Platform (MP) based on the "fj" version of their US emissions inventory (EPA, 2022b), and used it to project future ozone DVs for the years 2023, 2026 and 2032 (EPA, 2022c)[22]. EPA estimated that ozone DVs in Clark County would attain the 2015 ozone NAAQS in 2023 (Table 12-1) and more certainly would attain in 2026 and 2032. Table 12-1 also lists the 2023 future base case projected DVs determined in this study (Section 9.3), which are very similar to EPA's results.

In late 2022, EPA developed the 2016v3 MP (EPA, 2022c). In response to public comments on the 2016v2 base year and projected emissions inventories, the 2016v3 emissions platform (version "gf") includes "updates, corrections, improved methods, and refinements to some projection factors due to newly released data" (EPA, 2022c). Additionally, EPA replaced 36US3 North American grid BCs drawn from the Hemispheric CMAQ (H-CMAQ) model with new boundary concentrations derived from the GEOS-Chem global chemistry model. Biogenic emissions were developed using BEIS4/BELD6, replacing BEIS3.7/BELD5. Finally, EPA estimated three-dimensional model inputs for lightning NOx (LNOx) emissions.

EPA repeated their projections of future ozone DVs using the 2016v3 MP (EPA, 2023a)[23], which continued to show that Clark County will attain the 2015 ozone NAAQS in 2023 (Table 12-1). There was very little change in results from the 2016v2 projections, and the new results converged somewhat toward the projected DVs determined in this study.

[22] https://gaftp.epa.gov/Air/aqmg/2016v2_Platform_Modeling_Data/

[23] https://www.epa.gov/interstate-air-pollution-transport/final-disapproval-good-neighbor-state-implementation-plans

Table 12-1. Projected 2023 ozone DVs (ppb) at Clark County ozone monitoring sites based on EPA's 2016v2/fg and 2016v3/gf modeling platforms and from the 2023 future base case scenario in this study (CCNAA).

Site ID	2023fj Avg 3x3	2023gf Avg 3x3	CCNAA Avg 3x3
320030022	66.1	65.6	65.2
320030023	58.3	58.5	57.2
320030043	68.5	68.4	67.7
320030071	67.7	67.9	67.9
320030073	67.7	67.9	67.2
320030075	70.0	69.9	69.0
320030298	66.6	66.8	67.3
320030540	65.0	64.4	64.1
320030601	61.8	62.2	61.5
320031019	64.8	64.4	63.9
320032002	67.9	67.5	67.3
320037772	65.1	63.8	62.3

EPA also used the 2016v2 and 2016v3 MPs for their preliminary and final interstate ozone transport modeling for the 2015 ozone NAAQS (EPA, 2022d; 2023a). In both cases, 2023 DV contributions were estimated from individual states, foreign sources, fires and biogenic emissions. Table 12-2 shows results from the 2016v2 while Table 12-3 shows results from the 2016v3. From the 2016v2, EPA estimated that California's contribution to ozone DVs in Clark County is roughly as large as Nevada's own contribution, while most ozone is transported into the LVV from boundary conditions (BCs) reflecting total global contributions. Fires and biogenic emissions were estimated to be modest contributors (1-3 ppb each) and Canada plus Mexico were modeled to contribute even less (1-2 ppb).

Table 12-2. Projected 2023 ozone DV contributions (ppb) from Nevada, other states, foreign sources, fires, and biogenic emissions at Clark County ozone monitoring sites based on EPA's 2016v2 modeling platform (https://gaftp.epa.gov/Air/aqmg/2016v2_Platform_Modeling_Data/ accessed April 2022).

Site ID	AZ	CA	NV	Canada +Mexico	2023 Fires	IC/BC	Biogenic
320030022	0.31	6.90	6.58	1.33	1.57	47.03	1.83
320030043	0.37	6.96	8.19	1.48	2.30	46.43	1.94
320030071	0.19	7.40	6.31	1.31	3.10	46.72	1.70
320030073	0.19	7.40	6.31	1.31	3.10	46.72	1.70
320030075	0.21	7.44	8.46	1.28	0.67	49.59	1.75
320030298	0.46	7.60	6.47	1.84	1.77	45.58	1.99
320030540	0.42	6.89	8.45	1.73	1.84	42.94	1.86
320031019	0.13	6.66	0.99	1.61	2.21	51.22	1.42
320032002	0.36	7.79	10.57	1.31	0.78	44.48	1.97
320037772	0.07	5.54	1.66	0.79	1.90	53.25	1.29

Table 12-3. Projected 2023 ozone DV contributions (ppb) from Nevada, other states, foreign sources, fires, and biogenic emissions at Clark County ozone monitoring sites based on EPA's 2016v3 modeling platform (https://www.epa.gov/interstate-air-pollution-transport/final-disapproval-good-neighbor-state-implementation-plans/ accessed February 2023).

Site ID	AZ	CA	NV	Canada +Mexico	2023 Fires	IC/BC	Biogenic +LNOx
320030022	0.41	7.52	6.43	1.46	0.87	45.30	2.83
320032023	0.91	4.82	1.95	1.76	0.79	44.98	2.45
320030043	0.77	6.97	9.05	1.94	2.13	42.30	4.04
320030071	0.65	6.84	9.97	1.70	2.42	41.42	3.82
320030073	0.65	6.84	9.97	1.70	2.42	41.42	3.82
320030075	0.49	8.96	10.53	1.45	1.36	42.68	3.57
320030298	0.68	7.30	5.34	1.64	2.25	45.11	3.32
320030540	0.65	7.57	7.95	1.37	1.36	41.03	3.39
320030601	0.74	7.22	2.81	1.70	1.59	44.07	3.20
320031019	0.27	6.63	1.38	1.86	1.69	49.49	2.35
320032002	0.50	8.17	10.07	1.27	1.53	41.84	3.40
320037772	0.23	6.52	1.93	0.97	1.87	49.31	2.19

The ozone apportionment results in Table 12-3 are very similar according to the 2016v3 results, but with some notable differences. Contributions from Arizona, California, Nevada, and Canada plus Mexico increased somewhat, while contributions from fires and BCs decreased slightly. Contributions from biogenic emissions increased by about 0.5 ppb and the addition of LNOx in the 2016v3 increased the natural contribution to 2-4 ppb. Both sets of 2016 MP modeling results consistently show that California and fires together contribute about as much to Clark County 2023 DVs as Nevada's own contribution.

12.4 Alternative 2023 DV Projections

12.4.1 Flexibility in RRF Calculations

EPA's guidance includes some flexibility to modify the recommended ozone DV projection procedure. One is to consider shifting the base year DV period by a year or two from which to project the future year DV, to further account for variability in DV levels over the base year period.

Another consideration is to account for "exceptional event like" days (i.e., days that might not qualify as official exceptional events) such as wildfires. EPA (2019c) includes provisions for excluding such days with appropriate justification. There are two approaches to account for exceptional event like days in the attainment year DVF projection: (1) remove such days from the base year DV calculation so that the DV more faithfully reflects typical local to regional anthropogenic ozone conditions and patterns; (2) remove such days from the list of modeled highest 10 base year ozone days in the RRF calculation so that the projection more faithfully reflects impacts from typical local to regional emission reductions. As described in the Modeling Protocol (Ramboll, 2022a) several days of 2016 warrant exclusion, but it would be problematic to exclude a large number.

12.4.2 DV Projections Using Base DV Centered on 2017

We applied SMAT-CE with the most current monitoring database from EPA containing 2002-2020 4th high MDA8 ozone for all official sites operating in Clark County. In this analysis we ran SMAT-CE using

the 2017-2019 3-year DV period for base monitored ozone (2015-2019 4th highs centered on 2017), as opposed to the 2016-2018 DV used previously for the 2023 future base case and control measure scenarios. All other configuration options remained the same as our previous SMAT-CE runs, which employed default or standard settings throughout the setup menu. We made no special modifications to monitored data or specific selection of modeled days for the RRF calculation.

12.4.2.1 Results at Monitoring Sites

Table 12-4 shows projected DV results based on the original 2016-2018 base year DVs and the 2017-2019 base year DVs in this analysis. SMAT-CE continued to indicate no exceedances in 2023. The peak average projected DV was 68.4 ppb at Joe Neal and 68.5 ppb at Walter Johnson, respectively.

Table 12-4. 2023 projected DVs at each monitoring site within the LVV according to SMAT-CE calculations using the 2016-2018 and 2017-2019 average base year DVs. Red values indicate exceedances of the 2015 ozone NAAQS, green indicate values below the NAAQS. Sites noted with an asterisk continued to exceed the ozone NAAQS in 2020, leading to the bump up from Marginal to Moderate nonattainment status.

Site ID	Site Name	2016-2018 DV		2017-2019 DV	
		Base DV Avg 3x3	2023 DV Avg 3x3	Base DV Avg 3x3	2023 DV Avg 3x3
320030022	Apex	70.3	65.2	69.0	64.0
320030023	Mesquite	61.3	57.2	61.3	57.2
320030043	Paul Meyer*	72.0	67.7	71.3	67.1
320030071	Walter Johnson*	72.3	67.9	73.0	68.5
320030073	Palo Verde	72.3	67.2	71.0	66.0
320030075	Joe Neal*	75.0	69.0	74.3	68.4
320030298	Green Valley*	71.0	67.3	71.5	67.7
320030540	Jerome Mack	68.7	64.1	68.3	63.8
320030601	Boulder City	66.0	61.5	66.0	61.5
320031019	Jean	68.3	63.9	67.7	63.3
320032002	J.D. Smith	72.5	67.3	72.0	66.9
320037772	Indian Springs	68.5	62.3	68.3	62.1

12.4.3 DV projections With Fire-Influenced Days Removed

We re-ran SMAT-CE for the standard 2016-2018 base year DV period but with annual 4th high MDA8 ozone values during 2014-2018 recalculated by removing fire-influenced days from the monitored annual MDA8 ozone database. The DES/DAQ provided a list of fire-influenced dates compiled for the years 2016, 2018, and 2020-2022 (Table 12-5; Sonoma Technology, 2023). During the 2016-2018 DV period, individual 4th high MDA8 values in 2016 and 2018 were reduced at most sites by the removal of fire-influenced days, which further reduced all three DVs during 2016-2018.

Table 12-5. Fire-influenced days during 2016, 2018, and 2020-2022 identified and analyzed by DES/DAQ and Sonoma Technology (2023).

Event Date(s)	DES Identified Event Type
June 24-25, 2016	Southern California wildfire influence
June 27, 2016	Southern California wildfire influence
July 24, 2016	Southern California wildfire influence
July 26-29, 2016	Southern California wildfire influence
August 24, 2016	Southern California wildfire influence
June 23, 2018	Wildfire
June 27, 2018	Wildfire
July 14–17, 2018	Wildfire
July 25–27, 2018	Wildfire
July 30–31, 2018	Wildfire
August 6–7, 2018	Wildfire
August 3, 2020	Wildfire
August 7, 2020	Wildfire
August 18–21, 2020	Wildfire
September 26, 2020	Wildfire
June 11-12, 2021	Local smoke
June 16-17, 2021	Regional wildfire smoke
July 20, 2021	Regional wildfire smoke
August 2-3, 2021	Regional wildfire smoke
August 7, 2021	Regional wildfire smoke
August 19, 2021	Regional wildfire smoke
September 8, 2021	Regional wildfire smoke
June 16,2022	Regional wildfire smoke
July 17, 2022	Regional wildfire smoke
July 28-29,2022	Regional wildfire smoke
September 1-2, 2022	Regional wildfire smoke

12.4.3.1 Results at Monitoring Sites

Table 12-6 shows 2016-2018 base year and projected DV results including fire-influenced days (duplicated from the 2023 future base case results) and with fire-influenced days removed. In both cases, the standard CAMx 2016 base case and 2023 future base were used (including wildfire emissions) for the 2023 projections; i.e., only the 2016-2018 DVs were modified and not the CAMx results. According to SMAT-CE, reductions in 2016-2018 DVs of 0 to 2 ppb resulted from the removal of fire-influence days, and 2023 projected DVs were similarly lower with no exceedances among any monitoring site. The peak average 2016-2018 DV was reduced from 75 to 73 ppb. The peak average projected 2023 DV was reduced from 69 to 67 ppb at Joe Neal.

Table 12-6. 2016-2018 and 2023 projected DVs at each monitoring site within the LVV according to SMAT-CE calculations using the official 2016-2018 DVs and the modified 2016-2018 DVs reflecting the removal of fire-influenced days in 2016 and 2018 (Table 12-5). Projected 2023 DVs were determined using the 2023 future base case CAMx results that include influences from wildfires. Red values indicate exceedances of the 2015 ozone NAAQS, green indicate values below the NAAQS. Sites noted with an asterisk continued to exceed the ozone NAAQS in 2020, leading to the bump up from Marginal to Moderate nonattainment status.

Site ID	Site Name	2016-2018 DV		2016-2018 DV no fire days	
		Base DV Avg 3x3	2023 DV Avg 3x3	Base DV Avg 3x3	2023 DV Avg 3x3
320030022	Apex	70.3	65.2	69.7	64.7
320030023	Mesquite	61.3	57.2	61.3	57.2
320030043	Paul Meyer*	72.0	67.7	71.0	66.8
320030071	Walter Johnson*	72.3	67.9	71.0	66.6
320030073	Palo Verde	72.3	67.2	71.0	66.0
320030075	Joe Neal*	75.0	69.0	73.3	67.5
320030298	Green Valley*	71.0	67.3	70.0	66.3
320030540	Jerome Mack	68.7	64.1	68.0	63.5
320030601	Boulder City	66.0	61.5	65.3	60.9
320031019	Jean	68.3	63.9	68.0	63.6
320032002	J.D. Smith	72.5	67.3	70.5	65.5
320037772	Indian Springs	68.5	62.3	67.5	61.4

12.5 Clark County Emission Trends

Ramboll compiled historical and projected future Clark County anthropogenic emission inventories from which to develop NOx and VOC emission trendlines. Centered on 2017, the resulting trendlines span 9 years prior and 16 years forward. Historical emissions in 2008 and 2015 were taken from the Ozone Redesignation Request and Maintenance Plan for the 1997 Ozone NAAQS (Clark County, 2018), while 2017 anthropogenic emissions and projections to 2023 and 2033 were taken from the second Maintenance Plan (Clark County, 2021).

It is important to note that the historical inventories reported here for 2008, 2015 and 2017 were developed using different data sources, methods, and models unique to each inventory year. This leads to some inconsistencies in trendlines for those sectors affected by substantial updates, improvements, or refinements, e.g., the evolution of MOBILE, NONROAD, and MOVES models and associated local data used to estimate emissions for on-road and nonroad motor vehicle sectors. Additionally, substantial methodological and data updates for other sectors have occurred and are anticipated, e.g., the use of new information from field research and models from which to estimate emissions from volatile chemical products (VCP) that comprise a major fraction of the nonpoint VOC emissions sector. Nevertheless, the trendlines developed here provide a general sense for the evolution of NOx and VOC emissions over a 25 year span.

Tables 12-7 and 12-8 tabulate the Clark County anthropogenic emission estimates over 2008-2033 by major source sector and Figure 12-5 shows the resulting trendline for total anthropogenic NOx and VOC. A substantial NOx reduction has occurred between 2008 and 2023, by 56%. Continued

reductions are projected out to 2033, with an overall 2008-2033 reduction of 64%. NOx reductions over the entire period are driven primarily by large decreases among the on-road and nonroad motor vehicle sectors, only curbed by increases in airport-related emissions.

VOC emissions have also generally decreased over the 2011-2023 period by 25% and are projected to continue decreasing through 2033 for an overall reduction of 26%. VOC decreases over the period are driven primarily by on-road and nonroad mobile sources but are curbed by growth in the nonpoint sector because of historical and future burgeoning population and commercial activity. Recent growth in airport emissions also contribute to increasing VOC since 2017.

The area is expected to continue its evolution from a transitional NOx- and VOC-sensitive environment toward a relatively more NOx-sensitive environment out to 2033. Therefore, after a period of some NOx-disbenefits in certain areas, continued NOx reductions will be effective in lowering ozone into the future while VOC reductions will be increasingly less effective.

Table 12-7. Clark County anthropogenic NOx emissions trends (TPD) by major source category. Data from 2008 and 2015 are reported by Clark County (2018) while data from 2017 through 2033 are reported by Clark County (2021). Sectors noted in green (red) exhibit a net reduction (increase) from 2008 to 2023 and beyond to 2033.

Sector	2008	2015	2017	2023	2033
Point Source	28.97	11.60	12.34	11.41	11.33
Nonpoint Source	6.60	5.94	4.69	5.03	4.78
Mobile: On-road	89.5	64.30	42.20	22.22	11.13
Mobile: Nonroad	40.63	27.69	38.87	24.48	16.33
Aviation: Commercial + Federal	12.68	13.35	11.90	15.53	19.77
TOTAL	**178.38**	**122.88**	**110.0**	**78.67**	**63.34**

Table 12-8. Clark County anthropogenic VOC emissions trends (TPD) by major source category. Data from 2008 and 2015 are reported by Clark County (2018) while data from 2017 through 2033 are reported by Clark County (2021). Sectors noted in green (red) exhibit a net reduction (increase) from 2008 to 2023 and beyond to 2033.

Sector	2008	2015	2017	2023	2033
Point Source	1.50	2.42	2.95	2.62	2.63
Nonpoint Source	67.56	60.12	64.69	67.83	71.31
Mobile: On-road	42.46	33.04	26.27	17.85	11.50
Mobile: Nonroad	42.07	31.10	28.93	27.29	27.86
Airports: Commercial + Federal	3.39	3.75	1.96	2.64	3.05
TOTAL	**156.98**	**130.43**	**124.08**	**118.23**	**116.35**

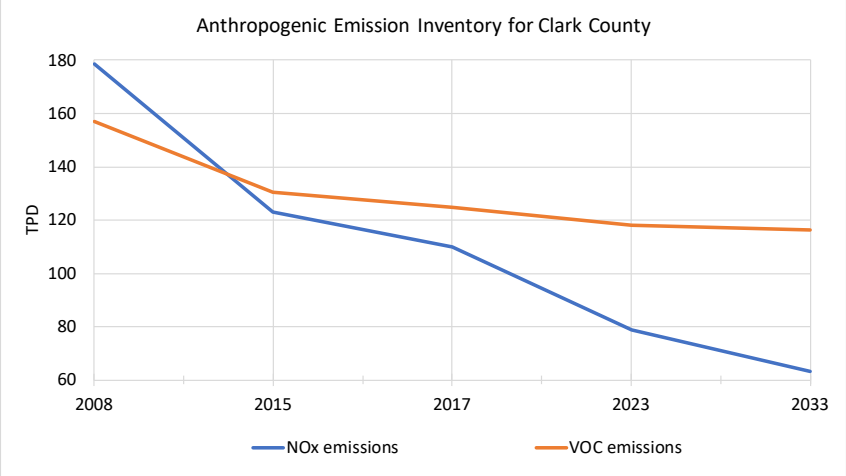

Figure 12-1. Clark County total anthropogenic NOx and VOC emission trends (TPD) from 2008 through 2033. Data from 2008 and 2015 are reported by Clark County (2018) while data from 2017 through 2033 are reported by Clark County (2021).

12.6 Meteorologically Adjusted Ozone Trends

Variations in interannual weather patterns affect ozone DVs year-to-year, which can obscure the assessment of air quality trends. Warm, clear and stagnant summers usually lead to more frequent high ozone episodes while cool, cloudy and breezy summers lead to better air quality. EPA uses a statistical model to adjust monitored ozone levels for the effects of seasonal weather variability "to provide a more accurate assessment of the underlying trend in ozone caused by emissions" (EPA, 2023e). In other words, by filtering interannual variations among key meteorological factors toward climatological averages, the adjusted long-term ozone trend should better reflect influences from long-term emission changes. In this context, we expect EPA is referring to anthropogenic emission reductions at local to regional scales that primarily influence ozone at specific monitors. It is important to note that, especially in the western US, ozone trends reflect contributions from several other substantial uncontrollable influences that are not addressed by meteorological filtering alone, such as interannual wildfire activity and sources of background contributions (including stratospheric intrusions, neighboring countries, intercontinental transport from Asia, etc.). The 2020 COVID-19 pandemic also impacted anthropogenic activities and emissions.

Wells et al. (2021) describe the statistical models used to determine the trendline adjustments and how they are fit independently for each ozone monitoring site using local ozone and weather data. The statistical technique, called forward selection, chooses the weather variables that are most important for ozone formation at each location. Variables are selected iteratively according to greatest improvement in the model fit, up to a maximum of 10 variables. As we would expect, the variables of greatest importance, and the resulting statistical adjustments applied, all tend to have a strong geographic coherence. Nevertheless, since the adjustment is statistical, it likely cannot remove all interannual weather influences from the trendlines.

12.6.1 Ozone Trends With Fire-Influenced Days Removed

Ramboll developed meteorologically adjusted 2000-2022 ozone trends and compared them to trends with fire-influenced or "EE-like" days removed since 2016 (as identified by DES/DAQ; Table 12-5). The analysis focused on the four consistently highest ozone monitoring sites in Clark County: Joe Neal, Walter Johnson, Paul Meyer, and Palo Verde. We obtained EPA's statistical software package, run

scripts, and input datasets (B. Wells, personal communication). The fire-influenced days from 2016 through 2022 listed in Table 12-5 were removed from EPA's May-September 2000-2022 MDA8 ozone database for the four sites listed above and the software scripts were used to calculate the 97th percentile trendlines, which closely corresponds to 4th highs for the number of days over the ozone season.

Figure 12-6 shows the resulting ozone trend lines at the four Clark County monitoring sites, where the 97th percentile trendlines for all-day (red) and no-fire (blue) cases are overlaid for direct comparison. The dotted lines show the meteorologically unadjusted trends while the solid lines show the trends after filtering the interannual weather variability. The trends in the all-day cases have tended to flatten over the past 10 years, with a substantial degree of remaining interannual variability after filtering for weather. It is likely that this remaining variability is related to other western regional influences that weather parameters cannot account for, particularly the significant increase in western wildfire activity over this later period. The flattened trends are in sharp contrast to large anthropogenic emission reductions achieved across the region during this time, further suggesting influences from uncontrollable sources. The significant uptick in 97th percentile ozone at Palo Verde over 2020-2021 (+13 ppb unadjusted, +9 ppb adjusted) is particularly notable as it is much larger than at all other sites and is reflected throughout the frequency distribution, from the median through the 90th percentile (EPA, 2023e; not shown). The cause for this behavior is not readily apparent.

The no-fire trendlines without the meteorological adjustment correctly show reduced 97th percentile MDA8 ozone only in the years when fire-influenced days were removed, by typically 2 to 3 ppb but as much as 5.5 ppb in 2020 at Joe Neal. Interestingly, the meteorologically adjusted no-fire trendlines change in all years. We suspect that removing high ozone days during the few later years changed the diagnosed statistical relationships and associated ozone adjustments enough to alter the data throughout the analysis period. The meteorologically adjusted no-fire trendlines exhibit a similar interannual variability as the all-day trendlines but result in a substantial reduction in recent ozone levels. Note that removal of fire days in 2020-2022 slightly reduces the large uptick in 97th percentile ozone at Palo Verde over this period.

Linear regressions were fit to the meteorologically adjusted trendlines to further clarify the 20-year mean trends and impacts from removing fire-influenced EE-like days, as well as to project the trends to 2023. Table 12-9 presents pertinent statistics and 2023 projections from the meteorological adjusted 97th percentile trendlines. The regressed projections to 2023 show MDA8 ozone below the NAAQS at three of the four sites in the all-day and no-fire cases.

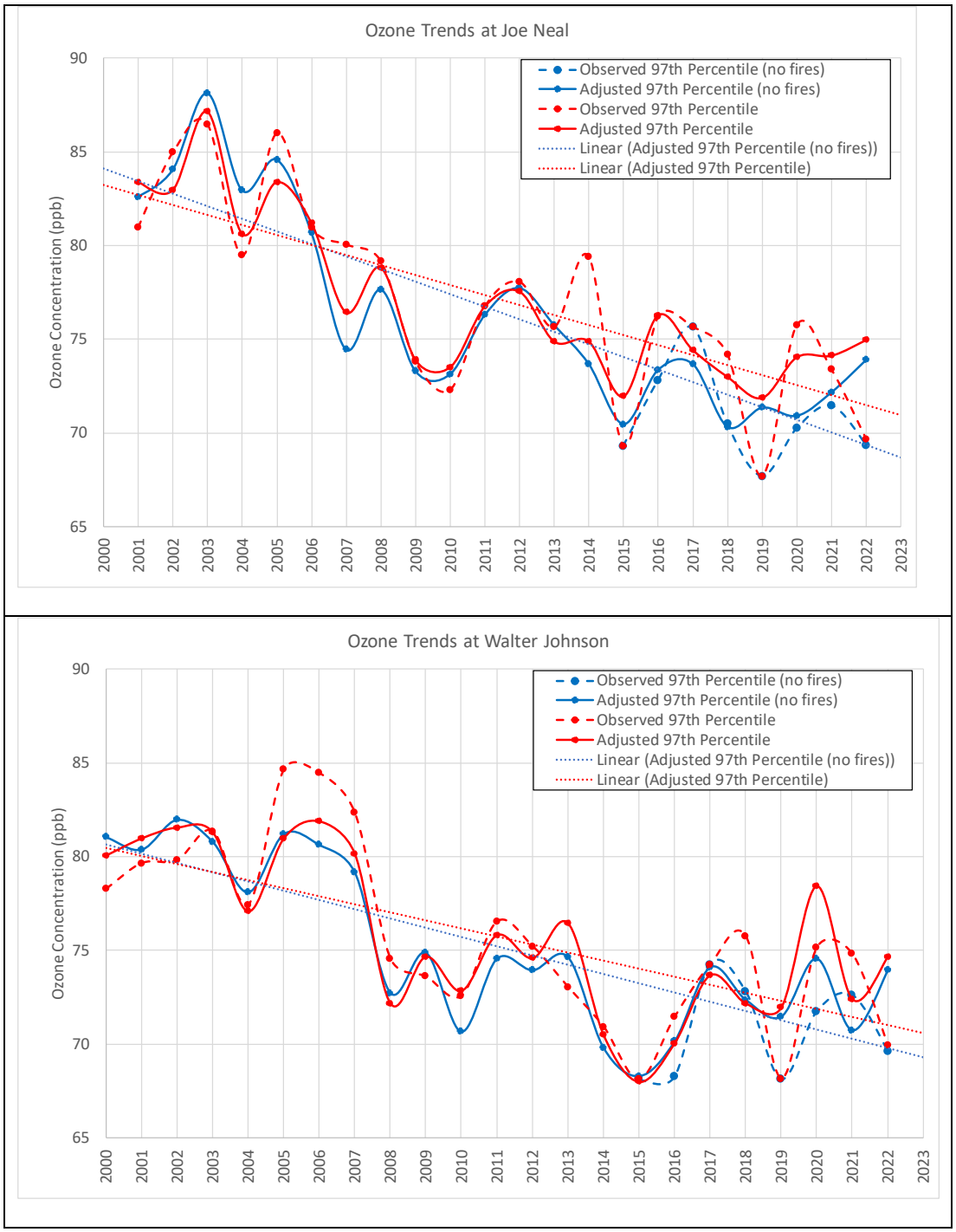

Figure 12-2. 2001-2022 ozone trends at Clark County monitoring sites: 97th percentile for all days (red) for observed (dashed line) and meteorologically adjusted (solid line) May-September MDA8 ozone; and 97th percentile resulting from removal of fire-influenced days in 2016 through 2022 (blue) for observed (dashed lines) and meteorologically adjusted (solid line) May-September MDA8 ozone. The linear regression lines for adjusted all-days and no-fire days are shown as the dotted lines and extend to 2023.

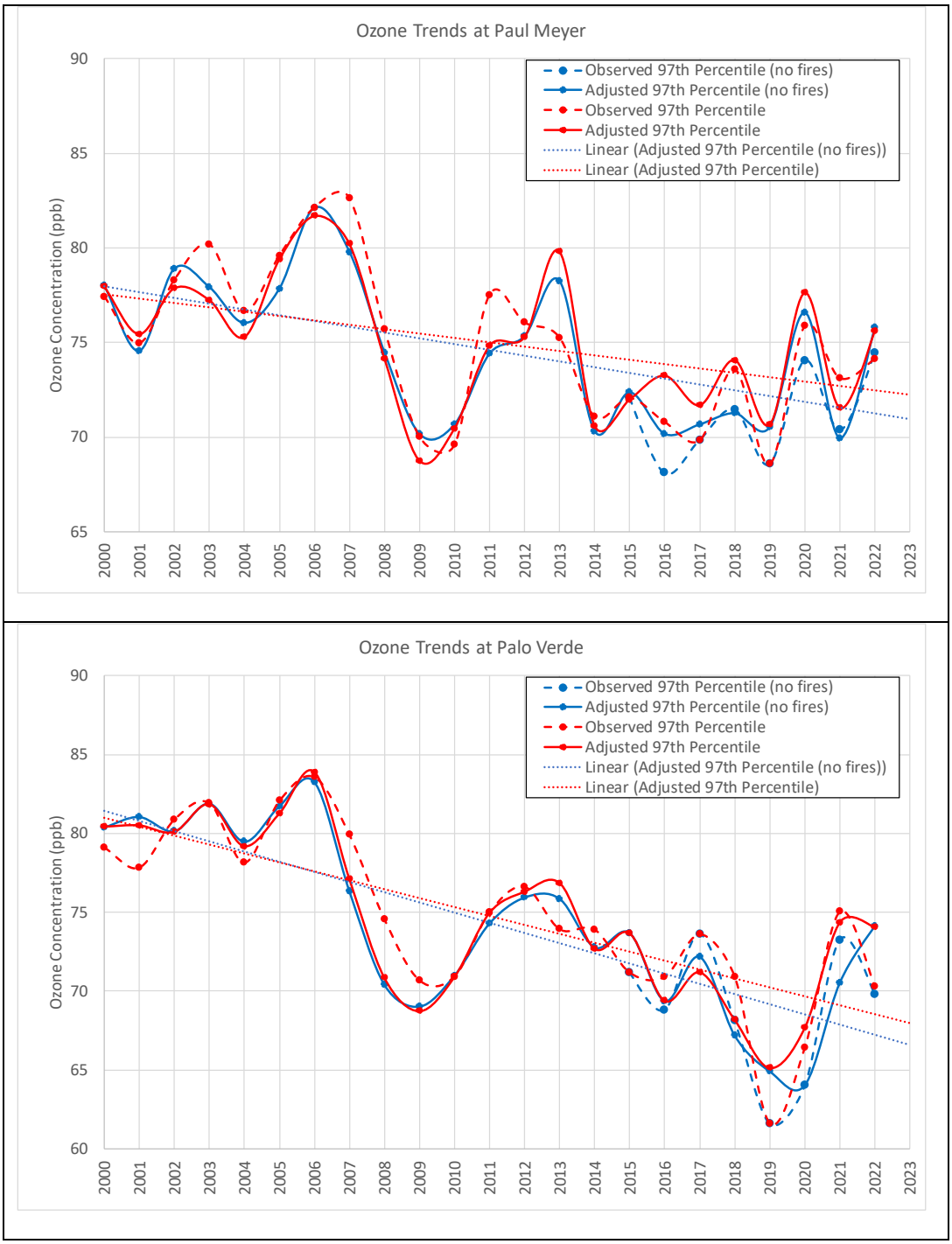

Figure 12-6 (concluded).

Table 12-9. Regression statistics for all-days and no-fire days meteorologically adjusted 97th percentile MDA8 ozone trendlines in Figure 12-6 along with the corresponding 2023 projected 97th percentile MDA8 ozone.

Site	Slope (ppb/yr)		R^2		20-year change		2023 Projection	
	All Days	No Fire	All Days	No Fire	All Days	No Fire	All Days	No Fire
Joe Neal	-0.5352	-0.6699	0.67	0.70	-10.7	-13.4	70.9	68.6
Palo Verde	-0.5661	-0.6444	0.54	0.61	-11.3	-12.9	68.1	66.7
Walter Johnson	-0.4281	-0.4946	0.47	0.61	-8.6	-9.9	70.7	69.3
Paul Meyer	-0.2304	-0.3037	0.19	0.31	-4.6	-6.1	72.3	71.0

12.7 CAMx 2023 Future Base Case With Wildfire Emissions Removed

The 2023 future year base case CAMx run was repeated but removing all wildfire emissions within the 12US2 and CC4c2 modeling domains. All other inputs were not modified (Table 12-10), and only the 12US2/CC4c2 2-way nested grids were run using the 2023 12US2 future base case boundary conditions extracted from the 36US3 grid. In this test we isolated the effects of wildfires on 2023 DV projections by considering a scenario where all wildfires that occurred in 2016 would not occur in 2023.

12.7.1 SMAT-CE Configuration

We applied SMAT-CE identically to the original 2023 future base case scenario, specifying 2016-2018 3-year DV period for base monitored ozone (2014-2018 4th highs centered on 2016). All other configuration options remained the same as the original SMAT-CE run, which employed default or standard settings throughout the setup menu. We made no special modifications to monitored data or specific selection of modeled days for the RRF calculation.

12.7.2 Results at Monitoring Sites

Table 12-11 shows projected DV results at monitoring sites that reported sufficient data during the 2016-2018 base year DV period. Projected DVs were all well below the ozone NAAQS and were 1-3 ppb lower than the DV projections that include the wildfire emissions in the 2023 future base case. Therefore, the modeled wildfire contribution to projected DVs of 1-3 ppb agree with EPA's source apportionment estimates from their 2016 MPs (Tables 12-2 and 12-3; EPA, 2022c, 2023a). The peak average projected DV was 67.6 ppb at Joe Neal.

Table 12-10. CAMx model configuration for the CCNAA 2023 future base case simulation with wildfires removed (noted in red).

Model Component	CCNAA Application	Comment
Model Code	CAMx v7.20 - May 2022	
Modeling Period	May 1 – August 31, 2016	
Horizontal Grids		
Map Projection	Lambert Conic Conformal	EPA 2016 MP
36 km (36US3)	172 x 148 cells	Not run
12 km (12US2)	396 x 246 cells (no buffer cells)	EPA 2016 MP (2-way nesting)
4 km (CC4c2)	50 x 62 cells (with buffer cells)	CCNAA grid (2-way nesting)
Vertical Grid	35 layers	EPA 2016 MP, defined by WRF
Initial Conditions	12US2/CC4c2 IC May 1 from 36US3	2023 future year base case
Boundary Conditions	12US2 BC from 36US3	2023 future year base case
Time Zone	UTC	EPA 2016 MP
Emissions		
36/12 km Data Sources	EPA 2023fj from 2016v2 MP	Wildfires removed from 12US2 grid
4 km Data Sources	EPA 2023fj from 2016v2 MP + 2023 Clark County Data, elevated Reid LTO emissions	Wildfires removed
Models/Processing Tools	SMOKE, MOVES3, SMOKE-MOVES, BEIS4/BELD6	CCNAA grid
Plume-in-Grid	Off	No large point sources in high-resolution CCNAA grid
In-line Ix emissions	On	Oceanic halogens
Chemistry		
Gas Phase Chemistry	CB6r5	Latest mechanism available
Aerosol Chemistry	Active	Gas phase only
Meteorological Interface	WRFCAMx v5.2	
Horizontal Diffusion	Smagorinsky	Spatially variant K-theory
Vertical Diffusion	YSU Kv formulation + KVPATCH	Minimum Kv 0.1 to 1.0 m^2/s
ACM2	Off	Non-local boundary layer convection
Sub-grid Cloud Convection	Off	
Deposition		
Dry Deposition	Zhang03	
Wet Deposition	On	rain/snow/graupel
Surface Chemistry Model	Off	
Bi-directional Ammonia	Off	For aerosol chemistry
Numeric Solvers		
Gas Phase Solver	Euler Backward Iterative (EBI)	Default fast and accurate solver
Vertical Advection	Piecewise Parabolic Method (PPM)	Default
Horizontal Advection	Piecewise Parabolic Method (PPM)	Default
Integration Time Step	Wind speed dependent	~0.5-1 min (4 km), 1-5 min (12 km), 5-15 min (36 km)
Super Stepping	On	Maximizes time step selection

Table 12-11. 2023 projected DVs at each monitoring site within the LVV according to SMAT-CE calculations using the 2016-2018 average base year DVs. Projected DVs are listed for the original 2023 future base case and for 2023 without contributions from wildfires. Green indicates values below the NAAQS while sites noted with an asterisk continued to exceed the ozone NAAQS in 2020, leading to the bump up from Marginal to Moderate nonattainment status.

Site ID	Site Name	2023 Future Base DV	2023 Future DV No Wildfires	Differences
		Avg 3x3	Avg 3x3	Avg 3x3
320030022	Apex	65.2	64.1	-1.1
320030023	Mesquite	57.2	56.5	-0.7
320030043	Paul Meyer*	67.7	65.8	-1.9
320030071	Walter Johnson*	67.9	65.6	-2.3
320030073	Palo Verde	67.2	64.9	-2.3
320030075	Joe Neal*	69.0	67.6	-1.4
320030298	Green Valley*	67.3	65.9	-1.4
320030540	Jerome Mack	64.1	62.4	-1.7
320030601	Boulder City	61.5	60.4	-1.1
320031019	Jean	63.9	62.2	-1.7
320032002	J.D. Smith	67.3	65.0	-2.3
320037772	Indian Springs	62.3	59.6	-2.7

13.0 REFERENCES

Adelman, Z. 2004. Quality Assurance Protocol – WRAP RMC Emissions Modeling with SMOKE, Prepared for the WRAP Modeling Forum by the WRAP Regional Modeling Center, Riverside, CA.

Appel, W., R. Gilliam, N. Davis, A. Zubrow, S. Howard, 2011. Overview of the atmospheric model evaluation tool (AMET) v1.1 for evaluating meteorological and air quality models. *Environmental Modelling & Software*, 26, 434-443. 10.1016/j.envsoft.2010.09.007.

Boylan, J.W. and A.G. Russell, 2006. PM and light extinction model performance metrics, goals, and criteria for three-dimensional air quality models. *Atmos. Env.*, 40/26, 4946-4959. https://www.sciencedirect.com/science/article/pii/S1352231006000690.

Buchholz, R. R., Emmons, L. K., Tilmes, S., and the CESM2 Development Team, 2019. CESM2.1/CAM-chem Instantaneous Output for Boundary Conditions. UCAR/NCAR - Atmospheric Chemistry Observations and Modeling Laboratory. https://doi.org/10.5065/NMP7-EP60.

Clark County, 2008. 8-Hour ozone early progress plan for Clark County, Nevada (June 2008). https://files.clarkcountynv.gov/clarknv/Environmental%20Sustainability/SIP%20Related%20Documents/Ozone_Early_Progress_Plan_2008_complete.pdf?t=1647046265375&t=1647046265375

Clark County, 2011. Ozone Redesignation Request and Maintenance Plan, Clark County, Nevada (March 2011). https://files.clarkcountynv.gov/clarknv/Environmental%20Sustainability/SIP%20Related%20Documents/Ozone_Maint_Plan_final.pdf?t=1647046265375&t=1647046265375

Clark County, 2018. Revision to Motor Vehicle Emissions Budgets in Ozone Redesignation Request and Maintenance Plan: Clark County, Nevada. Prepared by the Clark County Department of Environment and Sustainability, Las Vegas, NV (October 2018). https://files.clarkcountynv.gov/clarknv/Environmental%20Sustainability/SIP%20Related%20Documents/20181016_1997_8-Hr_Ozone_SIP_Revision_with_Appendices.pdf?t=1676558658217&t=1676558658217.

Clark County, 2019. Clark County Department of Air Quality, Ozone Advance Program Progress Report Update (August 2019). https://files.clarkcountynv.gov/clarknv/Environmental%20Sustainability/SIP%20Related%20Documents/2019%20Ozone%20Advance%20Progress%20Report%20Update.pdf?t=1647046265375&t=1647046265375.

Clark County, 2020. Revision to the Nevada state implementation plan for the 2015 Ozone NAAQS: emissions inventory and emissions statement requirements (September, 2020). https://files.clarkcountynv.gov/clarknv/Environmental%20Sustainability/SIP%20Related%20Documents/O3/20200901_2015_O3%20EI-ES_SIP_FINAL.pdf?t=1617690564073&t=1617690564073.

Clark County, 2021. Second Maintenance Plan for the 1997 8-hour Ozone NAAQS. Prepared by the Clark County Department of Environment and Sustainability, Las Vegas, NV (December 2021). https://files.clarkcountynv.gov/clarknv/Environmental%20Sustainability/SIP%20Related%20Documents/O3/20211221_1997_O3_2nd_MSIP_w_Appendices.pdf.

Clark County, 2023. Exceptional Events and Demonstrations website. https://www.clarkcountynv.gov/government/departments/environment_and_sustainability/division_of_air_quality/planning/exceptional_events.php.

Daley, C., M. Halbleib, J. Smith, W. Gibson, M. Doggett, G. Taylor, J. Curtis, P. Pasteris, 2008. Physiographically sensitive mapping of climatological temperature and precipitation across the conterminous United States. *Intl. J. Climate*, DOI: 10.1002/joc.1688. http://prism.oregonstate.edu/documents/Daly2008_PhysiographicMapping_IntJnlClim.pdf.

Emery, C., E. Tai, G. Yarwood, 2001. Enhanced Meteorological Modeling and Performance Evaluation for Two Texas Episodes. Prepared for the Texas Natural Resources Conservation Commission by ENVIRON International Corp., Novato, CA.

Emery, C.E., Z. Liu, A.G. Russell, M.T. Odman, G. Yarwood, N. Kumar, 2016. Recommendations on statistics and benchmarks to assess photochemical model performance. *J. of the Air and Waste Management Assoc.*, 67/5, DOI: 10.1080/10962247.2016.1265027. https://www.tandfonline.com/doi/full/10.1080/10962247.2016.1265027.

EPA, 1991. Guidance for Regulatory Application of the Urban Airshed Model (UAM). US Environmental Protection Agency, Office of Air Quality Planning and Standards, Research Triangle Park, NC.

EPA, 2008. Network design criteria for ambient air quality monitoring, 40 CFR Part 58, Appendix D.

EPA, 2015. Implementation of the 2015 Primary Ozone NAAQS: Issues Associated with Background Ozone, White Paper for Discussion" (December 30, 2015). https://www.epa.gov/ground-level-ozone-pollution/background-ozone-workshop-and-information.

EPA, 2018a. Modeling Guidance for Demonstrating Air Quality Goals for Ozone, PM2.5, and Regional Haze. Prepared by the US Environmental Protection Agency, Office of Air Quality Planning and Standards, Air Quality Assessment Division (EPA 454/R-18-009, November 2018). https://www3.epa.gov/ttn/scram/guidance/guide/O3-PM-RH-Modeling_Guidance-2018.pdf.

EPA, 2018b. Implementation of the 2015 National Ambient Air Quality Standards for Ozone: Nonattainment Area State Implementation Plan Requirements, Final Rule. US Environmental Protection Agency (November 7, 2018). https://www.epa.gov/sites/production/files/2018-11/documents/2015_ozone_srr_final_preamble_20181101.pdf.

EPA, 2019a. Meteorological Model Performance for Annual 2016 Simulation WRF v3.8. US Environmental Protection Agency, Office of Air Quality Planning and Standards, Air Quality Assessment Division (EPA-454/R-19-010). https://www.epa.gov/sites/default/files/2020-10/documents/met_model_performance-2016_wrf.pdf.

EPA, 2019b. Technical Support Document for EPA's Updated 2028 Regional Haze Modeling. US Environmental Protection Agency, Office of Air Quality Planning and Standards (September, 2019). https://www3.epa.gov/ttn/scram/reports/Updated_2028_Regional_Haze_Modeling-TSD-2019.pdf.

EPA, 2019c. Additional Methods, Determinations, and Analyses to Modify Air Quality Data Beyond Exceptional Events. U.S. Environmental Protection Agency, Office of Air Quality Planning and Standards (EPA-457/B-19-002, April 2019). https://www.epa.gov/sites/default/files/2019-04/documents/clarification_memo_on_data_modification_methods.pdf.

EPA, 2019d. Transboundary Air Pollution, Briefing for Clean Air Act Advisory Committee; November 7, 2019. https://www.epa.gov/sites/production/files/2019-11/documents/international_transport_.pdf.

EPA, 2020a. MOVES3 Technical Guidance: Using MOVES to Prepare Emission Inventories for State Implementation Plans and Transportation Conformity. US Environmental Protection Agency, Office of Transportation and Air Quality (EPA-420-B-20-052, November 2020). https://nepis.epa.gov/Exe/ZyPDF.cgi?Dockey=P1010LXH.pdf.

EPA, 2020b. Guidance on the Preparation of Clean Air Act Section 179B Demonstrations for Nonattainment Areas Affected by International Transport of Emissions. US Environmental Protection Agency, Office of Air Quality Planning and Standards, Research Triangle Park, NC (EPA-457/P-20-001F, December 2020). https://www.epa.gov/sites/default/files/2020-01/documents/draft_179b_guidance-final_draft_for_posting.pdf.

EPA, 2021a. Official Release of the MOVES3 Motor Vehicle Emissions Model for SIPs and Transportation Conformity. Federal Register, Vol. 86, No. 4 (January 7. 2021). https://www.govinfo.gov/content/pkg/FR-2021-01-07/pdf/2021-00023.pdf.

EPA, 2021b. Revised Cross-State Air Pollution Rule Update, Final Rulemaking. https://www.epa.gov/csapr/revised-cross-state-air-pollution-rule-update.

EPA, 2021c. 2017 National Emissions Inventory: January 2021 Updated Release, Technical Support Document (EPA-454/R-21-001, February 2021). https://www.epa.gov/sites/default/files/2021-02/documents/nei2017_tsd_full_jan2021.pdf.

EPA, 2022a. Hemispheric CMAQ Application and Evaluation for 2016. https://cfpub.epa.gov/si/si_public_record_report.cfm?Lab=NERL&dirEntryId=344092.

EPA, 2022b. Technical Support Document (TSD): Preparation of Emissions Inventories for the 2016v2 North American Emissions Modeling Platform (EPA-454/B-22-001, February 2022). https://www.epa.gov/system/files/documents/2022-02/2016v2_emismod_tsd_february2022.pdf.

EPA, 2022c. Air Quality Modeling for the 2016v2 Emissions Platform Technical Support Document. Office of Air Quality Planning and Standards (January 2022). https://gaftp.epa.gov/Air/aqmg/2016v2_Platform_Modeling_Data/AQ%20Modeling%20TSD_2016v2%20Platform_rev_2022_0119a.pdf

EPA, 2022d. Notice of Data Availability - Preliminary Interstate Ozone Transport Modeling Data for the 2015 Ozone NAAQS. https://www.epa.gov/airmarkets/notice-data-availability-preliminary-interstate-ozone-transport-modeling-data-2015-ozone.

EPA, 2022e. Biogenic Emission Inventory System (BEIS). https://www.epa.gov/air-emissions-modeling/biogenic-emission-inventory-system-beis.

EPA, 2022f. The Atmospheric Model Evaluation Tool. https://www.epa.gov/cmaq/atmospheric-model-evaluation-tool.

EPA, 2022g. Photochemical Modeling Tools: SMAT-CE. https://www.epa.gov/scram/photochemical-modeling-tools.

EPA, 2023a. Air Quality Modeling Technical Support Document: 2015 Ozone NAAQS SIP Disapproval Final Action. Environmental Protection Agency, Office of Air Quality Planning and Standards. https://www.epa.gov/system/files/documents/2023-02/AQ%20Modeling%20TSD_Final%20Action%20%281%29.pdf.

EPA, 2023b. Air Emission Inventories. https://www.epa.gov/air-emissions-inventories.

EPA, 2023c. Technical Support Document (TSD): Preparation of Emissions Inventories for the 2016v3 North American Emissions Modeling Platform. Environmental Protection Agency, Office of Air Quality Planning and Standards (EPA-454/B-23-001, January 2023). https://www.epa.gov/system/files/documents/2023-01/2016v3_EmisMod_TSD_January2023_0.pdf.

EPA, 2023d. Air Pollutant Emissions Trends Data. https://www.epa.gov/air-emissions-inventories/air-pollutant-emissions-trends-data.

EPA, 2023e. Trends in Ozone Adjusted for Weather Conditions. https://www.epa.gov/air-trends/trends-ozone-adjusted-weather-conditions.

Federal Register, 2018. Additional Air Quality Designations for the 2015 Ozone National Ambient Air Quality Standards. Vol. 83, No. 107 (June 4, 2018). https://files.clarkcountynv.gov/clarknv/Environmental%20Sustainability/SIP%20Related%20Documents/20180604_83_FR_25776_2015_O3_NAAQS_Designations.pdf?t=1647046265375&t=1647046265375z.

Federal Register, 2022. Finding of Failure To Attain and Reclassification of Las Vegas Area as Moderate for the 2015 Ozone National Ambient Air Quality Standard (Proposed Rule). Vol. 87, No. 140 (July 22, 2022) [EPA–R09–OAR–2022–0525; FRL–9961–01–R9]. https://www.federalregister.gov/documents/2022/07/22/2022-15674/finding-of-failure-to-attain-and-reclassification-of-las-vegas-area-as-moderate-for-the-2015-ozone.

Federal Register, 2023. Finding of Failure To Attain and Reclassification of Las Vegas Area as Moderate for the 2015 Ozone National Ambient Air Quality Standard (Final Rule). Vol. 88, No. 3 (January 5, 2023) [EPA–R09–OAR–2022–0525; FRL–9961–02–R9]. https://www.federalregister.gov/documents/2023/01/05/2022-28319/finding-of-failure-to-attain-and-reclassification-of-las-vegas-area-as-moderate-for-the-2015-ozone.

Jaffe, D.A., O.R. Cooper, A.M. Fiore, B.H. Henderson, G.S. Tonnesen, A.G. Russell, D.K. Henze, A.O. Langford, M. Lin, T. Moore, 2018. Scientific assessment of background ozone over the U.S.: Implications for air quality management. *Elem. Sci. Anth*., 6: 56. DOI: https://doi.org/10.1525/elementa.309.

Kemball-Cook, S., Y. Jia, C. Emery, R. Morris, 2004. 2002 annual MM5 simulation to support WRAP CMAQ visibility modeling for the section 308 SIP/TIP. Prepared for The Western Regional Air Partnership by ENVIRON International Corp, Novato, CA.

Langford A.O., 2014. Las Vegas Ozone Study (LVOS), Final Report (MOU #CBE 602948-13) to the Clark County department of Air Quality. (July 25, 2014). https://csl.noaa.gov/projects/lvos/LVOSfinalreportCBE602948-13.pdf.

Langford A.O., Senff C.J., Alvarez R.J., Brioude J., Cooper O.R., Holloway J.S., Lin M.Y., Marchbanks R.D., Pierce R.B., Sandberg S.P., Weickmann A.M., and Williams E.J., 2015. An overview of the 2013 Las Vegas Ozone Study (LVOS): impact of stratospheric intrusions and long-range transport on surface air quality. *Atmospheric Environment*, 109, 305-322, doi: 10.1016/j.atmosenv.2014.08.040, 2015/05/01/. http://www.sciencedirect.com/science/article/pii/S1352231014006426.

Langford A.O. et al., 2022. The Fires, Asian, and Stratospheric Transport–Las Vegas Ozone Study (FAST-LVOS). *Atmos. Chem. Phys*., 22, 1707–1737, 2022 https://doi.org/10.5194/acp-22-1707-2022.

Maricopa Association of Governments, 2016. MAG 2017 Eight-Hour Ozone Moderate Area Plan (December, 2016). https://azmag.gov/portals/0/Documents/EP_2016-12-09_MAG-2017-EightHour-Ozone-Moderate-Area-Plan-for-the-Maricopa-Nonattainment-Area.pdf.

McNally, D., G. Schewe, J. Johnson, R. Morris. 2008. Evaluation of Preliminary MM5 Meteorological Model Simulation for the June-July 2006 Denver Ozone SIP Modeling Period Focused on Colorado. Prepared for the Denver Regional Air Quality Council (RAQC) by Alpine Geophysics, LLC and ENVIRON International Corporation (February 2008). http://www.ozoneaware.org/documents/MM5_Eval_DENSIP_Feb25_2008.pdf.

NASA, 2022. Ozone Monitoring Instrument (OMI) FTP site. https://acd-ext.gsfc.nasa.gov/anonftp/toms/omi/data/Level3e/ozone/ or https://acd-ext.gsfc.nasa.gov/anonftp/toms/omps_tc/data/ozone/.

National Weather Service Forecast Office, 2020. Las Vegas, NV: general climatic summary. https://www.wrh.noaa.gov/vef/lassum.php.

NCAR, 2022. The Community Atmosphere Model with Chemistry (CAM-chem) website. National Center for Atmospheric Research, Atmospheric Chemistry Observations and Modeling. https://www2.acom.ucar.edu/gcm/cam-chem.

NDEP and Clark County, 2018. Clark County Response to 120-Day 2015 Ozone NAAQS Designations Letter; Docket ID EPA HQ-OAR-2017-0548. Letter to Acting Regional Administrator, EPA Region 9 (February, 2018). https://files.clarkcountynv.gov/clarknv/Environmental%20Sustainability/SIP%20Related%20Documents/20180223_%20NDEP_Lovato_Transmittal_ClarkCounty_2015_O3_NAAQS_%20Response.pdf?t=1647046265375&t=1647046265375.

NOAA, 2022. Las Vegas Field Measurements of Volatile Chemical Product and Mobile Source Emissions: Ozone Formation and its Sensitivity to NOx AND VOCs (Draft Final Report). Prepared by the NOAA Chemical Sciences Laboratory (NOAA CSL), Boulder, CO and CIRES, University of Colorado, Boulder (November 11, 2022).

RAQC, 2022. 2023 Local Source Apportionment Analysis. Regional Air Quality Council SIP Modeling website. https://raqc.egnyte.com/dl/VHRCCkBuru/Dashboard_LocalAPCA_mda8_v2021.03.17_(1).xlsx_.

Ramboll, 2018. Relative Reduction Factors Using Anthropogenic Ozone Increments. Prepared for the Coordinating Research Council, Report No. A-112, by Ramboll US Corporation, Novato, CA

(October, 2018). https://crcao.org/reports/recentstudies2018/A-112/CRC_A-112_Executive%20Summary_22Oct18.pdf.

Ramboll, 2019. 2020 and 2023 Attainment Demonstration Modeling for the Denver Metro/North Front Range Ozone Nonattainment Area. Prepared for the Denver Regional Air Quality Council (April 22, 2019) https://raqc.egnyte.com/dl/fcJZDcD3Ue/DMNFR_2023_2020_Ozone_Modeling_Protocol.pdf_.

Ramboll, 2021a. 2017 WAQS WRF Meteorological Modeling. Prepared for Western States Air Resources Council (WESTAR), Santa Fe, New Mexico (May 2021). https://views.cira.colostate.edu/docs/IWDW/Modeling/WRAP/2017/Ramboll_WESTAR_WRF_Report_May18_2021.pdf.

Ramboll, 2021b. Modeling International Ozone Contribution to Wasatch Front Nonattainment Areas. In the Utah Division of Air Quality Clean Air Act 179B(b) Demonstration, Northern Wasatch Front Ozone Nonattainment Area (05/05/2021). https://documents.deq.utah.gov/air-quality/planning/air-quality-policy/DAQ-2022-012013.pdf.

Ramboll, 2022a. Modeling Protocol for the Clark County Ozone State Implementation Plan (Version 5). Prepared for the Clark County Department of Environment and Sustainability, Division of Air Quality, Las Vegas, NV, by Ramboll US Consulting, Inc. Novato, CA (October 5, 2022).

Ramboll, 2022b. User's Guide: Comprehensive Air quality Model with extensions, version 7.2. https://camx.com/Files/CAMxUsersGuide_v7.20.pdf.

Ramboll, 2022c. Modeling Protocol for the Denver Metro/North Front Range Severe (2008) and Moderate (2015) 2023 Ozone State Implementation Plan (Draft). Prepared for the Denver Regional Air Quality Council and the Colorado Department of Public Health and Environment, Air Pollution Control Division (March 2022).

Ramboll, 2022d. METSTAT Meteorological Model Statistical Evaluation Package (December 9, 2013). http://www.camx.com/download/support-software.aspx.

Ramboll, 2022e. CBE NO. 606111-22: Clark County, Nevada Attainment Demonstration Modeling. Sub-Task 13: Design Document, Future Year Source Apportionment Modeling. Prepared for the Clark County Department of Environment and Sustainability, Division of Air Quality, Las Vegas, NV, by Ramboll US Consulting, Inc. Novato, CA (August 16, 2022).

Ramboll, 2023a. Clark County 15% VOC Rate-of-Progress Plan: Technical Support Document. Prepared for the Clark County Department of Environment and Sustainability, Division of Air Quality, Las Vegas, NV, by Ramboll US Consulting, Inc. Novato, CA (December 4, 2023).

Ramboll, 2023b. 2017 and 2023 Emission Inventories for the Clark County Ozone SIP. Prepared for the Clark County Department of Environment and Sustainability, Division of Air Quality, Las Vegas, NV, by Ramboll US Consulting, Inc. Novato, CA (November 30, 2023).

Ramboll, 2024a. Clark County 15% VOC Rate-of-Progress Plan: Technical Support Document. Prepared for the Clark County Department of Environment and Sustainability, Division of Air Quality, Las Vegas, NV, by Ramboll Americas Engineering Solutions, Inc. Novato, CA (June 27, 2024).

Ramboll, 2024b. 2017 and 2026 Emission Inventories for the 15% Rate of Progress (ROP) Plan for the Clark County Ozone Nonattainment Area. Prepared for the Clark County Department of Environment and Sustainability, Division of Air Quality, Las Vegas, NV, by Ramboll Americas Engineering Solutions, Inc. Novato, CA (April 5, 2024).

Ramboll and Alpine, 2017. Denver Metro/North Front Range 2017 8-Hour Ozone State Implementation Plan: 2011 Base Case Modeling and Model Performance Evaluation. Final Report prepared by Ramboll, Novato, CA and Alpine Geophysics, LLC, Arvada, CO (September 2017). https://raqc.egnyte.com/dl/pxHfZAhquy/TSD_2011_BaseCaseModeling%26MPE.pdf .

Seltzer, K., E. Pennington, V. Rao, B. Murphy, M. Sturm, K. Isaacs and H. Pye, 2021. Reactive Organic Carbon Emissions from Volatile Chemical Products. *Atmos. Chem. Phys.*, 21, 5079-5100. https://acp.copernicus.org/articles/21/5079/2021/.

Sillman, S., 1995. The Use of NOy, H2O2, and HNO3 as Indicators for Ozone - NOX-Hydrocarbon Sensitivity in Urban Locations. *J. Geophys. Res.,* 100, 14,175-14,188.

Simon, H., K. Baker, S. Phillips, 2012. Compilations and Interpretation of Photochemical Model Performance Statistics Published between 2006 and 2012. *Atmos. Env.*, 61, 124-139. http://www.sciencedirect.com/science/article/pii/S135223101200684X.

Skamarock, W.C., et al., 2019. A Description of the Advanced Research WRF Model Version 4. NCAR Technical Note TN-556+STR, Mesoscale and Microscale Meteorology Laboratory, National Center for Atmospheric Research, Boulder, CO (March). https://opensky.ucar.edu/islandora/object/opensky:2898.

Sonoma Technology, 2021. Exceptional Event Demonstration for Ozone Exceedances in Clark County, Nevada – September 26, 2020. Prepared for EPA Region 9 and Clark County Department of Environment and Sustainability (September 2021). https://files.clarkcountynv.gov/clarknv/Environmental%20Sustainability/Exceptional%20Events/20200926_ClarkCounty_Wildfire_EE.pdf?t=1647045765548&t=1647045765548.

Sonoma Technology, 2023. Wildfire Atypical Event Analysis for Ozone Attainment Demonstration State Implementation Plan (SIP). Prepared for EPA Region 9 and Clark County Department of Environment and Sustainability (November 2023).

Stoeckenius, T., T. Olevski, M. Zatko, 2018. Representativeness of Candidate Modeling Years for the Western U.S. Prepared by Ramboll, Novato, California (July 2018). https://www.wrapair2.org/pdf/WESTAR_RTOWG_Representativeness_final.pdf.

UCI, 2022. MEGAN web site, University of California at Irvine. https://bai.ess.uci.edu/megan.

UDAQ, 2021. Clean Air Act 179B(b) Demonstration: Northern Wasatch Front Ozone Nonattainment Area. Prepared by the Utah Division of Air Quality, Salt Lake City, UT (05/05/2021). https://documents.deq.utah.gov/air-quality/planning/air-quality-policy/DAQ-2022-012013.pdf.

UNC, 2020. SMOKE v4.8.1 User's Manual. University of North Carolina, Institute for the Environment, Center for Community Air Quality Modeling and Analysis (January 2020). https://www.cmascenter.org/smoke/documentation/4.8.1/manual_smokev481.pdf.

US Census, 2020. American Community Survey 5-year estimates. Retrieved from Census Reporter Profile page for Las Vegas-Henderson-Paradise, NV Metro Area. http://censusreporter.org/profiles/31000US29820-las-vegas-henderson-paradise-nv-metro-area/.

Wells, B., P. Dolwick, B. Eder, M. Evangelista, K. Foley, E. Mannshardt, C. Misenis, A. Weishampel, 2021. Improved estimation of trends in U.S. ozone concentrations adjusted for interannual variability in meteorological conditions. Atmos Environ., 248, 118234, https://doi.org/10.1016/j.atmosenv.2021.118234.

Wells, B., personal communication via e-mail (2/8/23). Delivery of EPA meteorologically adjusted trends software and database.

Zhang, L., et al., 2020. Characterizing sources of high surface ozone events in the southwestern U.S. with intensive field measurements and two global models. *Atmos. Chem. Phys*., 20, 10379–10400, 2020 https://doi.org/10.5194/acp-20-10379-2020.

APPENDIX A: FUTURE YEAR SENSITIVITY MODELING

MEMORANDUM

Date: **31 October 2023**

To: **Zheng Li, Clark County DES/DAQ**

From: **Chris Emery, Trang Tran, Chao-Jung Chien, Tejas Shah**

Subject: **CBE NO. 606111-22: Clark County, Nevada Attainment Demonstration Modeling**
Future Year Sensitivity Modeling

INTRODUCTION

In 2018, the US Environmental Protection Agency (EPA) designated a portion of Clark County, Nevada as a Marginal Nonattainment area under the 2015 ozone National Ambient Air Quality Standard (NAAQS) of 70 parts per billion (ppb) (Federal Register, 2018). The nonattainment boundary is defined as the Las Vegas Valley (LVV), hydrographic area 212 (HA 212), as recommended by the Nevada Division of Environmental Protection (NDEP) and Clark County (2018). Due to continued exceedances of the standard through 2020, the EPA reclassified the Clark County Nonattainment Area (CCNAA) to Moderate with an attainment date of August 3, 2024, based on the 2021-2023 8-hour ozone Design Value (DV) (Federal Register, 2022; 2023).

To support an ozone attainment demonstration for the Moderate CCNAA State Implementation Plan (SIP), Ramboll is conducting a complete photochemical modeling study and ancillary weight-of-evidence analyses. The Comprehensive Air quality Model with extensions (CAMx) is used for this purpose.

This memorandum describes CAMx future year sensitivity modeling scenarios and results from applying the modeled attainment test to project the 2016-2018 average DV to the 2023 future year. The methodology closely follows the approach described in EPA modeling guidance (EPA, 2018) and in the Modeling Protocol developed during the early phases of this project (Ramboll, 2022). A complete description of the Clark County CAMx modeling platform, results from 2016 base year performance evaluation and sensitivity testing, and results from the 2023 future year modeling applications are provided in the Technical Support Document (Ramboll, 2024).

Summary of Results

- We conducted a sensitivity test in which the 2023 future year model-ready on-road NOx emissions were scaled down by 50% within the CCNAA. All other emission sectors, emitted compounds, and other model inputs were unaltered from the 2023 future base case.
  - Projected 2023 DVs are all well below the ozone NAAQS but only 0-0.5 ppb lower than the DV projections from the 2023 future base case. The peak average projected DV is 68.5 ppb Joe Neal. Generally, these results are similar to the 15% VOC Rate of Progress scenario (Ramboll, 2024), but show NOx-disbenefit conditions in the urban center of the LVV and NOx-limited conditions in the

downstream rural areas to the north, consistent with OSAT analyses (Ramboll, 2024).

  - Spatial differences in projected 2023 DV relative to the 2023 future base case clearly show different chemical regimes in the LVV, with lower DV approaching -1 ppb in NOx-lean outer rural areas to the northwest and higher DV (NOx disbenefit) approaching 1 ppb in and around the NOx-rich urban core.

- We conducted a sensitivity test in which the 2023 future year model-ready non-road NOx emissions were scaled down by 50% within the CCNAA. All other emission sectors, emitted compounds, and other model inputs were unaltered from the 2023 future base case.
  - Projected 2023 DVs are all well below the ozone NAAQS but only 0-0.5 ppb lower than the DV projections from the 2023 future base case. The peak average projected DV is 68.5 ppb Joe Neal, as in the on-road NOx reduction case. While these results are also similar to the 15% VOC Rate of Progress scenario, this run suggests a slightly larger NOx-disbenefit condition in the urban center of the LVV than the on-road NOx reduction case.
  - Spatial differences in projected 2023 DV relative to the 2023 future base case again show different chemical regimes in the LVV, with lower DV approaching -1 ppb in NOx-lean outer rural areas to the northwest and higher DV (NOx disbenefit) approaching 0.4 ppb in and around the NOx-rich urban core.
- We conducted a sensitivity test in which Clark County emissions were held constant from 2016 to 2023 while emissions over the rest of the 12US2 and 36US3 domains evolved, thereby allowing us to characterize the effect that local emission changes between 2016 and 2023 have on the 2023 ozone projection.
  - All projected 2023 DVs in the "2016/2023 mix" hybrid scenario remain below the 70 ppb standard. Some sites show higher DVs and some lower relative to the 2023 future base case. The higher DVs in the hybrid case are an expected result since 2016 Clark County emissions are higher than in the 2023 future base case. The lower DVs at sites in and around the urban core show that higher 2016 emissions lead to lower ozone relative to 2023 emissions, i.e., a NOx disbenefit. Regional emission reductions on the 12US2 grid are key to reducing 2023 ozone in the LVV while a local NOx disbenefit condition in and around the core urban area mitigates those reductions to some extent.
  - Spatial differences in projected 2023 DV relative to the 2023 future base case clearly shows higher DV approaching 3 ppb in NOx-lean outer rural areas to the northwest and lower DV (NOx disbenefit) approaching -3 ppb in and around the NOx-rich urban core.
- We conducted a sensitivity test in which all 2023 future year model-ready anthropogenic NOx and VOC emissions were scaled down by 50% within the CCNAA. All other emission sectors, emitted compounds, and other model inputs were unaltered from the 2023 future base case.
  - Projected DVs are all lower than the 2023 future year base case. Reductions vary from 0.01 ppb at outer monitors to 1-3 ppb in central Las Vegas to almost 4 ppb at Joe Neal. Large reductions continue farther downstream to the northwest of the LVV. These results suggest that such deep cuts in both VOC and NOx are

sufficient to overcome the NOx disbenefit in central Las Vegas seen for smaller NOx-only reductions.

- Spatial differences in projected 2023 DV relative to the 2023 future base case exhibit deep ozone reduction patterns across the LVV. However, the vicinity of McCarran/Reid airport indicates higher ozone than the 2023 base case by several ppb. This is related to reducing McCarren airport NOx, which causes a very localized non-disbenefit. The 2016 base case and 2023 future case both generated a local ozone minimum at that location as a result of the large airport NOx emissions. Lifting that NOx burden in this scenario has filled in the ozone minimum because of a more efficient mix of NOx and VOC from the airport and other local sources in that area.

50% NOx REDUCTION TO ON-ROAD EMISSIONS

Emissions Processing

Model-ready 2023 on-road NOx (NO and NO_2) emissions were scaled by 50% over a rectangular subset of CC4c2 grid cells covering the CCNAA. This scaling was done for every day of the May-August modeling period. All other emission sectors, emitted compounds, and other model inputs were unaltered from the 2023 future base case. As a QA step, model-ready emissions were plotted to verify that only the CCNAA area of the CC4c2 grid was modified. Table 1 shows resulting CCNAA model-ready on-road emissions averaged over July weekdays.

Table 12. 2023 CCNAA model-ready July weekday average on-road emissions (TPD) and net change for the 50% NOx reduction sensitivity scenario.

Precursor	2023 Base	2023 50% NOx	Difference	Change (%)
NOx	18.60	9.30	-9.30	-50%
VOC	16.21	16.21	0.00	0%

CAMx Modeling

The 2023 future year base case CAMx run (Ramboll, 2024) was repeated but replacing 2023 on-road sector emissions on the CC4c2 grid with revised emissions reflecting 50% NOx reductions in the CCNAA. All other inputs were not modified, and only the 12US2/CC4c2 2-way nested grids were run using the 2023 12US2 future base case boundary conditions extracted from the 36US3 grid.

SMAT-CE Configuration

We applied SMAT-CE (EPA, 2022) identically to the original 2023 future base case scenario, specifying 2016-2018 3-year DV period for base monitored ozone (2014-2018 4^{th} highs centered on 2016). All other configuration options remained the same as the original SMAT-CE run, which employed default or standard settings throughout the setup menu. We made no special modifications to monitored data or specific selection of modeled days for the RRF calculation.

Results at Monitoring Sites

Table 2 shows projected DV results at monitoring sites that reported sufficient data during the 2016-2018 base year DV period. Projected DVs are all well below the ozone NAAQS but only 0-0.5 ppb lower than the DV projections from the 2023 future base case among sites within the CCNAA. The peak average projected DV is 68.5 ppb Joe Neal. Generally, these results are similar to the 15% VOC Rate of Progress scenario (Ramboll, 2024) as shown in Table 3. Note, however, that the 2023 ozone DV is unresponsive to the on-road NOx reduction at Paul Meyer and is higher at Green Valley, indicating VOC-limited, NOx-disbenefit conditions in the urban center of the LVV. Conversely, the DV reduction is largest at the downstream Indian Springs site well to the north, suggesting NOx-limited conditions in that rural area. These results are consistent with OSAT analyses (Ramboll, 2024) that indicate the modeled LVV environment represents a spatial mix of VOC- and NOx-sensitive conditions.

Table 2. 2023 projected DVs at each monitoring site within the LVV according to SMAT-CE calculations using the 2016-2018 average base year DVs. Projected DVs are listed for the original 2023 future base case and for the 2023 50% on-road NOx scenario. Green indicates values below the NAAQS while sites noted with an asterisk continued to exceed the ozone NAAQS in 2020, leading to the bump up from Marginal to Moderate nonattainment status.

Site ID	Site Name	2023 Future Base DV	2023 50% NOx DV	Differences
		Avg 3x3	Avg 3x3	Avg
320030022	Apex	65.2	65.0	-0.2
320030023	Mesquite	57.2	57.2	0.0
320030043	Paul Meyer*	67.7	67.7	0.0
320030071	Walter Johnson*	67.9	67.7	-0.2
320030073	Palo Verde	67.2	66.9	-0.3
320030075	Joe Neal*	69.0	68.5	-0.5
320030298	Green Valley*	67.3	67.4	0.1
320030540	Jerome Mack	64.1	64.0	-0.1
320030601	Boulder City	61.5	61.5	0.0
320031019	Jean	63.9	63.9	0.0
320032002	J.D. Smith	67.3	67.1	-0.2
320037772	Indian Springs	62.3	61.7	-0.6

Table 3. As in Table 2, but comparing projected DVs for the 2023 15% VOC ROP scenario and for the 2023 50% on-road NOx scenario.

Site ID	Site Name	2023 15% VOC ROP	2023 50% NOx DV	Differences
		Avg 3x3	Avg 3x3	Avg
320030022	Apex	65.2	65.0	-0.2
320030023	Mesquite	57.2	57.2	0.0
320030043	Paul Meyer*	67.5	67.7	0.2
320030071	Walter Johnson*	67.5	67.7	0.2
320030073	Palo Verde	66.9	66.9	0.0
320030075	Joe Neal*	68.8	68.5	-0.3
320030298	Green Valley*	67.1	67.4	0.3
320030540	Jerome Mack	64.0	64.0	0.0
320030601	Boulder City	61.5	61.5	0.0
320031019	Jean	63.9	63.9	0.0
320032002	J.D. Smith	67.1	67.1	0.0
320037772	Indian Springs	62.2	61.7	-0.5

50% NOx REDUCTION TO NON-ROAD EMISSIONS

Emissions Processing

Model-ready 2023 non-road NOx emissions were scaled by 50% over a rectangular subset of CC4c2 grid cells covering the CCNAA. This scaling was done for every day of the May-August modeling period. All other emission sectors, emitted compounds, and other model inputs were unaltered from the 2023 future base case. As a QA step, model-ready emissions were plotted to verify that only the CCNAA area of the CC4c2 grid was modified. Table 4 shows resulting CCNAA model-ready non-road emissions averaged over July weekdays.

Table 4. 2023 CCNAA model-ready July weekday average non-road emissions (TPD) and net change for the 50% NOx reduction sensitivity scenario.

Precursor	2023 Base	2023 50% NOx	Difference	Change (%)
NOx	23.10	11.55	-11.55	-50%
VOC	23.84	23.84	0.00	0%

CAMx Modeling

The 2023 future year base case CAMx run was repeated but replacing 2023 non-road sector emissions on the CC4c2 grid with revised emissions reflecting 50% NOx reductions in the CCNAA. All other inputs were not modified, and only the 12US2/CC4c2 2-way nested grids were run using the 2023 12US2 future base case boundary conditions extracted from the 36US3 grid.

SMAT-CE Configuration

We applied SMAT-CE identically to the original 2023 future base case scenario, specifying 2016-2018 3-year DV period for base monitored ozone (2014-2018 4th highs centered on 2016). All other configuration options remained the same as the original SMAT-CE run, which employed default or standard settings throughout the setup menu. We made no special modifications to monitored data or specific selection of modeled days for the RRF calculation.

Results at Monitoring Sites

Table 5 shows projected DV results at monitoring sites that reported sufficient data during the 2016-2018 base year DV period. Projected DVs are similar to the on-road NOx reduction case above and only 0-0.5 ppb lower than the DV projections from the 2023 future base case among sites within the CCNAA. This case, however, indicates a slightly larger NOx-disbenefit in the central urban core of the CCNAA. The peak average projected DV is 68.5 ppb Joe Neal, identical to the on-road NOx reduction case. Generally, these results are similar to the 15% VOC Rate of Progress scenario as shown in Table 6 but ozone is slightly higher in the NOx-rich areas around Paul Meyer, Walter Johnson, and Green Valley. Conversely, the DV reduction is largest at the downstream sites at Indian Springs, Apex, and Joe Neal as conditions become more NOx-limited. These results are again consistent with OSAT analyses that indicate the modeled LVV environment represents a spatial mix of VOC- and NOx-sensitive conditions.

Table 5. 2023 projected DVs at each monitoring site within the LVV according to SMAT-CE calculations using the 2016-2018 average base year DVs. Projected DVs are listed for the original 2023 future base case and for the 2023 50% non-road NOx scenario. Green indicates values below the NAAQS while sites noted with an asterisk continued to exceed the ozone NAAQS in 2020, leading to the bump up from Marginal to Moderate nonattainment status.

Site ID	Site Name	2023 Future Base DV	2023 50% NOx DV	Differences
		Avg 3x3	Avg 3x3	Avg
320030022	Apex	65.2	64.8	-0.4
320030023	Mesquite	57.2	57.2	0.0
320030043	Paul Meyer*	67.7	67.9	0.2
320030071	Walter Johnson*	67.9	68.0	0.1
320030073	Palo Verde	67.2	67.0	-0.2
320030075	Joe Neal*	69.0	68.5	-0.5
320030298	Green Valley*	67.3	67.4	0.1
320030540	Jerome Mack	64.1	64.0	-0.1
320030601	Boulder City	61.5	61.4	-0.1
320031019	Jean	63.9	63.9	0.0
320032002	J.D. Smith	67.3	67.1	-0.2
320037772	Indian Springs	62.3	61.6	-0.7

Table 6. As in Table 5, but comparing projected DVs for the 2023 15% VOC ROP scenario and for the 2023 50% non-road NOx scenario.

Site ID	Site Name	2023 15% VOC ROP	2023 50% NOx DV	Differences
		Avg 3x3	Avg 3x3	Avg
320030022	Apex	65.2	64.8	-0.4
320030023	Mesquite	57.2	57.2	0.0
320030043	Paul Meyer*	67.5	67.9	0.4
320030071	Walter Johnson*	67.5	68.0	0.5
320030073	Palo Verde	66.9	67.0	0.1
320030075	Joe Neal*	68.8	68.5	-0.3
320030298	Green Valley*	67.1	67.4	0.3
320030540	Jerome Mack	64.0	64.0	0.0
320030601	Boulder City	61.5	61.4	-0.1
320031019	Jean	63.9	63.9	0.0
320032002	J.D. Smith	67.1	67.1	0.0
320037772	Indian Springs	62.2	61.6	-0.6

2016 CC4C2 EMISSIONS WITH 2023 12US2 EMISSIONS

CAMx Modeling

The 2023 future year base case CAMx run was repeated but replacing all 2023 emissions on the CC4c2 grid with their 2016 counterparts. This run shows a hypothetical situation where Clark County emissions are held constant from 2016 to 2023 while emissions over the rest of the 12US2 and 36US3 domains evolve, thereby allowing us to characterize the effect that local emission changes between 2016 and 2023 have on the 2023 ozone projection. All other inputs were not modified, and only the 12US2/CC4c2 2-way nested grids were run using the 2023 12US2 future base case boundary conditions extracted from the 36US3 grid.

SMAT-CE Configuration

We applied SMAT-CE identically to the original 2023 future base case scenario, specifying 2016-2018 3-year DV period for base monitored ozone (2014-2018 4th highs centered on 2016). All other configuration options remained the same as the original SMAT-CE run, which employed default or standard settings throughout the setup menu. We made no special modifications to monitored data or specific selection of modeled days for the RRF calculation.

Results at Monitoring Sites

Table 7 shows projected DV results at monitoring sites that reported sufficient data during the 2016-2018 base year DV period. All projected DVs in the "2016/2023 mix" hybrid scenario remain below the 70 ppb standard. Some sites show higher DVs and some lower relative to the 2023 future base case. The higher DVs in the hybrid case are an expected result since Clark County emissions (maintained at 2016) are higher than in the 2023 future base case. The lower DVs at sites in and around the urban core show that higher 2016 emissions lead to lower ozone relative to 2023 emissions. This means that 2016 NOx emissions inhibit ozone formation in that area leading to a NOx disbenefit (higher ozone) when lower 2023 emissions are used. Since 2023 projected DVs are much lower than the 2016-2018 DVs in both cases at all sites, the wider regional emission reductions are key to reducing ozone in the LVV while a local NOx disbenefit conditions in and around the core urban area mitigates those reductions to some extent. These results are consistent with signals reported in the two sensitivity tests above, and with OSAT analyses that indicate the modeled LVV environment represents a spatial mix of VOC- and NOx-sensitive conditions.

Table 5. 2023 projected DVs at each monitoring site within the LVV according to SMAT-CE calculations using the 2016-2018 average base year DVs. Projected DVs are listed for the original 2023 future base case and for the 2016/2023 emissions mix scenario. Green DVs indicate values below the NAAQS while red differences indicate a NOx disbenefit signal.

Site ID	Site Name	2023 Future Base DV	2016/2023 Mix DV	Differences
		Avg 3x3	Avg 3x3	Avg
320030022	Apex	65.2	66.1	0.9
320030023	Mesquite	57.2	57.4	0.2
320030043	Paul Meyer*	67.7	67.1	-0.6
320030071	Walter Johnson*	67.9	67.2	-0.7
320030073	Palo Verde	67.2	67.4	0.2
320030075	Joe Neal*	69.0	69.3	0.3
320030298	Green Valley*	67.3	66.3	-1.0
320030540	Jerome Mack	64.1	63.7	-0.4
320030601	Boulder City	61.5	61.7	0.2
320031019	Jean	63.9	64.0	0.1
320032002	J.D. Smith	67.3	67.0	-0.3
320037772	Indian Springs	62.3	64.3	2.0

50% NOx AND VOC REDUCTION FOR ALL ANTHROPOGENIC EMISSIONS

Emissions Processing

Model-ready 2023 anthropogenic NOx and VOC emissions were scaled by 50% over a rectangular subset of CC4c2 grid cells covering the CCNAA. This scaling was done for every day of the May-August modeling period. All other emission sectors, emitted compounds, and other model inputs were unaltered from the 2023 future base case. As a QA step, model-ready emissions were plotted to verify that only the CCNAA area of the CC4c2 grid was modified. Table 6 shows resulting CCNAA model-ready anthropogenic emissions averaged over July weekdays.

Table 6a. 2023 CCNAA model-ready July weekday average anthropogenic NOx emissions (TPD) and net change for the 50% NOx reduction sensitivity scenario.

Sector	2023 Base	2023 50% NOx	Change (%)
afdust_adj	0.000	0.000	
airports_wo_McCarran_CD	8.386	4.193	-50%
fertilizer	0.000	0.000	
livestock	0.000	0.000	
nonpt	3.958	1.978	-50%
nonroad	23.097	11.555	-50%
np_oilgas	0.000	0.000	
onroad	18.603	9.301	-50%
pt_oilgas	0.151	0.075	-50%
ptegu	2.639	1.320	-50%
ptnonipm	5.938	2.969	-50%
rail	0.659	0.330	-50%
rwc	0.058	0.029	-50%
solvents	0.000	0.000	
airports_w_McCarran_CD	7.524	3.762	-50%

Table 6b. 2023 CCNAA model-ready July weekday average anthropogenic VOC emissions (TPD) and net change for the 50% VOC reduction sensitivity scenario.

Sector	2023 Base	2023 50% VOC	Change (%)
afdust_adj	0.000	0.000	
airports_wo_McCarran_CD	2.529	1.265	-50%
fertilizer	0.000	0.000	
livestock	0.002	0.001	-50%
nonpt	10.547	5.273	-50%
nonroad	23.843	11.928	-50%
np_oilgas	0.000	0.000	
onroad	16.212	8.106	-50%
pt_oilgas	0.020	0.010	-50%
ptegu	0.733	0.367	-50%
ptnonipm	0.585	0.293	-50%
rail	0.028	0.014	-50%
rwc	0.410	0.205	-50%
solvents	31.745	15.870	-50%
airports_w_McCarran_CD	0.098	0.049	-50%

CAMx Modeling

The 2023 future year base case CAMx run was repeated but replacing 2023 anthropogenic emissions on the CC4c2 grid with revised emissions reflecting 50% NOx and VOC reductions in the CCNAA. All other inputs were not modified, and only the 12US2/CC4c2 2-way nested grids were run using the 2023 12US2 future base case boundary conditions extracted from the 36US3 grid.

SMAT-CE Configuration

We applied SMAT-CE identically to the original 2023 future base case scenario, specifying 2016-2018 3-year DV period for base monitored ozone (2014-2018 4th highs centered on 2016). All other configuration options remained the same as the original SMAT-CE run, which employed default or standard settings throughout the setup menu. We made no special modifications to monitored data or specific selection of modeled days for the RRF calculation.

Results at Monitoring Sites

Table 7 shows projected DV results at monitoring sites that reported sufficient data during the 2016-2018 base year DV period. Projected DVs are all lower than the 2023 future year base case. Reductions vary from 0.01 ppb at outer monitors (Jean and Mesquite) to 1-3 ppb in central Las Vegas (Paul Meyer, Walter Johnson, Palo Verde, Green Valley, Jerome Mack and J.D. Smith) to almost 4 ppb at Joe Neal. Large reductions continue farther downstream to the northwest of the LVV (Indian Springs). These results suggest that such deep cuts in both VOC and NOx are sufficient to overcome the NOx disbenefit in central Las Vegas seen for smaller NOx-only reductions.

Table 7. 2023 projected DVs at each monitoring site within the LVV according to SMAT-CE calculations using the 2016-2018 average base year DVs. Projected DVs are listed for the original 2023 future base case and for the 2023 50% anthropogenic NOx and VOC scenario. Green indicates values below the NAAQS while sites noted with an asterisk continued to exceed the ozone NAAQS in 2020, leading to the bump up from Marginal to Moderate nonattainment status.

Site ID	Site Name	2023 Future Base DV	2023 50% NOx and VOC DV	Differences
		Avg 3x3	Avg 3x3	Avg
320030022	Apex	65.2	63.7	-1.5
320030023	Mesquite	57.2	57.1	-0.1
320030043	Paul Meyer*	67.7	65.7	-2.0
320030071	Walter Johnson*	67.9	65.0	-2.9
320030073	Palo Verde	67.2	64.4	-2.8
320030075	Joe Neal*	69.0	65.1	-3.9
320030298	Green Valley*	67.3	66.0	-1.3
320030540	Jerome Mack	64.1	62.4	-1.7
320030601	Boulder City	61.5	61.1	-0.4
320031019	Jean	63.9	63.8	-0.1
320032002	J.D. Smith	67.3	64.6	-2.7
320037772	Indian Springs	62.3	59.5	-2.8

REFERENCES

EPA, 2018. Modeling Guidance for Demonstrating Air Quality Goals for Ozone, PM2.5, and Regional Haze. Prepared by the US Environmental Protection Agency, Office of Air Quality Planning and Standards, Air Quality Assessment Division (EPA 454/R-18-009, November 2018). https://www3.epa.gov/ttn/scram/guidance/guide/O3-PM-RH-Modeling_Guidance-2018.pdf.

EPA, 2022. Photochemical Modeling Tools: SMAT-CE. https://www.epa.gov/scram/photochemical-modeling-tools.

Federal Register, 2018. Additional Air Quality Designations for the 2015 Ozone National Ambient Air Quality Standards. Vol. 83, No. 107 (June 4, 2018). https://files.clarkcountynv.gov/clarknv/Environmental%20Sustainability/SIP%20Related%20Documents/20180604_83_FR_25776_2015_O3_NAAQS_Designations.pdf?t=1647046265375&t=1647046265375z.

Federal Register, 2022. Finding of Failure To Attain and Reclassification of Las Vegas Area as Moderate for the 2015 Ozone National Ambient Air Quality Standard. Vol. 87, No. 140 (July 22, 2022) [EPA–R09–OAR–2022–0525; FRL–9961–01–R9]. https://www.federalregister.gov/documents/2022/07/22/2022-15674/finding-of-failure-to-attain-and-reclassification-of-las-vegas-area-as-moderate-for-the-2015-ozone.

Federal Register, 2023. Finding of Failure To Attain and Reclassification of Las Vegas Area as Moderate for the 2015 Ozone National Ambient Air Quality Standard (Final Rule). Vol. 88, No. 3 (January 5, 2023) [EPA–R09–OAR–2022–0525; FRL–9961–02–R9]. https://www.federalregister.gov/documents/2023/01/05/2022-28319/finding-of-failure-to-attain-and-reclassification-of-las-vegas-area-as-moderate-for-the-2015-ozone.

NDEP and Clark County, 2018. Clark County Response to 120-Day 2015 Ozone NAAQS Designations Letter; Docket ID EPA HQ-OAR-2017-0548. Letter to Acting Regional Administrator, EPA Region 9 (February, 2018). https://files.clarkcountynv.gov/clarknv/Environmental%20Sustainability/SIP%20Related%20Documents/20180223_%20NDEP_Lovato_Transmittal_ClarkCounty_2015_O3_NAAQS_%20Response.pdf?t=1647046265375&t=1647046265375.

Ramboll, 2022. Modeling Protocol for the Clark County Ozone State Implementation Plan (Version 5). Prepared for the Clark County Department of Environment and Sustainability, Division of Air Quality, Las Vegas, NV, by Ramboll US Consulting, Inc. Novato, CA (October 5, 2022).

Ramboll, 2024. Technical Support Document: Attainment Demonstration for the Clark County Ozone State Implementation Plan. Prepared for the Clark County Department of Environment and Sustainability, Division of Air Quality, Las Vegas, NV, by Ramboll Americas Engineering Solutions, Inc. Novato, CA (June 28, 2024).

APPENDIX B: SENSITIVITY MODELING TO DERIVE AN INTER-POLLUTANT TRADING RATIO

MEMORANDUM

Date: **14 December 2023**

To: **Zheng Li, Clark County DES/DAQ**

From: **Chris Emery, Trang Tran, Chao-Jung Chien**

Subject: **CBE NO. 606111-22: Clark County, Nevada Attainment Demonstration Modeling**
Sensitivity Modeling to Derive an Inter-Pollutant Trading Ratio

INTRODUCTION

This memorandum describes the approach to estimate a VOC:NOx inter-pollutant trading (IPT) ratio from two CAMx future year sensitivity modeling scenarios. The sensitivity runs involved applying across-the-board 10% NOx and 10% VOC reductions, relative to the 2023 15% VOC Rate of Progress (ROP) scenario, to all anthropogenic source sectors except airports within the Clark County Nonattainment Area (CCNAA or HA212). All other emissions sectors, emitted compounds, and other model inputs were unaltered from the 2023 15% VOC ROP case. Estimating an IPT ratio relative to the 15% ROP scenario considers the ambient chemical environment after all ROP measures have been fully implemented. For both sensitivity cases, the modeled attainment test procedure was used to project the monitored 2016-2018 average ozone Design Value (DV) to the 2023 future year. Ratios of resulting 2023 ozone DV impacts from the NOx and VOC cases relative to the 15% ROP case were calculated to yield the VOC:NOx IPT ratio for several combinations of monitoring sites within the CCNAA. A complete description of the Clark County CAMx modeling platform, results from 2016 base year performance evaluation and sensitivity testing, and results from the 2023 future year modeling applications are provided in the Modeling Technical Support Document.

Summary of Results

Following the approach summarized above, we determined ozone DV impacts from the 10% NOx and 10% VOC CCNAA anthropogenic emission reduction cases relative to the 15% ROP case. We then calculated a ratio of those DV changes normalized on a tpd basis to determine VOC:NOx IPT ratios for three different combinations of monitoring sites.

- VOC:NOx IPT averaged over six monitoring sites within the CCNAA: the IPT ratio is 0.08, meaning that it takes 0.08 tpd VOC for each 1 tpd of NOx to get an equivalent ozone impact; i.e., 1 tpd VOC reduction is ~12.5 times more effective at reducing ambient ozone concentrations than 1 tpd NOx reduction across the CCNAA (a VOC-limited, NOx-rich condition with NOx-disbenefits at three central locations).
- VOC:NOx IPT averaged over three monitoring sites within the CCNAA (with no NOx-disbenefits): the IPT ratio is 0.48, or 1 tpd VOC reduction is ~2 times more effective at reducing ambient ozone concentrations than 1 tpd NOx reduction among those sites.
- VOC: NOx IPT at the peak Joe Neal site: the IPT ratio is 0.75, or 1 tpd VOC reduction is ~1.3 times more effective at reducing ambient ozone concentrations than 1 tpd NOx reduction at that location.

EMISSIONS PROCESSING

Model-ready 2023 anthropogenic NOx and VOC emissions from the 15% ROP scenario were scaled down by 10% over a rectangular subset of CC4c2 grid cells covering the CCNAA. Estimating an IPT ratio relative to the 15% ROP scenario considers the ambient chemical environment after all ROP measures have been fully implemented. This scaling was performed for all anthropogenic sectors, except for airports, for every day of the May-August modeling period. All other emission sectors, emitted compounds, and other model inputs were unaltered from the 2023 15% ROP case. As a QA step, model-ready emissions were plotted to verify that only the CCNAA area of the CC4c2 grid was modified. Table 1 shows resulting CCNAA model-ready anthropogenic emissions averaged over July weekdays.

Table 13. 2023 CCNAA model-ready July weekday average anthropogenic emissions (tpd) and net change for the 10% NOx and VOC reduction sensitivity scenarios.

Precursor	2023 15% ROP	10% Reduction	Difference	Change (%)
NOx	55.10	49.59	-5.51	-10%
VOC	74.18	66.76	-7.42	-10%

CAMX MODELING

The 2023 15% ROP CAMx run (Ramboll, 2024) was repeated twice by replacing affected anthropogenic emissions on the CC4c2 grid with revised emissions reflecting 10% NOx and 10% VOC reductions in the CCNAA, respectively. All other inputs were not modified, and only the 12US2/CC4c2 2-way nested grids were run using the 2023 12US2 future base case boundary conditions extracted from the 36US3 grid.

SMAT-CE Configuration

We applied SMAT-CE (EPA, 2022) identically to the 2023 15% ROP scenario, specifying 2016-2018 3-year DV period for base monitored ozone (2014-2018 4th highs centered on 2016). All other configuration options remained the same as the original SMAT-CE run, which employed default or standard settings throughout the setup menu. We made no special modifications to monitored data or specific selection of modeled days for the relative response factor (RRF) calculation.

IPT Ratio Calculations

2023 ozone DV changes from the NOx and VOC cases relative to the 15% ROP scenario were determined at each monitoring site. Then, VOC:NOx IPT ratios were determined by normalizing the DV change by the total emission reductions (5.51 tpd NOx, 7.42 tpd VOC) produced by the 10% across the board emissions reductions. The resulting values represent the VOC:NOx IPT, which estimates the tpd of VOC for each 1 tpd of NOx to get an equivalent ozone DV impact.

$$VOC{:}NOx\ IPT\ ratio = \frac{\left[\frac{DV\ \Delta\ from\ NOx\ reduction\ (ppb)}{5.51\ NOx\ tpd}\right]}{\left[\frac{DV\ \Delta\ from\ VOC\ reduction(ppb)}{7.42\ VOC\ tpd}\right]} = \frac{VOC\ tpd)}{NOx\ tpd}$$

After calculating VOC:NOx IPT ratios for each monitoring site, we calculated several combinations as potential candidates for the VOC:NOx IPT ratio for the CCNAA:

- VOC:NOx IPT averaged over the six monitoring sites operating within the CCNAA in 2016 and 2023, to give a broad indication of precursor sensitivity across all simulated chemical regimes (JD Smith was excluded for purposes of calculating the future inter-pollutant trading ratio because the monitoring site shutdown in 2017 due to poor siting. It was replaced by Walnut Community Center which did not begin operating until 2021);
- VOC:NOx IPT averaged over three monitoring sites within the CCNAA with no NOx-disbenefits to give an average assessment in areas where NOx reductions are simulated to reduce ozone;
- VOC:NOx IPT at the peak Joe Neal site to estimate relative sensitivity for peak monitored ozone.

Table 2 shows results from the 2023 ozone DV changes and IPT ratio calculations for each site, and potential CCNAA VOC:NOx IPT ratios for the three combinations of monitoring sites. Note that SMAT only reports ozone DV projections to one decimal place, which is insufficient to calculate IPT ratios. However, SMAT also reports RRF to 4 decimal places, so we recalculated 2023 projected DVs at each monitor directly using RRFs reported by SMAT for the 15% ROP, 10% NOx and 10% VOC scenarios. The resulting DV differences from the NOx and VOC sensitivity cases relative to the 15% ROP DV were then calculated for each site. Table 2 shows the DV change at each monitoring site after modeling the emissions reductions and results of the VOC:NOx IPT calculations.

When considering all six monitoring sites within the CCNAA, the VOC:NOx IPT ratio is 0.08, meaning that meaning that it takes 0.08 tpd VOC for each 1 tpd of NOx to get an equivalent ozone impact. In other words, 1 tpd VOC emission reduction is 12.5 times more effective than 1 tpd NOx emissions reduction in reducing ambient ozone concentrations across the CCNAA, confirming a VOC-limited, NOx-rich condition with NOx-disbenefits at some central locations. Considering only three monitoring sites within the CCNAA with no NOx-disbenefits, the VOC:NOx IPT ratio is 0.48, or 1 tpd VOC reduction is ~2 times more effective than 1 tpd NOx reduction among those sites. At the peak Joe Neal site, the VOC:NOx IPT ratio is 0.75, or 1 tpd VOC reduction is ~1.3 times more effective than 1 tpd NOx reduction for reducing the ambient ozone concentration at that location.

Table 2. VOC for NOx tpd Inter-pollutant Trading Ratio based on 2023 projected DV change at each Clark County monitoring site according to SMAT-CE calculations using the 2016-2018 average base year DVs. Bold highlighted rows represent sites within the CCNAA. DV impacts in red indicate NOx-disbenefits where NOx reductions lead to ozone DV increases.

Site Name	2023 15% ROP DV (ppb)	10% NOx Reduction ΔDV (ppb)	10% VOC Reduction ΔDV (ppb)	ΔDV (ppb) / NOx (tpd)	ΔDV (ppb) / VOC (tpd)	VOC:NOx IPT Ratio
Apex	65.25246	-0.1476	-0.0562	-0.0268	-0.0076	3.53
Mesquite	57.23581	-0.0061	0.0000	-0.0011	0.0000	-----
Paul Meyer	**67.50720**	**0.0576**	**-0.3024**	**0.0105**	**-0.0408**	**-0.26**
Walter Johnson	**67.58604**	**0.0217**	**-0.3543**	**0.0039**	**-0.0477**	**-0.08**
Palo Verde	**66.99318**	**-0.0868**	**-0.2675**	**-0.0157**	**-0.0361**	**0.44**
Joe Neal	**68.82000**	**-0.1800**	**-0.3225**	**-0.0327**	**-0.0435**	**0.75**
Green Valley	**67.13760**	**0.0994**	**-0.2201**	**0.0180**	**-0.0297**	**-0.61**
Jerome Mack	**64.02840**	**-0.0344**	**-0.1855**	**-0.0062**	**-0.0250**	**0.25**
Boulder City	61.55160	-0.0396	-0.0264	-0.0072	-0.0036	2.02
Jean	63.90831	0.0000	-0.0137	0.0000	-0.0018	0.00
Indian Springs	62.25280	-0.2946	-0.0959	-0.0535	-0.0129	4.14
					Average over all 6 CCNAA sites	**0.08**
					Average over all 3 CCNAA sites <0 ΔDV	**0.48**
					Joe Neal	**0.75**

REFERENCES

EPA, 2022. Photochemical Modeling Tools: SMAT-CE. https://www.epa.gov/scram/photochemical-modeling-tools.

EPA 2023. EPA Interpollutant Trading Technical Support Document Proposed Contingency Measures Federal Implementation Plan for the Fine Particulate Standards for San Joaquin Valley, California. U.S. Environmental Protection Agency, Region IX (July 2023).

Ramboll, 2024. Technical Support Document: Attainment Demonstration for the Clark County Ozone State Implementation Plan. Prepared for the Clark County Department of Environment and Sustainability, Division of Air Quality, Las Vegas, NV, by Ramboll Americas Engineering Solutions, Inc. Novato, CA (June 28, 2024).